A STUDY OF POLY(PROPYLENE) BY GAS PERMEATION

by

WALTER F. WUERTH

B.A.Sc., University of Toronto, (1962)

S.M., Massachusetts Institute of Technology, (1964)

Submitted in Partial Fulfillment

of the

Requirements for the Degree of

DOCTOR OF SCIENCE

at the

Massachusetts Institute of Technology

December, 1967

Signature of Author _____
Department of Chemical Engineering

Certified by _____
Professor W. R. Vieth, Thesis Supervisor

Accepted by _____
Professor G. C. Williams, Chairman
Departmental Committee on Graduate Theses

ABSTRACT

A STUDY OF POLY(PROPYLENE) BY GAS PERMEATION

by

Walter F. Wuerth

Submitted to the Department of Chemical Engineering on December 7 , 1967, in partial fulfillment of the requirements for the degree of Doctor of Science.

The barrier and transport properties of semi-crystalline polymer membranes are strongly dependent on their crystalline microstructures which, at present, are still poorly understood. Thus, the object of this thesis was to investigate and, hopefully, clarify the microstructure of semi-crystalline poly(propylene) by studying the levels of gas sorption and the rates at which carefully-selected, small, inert gas molecules (He, A, CF_4) diffuse in isotactic and atactic poly(propylene), using the latter material as the completely amorphous analog of the crystalline, isotactic form. Time-lag and sorption experiments were employed to measure permeability, diffusivity and solubility constants in films cooled at various rates from the melt and subsequently annealed at varying temperatures near the melting point. These techniques allowed the preparation of poly(propylene) samples of a rather wide range of morphologies. In order to more fully characterize these films, experiments above (30 to 70°C) and below (0 to -40°C) the glass transition temperature were conducted.

While solubility constants in films annealed above 90°C showed the normal variation with the amorphous content of the polymer, solubility constants for all unannealed, quenched films were remarkably constant and independent of the rate of cooling. Thus, all quenched films appear to have the same amorphous content (ca. 41%). The remaining material is believed to be a mixture of monoclinic and hexagonal crystallinity, the volume ratio of the two being a function of the rate of quenching, and changing, on annealing, in favor of the more stable, monoclinic form; the transition occurring rather sharply at 90°C. In addition to the sorption and diffusion behavior of quenched films, diffraction patterns were analyzed and offer further evidence for the existence of the hexagonal crystals. Concerning the amorphous phase per se, the enhanced solubility in the glassy polymer points to a process of micro-void filling in addition to the process of ordinary dissolution, emphasizing the role of free-volume in transport behavior.

The diffusion behavior in crystalline poly(propylene) is normal and Fickian but instead of the usual steady decline with increasing crystallinity, diffusivities show definite enhancement for the annealed films. This suggests reduction in diffusional impedance by the formation of defects in existing crystallites, as the lamellae thicken, in a manner similar to that observed on annealing of poly(ethylene) single crystals. On the basis of an analysis of the relative diffusional enhancements of progressively larger molecules, a defect size distribution was estimated. From this, it was determined that the diameter of the most common defect is 4.2A, in excellent agreement with the estimated diameter of the poly(propylene) helix which is thought to leave row vacancies by translational motions in the lattice at the temperature of annealing.

The apparent activation energies of diffusion and average lengths of the activated diffusion step were essentially constant and independent of thermal history. This suggests that in a highly crystalline polymer diffusion is not so much impeded by the restricted mobility of chain segments but rather by the extremely small dimensions of the available diffusional paths. Thus, crystalline poly(propylene) appears to be a one-phase crystalline aggregate with numerous defects and lamellae borders in which diffusion and sorption take place.

In support of the argument that the transport properties of poly(propylene) are controlled at a level of microstructure well below the characteristic dimensions of spherulites, it was observed that bulk-crystallized poly(propylene) has a spherulitic structure whose size and texture do not change on annealing. Finally, electron microscopic examination suggests that, within the well-annealed spherulite, the structure is highly branched and interwoven.

This thesis has, it is believed, contributed to an improved understanding of the microstructure of semi-crystalline poly-(propylene), especially in relation to the way in which it governs the transport properties of the material. Additional studies of crystallizable poly(olefinic) materials are recommended, to further develop comprehensive structure-property relationships for this important class of materials.

Thesis Supervisor: Wolf R. Vieth
Associate Professor of Chemical Engineering

Department of Chemical Engineering
Massachusetts Institute of Technology
Cambridge, Massachusetts 02139
December 7, 1967

Professor Edward N. Hartley
Secretary of the Faculty
Massachusetts Institute of Technology
Cambridge, Massachusetts 02139

Dear Professor Hartley:

In accordance with the regulations of the faculty, I herewith submit the thesis, entitled "A Study of Poly(propylene) by Gas Permeation", in partial fulfillment of the requirements for the degree of Doctor of Science in Chemical Engineering at the Massachusetts Institute of Technology.

Respectfully submitted,

Walter F. Wuerth

ACKNOWLEDGEMENTS

The author gratefully acknowledges the expert guidance and kind encouragement of Professor Wolf R. Vieth throughout the course of this work. Appreciation is expressed to Professor Allan S. Hoffman, Dr. Alan S. Michaels and Dr. Harris J. Bixler for their valuable advice and continued interest.

The author acknowledges with gratitude the financial support of the National Science Foundation, whose Grant-in-Aid, GP-707, made this study possible. The polymer was furnished by Hercules, Inc., and the Avisun Corporation.

The author wishes to thank Messrs. R. Bates, C. L. Marx, and J. Del Pico for their assistance in collecting the low pressure sorption data, and Messrs. P. A. Tomlinson, A. Ogunbameru and D. L. Phipps for performing the high pressure sorption experiments.

Mr. S. R. Mitchell rendered valuable services in glass-blowing and electron microscopy.

The author also expresses his gratitude to his wife and parents for their encouragement, patience and confidence.

TABLE OF CONTENTS

LIST OF FIGURES

LIST OF TABLES

I. SUMMARY

A. Introduction

The relative impermeability of polymer films has long made them invaluable in innumerable and diverse packaging applications. This, together with their considerable potential as media for separating gas or liquid mixtures, has stimulated an enthusiastic and sustained interest in polymer films.

In the area of semi-crystalline polymers, it has been found that the crystalline microstructure plays an important role in the selectivity and the fluid-transport properties of the film. Knowing what this microstructure is and how it can be modified by suitable thermal, mechanical or solvent treatment make possible the development of materials with permeation properties most advantageous for a given application.

Although electron microscopy and x-ray diffraction provide means for observation of microcrystallinity, the extremely complex micro-structure of bulk polymers has made detailed morphological studies difficult by these means alone. On the other hand, analysis of data on the sorption and diffusion of small inert gas molecules has proven very successful, in the past, in elucidating aspects of polymer microstructures which may be insensitive to the other techniques.

Poly(propylene) was chosen as the subject of this investigation because of its present economic importance, its potential for many more applications, and its relatively poorly understood microstructure.

Specifically, the aims of this study were: (1) to use sorption and diffusion studies to establish the presence and nature of the crystalline phase in poly(propylene) and to determine the extent of its interaction with the amorphous phase; (2) to observe the effect of changes in thermal history on the microstructure by observation of the resulting changes in the permeation properties of the altered film; (3) to arrive at a model for diffusion and sorption in isotactic poly-(propylene) by interpretation of the gas permeation data, in conjunction with evidence from other polymer characterization; and (4) to generate engineering data for design considerations.

B. Theoretical Aspects

The material under consideration is the isotactic stereoisomer of poly(propylene). It is a linear polymer whose chain favors a helical conformation, due to its bulky methyl side-groups. The ability of the resulting helices to pack closely leads to crystallization. The most stable crystal mode is monoclinic. However, quenching of the polymer from the melt results in another crystal form often referred to as "smectic" or simply "quenched" material. The nature of this form has not been clearly resolved; however, existing evidence points to small hexagonal crystals.

It is believed that, even in the bulk polymer, chains crystallize into chain-folded lamellae which, on annealing, grow in lateral dimensions as well as thicken without new growth. The thickening process proceeds by self-diffusion of chains along their own backbones (45). This, in turn, necessitates introduction of chain ends into the crystal, with the diffusion of some right through the lamella, leaving behind a vacant row in the lattice. This introduces a defect into the lamella similar to the "swiss-cheese" effect observed for single crystals of poly(ethylene). To examine such morphological features, the solution and diffusion of small gas molecules in films of varied thermal history were studied.

The steady-state, uni-directional flow of gas across a polymer membrane can be described by Fick's first law of diffusion,

$$J = -D \frac{dc}{dx} \qquad (1)$$

where J is the permeation flux, D is the diffusion constant, and $\frac{dc}{dx}$ is the concentration gradient.

For the gases used in the present work,

$$D \neq f(c) \qquad (2)$$

and Henry's law describes the solubility,

$$C = kP \qquad (3)$$

where C is the dissolved gas concentration, k is the solubility constant and P is the gas phase pressure. Accordingly, equation (1) may be simplified to

$$J = Dk \frac{(P_1 - P_2)}{\ell} \qquad (4)$$

where P_1 and P_2 refer to the pressures at the film surfaces.

The product Dk is usually defined by $\bar{P}$, the permeability constant, so that

$$\bar{P} \equiv Dk \qquad (5)$$

The effect of temperature on these three parameters is generally expressed by:

$$\bar{P} = \bar{P}_o \, e^{-\frac{E_{\bar{P}}}{RT}} \qquad (6)$$

$$D = D_o \, e^{-\frac{E_D}{RT}} \qquad (7)$$

$$k = k_o \, e^{-\frac{\Delta H_S}{RT}} \qquad (8)$$

where $E_{\bar{P}}$ and E_D are the activation energies for permeation and diffusion, respectively, and ΔH_S is the enthalpy of sorption.

The above discussion is directly applicable to gas transport in completely amorphous polymers. However, the presence of crystallinity complicates the picture considerably, the most pronounced effect being a reduction in permeability.

Originally, this led to the concept of a two-phase model of impenetrable crystallites dispersed in a rubbery amorphous matrix (88).

Parker (88) expressed the effect on solubility as,

$$k = \alpha k^* \qquad (9)$$

where α is the volume fraction of amorphous material and k^* is the solubility in the completely amorphous polymer. In other words, gas is soluble only in the amorphous phase.

However, crystallinity decreases permeability not only by reducing the volume of amorphous material available for flow but also by creating more sinuous and/or restricted pathways for the diffusing molecule. Thus, diffusivity was found to obey the relationship,

$$D = \frac{D^*}{\tau\beta} \qquad (10)$$

where D, the diffusivity in the partially crystalline polymer, is reduced from what it would be in the completely amorphous polymer, D^*, by a "geometric impedance factor", τ, and a "chain immobilization factor", β. The latter parameter was initially designed to account for the cross-linking action of the crystallites on segmental mobility.

However, Jeschke and Stuart (51) and others (15, 17, 67) have observed inconsistencies in this picture of diffusion in crystalline polymers. For example, they have found that β

depends strongly on the molecular diameter of the diffusing gas but is essentially constant for each gas and independent of α and thermal history of the polymer. Another observation that is difficult to explain on the basis of a two-phase model is the small decrease - rather than anticipated increase - in diffusional activation energies with decreasing α. Furthermore, the recent study of Fein (33) showed that as regards the transport of the smallest gas molecule, helium, the crystalline phase in poly(ethylene) may be quite imperfect and may, in fact, contain pockets and channels of amorphous material accessible only to helium.

These observations, together with the lamellar concept which presently enjoys wide acceptance, suggest that the two-phase model may, indeed, be a gross oversimplification. The actual situation may more nearly resemble a one-phase crystalline aggregate with numerous defects and regions of disorder, such as lamellae borders, in which diffusion and sorption take place.

Of interest is also the marked change in permeation properties at the glass transition temperature. Meares (62, 63) and Vieth (111) observed a marked change in permeation properties at T_g in the case of poly(vinyl acetate) and poly(ethylene terephthalate). Diffusion and solubility constants below T_g are both higher than what one would predict on the basis of a linear extrapolation from above T_g. These observations led to the postulation of the existence of micro-voids as a stable phase,

in which sorption takes place by a Langmuir-type of sorption process. Sorption in the glassy polymer consists, consequently, of ordinary dissolution plus "hole-filling", the latter becoming noticeable whenever the polymer contains sufficient frozen-in free volume and the dispersion interactions between the gas and the polymer are pronounced.

C. Experimental Procedure

1. Materials

The isotactic poly(propylene) was type 651A Profax supplied by Hercules, Inc., Wilmington, Delaware in the form of molding pellets or unoriented, cast film. It had an average molecular weight of 320,000 and an isotactic content of 95%.

The atactic poly(propylene) is manufactured by the Avisun Corporation under the trade name Oletac 100. The material used in this study had a molecular weight of 16,000, a density of 0.858 and was completely soluble in hexane.

The gases most frequently used were He, A and CF_4. They were chosen for their inertness, molecular symmetry and variation in size. For greater polymer-gas interaction, CO_2 and CH_4 were used in some studies. For all gases, the minimum purity was 99%. No further purification was attempted, except for passing the gases through a bed of $CaSO_4$ to remove any last traces of water vapor.

2. Film Preparation

Except for the high pressure sorption studies, all films were molded in a laboratory platen press under heat (~204°C) and pressure (~300 psi) into films of the desired thickness (6 to 40 mils). The cast film was fabricated by the supplier by extruding polymer at 500°F onto a chill roll maintained at 85°F.

The tacky, atactic material was melted, cast into flat discs and cut into cubes.

Variations in the thermal history of the films were produced by cooling the films at three different rates from the melt. The resulting films were referred to as "slowly" cooled (S), "moderately" cooled (M) and "rapidly" cooled (R). Additional films were subsequently annealed. For the "MA" series, the annealing temperatures were 80°C, 100°C, 110°C, 130°C, 140°C and 150°C. All other films were annealed at 150°C only. The annealing time was in all cases 60 minutes.

3. Experimental Techniques

(a) Time-lag.

Most of the diffusion and permeation data generated in this study were obtained via the classic time-lag technique developed by Barrer (9). The experiment consists of evacuating the membrane, applying a constant pressure to one side, and recording the pressure rise in the previously evacuated downstream reservoir as a function of time. From the transient portion of

the experiment, D can be calculated by the relationship,

$$D = \frac{\ell^2}{6\theta} \quad \frac{cm^2}{sec} \tag{11}$$

while $\bar{P}$ is evaluated from the rate of pressure increase in the downstream volume during the steady-state period. The constant k is determined indirectly from equation (5).

Gas pressures between 150 and 600 mm Hg were used at the upstream side of the membrane while pressures in the downstream reservoir seldom rose over 150 microns. The temperature dependence of the transport coefficients was determined by making runs over a 30-40°C range.

One of the major innovations in the classical time-lag system was the use of a capacitance-type pressure transducer to measure the downstream pressure. It provided unequalled accuracy ($\pm$0.001 microns) and ease of operation. Another new feature was the use of quick-connect, O-ring seals to attach the metal diffusion cell to the glass vacuum system.

For the time-lag experiments, the precision of $\bar{P}$, D and k at the 95% confidence limits for a representative run was $\pm$5.2%, $\pm$9.6% and $\pm$11%, respectively. The major contribution to error arose from variations in sample thickness.

(b) Low pressure sorption.

To obtain permeation data for atactic poly(propylene) and to check on k's obtained indirectly from the time-lag technique, low pressure sorption and desorption experiments were performed. Briefly, the method consists of equilibrating an initially evacuated sample of polymer, in strip or pellet form, with the desired gas at pressures up to one atmosphere. By recording the initial and final equilibration pressures, a simple material balance yields the solubility constant. In the case of the desorption experiments, the equilibration is followed by a quick evacuation (ca. 15 secs), after which the system is again closed off and the desorption process is allowed to come to equilibrium. Pressure was monitored continuously via the pressure transducer. Diffusion constants were calculated from an analysis of the data using appropriate solutions of Fick's second law (25).

The estimated precision at the 95% confidence limits was $\pm$1.5% for k and $\pm$8.4% and $\pm$8.2% for D from sorption and desorption experiments, respectively.

(c) High pressure sorption.

The high pressure sorption experiments were designed to measure solubility constants of argon and carbon dioxide in unoriented, cast film over a pressure range of 30 atmospheres and temperatures ranging from -40°C to +40°C. An error analysis places the precision limits of this method at $\pm$8.2%.

(d) Polymer characterization.

The density of all films was determined using isopropyl alcohol-water density gradient columns. Generally, densities were determined in triplicate and agreed to ± 0.0003 gm/cc.

The amorphous volume fraction, α, of any sample was then calculated from the relationship

$$\alpha = \frac{\rho_c - \rho}{\rho_c - \rho_a} \qquad (12)$$

where $\rho_c = 0.9360$ gm/cc and $\rho_a = 0.8580$ gm/cc.

Microtomed sections of the film samples were viewed under crossed polarizers at a magnification of 400X (Wild M-20 optical microscope). For finer details of the structure, samples were examined under the Philips EM-200 electron microscope. Samples were in the form of microtomed sections, replicated fracture surfaces, or thin films of leached polymer.

X-ray diffraction was used to determine percent crystallinity, crystallite orientation and mean crystallite size.

Calorimetric measurements were made to establish glass transition temperatures and to check on crystallinities calculated from density determinations.

D. Results and Discussion

Figure 22 presents representative data showing variation of $\bar{P}$ with permeation temperature and thermal history for He, A, and CF_4. The Arrhenius relationship was obeyed for all gases over the range of temperatures (20-70°C) considered. The average activation energies for permeation of He, A and CF_4 are 6.4 ± 0.1, 10.9 ± 0.5 and 17.8 ± 0.5 Kcals/gmole. The activation energies were essentially constant and independent of the level of crystallinity and thermal history.

Two striking observations evolve from a comparison of gas permeabilities in crystalline poly(propylene) (Table VI) with those in natural rubber and atactic poly(propylene). Firstly, in isotactic poly(propylene) permeation rates decrease more than one thousand fold in going from helium to CF_4. This dramatically illustrates the extreme sensitivity of permeation processes to relatively small changes in diameter (2.2 to 4.6Å) of the permeants. Secondly, considering isotactic poly-(propylene) vis-a-vis the atactic form or natural rubber, the effect of crystallinity on permeability is remarkable. Permeability is up to 170 times lower in isotactic poly(propylene) than in its amorphous analog. However, separate analyses of the sorption and diffusion processes are necessary for understanding the morphological factors responsible for these observations.

1. Solubility Constants

Figure 49 summarizes the solubility data of A and He for all the films studied, in relation to their amorphous contents. If crystalline poly(propylene) were indeed a simple two-phase system, one would expect this data to fall on a straight line connecting the origin and the point for 100% amorphous polymer (since the latter is not obtainable, atactic poly(propylene) was chosen as its analog). However, the plot of k vs. α shows that the solubility of all quenched films is significantly lower, and apparently independent of amorphous content. Only for the annealed films does the difference seem to disappear, with solubility approaching the "two-phase" solubility line. The solubility data seems to reflect the presence of the "smectic" or "quenched" crystal modification, whose existence was postulated by many authors on the basis of evidence from x-ray diffraction, IR-absorption, NMR and dynamic mechanical measurements.

In the case of argon, the greatest number of runs were made and the above solubility behavior is best delineated. The solubility is initially constant, apparently independent of amorphous content, and then drops off rather suddenly, reminiscent of a phase change, as the material is annealed at 100°C and above. The inflection point is in agreement with the results of Gailey and Ralston (36), who in extensive DTA studies observed that the "quenched" material underwent complete conversion to monoclinic crystallinity, if annealed

for at least 20 minutes at about 90°C. They concluded that the quenched phase consists most probably of very small hexagonal crystallites whose intrinsic density is 0.907 gm/cm^3. The presence of such hexagonal crystals in the films studied here is supported by the fact that the x-ray diffraction curves of film 2, a "rapidly" cooled sample, showed the two, typical, broad scattering maxima attributed by many authors to hexagonal crystals of very small size.

The following picture evolves from these observations: On quenching of polymer from the melt, a mixture of monoclinic and hexagonal crystallites are produced, the ratio of the two being a function of the rate of quenching from the melt. Based on the point of inflection at $\alpha = 0.41$, the total amount of crystallinity seems to be fixed at approximately 59% by volume. Since both morphological forms are crystalline, it is not unreasonable to assume that both are impermeable to gas, thus accounting for the constant solubility up to the point where films were either "slowly" cooled from the melt or annealed at temperatures greater than 90°C. Beyond this point only one crystal form is present, namely the more stable, monoclinic mode.

The solubility of helium is intrinsicly quite low and only slightly lower in the quenched material. Nevertheless, the helium data at least indicate the same break at $\alpha = 0.41$.

The solubility data for CF_4, the largest molecule studied also deviates considerably from the "two-phase" line and is even slightly low for the annealed films. The later is probably the result of inaccessibility, inasmuch as the large molar volume of CF_4 prevents it from reaching all interlamellar amorphous material.

Thus, the relationship $k = \alpha k^*$, which described the solubility in poly(ethylene) and poly(ethylene terephthalate) so well, is at best only valid for the solution of small gases in well-annealed poly(propylene) films. In such cases, the solubility at any crystallinity could be estimated from a knowledge of α and k^*, where k^* is readily obtained from the successful correlation of $\ell n\ k^*$ vs. $\varepsilon/\bar{k}$.

With the glass transition of crystalline poly(propylene) in the vicinity of zero degrees centigrade, it is conceivable that in some of its applications poly(propylene) will be used in the glassy state. The work of Meares (62) and Vieth (111) has shown that the solubility behavior of the glassy material may be quite different from that of the rubbery material. Not only did they observe an inflection in the plot of $\ell n\ k$ vs. $\frac{1}{T}$, but they also found that the solubility in the glassy polymer was considerably higher than what one would predict on the basis of an extrapolation from the rubbery region. The same was observed for argon solubility in glassy poly(propylene). As before, the additional solubility in the glassy polymer can

be explained by the presence of a Langumir-type of adsorption in "frozen-in" micro-voids. However, the processes of hole-filling and ordinary dissolution could not be separated due to the weakness of the gas-polymer interactions and the experimentally limited pressure range (3-30 atm.).

The variation of k with temperature (Figure 25 is a typical plot above T_g) both above and below T_g, was well described by the van't Hoff expression $k = k_o e^{-(\Delta H_S/RT)}$. Average values of ΔH_S above T_g for He, A and CF_4 were 1.7, -0.6 and 2.2 Kcals/gmole and, except for CF_4, fit well on the plot of ΔH_S versus $\varepsilon/\bar{k}$ for poly(ethylene), evincing the identity of solubility parameters for the two polymers, as also found by Alcalay (1). As with SF_6 in poly(ethylene) (15) the deviation of CF_4 is readily explained by its high partial molar volume and relatively low $\varepsilon/\bar{k}$. Finally, entropies of sorption were correlated well with solute mole fractions using the Jolley-Hildebrand correlation (52).

For argon, ΔH_S is significantly more exothermic in the glassy polymer (-3.0 vs. -0.6 Kcal/gmole) which is further evidence for the existence of the hole-filling process. Although separation of the modes of sorption was not possible directly from the isotherms, an analysis of all the existing data for glassy poly(propylene), poly(ethylene terephthalate) (111) and poly(styrene) (112) made it possible to estimate not only the micro-void saturation limit for poly(propylene) but also the size of the micro-voids and the enthalpy of adsorption,

using a statistical mechanical formulation for the latter. Based on this analysis, the micro-voids appear to be 32Å in radius and ΔH_{ads} = -1.6 Kcals/gmole for CO_2. The former value is in good agreement with estimates from light scattering work and, the latter, with the measured value of ΔH_S for CO_2 (-2.6 Kcals/gmole).

2. Diffusion Constants

All the diffusion data could be represented by a plot such as shown in Figure 34. Without exception, the data were well correlated by the relationship, $D = D_o e^{-(E_D/RT)}$ with average values of E_D = 4.7, 11.5 and 15.7 Kcals/gmole for He, A and CF_4, respectively. In addition, agreement between time-lag and static sorption diffusion constants supports the assumption in equation (1) of isotropic diffusion.

Figure 56 represents a typical plot of diffusivity as a function of the percent amorphous volume. If the crystalline polymer were, indeed, a two-phase system of impenetrable crystallites suspended in an amorphous matrix, one would expect the diffusivity to decrease monotonically as the percent amorphous volume decreases. However, instead of observing that, the curve of diffusivity versus α appears to pass through a minimum. Initially, diffusivity decreases rapidly but then, as the films are annealed above 90°C, the diffusivity curve flattens and eventually turns upward again.

This behavior can be explained on the basis of a defect model, the qualitative features of which are summarized in Figure 58. From the solution behavior, it was concluded that the apparent change in amorphous content from 60 to 41% is not the result of additional crystallization but rather the consequence of a transformation of the smectic to the monoclinic crystal habit. The transformation is accompanied by an association of many very small hexagonal crystals into larger but fewer monoclinic crystals. This tends to make the diffusional path more tortuous and explains the decrease in diffusivity without additional crystal growth.

On annealing, two more effects come into play: namely, additional crystallization and thickening of existing crystals without new growth. The additional crystallization reduces the volume available for flow, making existing crystals more anisometric and generally decreasing diffusivity. Thickening, on the other hand, is pictured as a process whereby chains increase their fold-period by self-diffusion of molecules along their own backbones. To proceed, the process pulls chain ends into the crystal surface and, in some cases, right through the lamella, introducing vacant rows into the crystal lattice. These defects open new passages for the diffusing molecule, and thus, reduce geometric impedance and enhance diffusion. To a lesser degree, diffusion is further eased by the reduction in the number of interlamellar links which accompanies lamellar thickening.

The conclusion that crystalline defects rather than changes in the amorphous phase are responsible for the observed diffusional enhancement was reached on the basis of the following analysis. A change in the properties of the amorphous phase, on annealing, should be reflected by a change in the values of E_D and ΔH_S, a change which should be greatest for the largest molecule, CF_4. Neither was observed - the values of E_D and ΔH_S did not change on annealing and CF_4 showed the smallest diffusional enhancement. Thus, the increase in diffusivity in spite of the increased crystallinity must be due to a decrease in the tortuosity of the diffusional path. This, in turn, could occur either by the crystals becoming more isometric or by the formation of crystalline defects large enough to allow passage of the diffusing molecule. The first possibility is unlikely because the crystals are chain-folded lamellae with additional growth at the crystal edges preferred over growth at the crystal faces. Furthermore, observations with single-crystal lamellae of poly(ethylene) have shown that lamellar thickening produced no decrease in the lateral dimensions of the lamella. This strongly suggests the formation of crystal defects, i.e., vacant micropores through the lamella.

The mechanism of diffusion in the defects is probably non-activated and analogous to gas diffusing in very small pores, i.e., Knudsen diffusion, where the diffusion coefficient is a factor of several hundred-fold larger than those measured in this work. However, in annealed films activation energies equal to those in the unannealed films were observed. This militates against the possibility that there exist interconnected defect pathways through the entire film, but still allows for the

existence of non-interconnected defects passing through individual lamellae. This leads to a picture of diffusion through an amorphous phase containing a suspension of partially permeable crystallites, where the diffusing molecule spends most of its time in the amorphous phase and only occasionally passes through a lamellar defect.

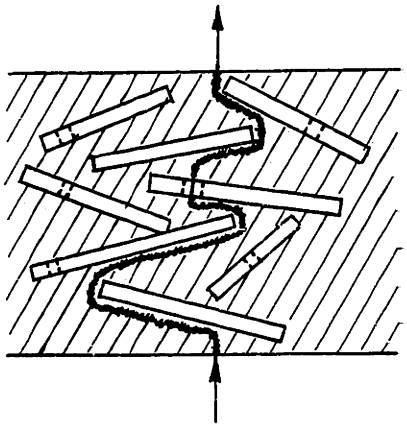

Since diffusion through defects is so much easier than through the amorphous phase, the number of defects necessary to account for the observed diffusion enhancement is governed primarily by the ability of the diffusing molecule to find defects. Unfortunately, it is impossible to establish a realistic two-dimensional model for the size, shape, and orientation of the crystals in an isotropic sample of poly(propylene). Therefore, it is difficult to accurately estimate the volume fraction of defects necessary so that, on the average, a diffusing molecule finds enough defects to reduce its diffusion path length through the membrane by 97%, in the case of helium for example.

However, one can obtain some indication of the volume fraction of defects present from the following analysis. From entropy considerations, one finds that for the gases studied the length of an average diffusion step in the amorphous phase is on the order of 30Å, a value which compares well with the value of 27Å observed by Meares (63) for similar gases in poly(vinyl acetate).

For a molecule to be never more than one diffusion step length away from a defect, it would require 0.6% defects based on total sample volume (Appendix G). This estimate implies defects of uniform size (4.5Å in diameter), homogeneously distributed. This is an admittedly oversimplified picture. Nevertheless, this calculation tends to over-estimate the volume fraction of defects actually present because the crystalline phase does not act like a sieve as is apparent from the observation that τ is still approximately four for the annealed films.

Another estimate of required defect-fraction may be obtained from an application of a series resistance law for transport in an amorphous phase containing a suspension of partially permeable crystallites. The simplest assumption would be that the defective crystallites are homogeneously distributed. This, however, is again an over-simplification, as accepted models of the crystallization process show that it is the older, more highly annealed crystals which will be defective. Consequently, the distribution of defects will be spatially non-randomized, and one again would require only a very small volume fraction of defects to account for the observed diffusional enhancement.

Finally, considering especially the presence of only minor differences (1.9%) between X-ray diffraction and density gradient-method estimates of crystallinity in annealed samples, one is led to the conclusion that a very small fraction of the sample (ca. a few percent) would have to be defective to account for the observed diffusional enhancement.

Experimentally, one finds that the diffusivity of the smallest molecule, helium, is enhanced much more than that of CF_4, the largest molecule studied. If one assumes that the mode of transport in the defects is non-activated and that the diffusional resistance in the defects is thus negligible compared to the resistance in the amorphous regions, it becomes possible to calculate a size distribution for the accessible defects, i.e., all defects large enough to accommodate helium. Based on such an analysis, at the 30% amorphous level, the most common defect size appeared to be 4.2Å in diameter. An examination of the monoclinic crystal lattice for poly(propylene) shows that this value compares well with the size of a vacant lattice site (~4.5Å). This strongly suggests that, indeed, many of the crystalline defects are single, vacant rows in the crystal lattice.

In the light of the morphological picture evolving from the above analysis of the sorption and diffusion data, the parameters τ and β are no longer as definite and easily calculated. Previous investigators have calculated τ on the assumption that $\beta = 1$ for helium. They further assumed that τ for helium remained the same for the other gases. Figure 61 is a plot of τ vs. α for helium. The correlation for the quenched films falls half-way between that for linear and branched poly(ethylene), indicating that crystallite size and shape are comparable to those in poly(ethylene). The curve for the annealed films shows the significant decrease in τ due to the introduction of these lamellar defects.

A plot of β vs. d^2, the square of the molecular diameter, shows that for the quenched films β is a direct function of the cross-sectional area of the diffusing molecule. This suggests that β is much more an index of interlamellar spacings rather than a measure of the restrictions on segmental mobility.

This view is further supported by the finding that the activation energies for diffusion were essentially constant and independent of the film's thermal history. The values of E_D for the isotactic polymer ranged from 4.7 to 11.5 to 15.7 Kcals/gmole for He, A and CF_4, respectively, and correlated well with the diameter of the diffusing molecule. This clearly illustrates the activated nature of the overall diffusion process, even in well-annealed films where non-activated flow in the defects contributes to diffusion. In comparison with natural rubber and poly(ethylene), the curve of E_D vs. d lies higher and shows a more pronounced dependence on d. The explanation for this can probably be found in poly(propylene)'s lower chain mobility, resulting from the bulky methyl side groups and the chain's propensity to coil.

Applying a modification of Eyring's (42) theory of absolute reaction rates to diffusion, one finds that the diffusion step can be evaluated in terms of the length of the diffusion jump and the entropies of activation for diffusion. The average diffusional jump length was 30Å and compared favorably with the value of 27Å quoted by Meares (63) for poly(vinyl acetate). The entropies of activation for diffusion correlate well with

the size of the diffusant when considered separately. As expected, ΔS_P^*, the entropy of activation for the polymer, increases markedly with the size of the diffusing molecule and reflects the disturbance of the polymer matrix by the diffusing molecule. ΔS_G^*, on the other hand, decreases linearly with the size of the diffusant, because larger molecules experience greater restraint on their remaining vibrational modes as they diffuse. As a result, plotting ΔS^* against E_D gives a linear relation as predicted by Barrer (7) for a process in which the activation energy is shared between a number of degrees of freedom in a zone of activation.

3. Polymer Characterization

To relate the effect of thermal history to changes in the micro-structure of the polymer, it becomes imperative to find a convenient way to characterize the polymer. Determination of the crystalline/amorphous ratio from polymer densities was found to be one convenient way to observe changes in the polymer. However, for quenched poly(propylene), the amorphous content calculated on the basis of a two-phase system is deceiving because changes in the amorphous content are probably due solely to the conversion of hexagonal to monoclinic crystals. Therefore x-ray diffraction data were useful in indicating the presence of the two separate crystal phases.

Generally speaking, polymer characterization by the other analytical methods used has on the whole proven difficult,

nevertheless, as mentioned above, it has in some instances, provided valuable supporting evidence for the morphological picture evolving from permeation studies.

E. Conclusions

1. The solubility constants of He, A, and CF_4 in quenched samples of poly(propylene) are all anonamously low, and independent of thermal history as well as level of crystallinity. All quenched films appear to have an overall amorphous content of 41%, independent of the rate of cooling from the melt, with the remainder of the material being a mixture of monoclinic and hexagonal crystallinity. The ratio of the crystal modes is a function of the rate of quenching and changes on annealing in favor of the more stable, monoclinic form. On annealing above 90°C, the conversion to the monoclinic form goes to completion.

2a. The solubility constants of argon and helium in the annealed samples are more normal, varying linearly with the amorphous volume fraction. For CF_4, even the solubility in annealed films is low, suggesting exclusion of the large molecules from some of the interlamellar, amorphous regions.

b. Solubility constants and sorption enthalpies are well correlated with gas molecular force constants, $\varepsilon/\bar{k}$, and entropies of solution correlate well on a Jolley-Hildebrand plot.

3. Below T_g, the solubility of argon is greater than what one would predict from solubility behavior above T_g. The enhanced solubility and large exothermic heat of sorption of argon in glassy poly(propylene) point to the presence of microvoids and sorption by microvoid-filling in addition to ordinary dissolution.

4. The diffusivity of helium, argon and CF_4 is a function of the level of crystallinity and dependent on the films' thermal history. In the quenched-films the diffusion constants decrease up to the point of complete conversion of hexagonal to monoclinic crystallinity. This is attributed to an increase in the geometric diffusional impedance with the consolidation of very small hexagonal crystals into fewer but larger monoclinic crystals.

5. On annealing, diffusivity actually increases with decreasing amorphous volume fraction. This suggests a marked decrease in impedance with increasing crystallinity and the formation of defects in the existing crystallites as the lamellae thicken, in a manner similar to that observed on annealing of poly(ethylene) single crystals.

6. Activation energies for diffusion are higher for poly-(propylene) than for poly(ethylene) or natural rubber and show a strong dependence on penetrant size. This reflects greater rigidity of the poly(propylene) chain and may be evidence for the helical conformation of the amorphous polymer.

7. The fact that the activation energies for diffusion are essentially constant and independent of the level of crystallinity or thermal history suggest that the chain immobilization factor reflects the impedance to diffusion arising from the extremely small dimensions of the inter-lamellar, amorphous channels rather than any restriction on chain mobility.

II. INTRODUCTION

A. Motivation and Objectives

The relative impermeability of polymer films has long made them invaluable in innumerable and diverse packaging applications. This, together with their considerable potential as media for separating gas or liquid mixtures, has stimulated an enthusiastic and sustained scientific interest in polymer films.

The ability of polymeric films to selectively transmit one component in preference to another has made possible separations which would be extremely difficult otherwise. But, whereas selective membranes have always played a vital role in living systems, extensive research was required before comparable synthetic membranes could be developed. Membranes which have a high selectivity for a given ionic species, i.e., either for anion or cation, are now available, making attractive many chemical operations such as the electrodialysis of saline waters and the demineralization of chemically related solutions. Selective membranes make possible separations that are difficult to obtain by distillation or absorption techniques. For example, they allow dehydration of food products at low temperatures, thus preserving the delicate taste and aroma components. Much attention has recently centered on membranes that are permeable to water and serve as barrier to salts for use in water demineralization by reverse osmosis. In medicine, synthetic membranes have become indispensible in prosthetic

devices such as the artificial kidney. Furthermore, it is possible that future discoveries will open the way to the use of membranes in the large-scale recovery of helium from natural gas and other such processes of importance in the process industries.

All these applications have benefited from a better understanding of the permeation process and the factors that influence gas or liquid transport in polymers. Specifically, in the area of semi-crystalline polymers, it has been found that the crystalline microstructure plays an important role in the selectivity and the level of fluid transport. Knowing what this microstructure is and how it can be modified by suitable thermal, mechanical, or solvent treatment has, in turn, made possible the development of materials with permeation properties most advantageous for a given application.

Although electron microscopy and x-ray diffraction provide means for direct observation, the extremely complex microstructure of bulk polymer crystallized from the melt has made detailed morphological studies difficult by these means. On the other hand, the study of polymer morphology by observing how small, inert gas molecules dissolve in - and diffuse through - the polymer has proven very successful (68, 71, 111). Much like the electrons or x-rays in the other methods, the gas molecule diffusing through the film may be thought of as an analytical probe of the microstructure. Yet, gas permeation has the advantage of being less specific than x-ray diffraction, which

can only yield information about the perfectly ordered regions of the polymer.

Isotactic poly(propylene) was chosen as the subject of this study for several reasons. First, poly(propylene) ranks today with poly(ethylene), poly(vinyl chloride) and poly-(styrene) as one of the most important thermoplastic materials, in terms of tonnage and diversity of application. In order to improve upon poly(propylene)'s performance in many of the existing applications, as well as to develop other potential applications, it becomes very necessary to understand what controls the morphology of isotactic poly(propylene) and its attendant gas permeability.

Furthermore, isotactic poly(propylene) belongs to the same family of semicrystalline, olefin polymers as does poly-(ethylene) and, as such, forms the logical continuation of the extensive work done on gas permeation in poly(ethylene). It is of interest to see if the model developed for the permeation process in crystalline poly(ethylene) can be extended to stereo-isomers such as poly(propylene); the ultimate aim being to establish a comprehensive theoretical foundation for understanding the transport properties of crystalline polymers as a class. Finally, the shorter range benefits of such a study are the generation of useful engineering correlations and data to predict the premeability of poly(propylene) generally to permanent, non-polar gases.

Thus, the present investigation was initiated with the following objectives in mind: (1) To use sorption and diffusion studies to establish the presence and nature of poly(propylene)'s crystalline phase(s) and to determine the extent of their interaction with the amorphous phase. (2) To observe the effect of changes in thermal history; i.e., quenching and annealing, on the microstructure, by observation of the resulting changes in the permeation characteristics of the altered film. (3) To arrive at a model for diffusion and sorption in isotactic poly-(propylene) by interpretation of the gas permeation data in conjunction with x-ray diffraction, optical and electron microscopic data. (4) To generate engineering data and correlations which allow one to design membranes of optimum permeation characteristics for a given application.

B. Poly(propylene)

1. Stereoisomerism

Before the discovery of stereospecific polymerization processes, only a relatively limited number of synthetic, semi-crystalline, hydrocarbon polymers were known. Only highly symmetrical monomers such as ethylene and vinylidene monomers or isobutylene were convertible to semi-crystalline polymers. Synthetic polymers of α-olefins, vinyl monomers and diolefines were generally amorphous and stereoirregular.

Concerning the matter of stereoregularity, there are two forms of stereoisomerism, embodied in the cis and trans

configurations (for example, in compounds containing a double bond) and optical stereoisomerism, manifesting the presence of assymetric carbon atoms which are linked to four different substituents. Methods of polymerization leading to the latter types of configuration made possible the crystalline, olefin polymers which are much superior to their amorphous counterparts in tensile strength, elongation, flexural strength, heat distortion, and barrier properties.

To obtain crystalline polymers, the monomer units in a long chain must either maintain identical configurations or alternate their configurations in a systematic way. The crystalline, α-olefin polymers owe their existence to the development of stereospecific polymerization processes, i.e., polymerization using a reduced transition metal catalyst (Ziegler catalysts), which assured the same configuration of each tertiary carbon atom along the chain of the molecule.

The different stereoisomeric, α-olefin polymers are illustrated below:

Isotactic

(all in the same plane)

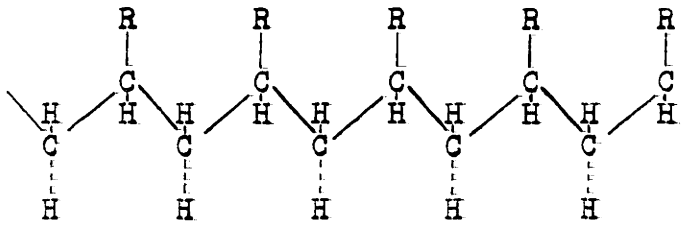

Syndiotactic

(alternating regularly)

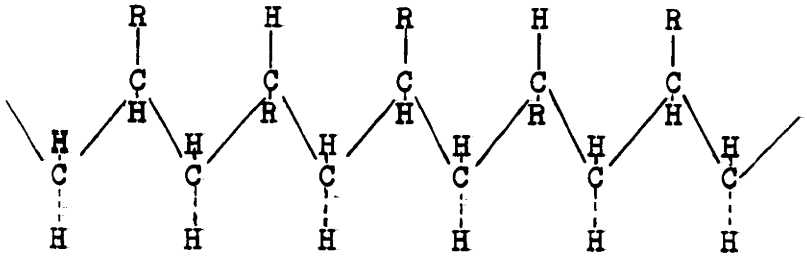

Atactic

(completely random)

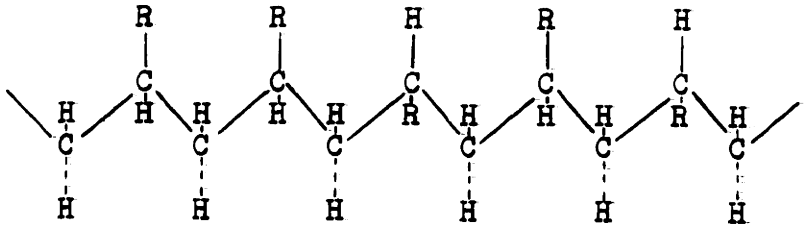

As mentioned above, only the isotactic and syndiotactic polymers are crystallizable and of the two, the isotactic polymers have the most interesting physical and technological properties.

Poly(propylene) can be made in the isotactic, syndiotactic or atactic forms. However, the crystallizability of isotactic poly(propylene) makes it the sole form with properties of commercial interest.

2. Isotactic Poly(propylene)

Isotactic poly(propylene) is a linear polymer of high stereoregularity and with the configuration

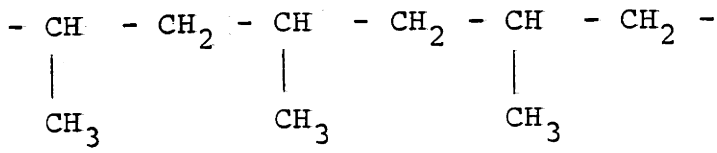

The methyl group substituents on the chain cause steric hinderance which is relieved by the assumption of a helical conformation. Thus each molecule arranges itself into a compact helical chain which, in turn, can pack very closely with neighboring chains during cooling and crystallization. This leads to the high crystallinities observed for isotactic poly-(propylene) in spite of the bulkiness of the methyl side groups.

3. Crystalline Phase

Traditionally, one has attempted to characterize semi-crystalline polymers as a mixture of two phases: amorphous and crystalline. However, it appears that in isotactic poly-(propylene) the added complication of helical chains has given rise to a somewhat controversial crystalline phase. Soon after Natta (83) disclosed that propylene could be polymerized to yield a high molecular weight, semi-crystalline polymer, he studied well-annealed samples of poly(propylene) by x-ray diffraction. He, and several investigators after him (66, 74, 82, 59), observed a monoclinic crystal structure with the polymer chains in a helical conformation. The repeat distance along the axis of the helix was 6.5Å and included three monomers. The axes of the pendant methyl groups are consequently at an angle of 120° with respect to one another in the plane perpendicular to the chain

axis. The angle between adjacent carbon-carbon atoms in the chain backbone is believed to be 114°. Natta (81) has further postulated that the helices of the poly(propylene) molecules are regularly spaced with their axes parallel and with right- and left-handed helices alternating regularly, much as schematically illustrated in Figure 1.

Apparently, arbitrary events during polymerization establish the winding direction of each helix. The helices, in turn, are arranged in the crystallites as pairs with enantiomorphous helices facing one another across a glide plane (see dotted line in Figure 1) along which the molecules are translated by one half of the pitch of the helix. This achieves the closest lateral packing. Obviously, as the ability of the chains to pack closely depends greatly on steric regularity, the degree of crystallinity of the solid polymer is closely related to its isotactic content (89). In other words the maximum crystallinity of a sample of isotactic poly(propylene) is set by the isotactic content of the sample. However, it is only rarely that all of the available isotactic material crystallizes. The extent of crystallization depends further upon the molecular weight distribution and the potential mobility of smaller molecular segments, as well as the time the material spends under crystallizing conditions -- assisted thermally or by a liquid swelling agent.

When isotactic poly(propylene) is rapidly cooled or quenched from the melt, a second "crystalline" form is observed. Natta (84) referred to this modification as the smectic state and

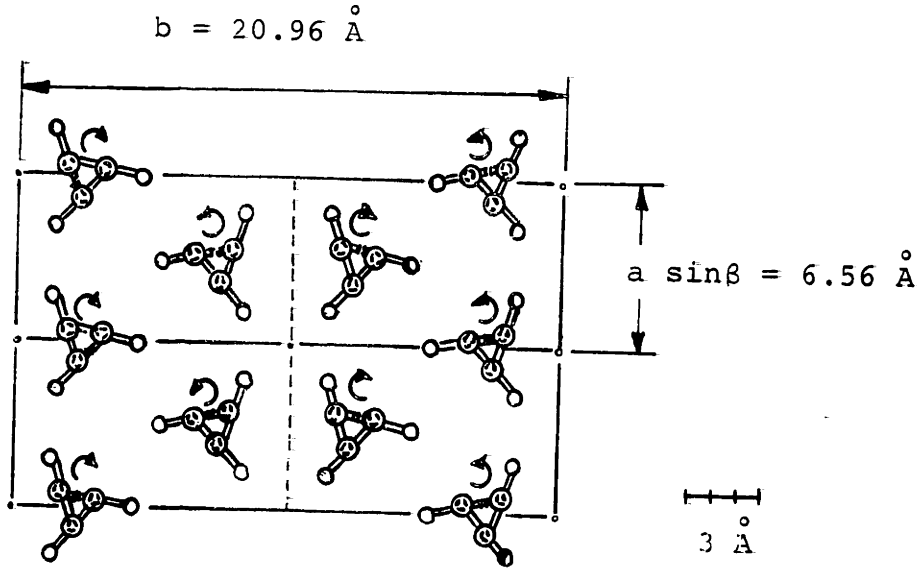

Figure 1 Packing of Helices in Monoclinic Crystallites of Isotactic Poly (propylene) (Left- and right-handed helices alternating regularly.) (79)

suggested that in this material the helices are arranged in parallel as in the monoclinic material except that right- and left-hand helices occur at random (see Figure 2).

Although numerous other investigators (53, 73, 97) have found evidence for this second "crystalline" form and have studied it, there is still considerable question as to what its structure is. Miller (73) studied the quenched material extensively by means of x-ray scattering, IR-absorption and NMR but could only conclude that in this state the poly(propylene) was in a form intermediate between that of the amorphous and that of the crystalline (monoclinic) isotactic poly(propylene). He suggests that the order existing in the quenched material may be that described by Hosemann (49) as "paracrystalline". Keith and co-workers (53) have observed a hexagonal structure in a somewhat rare type of poly(propylene) spherulite. The hexagonal crystal gave an x-ray diffraction pattern consisting of two strong lines which lie close to the midpoints of the two broad scattering maxima of the quenched form. It has consequently been assumed (50) that the quenched state may consist of very small crystallites of the hexagonal form. Geil (39) in his study of single crystals with electron diffraction has also detected a poly(propylene) form of hexagonal symmetry.

In the latest review of the quenched state of poly-(propylene) Gailey and Ralston (36) provide additional evidence for the existence of the hexagonal crystal form. They found a

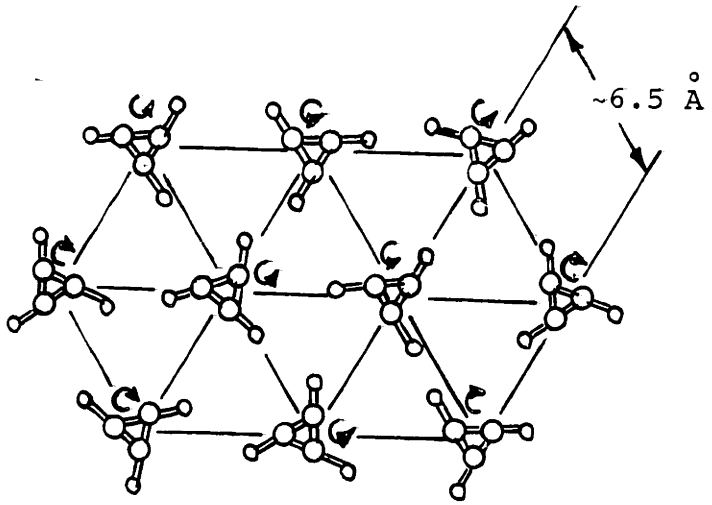

Figure 2 Packing of Helices in the Smectic (Quenched) State of Poly(propylene) (79)

relationship between density and IR-absorption which led to a calculated, apparent density of 0.907 gm/cc for the ordered phase in the quenched material. This they suggest is in good agreement with the density value for the hexagonal crystal calculated from its unit cell. Furthermore, they observed a rather sharp change in crystallization behavior near 115°C and a large energy of activation of conversion to the monoclinic form. They argue that if the quenched material were indeed in a "paracrystalline" state one would expect neither of these observations, since the paracrystalline state should be able to settle into a regular crystalline state by the motion of one or two monomer units at a time.

Since in any quenched sample of poly(propylene) a substantial fraction is in this intermediate state of order it is vital that consideration be given to this form in discussing the structure and morphology of poly(propylene).

4. Lamellar Structure

The earliest model proposed to explain the crystalline properties observed in many polymers was the "fringed-micelle" concept. The solid polymer was pictured as a tangled mass of molecular chains each of which passed randomly through a number of small crystallites and intervening amorphous areas. This concept successfully accounted for a large number of the early observations such as the good mechanical properties of crystalline polymers.

However, over the years, an increasing amount of experimental evidence accumulated which could not be convincingly explained by the fringed micelle theory. For example, in 1947, Bunn and coworkers studied poly(ethylene) (18) and nylon (19) spherulites and showed that they contained molecular chains arranged in a regular manner and tangentially to the radial growth elements of the spherulite. Then in 1957, Keller (54) and others (104, 35) reported the growth, from dilute solution, of single crystals of linear poly(ethylene). Subsequent electron diffraction showed that in these single crystal platelets the molecular chains were oriented in a direction normal to the flat surface of the crystal. This fact together with the observation that these platelets were only about 100Å thick, while the extended length of an average molecular chain is many 1000Å's, led Keller (54) to the logical conclusion that the chains must be folded with the fold period corresponding to the thickness of the platelet.

Since then, solution growth of single crystals has been reported for many other polymers (12). Their appearance is generally the same, being composed of thin platelets or lamellae about 100Å thick and usually many microns in lateral dimensions. In each case electron diffraction showed the chains oriented perpendicular to the flat surface of the crystal, further discrediting the fringed micelle model while strengthening the newly evolving lamellar theory.

Although the most conclusive evidence for a chain-folded, lamellar structure has initially come from the study of single crystals grown from solution, it is now widely believed (40) that bulk samples of crystalline polymers also consist largely of lamellar structures. Electron microscopic examination of surfaces of spherulitic films (39), fracture surfaces (20, 34, 3, 38), and samples of bulk polymer dispersed by means of a nitric-acid digestive treatment (87) provides strong evidence that lamellae exist throughout melt-crystallized specimens of most crystalline polymers, including poly(propylene) (39, 86).

Furthermore, several investigators (39, 60, 102) have studied thin films crystallized from the melt by electron diffraction and have presented convincing evidence that here too the molecular chains are oriented perpendicularly within the thickness of the lamellae. Since the thickness, as seen from the micrographs, was again only about 100Å and thus considerably less than the extended chain length, the polymer molecules must be folded within these lamellae.

The regularity of the folds within the lamellae appears to be open to some speculation. Geil (40) suggests that there are at present at least three models (see Figure 3) of the way the molecules are arranged in the lamellae: (1) Adjacent re-entry with sharp, regular folds and a uniform fold period similar to those postulated for solution-grown single crystals. (2) Adjacent re-entry with an irregular fold period and (3) Random re-entry or "switchboard" model in which the molecules meander through an

Smooth Chain-Folded Surface
(Sharp Phase Boundary)

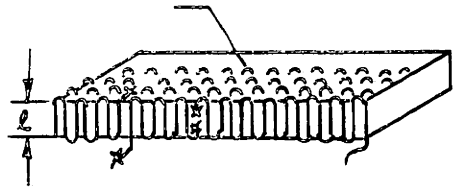

(i) Adjacent re-entry model with regular folds

Rough Chain-Folded Surface

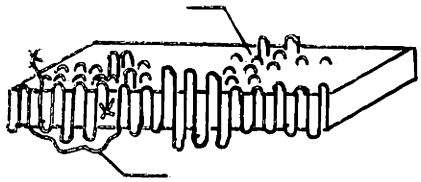

Example of Multiple Nucleation of Molecule on Growth Face

(ii) Adjacent re-entry model with irregular folds

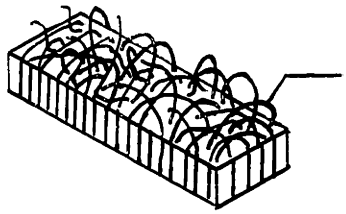

Random Loops (Diffuse Phase Boundary Layer)

(iii) Random re-entry or "Switchboard" model

Figure 3 Three Models for the Lamellar Crystals Observed in Polymers Crystallized from the Melt. Geil (40)

amorphous surface layer on the lamellar before re-entering the lamella. The actual structure is probably a combination of all three models and a function of the thermal history of the sample, with the tendency being to achieve regular folds. The fold period appears to depend on the crystallization temperature, increasing with increasing temperature.

Once the polymer is crystallized the chain-folded lamellae tend to thicken on annealing. Thickening by a factor of two to four is typical and has been observed in poly(ethylene) (41) and poly(chlorotrifluoroethylene) (44). Thickening occurs in both bulk and single crystals (45) and is accompanied by the formation of microholes. At relatively low annealing temperatures, the increase in fold period is thought (40) to occur by self-diffusion of the molecules along their own backbones. At higher temperatures and rapid heating rates, partial melting and recrystallization with a larger fold period probably predominates.

To explain the microhole formation process (the "swiss-cheese" effect) accompanying lamella thickening, one must examine the thickening process in chain-folded crystals more closely. Since the lamella retains its lateral dimensions, chain ends must continuously be introduced into the crystal interior to allow the process to proceed (47, 48). As thickening progresses whole rows become vacant and microholes form. The process may be best understood by reference to Figure 4, suggested by Hoffman and coworkers (45). The first step in the thickening process involves

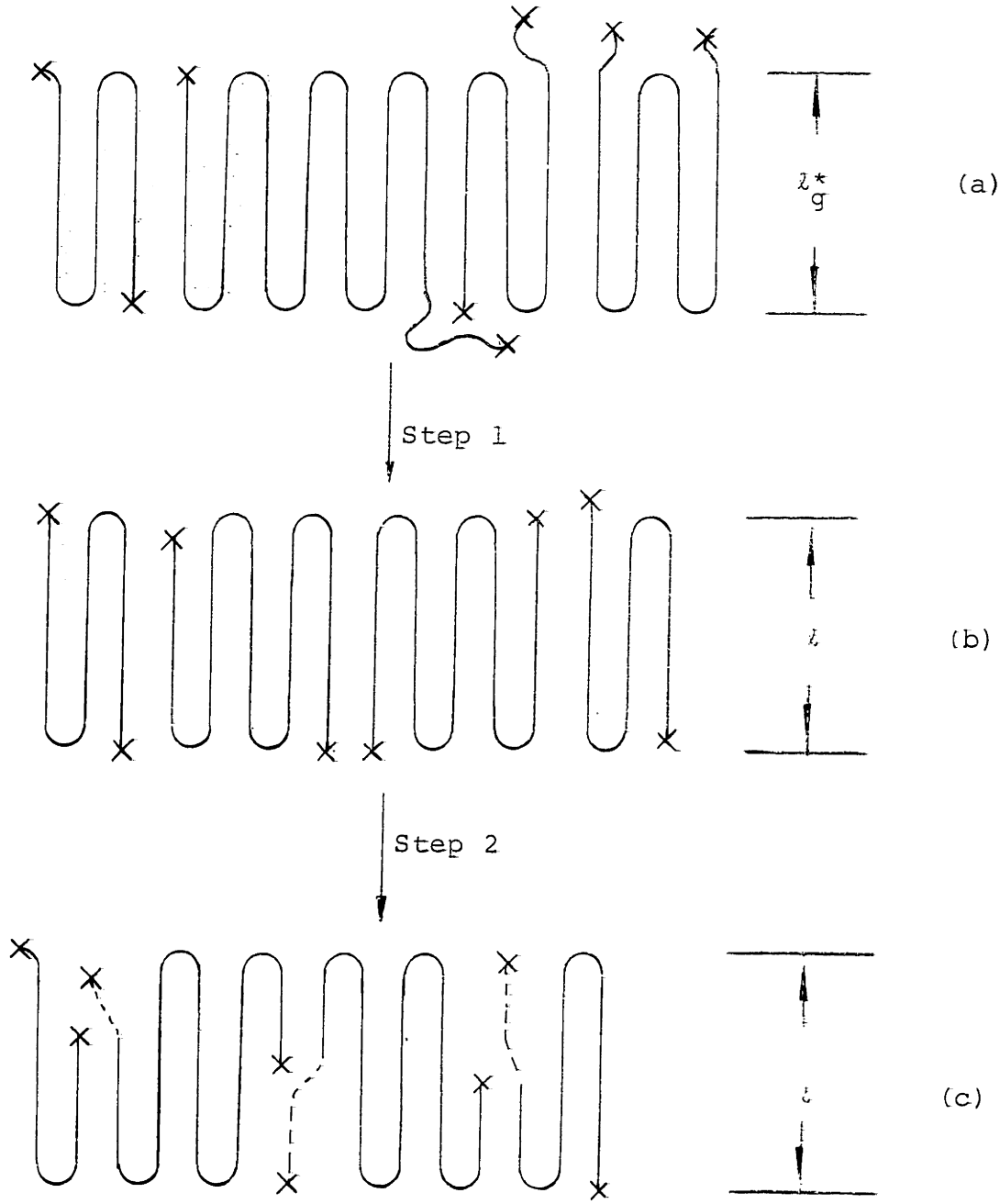

Figure 4 (a, b, c) Schematic Diagram of the Thickening Process of a Chain-Folded Crystal, Indicating a Mechanism for the Injection of Chain Ends Creating a Row of Vacancies into the Lamella; (d) Rate of Thickening. Hoffman, Williams and Passaglia (45)

pulling chain ends into the crystal surface with the formation of some "row-vacancy" defects and occurs at a rate approximated by (45):

$$\ell = \ell_g^* + B_1 \log [(t - t_o/t_o)] \qquad (1)$$

where ℓ_g^* is the initial crystal thickness,

$$B_1 = 2.303 \ kT/(2g\sigma^2/\sigma_e) \qquad (2)$$

$(t - t_o)$ is the age of the crystal, and g is a constant with the value 2.54×10^{-8} cm for the carbon skeleton polymers. As annealing proceeds, step (2) continues the thickening process. This step involves a high rate of "row-vacancy" defect formation and proceeds at a slower rate, approximated by equation (1) with B_1 replaced by:

$$B_2 = 2.303 \ kT/(2g\sigma^2/\sigma_e + E/\ell_o) \qquad (3)$$

where $\ell_o = 1.27 \times 10^{-8}$ cm for the carbon skeleton polymer and E is the energy required to form a row vacancy per -C- unit. While both these steps are known to occur in bulk poly(ethylene) (48), only the second thickening step has been observed in single crystals of poly(ethylene). However, it may be that single crystals are formed initially with the chain ends near the surface.

The experimental observations of the present study greatly support this concept of "row-vacancy" defect formation. It was

found that the diffusivity of small gas molecules is markedly enhanced by the appearance of just such defects on annealing of films crystallized from the melt.

Although the microstructure of poly(propylene) in its monoclinic modification appears to be quite typical in that it is definitely lamellar, there is evidence for a unique, highly branched or woven structure (see Figures 47 and 48). Crystalline regions of this type were observed both in crystallization from solution (97, 55) and in thin films of melt (41). Padden and Keith (85) have recently studied these structures in more detail by an ingenious procedure of growing spherulites in films thin enough - and with textures open enough - to expose the woven structures. They found that the center of spherulites invariably consisted of complex arrays of intercrossing lamellae. The coarse fibers visible in spherulites by optical microscopy are frondlike growths which radiate from the spherulite centers. Each of these fronds is composed of a cluster of ribbonlike leaders, each of which, in turn, is covered with dense arrays of lamellar branches. By electron diffraction they were, furthermore, able to show that all constituent lamellae are chain-folded single crystals.

From fracture studies of solution-grown lamellae of poly(propylene) Morrow and coworkers (77) concluded that chain-folding always occurs parallel to the long direction of the lamellae. They fractured lamellae by ultrasonic vibration and

found that fracture parallel to the a axis of the crystal resulted in clean fracture surfaces with no fibrils protruding, while for fractures roughly at right angles to the a-direction, numerous fibrils were seen to run between cleaved parts of the crystal.

As suggested throughout this discussion, poly(propylene) crystallized from the melt has a prominent structural organization on a scale larger than the lamellae, namely a typical spherulitic structure. When viewed in the polarizing microscope (see Figures 42, 43 and 44), poly(propylene) films show the dark Maltese cross patterns observed in many other polymers. However, in contrast to poly(ethylene), no ring structure is apparent. The spherulites range widely in size, with slow cooling from the melt leading to structures several 100 microns in diameter. Although spherulites may give a qualitative indication of a film's thermal history, it is generally felt that these structures are too large to be "seen" by the diffusing gas molecule. Instead, the gas molecule interacts with the intra- and interlamellar details on its passage through the film. Spherulites are thus of secondary importance in permeation.

The discussion will now move on to a brief summary of the permeation process and the factors that influence it.

C. Permeation Process

1. General

By "permeation" is meant the transport of matter across a membrane along an activity gradient. The process by which gases, vapors or liquids are transmitted varies and depends on the structure of the membrane. For a membrane with gross pores, mass transport occurs primarily by viscous processes when there exists a pressure difference across the pores, and by ordinary or Fickian diffusion in the presence of a concentration difference across the pores. If the diameter of the pore is smaller than the mean free path of the gas molecule, then still another form of diffusion, namely Knudsen flow, controls the process. Knudsen diffusion, in turn, may be enhanced by diffusion of the material in an adsorbed surface layer. This type of diffusion is referred to as surface-diffusion and combines characteristics of both adsorption and ordinary diffusion. Finally, one may consider the limiting case where the molecular and pore dimensions closely approach one another. The transport mechanism is not well understood in this case but is often assumed to be of a non-activated type in the absence of strong sorbate-sorbent interactions.

However, it is possible to fabricate membranes from polymers without pores (including micro-cracks or pin-holes). The fluid transport in such membranes is though to be of the activated diffusion type; that is, a process in which the gas dissolves in the film at one surface, then diffuses through the film under a

concentration gradient and finally desorbs or evaporates from the surface at the lower concentration. The total permeation process consists then of absorption, Fickian diffusion and desorption and is, consequently, best studied by considering sorption and diffusion separately. Since this investigation deals solely with gas permeation, interest will henceforth be only focused on the transport of gases in polymer membranes.

With a constant concentration difference across the membrane (see Figure 5) the steady-state, uni-directional flux of gas can be described by Fick's first law of diffusion

$$J = -D \frac{\partial c}{\partial x} \qquad (4)$$

where J is the flux and $\partial c/\partial x$ the concentration gradient.

The diffusion constant, D, is generally a function of concentration. However, for permanent gases (i.e., gases which at room temperature are well above their critical temperature) the sorption of gas in polymeric membranes is so low that gas-gas interactions are negligible and D is independent of concentration.

Thus with $D \neq f(c)$ (5)

$$J = D \left(\frac{c_1 - c_2}{\ell}\right) \qquad (6)$$

where c_1 and c_2 are the concentrations at the upstream and downstream surface of the membrane, respectively, and ℓ is the thickness of the membrane.

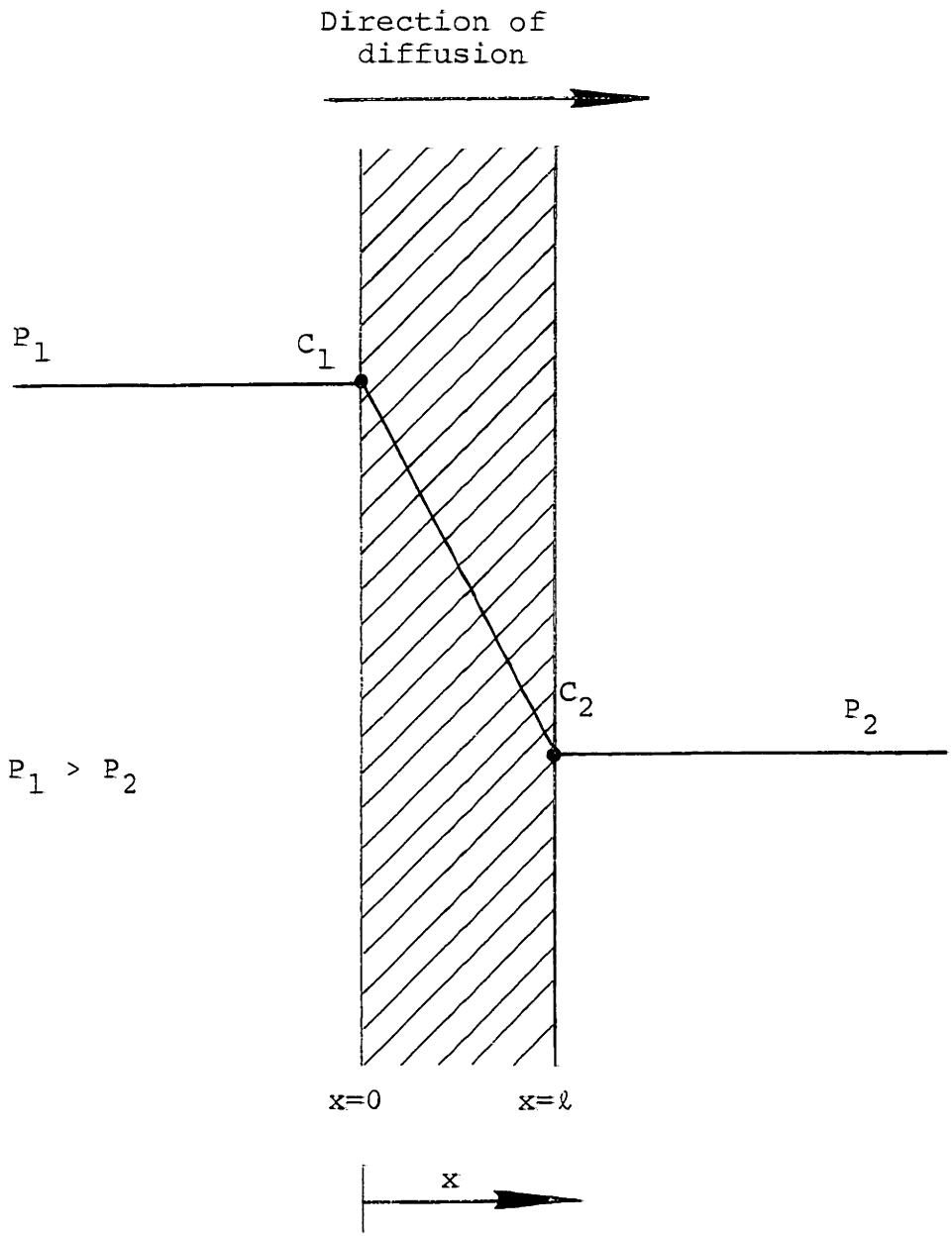

Figure 5 Gaseous Diffusion Across a Polymer Membrane

Accumulated evidence (64, 67, 70) has shown that sorption of gases in polymers is often well-described by Henry's Law, so that the concentration of the gas, c, at either surface of the membrane can be related to its partial pressure:

$$c = kP \tag{7}$$

Thus,

$$J = Dk \frac{(P_1 - P_2)}{\ell} \tag{8}$$

where k is the Henry's Law solubility constant, and P_1 and P_2 refer to the pressures at the film surfaces.

By definition, the product of D and k is usually defined by $\bar{P}$, the permeability constant,

$$\bar{P} \equiv kD \tag{9}$$

and

$$\bar{P} = \frac{J\ell}{(P_1-P_2)} = \frac{\Delta Q}{\Delta t} \frac{\ell}{A(P_1-P_2)} \tag{10}$$

where ΔQ is the amount of gas transmitted in the given interval of time, Δt, and A is the area of the membrane exposed to the diffusing gas. Throughout this study, $\bar{P}$ is expressed in units of cc(STP)/cmxsecxatm, D in cm^2/sec and k in cc(STP)/cc of polymer x atm.

Equation (8) is rigorously correct only when the following conditions exist:

(1) Diffusion must be truly one-dimensional, i.e., there exists a concentration gradient along the x-axis only. This is

generally true for unoriented polymer membranes since their thickness is usually very small in comparison to their large surface area.

(2) Equilibrium is established between the gas phase and the polymer surface, i.e., the attainment of sorption equilibrium is much faster than the rate of diffusion. Most investigators have accepted this to be the case, and Bixler (15) shows with a calculation based on the kinetic theory of gases that this assumption is definitely reasonable.

(3) Diffusion has reached steady state.

(4) Henry's Law is applicable, i.e., the solubility coefficient is not a function of concentration.

2. Effect of Temperature

The dependence of the three constants on temperature is of the Arrhenius type for rubbery materials. Strictly speaking, the activation energies should be slightly temperature-dependent; however, over small temperature ranges the following equations are very good approximations:

$$\bar{P} = P_o e^{-E_{\bar{P}}/RT} \qquad (11)$$

$$D = D_o e^{-E_D/RT} \qquad (12)$$

$$k = k_o e^{-\Delta H_S/RT} \qquad (13)$$

where E_P is the activation energy of permeation, E_D is the activation energy of diffusion, and ΔH_S is the enthalpy of sorption. Since the diffusion through a non-porous membrane is an activated process, E_D is always a positive quantity. Therefore, diffusion is enhanced by higher temperatures.

According to Gee (37) the sorption process may be considered to consist of two separate thermodynamic processes: (1) condensation of the gas, an exothermic process, and (2) mixing of the condensed gas with the polymer, an endothermic process. In other words, the heat of sorption is equal to the sum of the heat of condensation, ΔH_c, and the partial molar heat of mixing, $\overline{\Delta H}_m$:

$$\Delta H_S = \Delta H_c + \overline{\Delta H}_m \qquad (14)$$

For permanent gases, the heat of condensation is always small so that ΔH_S is essentially composed of $\overline{\Delta H}_m$, which is small and positive in the absence of solute-polymer interactions. Thus, for permanent gases, the permeation flux, too, increases with temperature.

On the other hand, for more readily condensible gases and vapors the contribution of the heat of condensation may become significant and the level of sorption may decrease with increasing temperature. Furthermore, these Arrhenius-type relationships may break down altogether in the presence of plasticizing penetrants or in the region of the glass transition. The former was

observed during water permeation in nylon and poly(vinyl alcohol) (100), while both Vieth (111) and Meares (62) observed a change in the slope of the diffusivity versus 1/T in the glass transition region for poly(ethylene terephthalate) and poly(vinyl acetate), respectively.

3. Effect of Penetrant

Several theories have been advanced to explain the mechanism of activated diffusion. Eyring (42) in his "transition state theory" focuses solely on the diffusing molecule and suggests that the diffusing molecule must pass through an activated state of sufficient energy to creat a "hole" into which the molecule can move. Applying the theory of rate processes he relates D to the entropy and energy of activation for a diffusion jump, through the equation:

$$D = \frac{e\lambda^2\bar{k}T}{h} e^{\frac{\Delta S^*}{R}} e^{-\frac{E_D}{RT}} \qquad (15)$$

where λ is the length of a successful diffusion step, $\bar{k}$ the Boltzmann and h the Planck constant. The main objection to this model stems from the observation that the values of ΔS^* calculated from equation (15) are very large, in fact so large that the activation process would have to involve the breaking of primariy bonds (5).

Barrer's zone theory of diffusion (6), on the other hand, proposes that the energy of activation is shared between the

diffusing molecule and the surrounding polymer segments. Thus the entropy is no longer concentrated in a single translational degree of freedom and the high entropies of activation encountered in the transition state theory are reduced to reasonable values.

Brandt (16) has attempted to take the zone theory one step further by picturing an average diffusion jump as the movement of the gas molecule down a cylindrical void created by the separation of four, roughly parallel chains. The activation energy for diffusion would thus consist of two separate contributions, one being the result of inter-molecular or cohesive forces, E_a, between adjacent chains, and one resulting from intra-molecular forces, E_b, such as chain stiffness. Brandt went on to show that E_a is proportional to the first power of the permeant's molecular diameter, d, whereas E_b is proportional to d^2.

Although none of these models are entirely successful in quantitatively predicting values of E_D, they do point out that the diffusion constant is related to the "looseness" of the polymer structure and the "ease" of chain separation to accommodate the diffusing gas molecule. This, in turn, implies that the diffusivity should vary considerably with the size of the diffusing molecule. Indeed, one finds that the rate of diffusion decreases as the molecular diameter of the permeant increases. Moreover, the shape of the molecule is also

important. This was pointed out by the findings of Binning et al. (14) in their study of three hexane isomers. The flux of n-hexane was considerably greater than that of either iso- or neo-hexane.

The chemical nature of the permeant is important to permeation insofar as it affects the solubility of the gas. Generally speaking, the solubility of a gas in a polymer depends on their mutual compatibility, and the principle of "like dissolves like" is followed (98). Polar gases, for example, are more soluble in polar liquids or polymers with polar groups. Differences in solubility of various gases in the same polymer arise from variations in their tendencies to condense. This explains why vapors are more soluble than gases and why Jolley and Hildebrand (52) were successful in their correlation of solubility with the force constants of the gases, $\varepsilon/\bar{k}$, as defined by the Lennard-Jones potential field equation.

4. Effect of Polymer Microstructure

The above discussion is directly applicable to gas transport in completely amorphous polymers. However, the presence of crystallinity in many polymer membranes complicates this picture considerably. Just as crystallinity greatly improves strength, heat resistance and other desirable mechanical properties, so it also has a marked effect on the transport properties of the polymer - the most pronounced effect being a reduction in permeability. This observation led to the postulation of the

"two-phase" model of well-ordered, crystalline regions dispersed in a less rigid, amorphous matrix. The crystalline regions are imagined to dissolve no gas and to be quite impermeable, so that all the transport takes place in the amorphous phase. The latter is thought to have the same specific permeability irrespective of the extent of crystallization. This model further suggests that increasing crystallinity decreases permeability by the combined effect of reducing the volume of amorphous material available to carry the flux and impeding the flow by forcing the diffusing molecule to by-pass impenetrable crystallites.

The relationships that evolve from this model are

$$k = \alpha k^* \qquad (16)$$

which states that the solubility in a partially crystalline polymer, k, is directly proportional to the amorphouse volume fraction with the proportionality constant, k*, being the solubility in completely amorphous polymer, and

$$D = \frac{D^*}{\tau} \qquad (17)$$

which says that D, the diffusivity in the partially crystalline polymer, is reduced from what it would be in completely amorphous polymer, D*, by the "geometric impedance factor", τ. The latter is, in turn, a function of the degree of crystallinity as well as the size and shape of the crystallites.

Numerous investigators (57, 58, 68, 70, 80, 111) studied the transport of gases and vapors in crystalline polymers,

especially poly(ethylene). Although the majority of the data could be explained in terms of the two-phase model, it soon became evident, particularly in the case of highly crystalline polymers (68), that the effect of crystallinity on diffusion was not only impedance by obstruction but also impedance by restricting polymer chain mobility in the amorphous phase. This led to the introduction (68) of the term β, called the "chain immobilization factor", in equation (17):

$$D = \frac{D^*}{\tau\beta} \qquad (18)$$

However, in time, new experimental evidence appeared which indicated that even this "modified, two-phase model" must be an over-simplification of the actual situation. Jeschke and Stuart (51) studied the diffusion of gases in poly(ethylene terephthalate) and poly(propylene) and observed that for a given level of crystallinity the decrease in solubility and diffusivity is a function of the temperature as well as the type of gas. Others (17, 70), too, have found that β depends strongly on the molecular diameter of the diffusing gas. This is contrary to what one would expect if one were dealing with a truly two-phase system where the solubility and diffusivity should be functions of the distribution and volume fraction of amorphous material only, at least at low levels of crystallinity. This, they conclude, is convincing evidence that the two-phase model which completely disregards any physical change of the amorphous phase with increasing crystallinity is inadequate.

Another observation that is difficult to justify even on the basis of the modified two-phase concept is the small decrease, rather than the anticipated increase, in the activation energy of diffusion and permeation with increasing crystallization. This decrease in activation energy was observed both in poly(ehtylene terephthalate) (51) and poly(ethylene) (68).

In a more recent gas permeation study, Fein (33) showed that the crystalline phase in poly(ethylene) films, cooled from the melt, may be quite imperfect and may in fact contain pockets and channels of amorphous material accessible only to the smallest molecules such as helium. Fein subsequently concluded that, rather than being a measure of chain immobilization, β is a function of the size of the diffusing molecule and the inter-crystallite distances.

All these observations, together with the lamellar picture which presently enjoys wide acceptance (see section B.4 of this chapter), suggest that the two-phase model may indeed be an over-simplification of the actual situation. Indeed, one is led to the conclusion that after crystallization only one "phase" remains, namely an imperfect crystalline aggregate with numerous defects, regions of disorder and lamellae borders in which diffusion and sorption take place. Jeschke and Stuart (51) discuss how this "one-phase" model could account for the variation in the decrease of solubility and diffusion constants for the

different gases as well as provide an explanation for the lowering of the activation energy of diffusion. The former they attribute to the inaccessibility of some amorphous regions to large penetrant molecules and the latter to the decreased length of individual diffusion jumps in the highly confined, amorphous channels.

Thus, in the light of this modern, single phase concept, crystallinity tends to reduce permeability by the combined effects of reduction of volume available for flow, diffusional impedance by the crystallites, and exclusion of some molecules from some amorphous areas.

5. Gas Transport in Poly(propylene)

Observations on gas permeation through poly(propylene) films were made by several investigators (51, 23, 79, 75) in the past. In 1959, Myers, Stannett and Szwarc (79) published the first results on the permeability of poly(propylene). They obtained permeability constants for N_2, O_2, CO_2 and water vapor and found that the permeability values for poly(propylene) lie between those found for the low and high density poly(ethylenes). They attributed the somewhat larger energies of activation for poly(propylene) to the methyl groups which, they suggest, necessitate larger zones of activation for diffusion.

Conner and Schertz (23) were mainly interested in establishing a relationship between poly(propylene) permeability, density and orientation. They obtained only permeability

constants and on the basis of a rather brief analysis concluded that the gas transport in poly(propylene) was well described by the modified two-phase model. However, it is noteworthy to point out that they, too, found that β depended on the diameter of the diffusing molecule and that the larger molecules diffuse less easily through poly(propylene) than through poly(ethylene). Both these observations point to poorly segregated crystalline and amorphous phases, much more in line with the one-phase concept.

The only other study of importance is the work of Jeschke and Stuart (51). As mentioned in the immediately preceding discussion they studied gas permeation in poly(propylene) using helium and hydrogen and strongly advocate abandoning the two-phase model in favor of the one-phase concept to describe the microstructure of crystalline polymers.

D. The Glass Transition Temperature

For every amorphous polymer there exists a narrow temperature region in which it changes from a viscoelastic, rubbery material at temperatures above this region to a hard, relatively brittle one below it. Although no phase transition is involved, one observes a rather abrupt change in the curve of volume versus temperature at the point called the glass transition temperature, T_g. However, since T_g depends on the rate of observation, it is not correct to think of it as a true thermodynamic transition. In the rubbery state, the polymer chain segments enjoy translational and rotational movement, while in

the glassy state their motion is essentially reduced to vibration against the local constraints of van der Waal forces.

In polymers capable of crystallization, one observes that the T_g is considerably higher than in completely amorphous polymer. It appears that the crystalline phase imposes considerable constraint on the rotational freedom of the chains in the amorphous phase. Consequently, the temperature at which rotational mobility can be achieved is higher than in the completely amorphous polymer.

Though there is some uncertainty (10) as to the exact location of the glass transition in poly(propylene), the values most frequently quoted for the T_g of atactic and isotactic poly-(propylene) are -12°C (109, 30) and 0°C (22, 78, 108, 101, 106), respectively. The uncertainty may in part be attributed to the fact that the different analytical methods (e.g., dilatometry, torsion pendulum, nuclear magnetic resonance, specific heat, etc.) used to determine the glass transition temperature all measure slightly different properties and at slightly different rates, and in part to the fact that the transition may shift to higher temperatures as the crystalline content of the polymer increases (10).

Besides the change in mechanical properties which takes place over the transition region, Meares (62, 64) and Vieth (69) observed a marked change in permeation properties of T_g in the case of poly(vinyl acetate) and poly(ethylene terephthalate), respectively. Both found that the diffusion

coefficients below T_g were lower than above but higher than would have been expected from a linear extrapolation of the log D against 1/T graph from above T_g. This behavior is identical to the behavior of specific volume with temperature.

To explain these observations Meares visualizes the unit diffusion step as the creation of a cylindrical void down which the activated molecule jumps. Furthermore, from the smaller activation energies of diffusion in the glassy state he concluded that there the length of the diffusion step is shorter in line with the restriction on segmental rotation.

Perhaps even more striking were the observations made for the solubility behavior above and below T_g. Again Meares and Vieth found much greater solubility than what one would predict on the basis of a linear extrapolation from above T_g. In addition the heats of sorption were large and exothermic. Both came to the conclusion that for these polymers in the glassy region, sorption is a combination of simple dissolution and "hole-filling". In reference to the "hole" theory of liquids they suggested that in the glassy region the polymer contained immobilized "frozen-in" holes or microvoids in which sorption takes place by a Langmuir-type of sorption process. The exothermic heats observed are characteristic of dispersion interactions between the gas molecules and the surrounding polymer. As further evidence for this hypothesis they point to the appearance of the sorption isotherms which seem to tail off at high pressures similar to the Langmuir isotherms.

In marked contrast to the results of Meares and Vieth, Barrer (8) and Stannett (99) observed no glass transition effect in their work on the solution and diffusion of vapors and permanent gases in ethyl cellulose and poly(ethyl methacrylate), respectively. It has consequently been suggested that this hole-filling process below T_g becomes noticeable only if the dispersion interactions between the gas and the polymer are pronounced.

Since the glass transition of poly(propylene) is not far below room temperature, its sorption and diffusion behavior below T_g is of interest and is also an integral part of this study.

III. MATERIALS, APPARATUS AND PROCEDURE

A. Materials

1. Polymer Samples

The isotactic poly(propylene) used in this study was of type 651A Profax (Lot No. 86933) supplied by Hercules, Inc. For this polymer, the manufacturer reported "a reduced specific viscosity" of 2.6, corresponding to a weight-average molecular weight of 320,000 (23), and an isotactic content of 95%, based on customary x-ray and solubility measurements (76). Furthermore, the polymer contained 0.1% oxidation inhibitor.

The polymer was supplied in the form of molding pellets and unoriented, cast film. Except for the high pressure sorption studies, all films were molded by the author from pellets.

The atactic poly(propylene) is manufactured by the Avisun Corporation under the trade name Oletac 100. The specific material used in this study was of low molecular weight, identified as TD-108 and had the following properties:

molecular weight	16,000
density (gm/cc)	0.858
capillary viscosity at 175°C (cp)	1,700
% solubles in boiling hexane	100

2. Gases

The purity and source of the gases used in this investigation are listed below. The gases were passed through

a bed of $CaSO_4$ to remove any last traces of water vapor, but were otherwise used as received.

Table I

Purity and Source of Gases

Gas	Grade	Minimum Purity (%)	Supplier
He	-	99.9	U. S. Navy
A	Welding Grade	99.99	Air Reduction Co.
CF_4	Pharmaceutical	99.8	Du Pont Co.
CO_2	Bone Dry	99.8	The Matheson Co.
CH_4	C. P.	99.0	The Matheson Co.

B. Film Preparation

1. Molding

Almost all isotactic poly(propylene) films were prepared by molding polymer pellets under heat and pressure into films of the desired thickness.

The films were molded in an electrically heated, hydraulic press as shown in Figure 6. To obtain reasonable time lags for helium, argon and CF_4, film thicknesses were controlled at 40 mils, 16 mils and 6 mils, respectively, by using brass shims of the appropriate thicknesses. The complete molding assembly consisted of two 1/4 inch stainless steel plates, two photo-printing plates and a square, brass shim. Figure 7 is a sketch of the assembly.

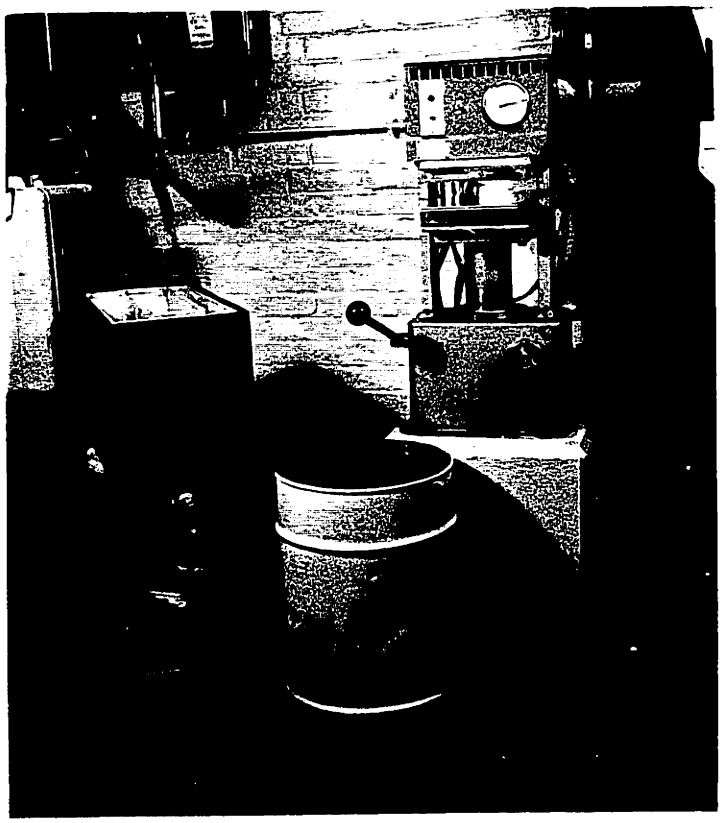

Fig. 6 -- Photograph of Film Molding Equipment

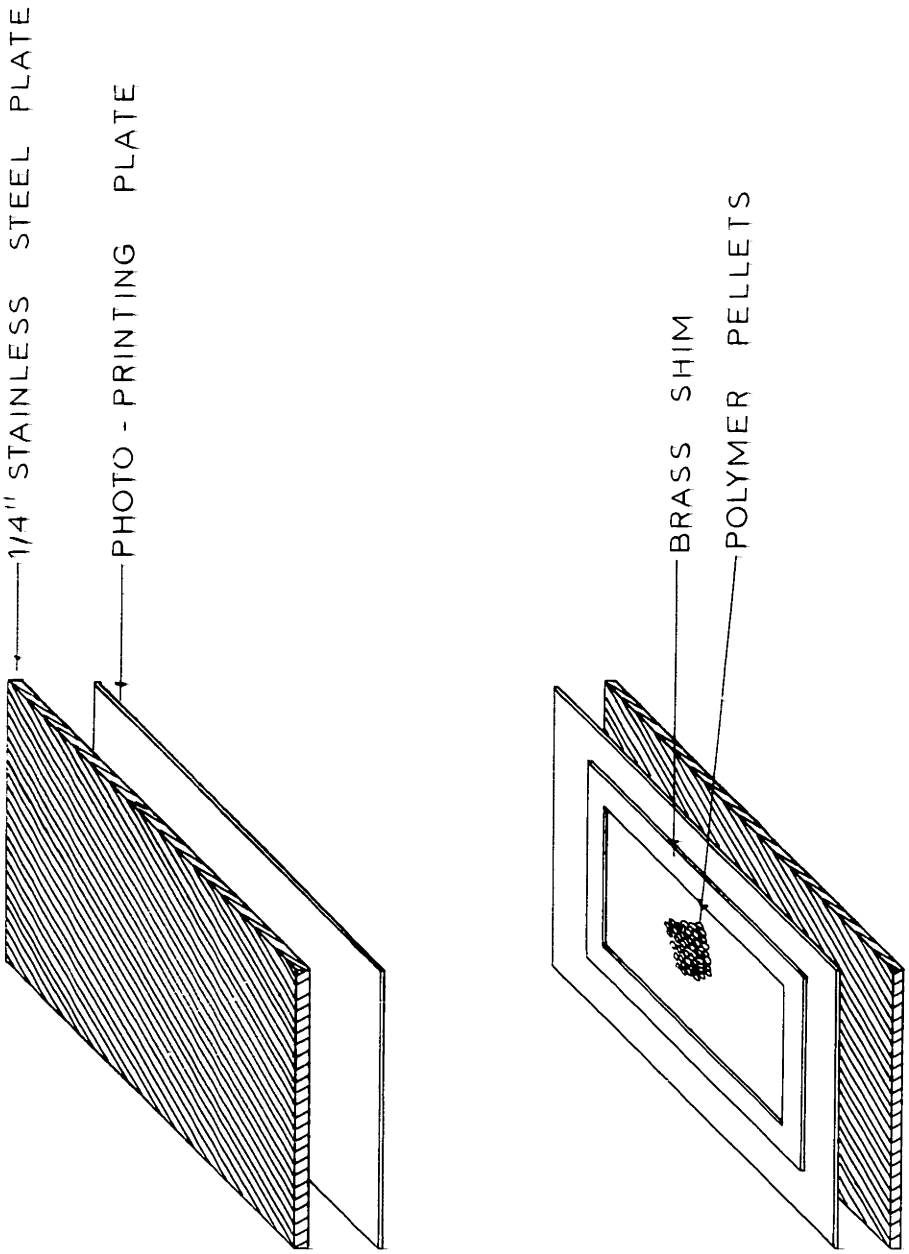

FIGURE 7. FILM MOLDING ASSEMBLY

To mold a film, the approximate weight of polymer pellets (calculated from the intended film thickness) was evenly distributed at the center of the shim resting on one of the photo-printing plates. The plate, shim and polymer were then covered with the other photo-printing plate, and the resulting "sandwich" was carefully inserted between the two outer stainless steel plates, already preheating in the press. Since poly-(propylene) is prone to oxidation at elevated temperatures, preheating of the press and outer plates was thought to minimize exposure to high temperatures.

The platen temperature was set at 400°F (~204°C) and was automatically held to within $\pm$5°F of this preset temperature. After inserting the molding assembly in the press, the press was closed just enough to make good contact between the plates and platens to allow the mold to come to temperature. In the case of the 6 and 16 mil films 5 minutes were allowed for this and 10 minutes in the case of the 40 mil films. By imbedding a thermocouple in the polymer and recording the temperature as a function of time it was found that this was enough time for the polymer to come to the preset temperature. The pressure was then slowly raised to a loading of 20,000 lbs which is equivalent to about 300 psi (based on the area of the shim plus film). The pressure had to be raised in small increments to allow the highly viscous melt to flow smoothly into the cavity provided by the shim. Too rapid pressure application resulted in occlusion of tiny air bubbles. Furthermore, orientation resulting from too

rapid flow of the polymer could be avoided by raising the pressure slowly.

The film used for the high pressure sorption work was manufactured by the supplier by extruding polymer at 500°F onto a chill roll maintained at 85°F.

In the case of the atactic material a slightly different molding procedure had to be adopted because of the inherently tacky nature of the material. The atactic material was heated to about 200°C in a stirred, round bottom flask. At this temperature the viscosity of the material was quite low and it could be poured onto cold glass plates. The material spread in a pancake-like fashion to form remarkably uniform discs which, upon solidification, could be cut up into small cubes and used in the statis sorption system. However, the discs were too thick and too weak structurally to be used in the time-lag system.

2. Quenching

After a total time of either 10 or 15 minutes in the press the next step was cooling of the melt.

For the "slowly" cooled films four "C" clamps were used to hold the stainless steel plates together. The clamps were applied hand-tight while the mold assembly was still under pressure. Then the press was opened and the whole mold assembly plunged into hot water (~90°C).

For the "moderately" and "rapidly" cooled films the press was opened, the upper, outer plate was removed and the inner plates alone were clamped together with four binder clips and then immersed in the cooling bath. It was felt that this would result in more uniform cooling across the whole film sample. It was suspected that at the higher rates of cooling the thick outer plates may produce somewhat slower cooling at the center of the film.

The "moderate" cooling was provided by an ice-water bath while a bath of ethyl-ortho-silicate at -72°C provided the "rapid" cooling. The ethyl-ortho-silicate was used because it is chemically inert (checked by soaking a sample of poly-(propylene) in ethyl-ortho-silicate at room temperature for five days) and has an unusually low viscosity at these low temperatures. This was necessary because it was found that if anything was quenched directly in the acetone-dry ice slurry, vapor locking resulted. Apparently the acetone dissolves large quantities of CO_2 which are liberated on quenching. This was also observed by Fein (33) who observed that the cooling rates in dry ice-acetone were lower than those in ice-water.

The cooling systems are listed in Table II and were used throughout this study.

Table II

Quenching Rates Used in Film Molding

Symbol	Rate	Quenching Temperature (°C)	Medium
R	rapid cooling	-72°C	ethyl-o-silicate
M	moderate cooling	0°C	ice-water
S	slow cooling	+90°C	water

The reason for the choice of these quenching rates was the observation that slower cooling (i.e., allowing the press to cool by natural radiation, or by flowing cooling water through the platens directly) resulted in films which were quite hazy and full of tiny "cracks" and craze-like inhomogeneities. Under the optical microscope these "cracks" appeared as voids at the borders of well-developed spherulites.

It is believed that, at slow rates of cooling, a relatively small number of spherulites grow by "feeding" on the interstitial amorphous areas and by pushing ahead of their growth fronts non-crystallizable, atactic and low molecular weight material. When most of the isotactic material has been incorporated in the spherulites growth ceases and these "holes", partially void and partially filled with exuded material, are left. Quite obviously, films of this nature are unsuitable in permeation work.

Due to the size of the film sample required for time-lag experiments, the whole molding assembly was relatively large and

it was consequently not practical to set up a bath at liquid nitrogen temperatures. Again, the actual quenching bath would have had to be some material other than liquid nitrogen to avoid the inevitable vapor binding.

Cooling curves were obtained for several films for each mode of cooling by means of imbedding a thermocouple in the polymer. The iron-constantan thermocouple (16 gauge) was first imbedded in a polymer pellet which then was placed together with the rest of the pellets at the center of the mold assembly. Since the cooling curves were surprisingly reproducible, it could be concluded that at least the quenching aspect of the molding procedure was quite reproducible. What was not so reproducible was the time required to fasten the clamps to the inner plates in the case of the "rapidly" and "moderately" cooled films. This meant that the temperature just prior to quenching was less than 204°C yet always more than the melting point of the material (i.e., ~162°C).

3. Annealing

After formation of the films by quenching from the melt, their morphology was further changed by annealing. For the "MA" series films the annealing temperatures were 80°C, 100°C, 110°C, 130°C, 140°C and 150°C. All other films were annealed at 150°C only. In each case the films were held at their specific temperature for 60 minutes.

The reason for not annealing the films at temperatures above 150°C was the observation that the surfaces of the films became extremely uneven, i.e., exhibiting steps in the plane of the film. Films annealed above 160°C developed innumerable fine cracks and air pockets.

Before annealing, each film was sealed with silicone rubber (Dow Corning's Silastic 732 RTV) between two photo-printing plates. In the upper edge was imbedded a small hypodermic needle, 24 gauge, to allow the gas sealed in with the film to escape. This "sandwich" was then immersed in a silicone oil bath (Dow Corning's 550 Fluid) so that only the end of the hypodermic needle projected above the surface. The bath was heated by spirals of nichrome wires to give rapid, lag-free heat transfer. The temperature could be controlled to within $\pm$0.02°C by a Sargent Model S Thermonitor.

C. Time-Lag Experiments

1. Method

Most of the diffusion and permeation data generated in this study were obtained via the classic time-lag technique developed by Barrer (9). In essence, the process is one of diffusion in a plane sheet, initially at some uniform concentration which then experiences a sudden change in surface concentrations.

In practice, the polymer film is first evacuated, then a constant pressure, P_1, is suddenly applied to one side, and the pressure rise in a calibrated downstream reservoir is recorded.

A typical plot of pressure versus time in the receiving reservoir is shown in Figure 8.

If the pressure, P_1, on the upstream side of the membrane is kept constant and the pressure rise, P_2, in the receiving reservoir is kept negligible compared with P_1, then the unidirectional diffusion of gas across the membrane is described by the partial differential equation

$$\frac{\partial c}{\partial t} = D \frac{\partial^2 c}{\partial x^2} \qquad (19)$$

where c is the concentration of gas in the polymer at any t and x (in $cc(STP)/cc_p$), D is the diffusivity (in cm^2/sec), x is the distance from the upstream surface (in cm), ℓ is the film thickness (in cm), and t is the time measured from the instant gas is introduced on the upstream side of the film (in sec).

The total amount of gas, Q, that has diffused through the membrane in time t is then given by

$$Q = -\int_0^t D \left(\frac{\partial c}{\partial x}\right)_{x=\ell} dt \qquad (20)$$

For the experimental conditions mentioned above, the solutions to equations (19) and (20) are readily obtained (25) and equation (21) evolves as:

$$\frac{Q}{\ell C_2} = \frac{Dt}{\ell^2} - \frac{1}{6} - \frac{2}{\pi^2} \sum_1^\infty \frac{(-1)^n}{n^2} e^{-\frac{Dn^2\pi^2 t}{\ell^2}} \qquad (21)$$

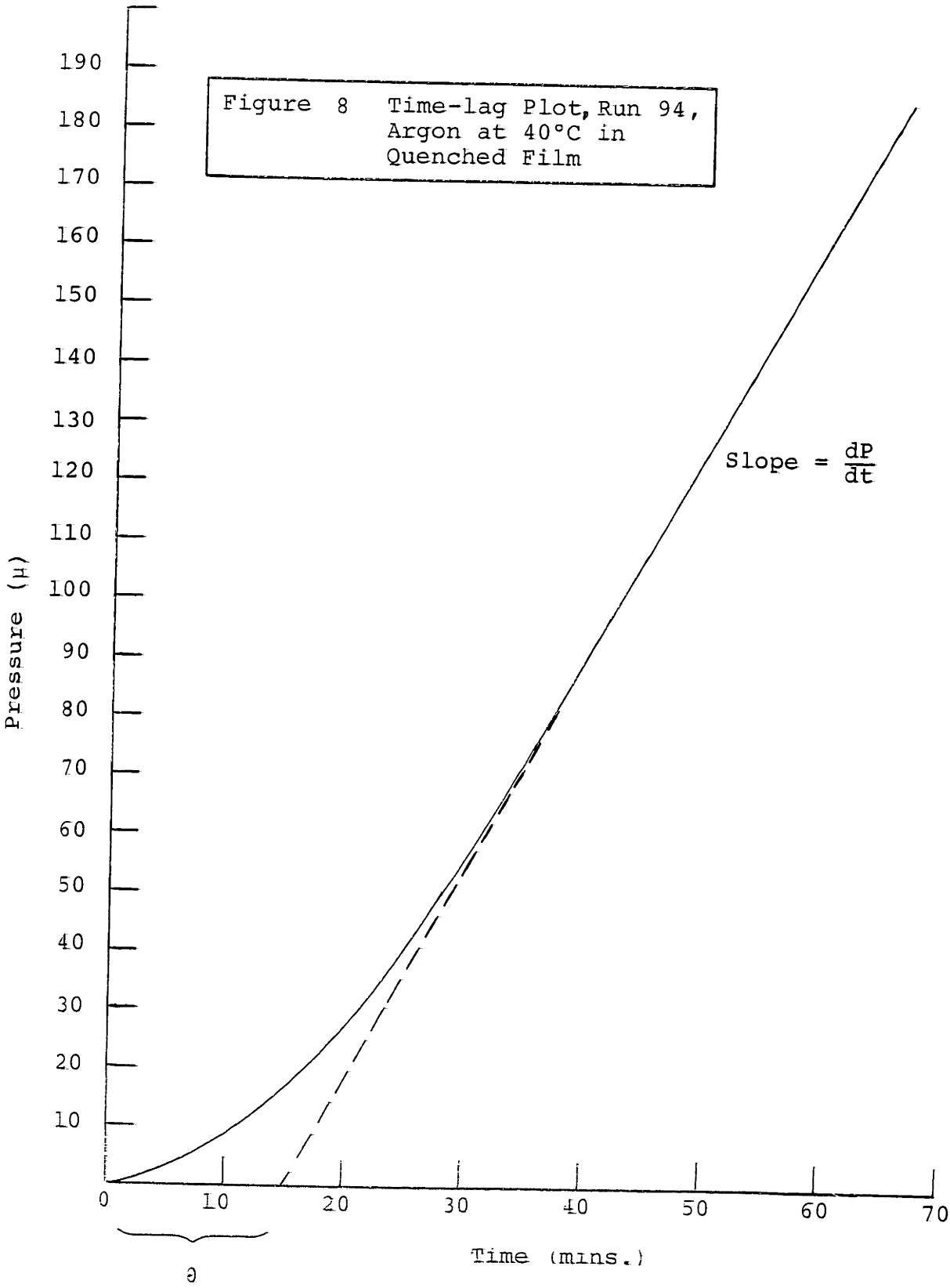

Figure 8 Time-lag Plot, Run 94, Argon at 40°C in Quenched Film

As t becomes very large, this expression approaches the linear relationship

$$Q = \frac{DC_2}{\ell}\left(t - \frac{\ell^2}{6D}\right) \qquad (22)$$

If this straight line is extrapolated to Q = 0, the intercept on the time axis will be some time θ. Setting Q = 0 in equation (22) shows that θ is related to diffusivity as

$$D = \frac{\ell^2}{360\theta} \quad \frac{cm^2}{sec} \qquad (23)$$

where θ is the time-lag in minutes.

The permeability is determined by performing a material balance on the downstream reservoir during the period when the pressure increases at a constant rate. The permeability is then given by:

$$\bar{P} = \frac{(dP/dt \times 10^{-3})(\ell)(V_S)(273)}{(A)(P_1)(60)(T_a + 273)} \quad \frac{cc\,(STP)}{cm\text{-}sec\text{-}atm} \qquad (24)$$

where dP/dt is the steady state pressure rise (in μ/min), V_S is the downstream collecting volume (in cc), A is the area of the membrane (in cm^2), P_1 is the upstream pressure (in mm Hg), and T_s is the temperature of the ambient air surrounding the collecting volume (in °C).

Although the solubility constant, k, cannot be determined directly, it can be calculated from the relationship

$$k = \frac{\bar{P}}{D} \quad \frac{cc(STP)}{cc_{polymer}\text{-}atm} \qquad (25)$$

which applies whenever the diffusion process is isotropic with a constant D and the solubility behavior obeys Henry's law, both the case in this study.

2. Apparatus

The time-lag apparatus used for this study was patterned after that of Bixler, Vieth and Fein (33, 15, 111). The two stations are shown schematically in Figure 9 and pictorially in Figure 10.

As before, the vacuum system was entirely glass using high vacuum stopcocks, lubricated with Apiezon N grease throughout. The vacuum was provided by an oil diffusion pump backed by a Welch Duo Seal mechanical pump. The system was capable of pressures of less than 10^{-5} mm Hg. A separate vacuum pump and mercury manometers were used for the gas feed stations.

One of the major innovations in the present experimental system was the use of a capacitance-type pressure transducer to measure the downstream pressure. Previous systems used a sensitive McCleod guage. The advantages of the pressure transducer are their unequalled accuracy ($\pm$0.001 microns) and ease of operation. The signal from the transducer is fed directly to a Sargent Model MR recorder.

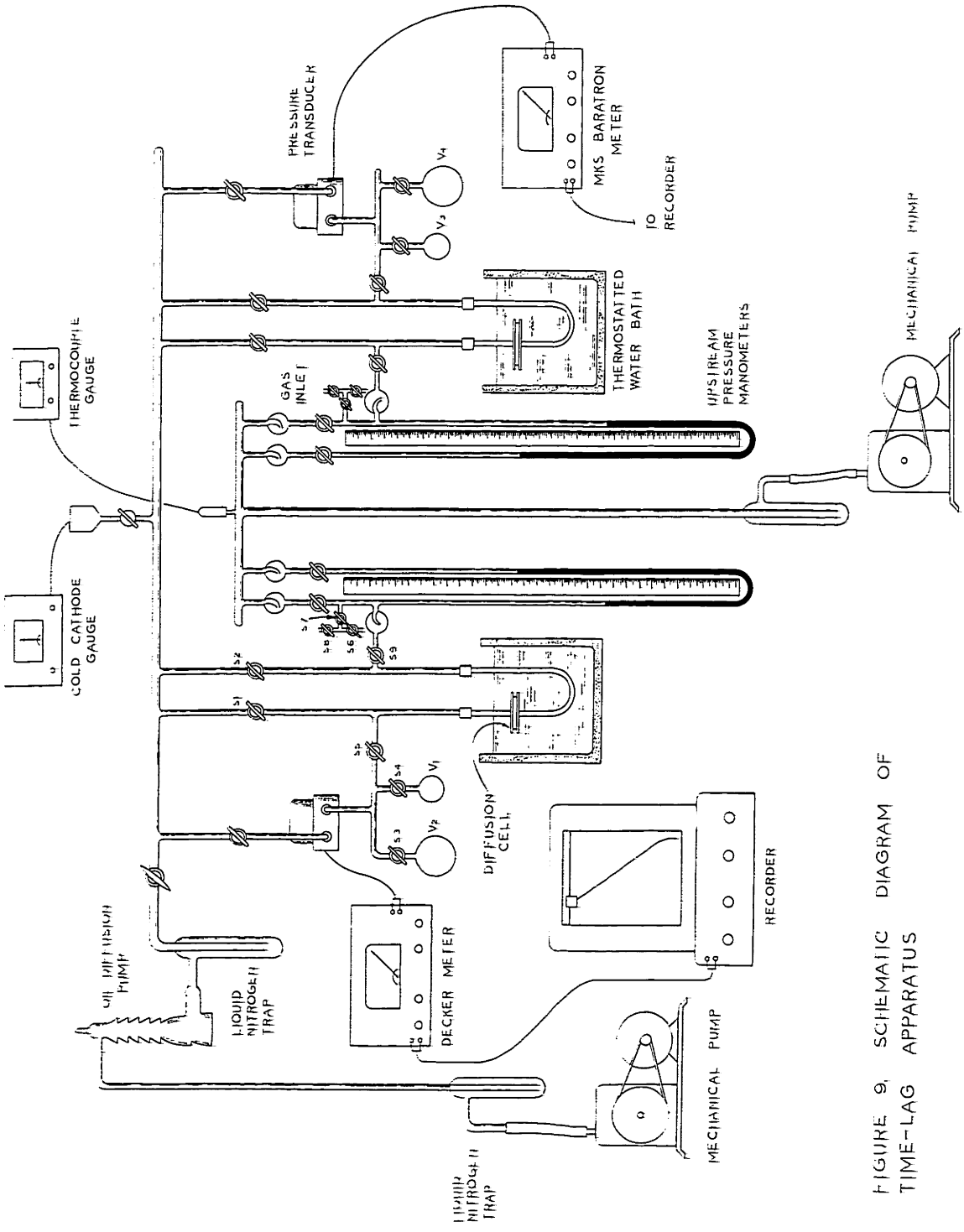

FIGURE 9. SCHEMATIC DIAGRAM OF TIME-LAG APPARATUS

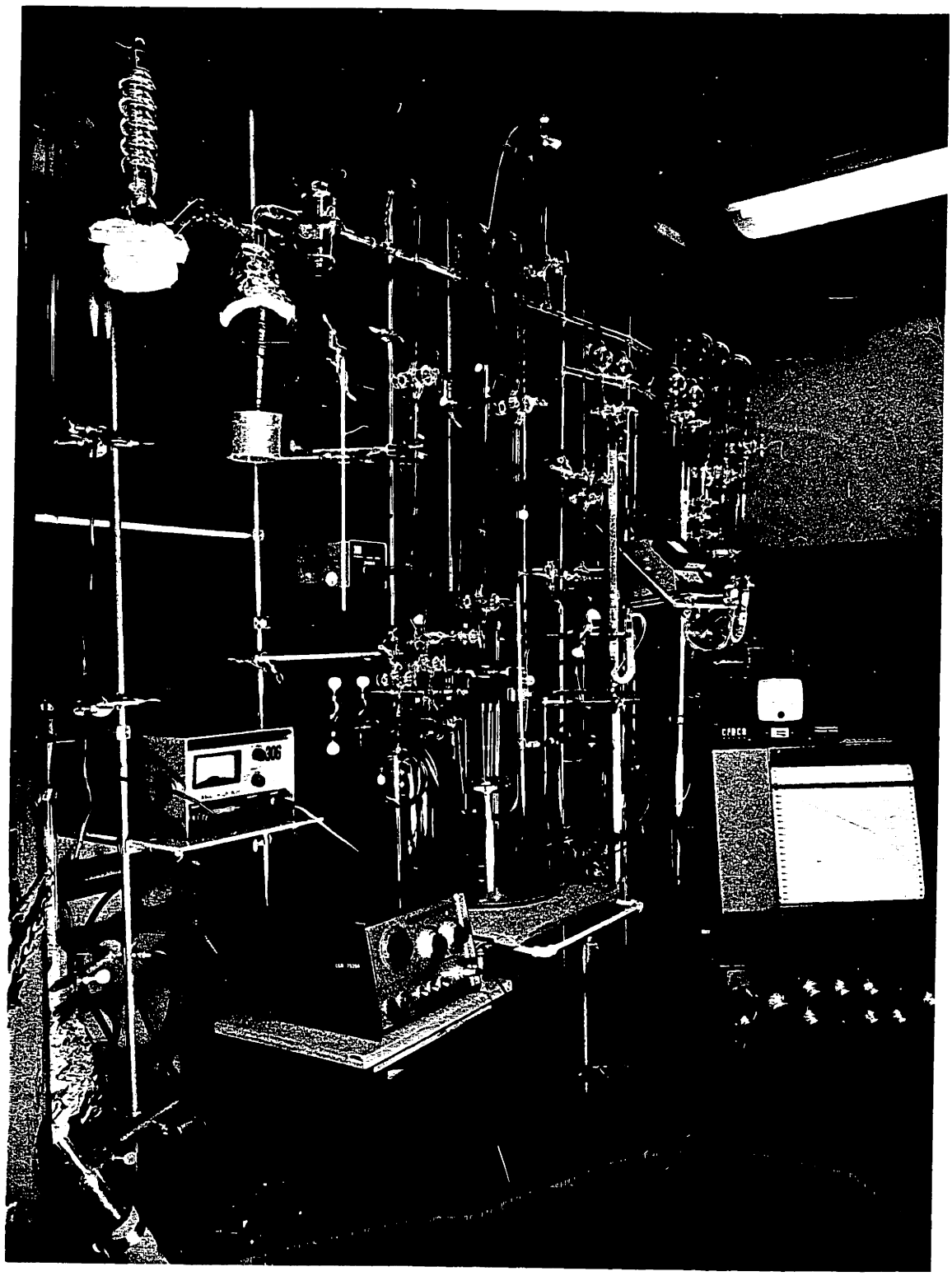

Fig. 10 -- Photograph of Time-Lag Apparatus

The other new feature of the system was the use of quick-connect, O-ring seals to attach the metal diffusion cell to the glass vacuum system. These connectors gave a remarkably good seal even at pressures as low as 10^{-5} mm Hg and made it easy to change films.

The diffusion cells were fashioned after a design used by the Amicon Corporation. Initially the cells were used without O-rings, however, the need to operate at higher temperatures with thin (<10 mils) membranes forced a change to Buna N or Butyl rubber O-rings. One of the cells is shown in Figures 11 and 12. The membrane is held by the outer lips of each half of the cell with one O-ring on each side of the membrane providing the seal. The effective area for diffusion is assumed to be the area of the slight depression in each cell half. On the downstream side the membrane was supported by a small perforated metal disc. In addition, a piece of porous filter paper served as spacer on both sides of the membrane. The cells were so designed that the fraction of the downstream volume immersed in the thermostated bath was negligible. Consequently, the collecting reservoirs could be considered to be at ambient temperature.

The thermostated waterbaths had a temperature range of 30 to 70°C with a temperature stability of $\pm$0.1°C.

The level of the vacuum in the main vacuum system was monitored by a Veeco Cold Cathode Discharge Gauge (Type TG-2). A Cenco thermocouple gauge indicated the pressure level in the upstream pressure manometers.

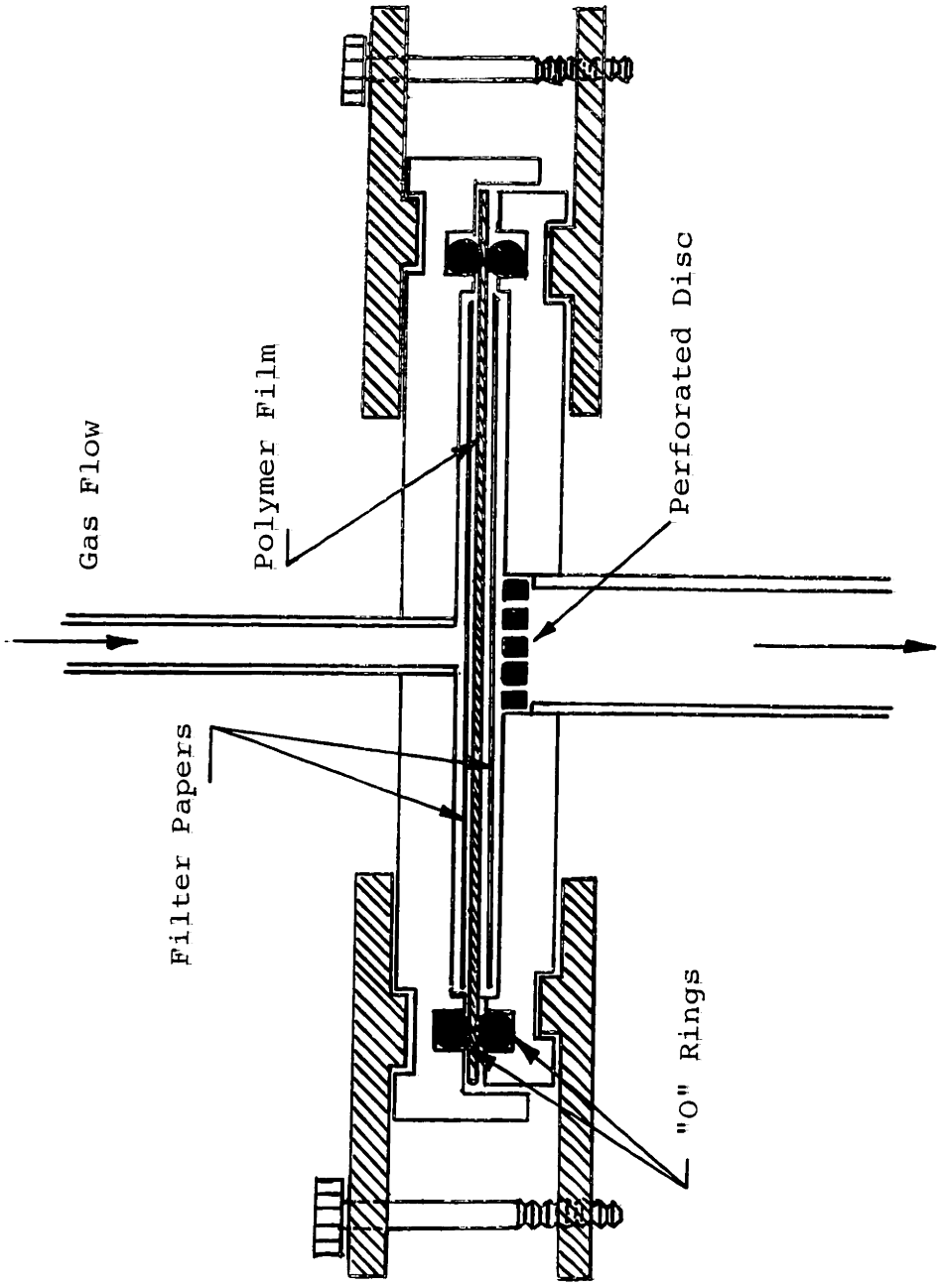

Figure 11 Schematic Diagram of Time-Lag Diffusion Cell. (Approximately 1-1/2 times actual size.)

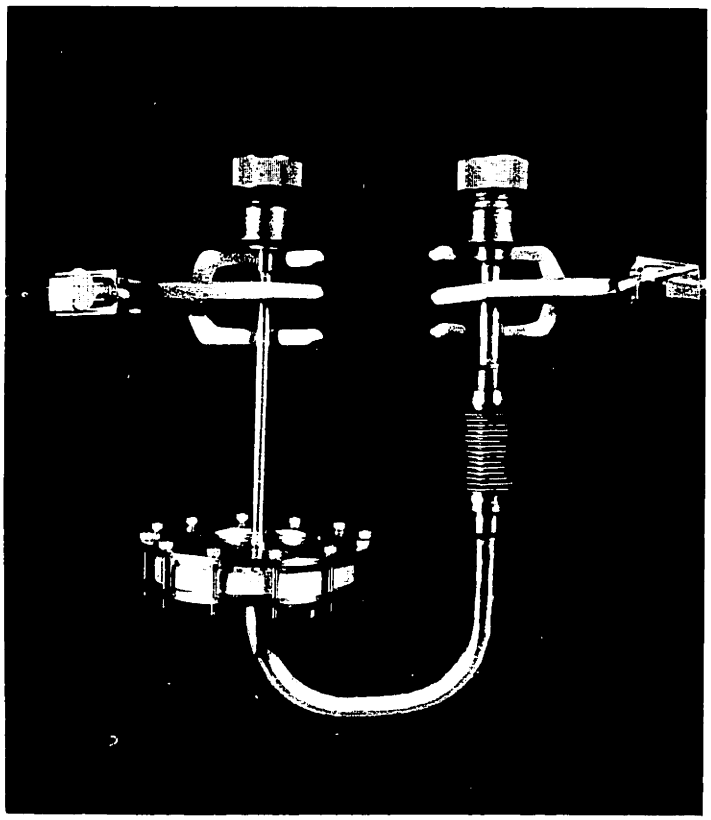

Fig. 12 -- Photograph of Time-Lag Diffusion Cell

3. Operating Procedure

Since the operation of the two time-lag stations was very similar to that of previous investigators (33, 15, 111), only the procedures unique to this apparatus will be explained in detail.

After the vacuum system became operationsl, i.e., capable of maintaining pressures of less than 10^{-5} mm Hg, the first step was to determine the downstream collecting volume. This was accomplished by a well-known gas expansion technique. A gas sample was isolated in the calibrated volume, V_1, at a known pressure, P_1. The gas was then expanded into the whole downstream gas space (previously evacuated) and the resulting pressure, P_2, noted. Since the number of moles of gas and temperature (ambient) were constant, the collecting volume, V_T, was given by the equation

$$V_T = V_1 \frac{(P_1 - P_2)}{P_2} \qquad (26)$$

The bulbs V_1, V_2, V_3, and V_4 were all calibrated prior to installation by weighing the volume of water which each held.

Prior to the start of a run the sample was generally evacuated for a period of at least 48 hours at a pressure of 10^{-5} mm Hg or less. Between runs with the same sample the pump-down time was shortened. Although Bixler showed (15) that 99.99% of the gas are removed after degasing for a period of 5.6 times the time lag, the time allowed for evacuation was always more than 10θ to allow for complete outgassing of the O-rings and the finite pumping speed of the vacuum system.

Immediately preceding an actual run a leak test was performed. This consisted of zeroing the Baratron or Decker pressure meter with both sides of the transducer open to the vacuum, closing stopcocks S_1, S_3 and S_4 (Figure 9), and recording the pressure after 10 minutes. If the leak rate was less than 10% (usually <3%) of the expected steady state permeation rate, then stopcock S_1 was again opened and after a further 10 minutes the system was ready for a run. (In all runs the value of $\bar{P}$ was corrected for the leak rate.)

During this time the recorder was zeroed, and a suitable (based on the anticipated time-lag) recorder speed and range were selected. At the other end of the system the upstream pressure manometer was charged by passing the gas from its compressed tank over "Drierite" ($CaSO_4$) to the gas inlet. After flushing the gas through stopcock S_8 for a few minutes, the flow rate of the gas was greatly reduced, stopcocks, S_8 and S_9 were closed, and stopcock S_7 was slowly opened until the pressure indicated on the manometer was in the desired range (100 - 700 mm Hg).

Then the recorder was started, stopcocks S_1 and S_2, and stopcocks S_3 and/or S_4 were closed (depending on the anticipated permeation rate), and at time zero, stopcock S_9 was opened. While the run was proceeding, the upstream pressure, bath and ambient temperatures were recorded. Usually the run was continued for a time equal to 5 times the time lag and never less than 3θ, since Van Amerong (2) predicted theoretically and the author

observed experimentally, that the time required to reach steady state is 3.5 to 3 times θ. The values of θ and dP/dt were read directly from the recorder plots.

D. Low Pressure Sorption Experiments

1. Method to Obtain Solubility Constants

The difficulty with static sorption experiments in the case of polymers is the characteristically low solubility of permanent gases in polymers. However, with the advent of capacitance-type pressure transducers it became possible to measure pressure changes in the micron range very accurately. This provided the opportunity to design a static sorption system which would yield diffusivity as well as solubility data. Since "sorption" experiments are inherently quicker (i.e., they required only one equilibration), all initial experiments were of the "sorption" kind. However, at a later stage difficulty in obtaining diffusion data necessitated a switch to "desorption" experiments.

In a "sorption" experiment, the polymer sample is initially thoroughly evacuated and then pressurized with the gas under study. The pressure drops as gas diffuses (sorbs) into the polymer. Since the polymer is contained within a system of known volume, V_T, and the weight and density of the polymer are also known, the void volume, V_v, of the system can be calculated. Then if one records the pressure in the system immediately after introduction of the gas and at the end of equilibration, one can by a simple mass balance on the system (Appendix D.2) obtain the solubility constant, k, as

$$k = \frac{V_v}{V_p} \cdot \frac{273}{T} \cdot \frac{P_i - P_e}{P_e} \qquad \frac{cc(STP)}{cc\text{-}atm} \qquad (27)$$

where V_v is the void volume in cc, V_p is the volume of the polymer in cc, T is the temperature of the system in °K, P_i is the pressure immediately after introduction of the gas in mm Hg, P_e is the equilibration pressure in mm Hg.

Previous investigators (33, 15) had some difficulty using this method for gases with high diffusivities such as helium and argon because pressures were measured with mercury manometers and it was difficult to establish P_i accurately. However, in this study the use of a pressure transducer made it possible to design the experimental apparatus in such a way that the pressure difference ($P_i - P_e$) could be measured very accurately and P_i could be measured at the operator's convenience any time during the run.

Nevertheless, "desorption" experiments had to be resorted to due to another problem. Experimentally, it was observed that pressurizing the sample so suddenly produced a marked thermal effect which completely obscured the initial gas diffusion into the polymer. Theoretical calculations, presented in Appendix D.4, showed that the temperature of the free volume of gas surrounding the polymer could rise as much as 200°C due to the adiabatic compression. In practice this effect was probably considerably less due to the presence of the polymer and the glass walls, with their finite heat capacity. However, since it

was important to get reproducible diffusion data, all experiments in the later part of this study were of the "desorption" kind.

Basically, a "desorption" experiment consists of completely degasing a polymer sample, allowing it to equilibrate with the gas at some pressure P_i, rapidly evacuating the void volume, isolating the system again and allowing it to reach equilibrium for a second time. As the gas diffuses out of the polymer, i.e., desorbs, the pressure rises in the sample volume.

As before, a mass balance on the system (Appendix D.3) readily yields the solubility constant, k, as

$$k = \frac{V_v}{V_p} \cdot \frac{273}{T} \cdot \frac{P_e}{[(1 - f)P_i - P_e]} \quad \frac{cc(STP)}{cc_p \text{ atm}} \qquad (28)$$

where V_v is the void volume in cc, V_p is the polymer volume in cc, T is the temperature of the system in °K, P_i is the equilibrium pressure before pumpdown in mm Hg, P_e is the pressure at the second equilibration in mm Hg, and f is the fraction of gas lost during pumpdown.

In practice, a small corrected had to be made in the equilibrium pressure, P'_e, actually observed, because the 15 second pumpdown was not perfect, and consequently, the pressure in the sample volume was some small, but finite, value P' at time zero. Thus by definition, $P_e = (P'_e - P')$.

The fraction of gas lost during pumpdown was estimated according to Fein (33) by adopting Crank's (26) solution for diffusion from a plane sheet to diffusion from a cube in a way suggested by Treybal (105).

For desorption from a plane sheet Crank gives the following solution for small times

$$\frac{M_t}{M_\infty} = 2\left(\frac{Dt}{\ell^2}\right)^{1/2} \left\{\pi^{-1/2} + 2\sum_{n=1}^{\infty} (-1)^n \text{ ierfc } \frac{n\ell}{\sqrt{Dt}}\right\} \qquad (29)$$

where M_t is the total amount of gas which has desorbed from the sheet at time t, M_∞ is the corresponding quantity after infinite time, D is the diffusivity of the gas in the polymer in cm^2/sec, t is the time in seconds and ℓ is the half-thickness of the film in cm.

For small D's and times, equation (29) may be approximated by

$$\frac{M_t}{M_\infty} = 2\left(\frac{Dt}{\pi\ell^2}\right)^{1/2} \qquad (30)$$

where M_t/M_∞ is by definition equal to f, the fraction of gas lost from a plane sheet. Now according to Treybal the fraction of gas still residing in the cube at any time t is simply equal to the cube of $[1 - (M_t/M_\infty)]$ for the plane sheet, i.e.,

$$(1 - f) = \left(1 - \frac{M_t}{M_\infty}\right)^3 \qquad (31)$$

Therefore

$$(1 - f) = [1 - 2(\frac{Dt}{\pi \ell^2})^{1/2}]^3 \qquad (32)$$

where t is duration of the pumpdown in seconds.

In the few instances when the polymer under study was in the form of small rectangular strips, a reciprocal average was taken for the thickness. In other words, it was assumed that, for short pumpdown times, the fraction of gas lost from the polymer particle is directly proportional to its area and inversely proportional to its volume. Thus the value of ℓ in equation (30) was taken as

$$\ell = \frac{3}{(\frac{1}{\ell_1} + \frac{1}{\ell_2} + \frac{1}{\ell_3})} \qquad (33)$$

where ℓ_1, ℓ_2 and ℓ_3 are the <u>half</u> lengths of each side of the rectangular strip in cm.

At least for the experiments with the polymer in the shape of cubes, the fraction of gas lost may have also been estimated by Crank's (<u>27</u>) solution for diffusion from a sphere. However, Treybal seems to indicate that the former solution is the better approximation.

2. <u>Method to Obtain Diffusion Constants</u>

As was previously pointed out, obtaining diffusion constants from "sorption" experiments was difficult because of the adiabatic compression effect. Nevertheless, by carefully observing the

magnitude of this effect with blank runs (i.e., identical experiments without polymer) it was possible to correct for this effect and obtain some reliable solubility and diffusion data from sorption experiments.

The model selected for obtaining diffusion constants from the sorption studies was that of diffusion into a plane sheet. This model assumes that (i) the initial concentration of the gas in the polymer is uniform, (ii) the surfaces of the polymer film are kept at constant concentration, and (iii) the amount of solute taken up by the polymer sheet is a negligible fraction of the whole. All these conditions are met at the beginning of any "sorption" experiment. Since the polymer was initially fully evacuated, condition one was fulfilled automatically. Furthermore, the total fractional uptake was never more than 1%, with the concentration change for the first 10 minutes of any run being 0.3% or less. Thus conditions (ii) and (iii) seem to apply.

The biggest approximation may be that of assuming the diffusion into the individual polymer strip is one-dimensional. However, since the strips were in the form of rectangular parallelopipeds with the thickness to width to length ratio being 1:13:62 it was valid to assume that effectively all the diffusion substance enters through the plane faces and a negligible amount through the edges.

The solution for this diffusional process is identical to that previously quoted for desorption. Thus equation (29)

$$\frac{M_t}{M_\infty} = 2\left(\frac{Dt}{\ell^2}\right)^{1/2} \left\{\pi^{-1/2} + 2\sum_{n=1}^{\infty} (-1)^n \text{ ierfc } \frac{n\ell}{\sqrt{Dt}}\right\} \quad \ldots\ldots (29)$$

applies again, except now M_t is the total amount of gas which has diffused into the polymer strip at time t and M_∞ is the total amount of gas that has diffused into the polymer after infinite time.

Again for short times the fractional uptake of gas by the polymer is approximated well by

$$\frac{M_t}{M_\infty} = 2\left(\frac{Dt}{\ell^2\pi}\right)^{1/2} \quad (30)$$

Thus a plot of P_t/P_e versus $t^{1/2}$ $(\text{min}^{1/2})$ for the first 10 minutes yields essentially a straight line with a slope equal to $2(D/\pi\ell^2)^{1/2}$ which is readily solved for D. A typical plot of P_t/P_e versus $t^{1/2}$ (corrected for the blank effect) is shown in Figure 13.

In the case of the "desorption" experiments the process was one of diffusion from a plane sheet into a constant, limited volume. As gas desorbs from the polymer, the pressure in the gas space (i.e., void volume) increases. By experimentally observing this pressure rise as a function of time while the system comes to equilibrium, it is possible to determine the diffusivity of a specific gas in the polymer.

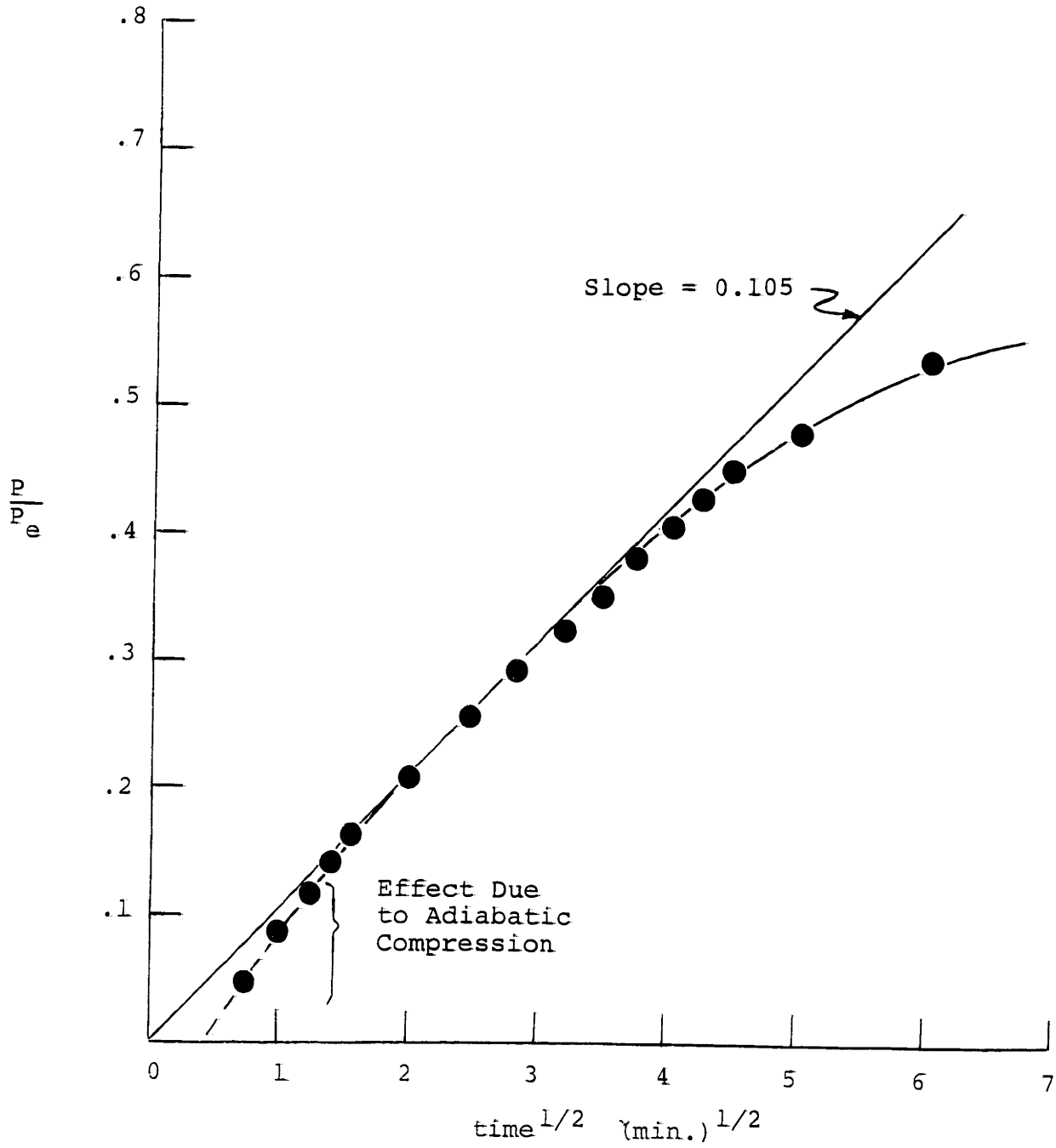

Figure 13 Low Pressure Sorption Data - Run 24 - Argon Sorption at 40°C

Two methods were used to obtain D's from "desorption" experiments. One relied upon an accurate record of the pressure change as a function of time during the initial period of the experiment and the other, on the observation of diffusion at long times.

In the case of diffusion at short times, the D's were calculated by comparing the experimentally observed rise in pressure with the corresponding numerical solution for diffusion out of a cube. Evans and Ma (32) presented a solution for this case in the form of plots of M_t/M_∞ versus $(Dt/\ell^2)^{1/2}$ for five values of final fractional uptake (see Figure 14). As before, M_t is the total amount of gas having diffused out of the polymer at any time t, M_∞ is the corresponding value at infinite time, D is the diffusivity in cm^2/sec, t is the time in seconds, and ℓ is the half-thickness in cm. For desorption, the final fractional uptake (ffu.) is defined as

$$\text{ffu.} = 1 - \frac{\text{total amount of gas in the polymer at equilibrium}}{\text{total amount of gas in the polymer initially}} \quad \ldots\ldots (34)$$

Since solutions for only five fractional uptakes were available, a solution at any other ffu. value was obtained by graphical interpolation. This was not as difficult as it may appear, since the plots of M_t/M_∞ versus $(Dt/\ell^2)^{1/2}$ were approximately linear up to $M_t/M_\infty = 0.3$.

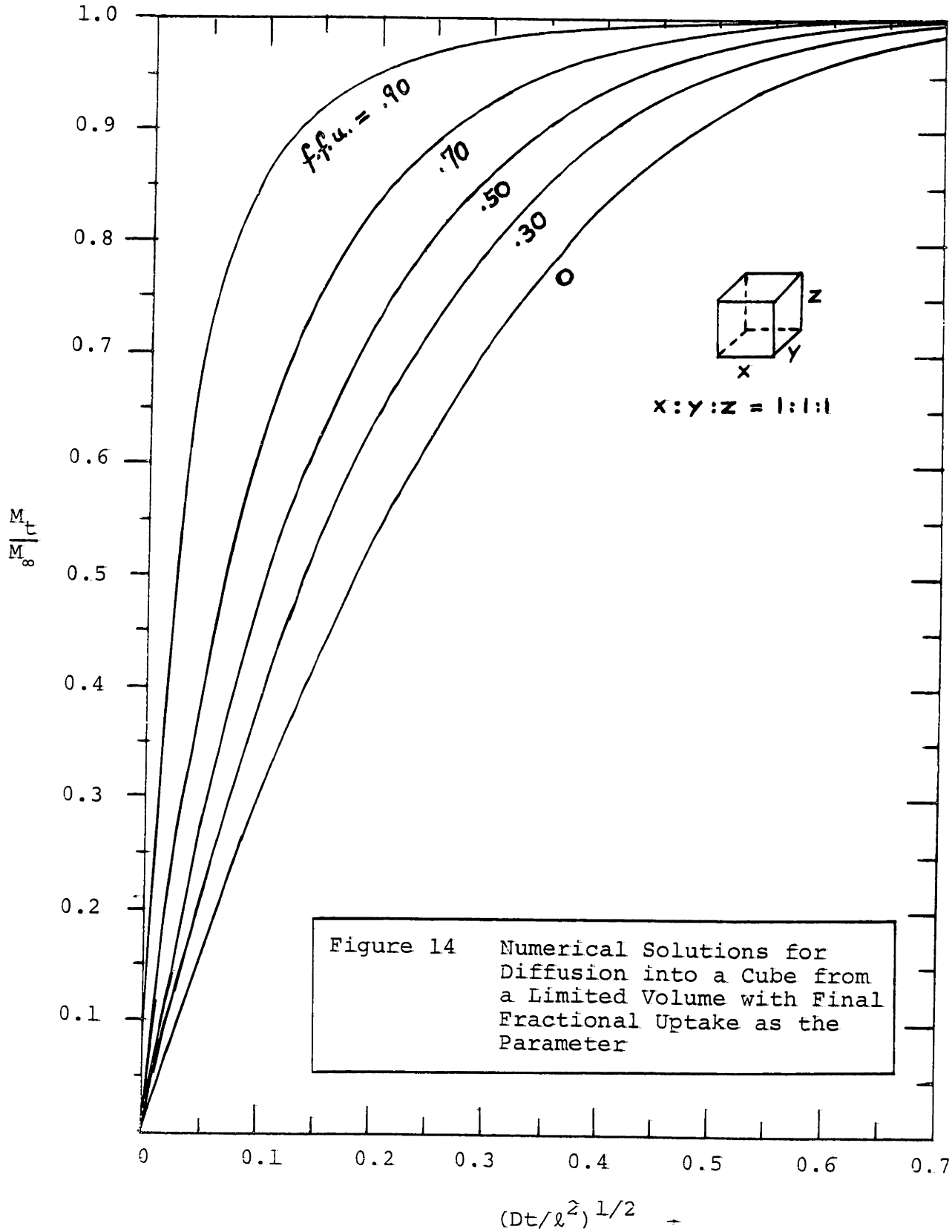

Figure 14 Numerical Solutions for Diffusion into a Cube from a Limited Volume with Final Fractional Uptake as the Parameter

Thus in practice, for any desorption run one would record P as a function of time, construct a plot of P/P_e versus $t^{1/2}$ from this, and equate the slope of the initial, straight line portion of this plot to the initial slope of the numerical solution at the ffu. value of this particular run.

Although no analytical solutions are available for the case of diffusion out of a cube into a limited volume, one can approximate this process by the simpler case of diffusion out of a sphere. This approximation is especially good at short times where, as both Crank (27) and Evans (32) point out, differences in geometry become quite unimportant. However, even at long times, diffusion from a sphere and a cube is very similar, because diffusion is related to the area to volume ratio of the particle and that ratio is identical for the two geometries. Nevertheless, the following method to obtain diffisuvities was used only in a few instances to verify the results obtained from the numerical solution.

Crank (28) outlines a solution for diffusion from a sphere into a limited volume and Bixler (15) suggests how it can be simplified to readily yield a numerical value of D. The fractional loss of gas by the polymers is given by

$$\frac{M_t}{M_\infty} = 1 - \sum_{n=1}^{\infty} \frac{6\emptyset(1 + \emptyset)}{(9 + 9\emptyset + \emptyset^2 q_n^2)} \exp - \frac{Dq_n^2 t}{\ell^2} \qquad (35)$$

For sufficiently long times, this reduces to

$$\frac{M_t}{M_\infty} = 1 - \frac{6\phi(1+\phi)}{9 + 9\phi + \phi^2 q_1^2} \exp - \frac{Dq_1^2 t}{\ell^2} \qquad (36)$$

where

$$\frac{M_t}{M_\infty} = \frac{P}{P_e} = \frac{\text{pressure at any time}}{\text{pressure at infinite time}} \qquad (37)$$

$$\phi = \frac{\text{free volume}}{\text{polymer volume x solubility}} \qquad (38)$$

and q_1 is the positive non-zero root of

$$\tan q_1 = \frac{3q_1}{3 + \phi q_1^2} \qquad (39)$$

and is tabulated by Crank (29).

Therefore a plot of $\ell n(1 - P/P_e)$ versus t should result in a curve which eventually becomes a straight line with slope (Dq_1^2/ℓ^2). Such a plot is shown in Figure 15. Then knowing q_1 and ℓ, the half-thickness of the cube, a value of D is readily calculated.

3. Apparatus

The equipment for the low pressure sorption experiments is schematically presented in Figure 16 and is shown in detail in Figure 17. The apparatus was so designed that it allowed both sorption and desorption experiments. This flexibility is largely attributable to the use of a capacitance-type transducer which made it possible to accurately measure the small pressure

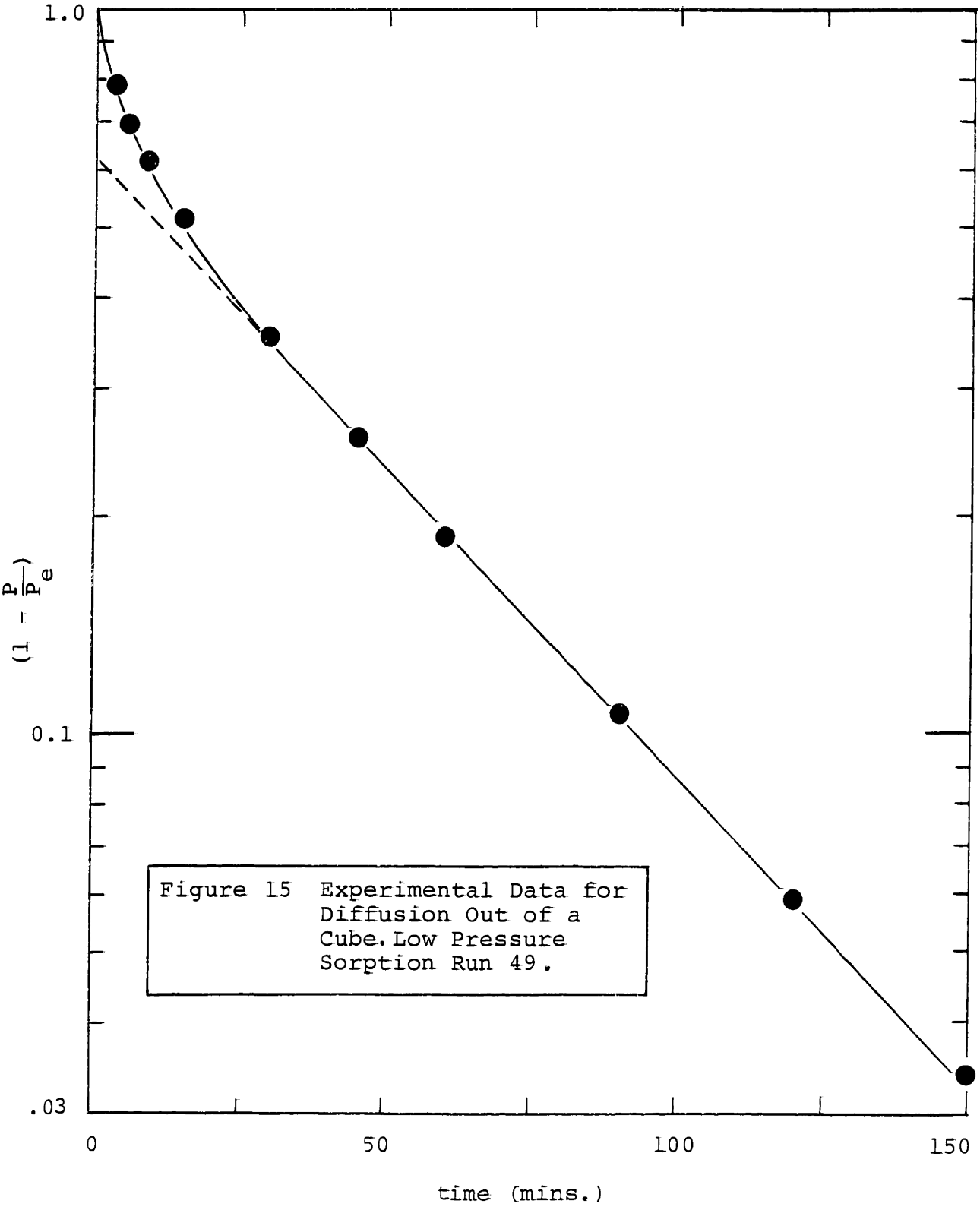

Figure 15 Experimental Data for Diffusion Out of a Cube. Low Pressure Sorption Run 49.

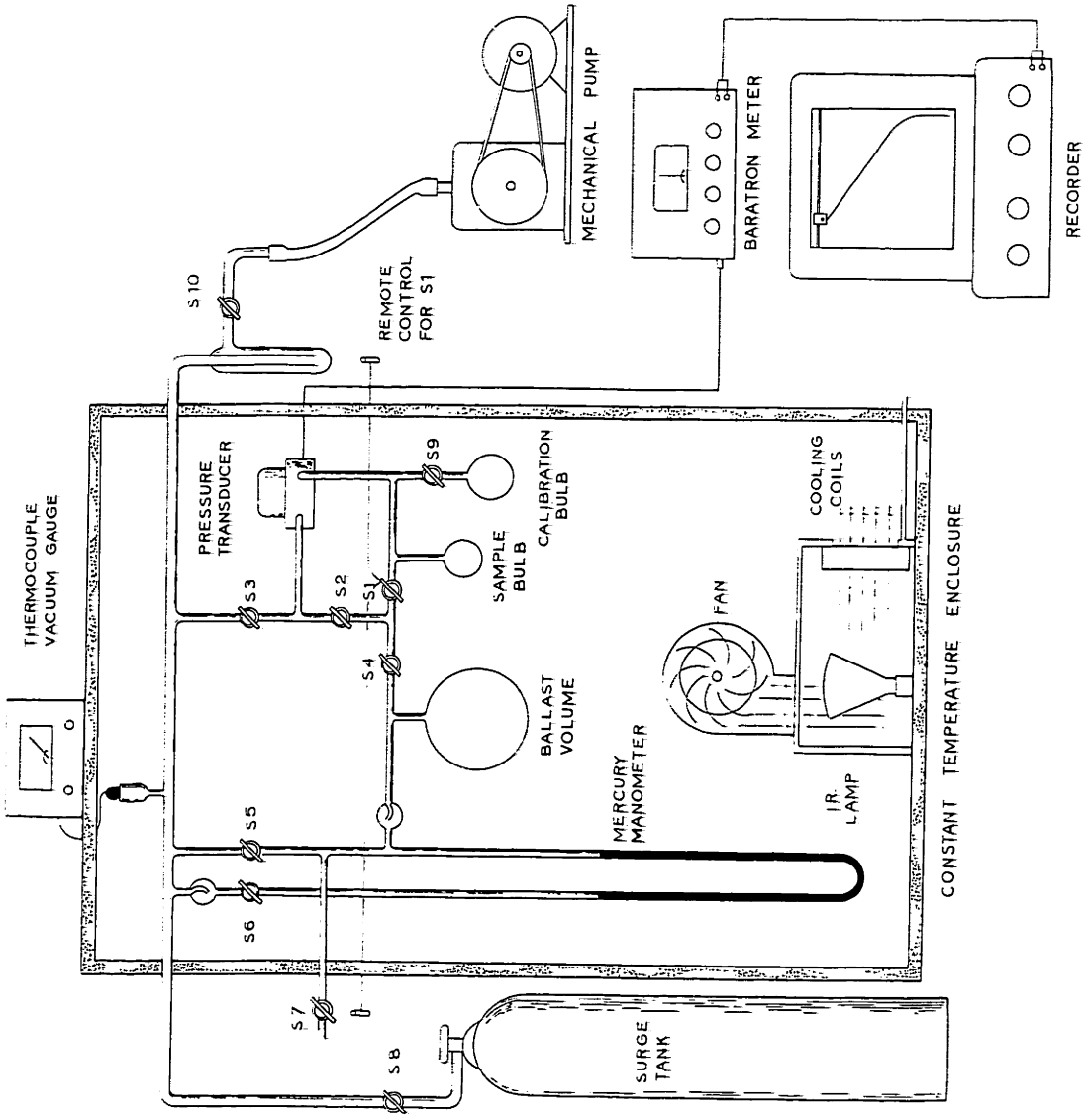

FIGURE 16. SCHEMATIC DIAGRAM OF THE LOW PRESSURE SORPTION APPARATUS

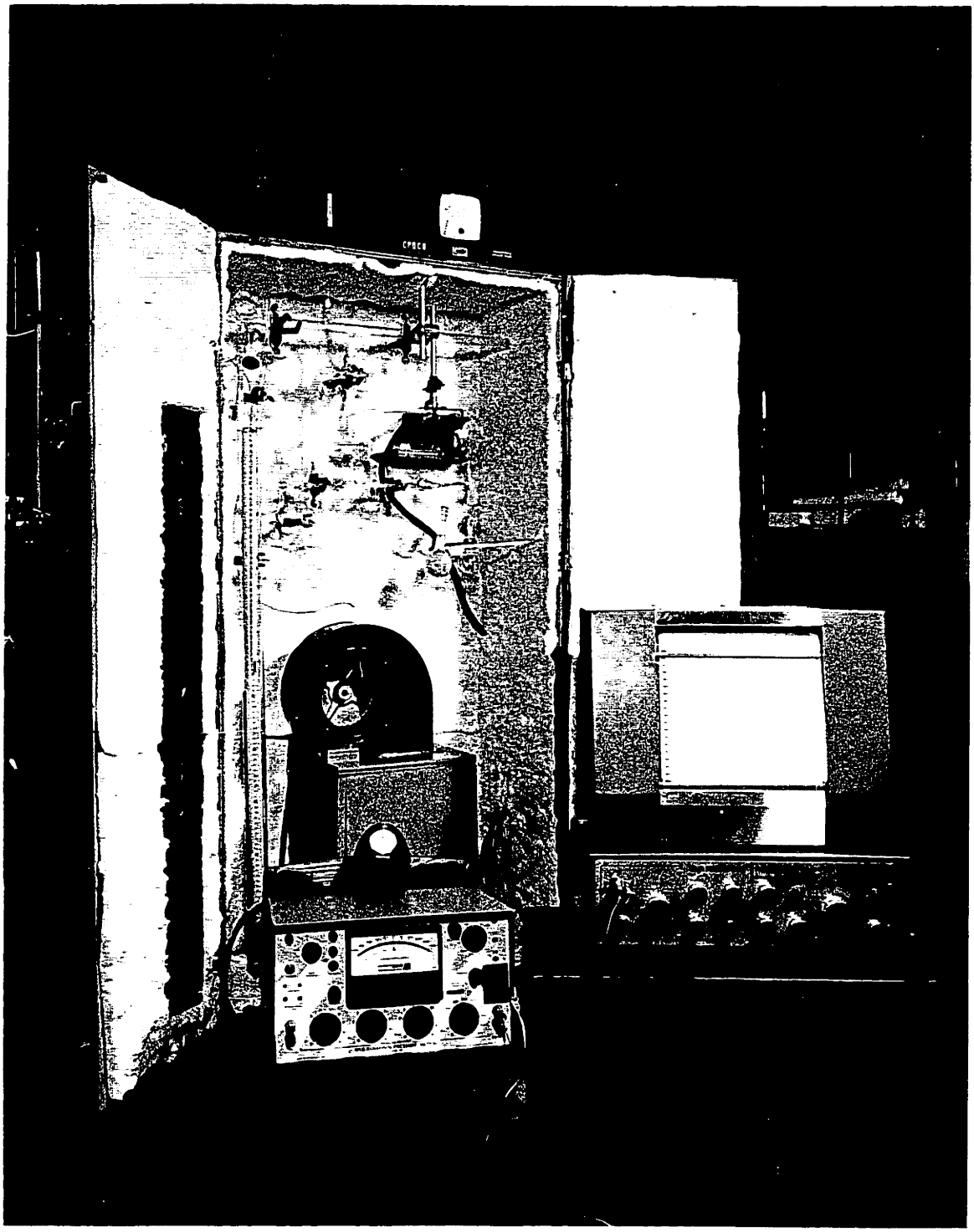

Fig. 17 -- Photograph of Low Pressure Sorption Apparatus

changes associated with the sorption of permanent gases in small samples of poly(propylene). Previous investigators (33, 15, 111) used mercury manometers and encountered definite difficulty in measuring solubilities accurately.

As in the case of the time-lag apparatus, feeding the amplified signal from the pressure transducer to a recorder provided a continuous record of the early stages of any experiment and thus allowed determination of diffusion constants.

The sample was either sealed into an elongated ampule which was directly blown into the system or held in a 50 cc or 100 cc flask which was attached to the system by means of a ground glass joint. The sample and system were degassed by a Welch Duo-Seal vacuum pump which provided consistent pressures as low as 0.1μ.

To meter the test gas to the sample, as well as to measure equilibration pressures, a mercury manometer was used.

Rapid evacuation of gas from the sample volume in the second stage of a desorption experiment was achieved by using an empty oxygen cylinder as a surge tank. This made it possible to reduce the pressure in the sample volume from an initial 600 mm Hg to less than 0.5 mm Hg in 15 seconds.

The apparatus was housed in a thermostatted cabinet which allowed operation over a temperature range of 25 to 70°C at a

temperature stability of $\pm$0.1°C. To cope with the wide experimental temperature range, all stopcocks were of the high vacuum type greased with Dow Corning silicone grease (Apiezon N was not adequate).

4. Operating Procedure

Although two types of experiments - sorption and desorption - were performed in the low pressure sorption system, the operating procedure of the latter was essentially only an extension of the former.

Before the apparatus was ready for the first experiment the total volume, V_T, of the sample bulb and its associated connecting lines was determined by the previously outlined method of gas expansion from the calibration bulb (see Appendix D.1). Except for this operation stopcock S_9 (Figure 16) was always kept closed.

To fill the sample bulb with polymer it was either cut from the system or disconnected at the ground glass joint. If the sample bulb had to be cut and reblown to the system, then the sample bulb was designed with a very narrow neck to ensure that the change in V_T during this procedure would be negligible. Once removed, the bulb was weighed, filled with polymer, and reweighed, to determine the weight and volume (knowing the density) of the polymer in the bulb.

In the case of the isotactic samples the polymer was in the form of small strips (cut from a film) of dimensions:

25 mm x 15 mm x 0.39 mm, while the atactic material was in the form of 6 mm cubes.

The bulb was then reattached to the system. In the case of the bulbs that had to be reblown into the system, care was exercised not to bring the torch too close to the polymer so that tis morphology remained unaltered.

With the sample in place the whole system was evacuated for at least 24 hours. During this time, the temperature of the box was raised to the level desired for the first run. To check if the polymer has been thoroughly outgassed, the stopcock sealing off the sample volume, S_1, was closed for 15 minutes while the other leg of the pressure transducer was kept open to the vacuum. If the pressure rise observed on the Baratron was significant, say >10 μ/hour, the evacuation was continued for another few hours and then the check repeated.

The rest of the system was checked for leaks by isolating the polymer with stopcock S_1 and closing the main stopcock just upstream of the pump, S_{10}. For a tight system no loss of vacuum would be detected by the thermocouple gauge over a period of 15 minutes. Occassionally a leak test was performed for the reference leg of the pressure transducer by closing stopcocks S_3 and S_2 (Figure 16) and exposing the other side of the transducer to the vacuum. If all those leak tests indicated that the system was neither leaking nor outgassing, then the system was ready for a run.

The following procedure was used for the sorption runs. The gas from the gas cylinder was passed over "Drierite" and delivered to a three-way stopcock through which the gas was flushed to the atmosphere for approximately 3 minutes. Then with stopcocks S_5, S_3 and S_1 closed the mercury manometer was pressurized and again degassed. This was repeated two more times whenever a change was made to a different gas. Following this, the manometer was pressurized to some convenient level, usually between 100 and 700 mm Hg, and allowed to come to the temperature of the box. Meanwhile the recorder was started.

Then at time zero stopcock S_1 was quickly opened and closed from the outside of the cabinet by means of wires attached to S_1, so as not to disturb the temperature equilibrium of the box. The pressure transducer followed the progress of diffusion by comparing the reference side, which was still at a vacuum, with the pressure in the sample volume. The pressure was recorded for the first 30 minutes and the data thus obtained was used to calculate diffusivities. While the run was proceeding, the initial pressure was read on the mercury manometer through a glass window at the front of the cabinet. Then after equilibrium was reached, i.e., no further pressure change was observed, the final pressure difference was read from the Baratron and used to calculate the solubility constant, k.

For desorption experiments the procedure was almost identical, except that when the gas was first introduced into the manometer, the stopcock to the sample volume, S_1, was left open. Thus, the

first significant measurement was the pressure after equilibration. To check if the polymer had come to equilibrium, stopcock S_1 was periodically closed. If no significant pressure drop across the transducer became apparent, the system had reached equilibrium.

At this point the Baratron meter was zeroed and set to "Null". The latter was recommended procedure whenever a pressure drop greater than what the transducer was designed for (30 mm Hg) was anticipated. Now the system was ready for the second stage of the experiment.

First, stopcock S_1 was closed and stopcocks S_3 and S_5 (Figure 16) were opened to evacuate that part of the system. The surge tank which was evacuated prior to the run was opened to the system by turning stopcock S_8. Next, the recorder was set into motion. Then, at time zero the sample volume was opened, at $t = 5$ seconds the ballast volume was closed, at $t = 10$ seconds the Baratron was turned from "Null" to "Operate", and at $t = 15$ seconds the sample volume was again isolated by closing S_1.

Depending on the method chosen to evaluate the data for diffusion constants, pressure was recorded for the first 30 minutes or first 6 hours. Finally, when the polymer had again come to equilibrium, the pressure was recorded once more and the solubility constant calculated.

E. High Pressure Sorption Experiments

1. Method

In principle, the high pressure sorption experiments were identical to those performed at low pressure. An evacuated sample of polymer was pressurized with gas and the solubility calculated from an observation of initial and equilibrium pressures.

The concentration of the sorbed gas in the polymer was determined from a material balance on the gas phase.

$$\begin{matrix}\text{moles of gas} \\ \text{admitted}\end{matrix} = \begin{matrix}\text{moles of gas} \\ \text{sorbed}\end{matrix} + \begin{matrix}\text{moles of gas in} \\ \text{void space}\end{matrix}$$

$$\left[\frac{V_a P_i}{RT_{a_i} Z_{a_i}} + \frac{V_b P_i}{RTZ_i}\right] = \left[\frac{CV_P P_o}{RT_o Z_o}\right] + \left[\frac{V_a P_f}{RT_{a_f} Z_{a_f}} + \frac{V_b P_f}{RTZ_f}\right] \quad (40)$$

In its most general form this reduces to

$$C = \frac{273 Z_o V_b}{TV_P}\left(\frac{P_i}{Z_i} - \frac{P_f}{Z_f}\right) + \frac{273 Z_o V_a}{V_P}\left(\frac{P_i}{Z_{a_i} T_{a_i}} - \frac{P_f}{Z_{a_f} T_{a_f}}\right) \quad \ldots. \quad (41)$$

where: C = concentration in cc(STP)/cc

P_i & P_f = initial and final pressures in atm

T_{a_i} & T_{a_f} = initial and final ambient temperatures in °K

T = thermostatted bath temperature in °K

V_p = volume of polymer in cc

V_a = volume of tubing in cc

V_b = void volume of bomb in cc

Z_i & Z_f = compressibility factors at (T & P_i) and (T & P_f)

Z_{a_i} & Z_{a_f} = compressibility factors at (T_a & P_i) and (T_a & P_f)

Z_o = compressibility factor at 273°K and 1 atm.

To generate the sorption isotherms more quickly, sequential operation was used. In other words, the pressure was raised immediately after each equilibration without prior degassing. The concentration after the second equilibration was then simply the sum of the initial concentration plus the change in concentration due to the sorption accompanying the incremental pressure change (see Appendix B.3 for sample calculation).

2. Apparatus

The equipment used for the high pressure sorption work is schematically shown in Figure 18. It was used essentially as built by Tam (103).

The major new feature was the use of a refrigeration unit (a 3/4 H.P. Freon compressor) which significantly extended the temperature range previously possible for the system. In conjunction with the heaters of the thermostatted bath, it facilitated operation at room temperature and made it possible to operate down to -40°C. Temperature stability was generally better than ±0.2°C over the temperature range of -40°C to 50°C.

All parts of the apparatus were fabricated from stainless steel (in contrast to all other equipment used in this study)

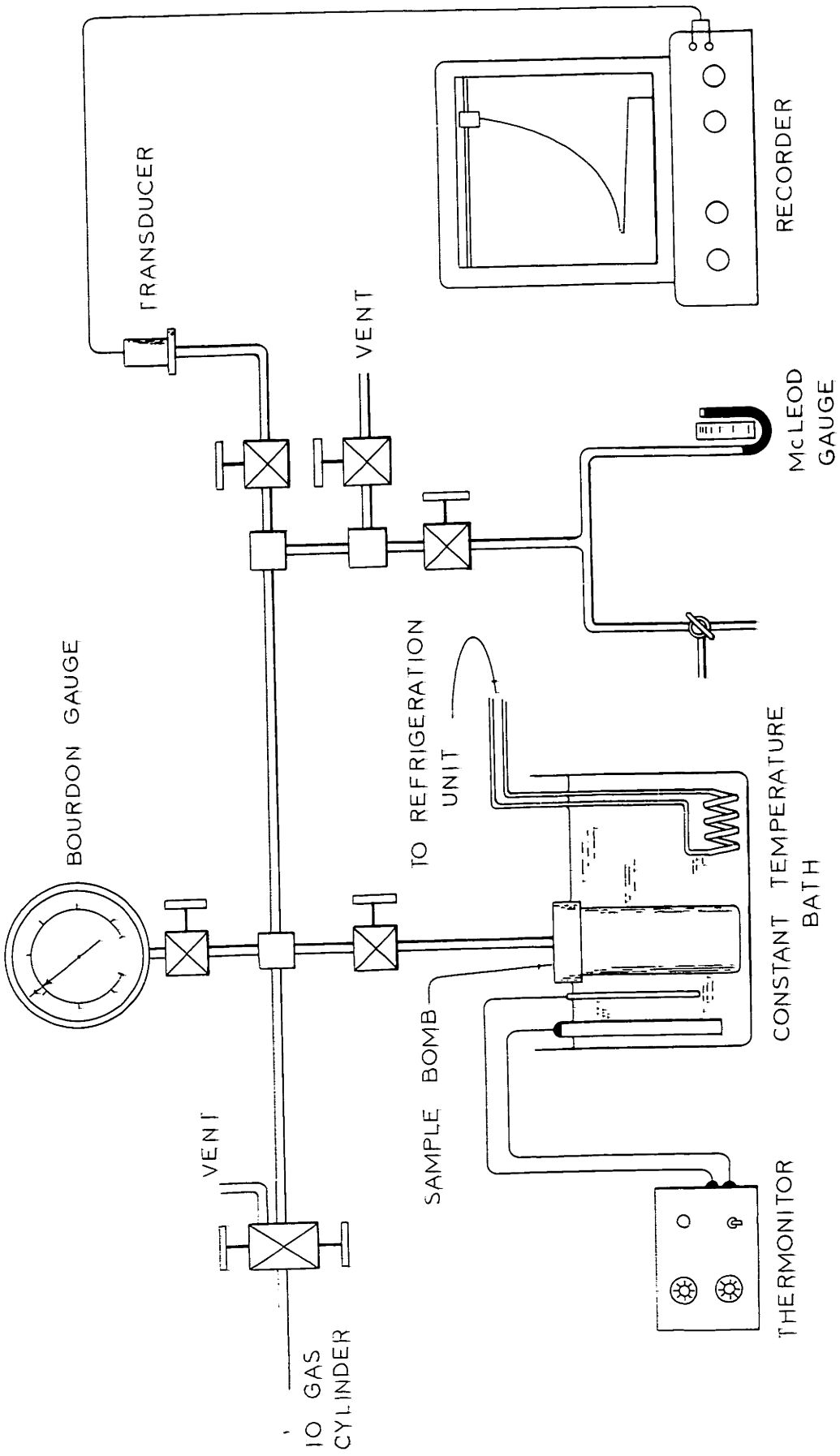

FIGURE 18, SCHEMATIC DIAGRAM OF THE HIGH PRESSURE SORPTION APPARATUS

and designed for 33 atmospheres pressure. Up to 20 atmospheres, the pressure was observed by a pressure transducer connected to a recorder but higher pressures could only be measured by a Bourdon gauge (with 5 psi being the smallest division).

The sample bomb was designed to accept a roll of polymer film so as to minimize the void space. The polymer film was rolled-up together with a thin, 1/4 inch, strip of film to ensure that each loop of the coil would be accessible to the gas. The bomb itself was immersed in the thermostatted bath mentioned above. The bath fluid was a 1:1 (by volume) mixture of ethylene glycol and water which gave ice-free operation down to -40°C. The percentage of the total volume of the system contained in the tubing (~7%) was always at the ambient temperature inside the enclosure surrounding the apparatus.

3. Operating Procedure

The volume of the empty system had previously been determined by Tam (L03). Then, knowing the density and weight of the polymer deposited in the bomb, the void volume, V_c, and the polymer volume, V_p, could be calculated.

Prior to any series of experiments the polymer was degassed for 18 - 24 hours. During the last two hours of degassing the desired bath temperature was established by proper adjustment of the refrigeration unit and the heaters.

Finally, with the recorder turned on and the valve to the pump closed, the gas was admitted to the system at the desired

initial pressure (2 - 3 atmospheres). After the pressure had dropped to its equilibrium value, more gas was admitted and again allowed to equilibrate. This process was repeated in increments of approximately 5 atmospheres until the maximum experimental pressure of about 30 atmospheres was reached.

After each addition of gas and at each equilibration the transducer pressure, gauge pressure and ambient temperature were recorded.

F. Film Characterization

1. Density

The density of all polymer films was determined using isopropyl alcohol-water density gradient columns. Three columns with density ranges of 0.8750-0.8950 gm/cc, 0.8900-.9100 gm/cc, and 0.9050-0.9250 gm/cc were established at 23°C and calibrated with glass beads accurately ground to specific densities (supplied by Scientific Glass Apparatus Co.). Generally, the densities of three samples, cut from different regions of the same film, were determined and agreed to $\pm$0.0003 gm/cc.

Knowing the density of completely crystalline (monoclinic) material, ρ_c = 0.9360 gm/cc (94), and the density of completely amorphous material, ρ_a = 0.858 gm/cc (94, 95) the amorphous volume fraction, α, in any partially crystalline sample could be calculated from:

$$\alpha = \frac{\rho_c - \rho}{\rho_c - \rho_a} \qquad (42)$$

where ρ is the measured density of the sample.

The density of the atactic material was determined by weighing a consolidated piece of it in air and in water. A trace of wetting agent was used to prevent bubbles from clinging to the surface.

2. Film Thickness

The thickness of most film samples was measured with a Pratt and Whitney supermicrometer, having an accuracy of ±.00001 inches. Occassionally an Ames micrometer with an accuracy of ±.00005 inches was used.

For each film the test area was roughly divided into 15 to 20 equal areas and the thickness measured at each location. An arithmetic average of the values obtained was taken as the film thickness. For a number of films this average value was compared with one evaluated on the basis of a more exact and elaborate technique suggested by Parker (88). Even for the thinnest films the difference between the two averages was never more than 0.5%.

3. Optical Microscope

One of the techniques used to detect differences in morphology was observation of the films under the Wild M-20 optical microscope. Since the films, as molded, were too thick for light transmission microscopy and lacked surface texture, film samples were imbedded in expoxy and thin sections microtomed on the LKB 4800A Ultrotome (Sweden). The samples were usually viewed under crossed polarizers at a magnification of approximately 400.

4. Electron Microscope

For finer details of the structure various samples were viewed under the Philips EM-200 electron microscope. Three different approaches were used.

In one case thin cross-sections (~600Å) were microtomed from samples of the films and observed under direct electron transmission of an enlargement of 31,000.

Other micrographs were taken of samples broken in liquid helium and some broken in liquid nitrogen. A long-handled, brass screw-device illustrated in Figure 19 was designed to break film samples while completely submerged in liquid helium. The fracture surface was then replicated by the following technique.

First, an impression was taken of the fracture surface by overlaying it with cellulose nitrate replicating tape moistened in methyl acetate, allowing the tape to dry and peeling it carefully from the specimen. Then the imprint on the tape was shadowed with chromium at an angle of 27° and coated with a thin layer of carbon. Finally the carbon-chromium replica, left after dissolving away the cellulose nitrate tape in butyl acetate at 60°C, was examined under the electron microscope.

A third approach followed a technique recently developed by Keith and Padden (85). Isotactic poly(propylene) was crystallized in the presence of 50% (by weight) atactic material which was later leached out, leaving behind a crystalline skeleton

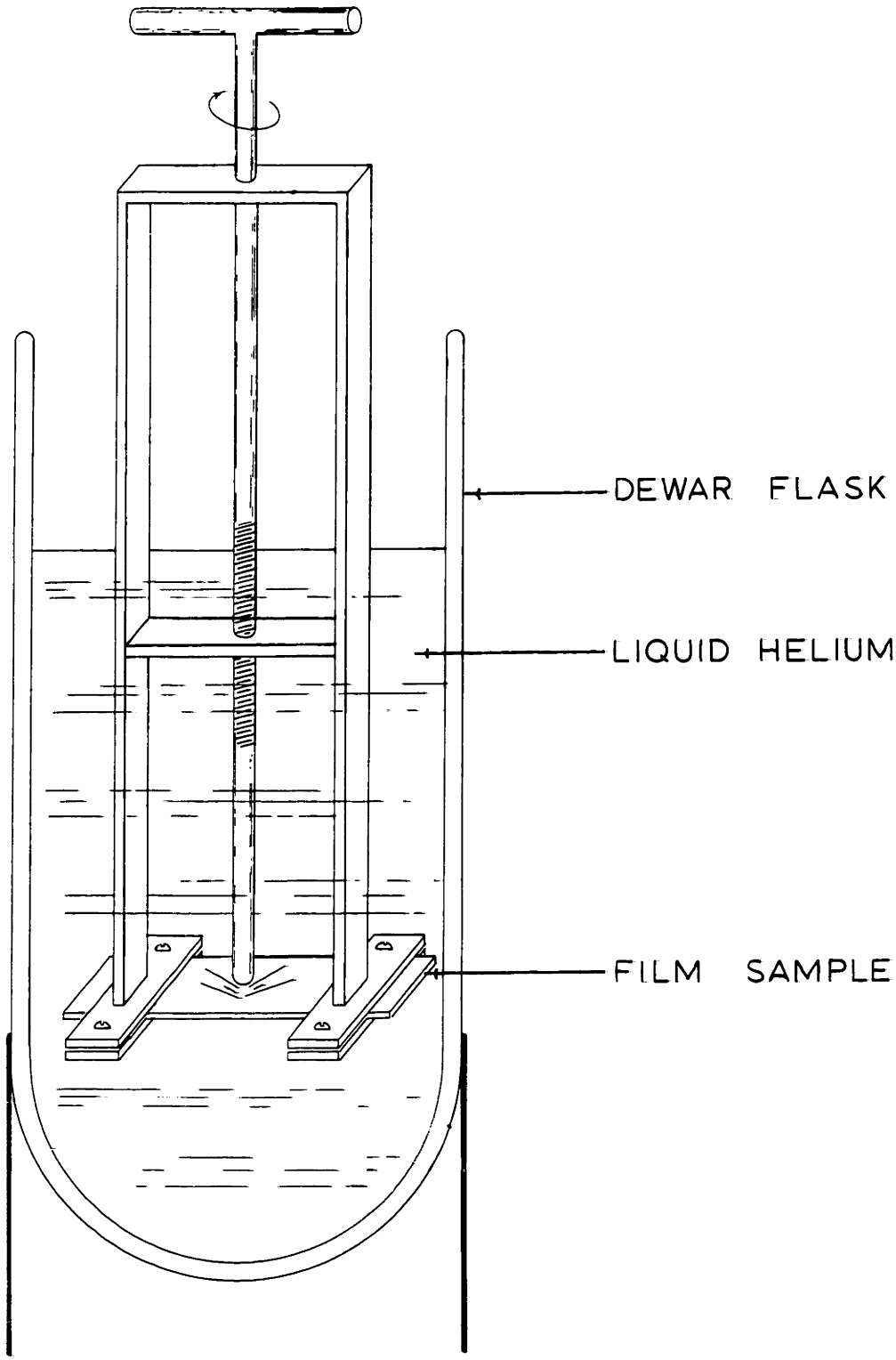

FIGURE 19. DEVICE FOR FRACTURING SAMPLES IN LIQUID HELIUM

suitable for examination by transmission electron microscopy. Although this system represents crystallization in a "very impure" melt, the situation in an actual melt may be much like this because of the inevitable presence of low molecular weight and stereo-irregular material in any commercial isotactic poly(propylene).

5. X-Ray Diffraction

Through the generous assistance of the Dow Chemical Company (107) it became possible to examine two films of widely different thermal histories by x-ray diffraction. By carefully analyzing the x-ray diffraction patterns obtained, it was possible to determine percent crystallinity, crystallite orientation and mean crystallite size. Crystallinity was determined in the customary way by measuring the area under the Bragg peaks, distinguishing between an amorphous halo and the area under the crystalline peaks. Crystallite size was calculated from line broadening according to the method described by Klug and Alexander (56) using angular width at half maximum intensity over the five peaks observed for propylene.

6. Calorimetric Measurements

a. DTA.

Du Pont's 900 Differential Thermal Analyzer (DTA) was used to detect first- and second-order transitions in samples of atactic and isotactic poly(propylene). The DTA measures differences in temperature between the sample and an inert reference while both are being heated at a uniform rate.

Whenever the sample undergoes a physical change during the heating, its temperature will change momentarily with respect to the reference material and this is recorded by the instrument. The instrument is capable of detecting temperature differences as small as 0.025°C.

The samples were scanned over a temperature range of -80°C to 200°C at heating rates of 10 to 30°C/min. The reference material was fine glass beads. The isotactic samples were either molding pellets ground to powder or finely cut-up pieces of film. The soft, tacky atactic material could be analyzed as supplied.

b. DSC.

Further attempts at characterizing the thermal behavior of isotactic and atactic samples centered around Perkin-Elmer's Differential Scanning Calorimeter (DSC-1). The instrument observes thermal changes in a sample by recording differences in power requirements, between the sample and an inert reference, to maintain both at the same temperature.

The thermograms were analyzed by comparing the area under the endothermic peak for crystalline poly(propylene) with the area observed for a known weight of Indium. Since every melting peak on the DSC was accompanied by a marked base-line shift, the area under the peak was evaluated according to a method suggested by Ralston (92). A vertical line was drawn through the lowest point of each peak and tangents were drawn from it to the lines "approaching" and "leaving" the peak. This method is

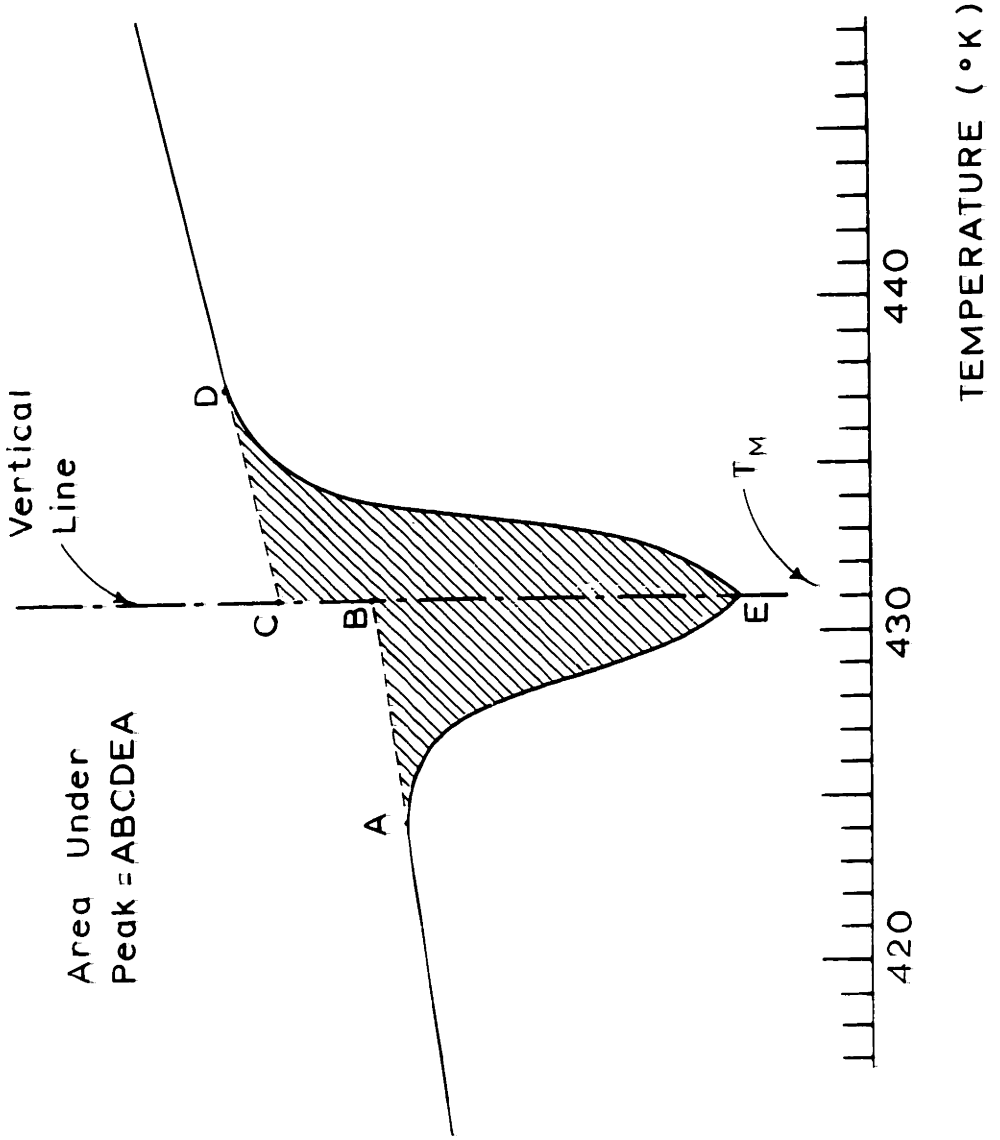

FIGURE 20. DSC THERMOGRAM

illustrated in Figure 20. The lowest point of each peak was interpreted as the melting point, T_M.

Heating rates of 10 to 20°C/minute were used with sample weights of 4 to 12 mg, determined on a Model 1801 Satorius Balance to an accuracy of $\pm$.0005 mg. The temperature range was room temperature to approximately 30°C above the melting point.

To check for glass transition temperatures several atactic and isotactic samples were scanned separately over a temperature range of -100°C to 100°C.

IV. RESULTS

TABLE III

PROPERTIES OF FILMS STUDIED

Film	Description	ℓ	$\rho_{23°C}$	α^*
		cm.	g/cm.	%
1	RA	0.0388	0.8920	56.5
2	RA	—	o.8923	56.0
3	RA	0.0370	0.8940	53.0
3a	RA-150	0.0364	0.9145	27.5
4	RA-150	0.0388	0.9132	29.0
5	RA-150	—	0.9135	28.7
6	MA	0.0427	0.9012	44.5
7	MA-80	0.0427	0.9020	43.5
8	MA-100	0.0442	0.9065	37.8
9	MA-110	0.0405	0.9069	37.3
10	MA-130	0.0410	0.9106	32.6
11	MA-140	0.0436	0.9105	32.7
12	MA-150	0.0431	0.9136	28.8
13	MA-150	0.0388	0.9132	29.0
14	MA	0.0372	0.8963	51.0
14a	MA-150	0.0369	0.9136	28.8
15	SA	0.0383	0.9055	39.0
16	SA-150	0.0396	0.9123	30.5
17	RH	0.1161	0.8971	50.0
18	RH	0.1039	0.8963	51.0
19	RH-150	0.1105	0.9119	31.0
20	MH	0.0901	0.8970	50.0

TABLE III (Cont'd.)

Film	Description	ℓ	$\rho_{23°C}$	α^*
		cm.	g/cm.^{3}	%
21	MH-150	0.0899	0.9127	29.5
22	SH	0.1129	0.9055	39.0
23	SH-150	0.1130	0.9117	31.0
24	RF	0.0148	0.8953	52.2
24a**	RF-150	0.0148	0.9150	27.0
25	MF	0.0169	0.8952	52.4
25a**	MF-150	0.0169	0.9144	27.5
26	SF	0.0154	0.9063	38.2
26a**	SF-150	0.0154	0.9148	27.4
27	cast	0.0178	0.8907	58.0
atactic	cubes	0.60	0.8580	100.0

*calculated from $\alpha = \frac{\rho_c - \rho}{\rho_c - \rho_a} \times 100$, where: $\rho_c = 0.9360$ g/cm. $\rho_a = 0.8580$ g/cm.

**in each case the "a" film is the immediately preceeding film, after annealing

Key: RA-150
- annealing temperature (°C)
- gas studied with (Argon, Helium, Freon 14)
- rate of cooling from melt

For fuller explanation see Table II and section III B,3

TABLE IV

PHYSICAL PROPERTIES OF THE GAS MOLECULES USED

Gas	Mol.Wt.	d	d^2	ϵ/k	$\bar{V}$	T_c
		(A°)	$(A°)^2$	°K	cc/gmole	°K
He	4	2.2	4.8	10	39	5.3
A	40	3.6	12.9	122	42	151
CO_2	44	3.7	16.4	189	40	304
CH_4	16	4.2	17.6	148	52	191
CF_4	88	4.6	21.1	152	75*	228

* estimated from plot of $\frac{\bar{V}}{V_c}$ vs. $\frac{T}{T_c}$ by Prausnitz (90)

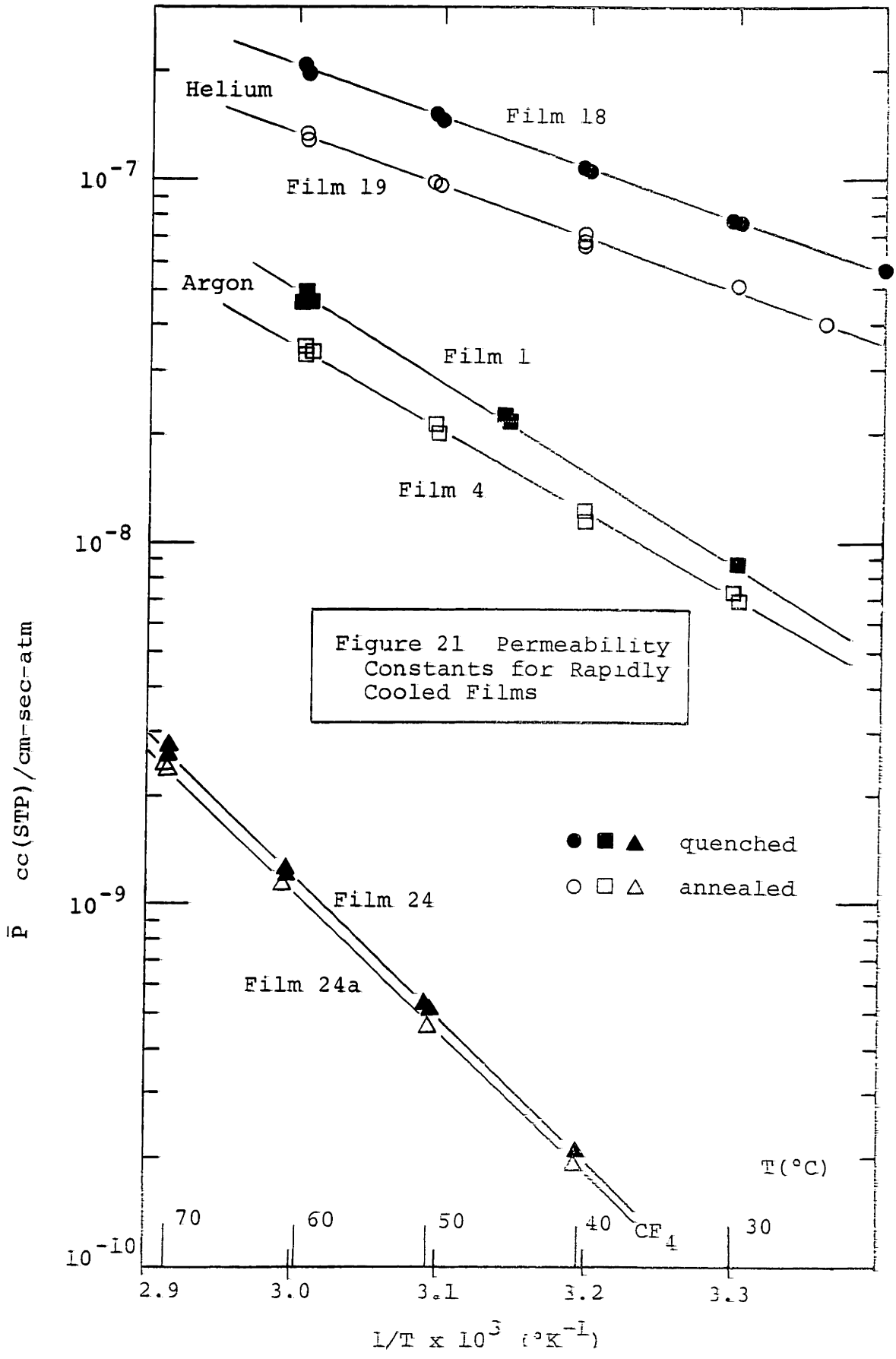

Figure 21 Permeability Constants for Rapidly Cooled Films

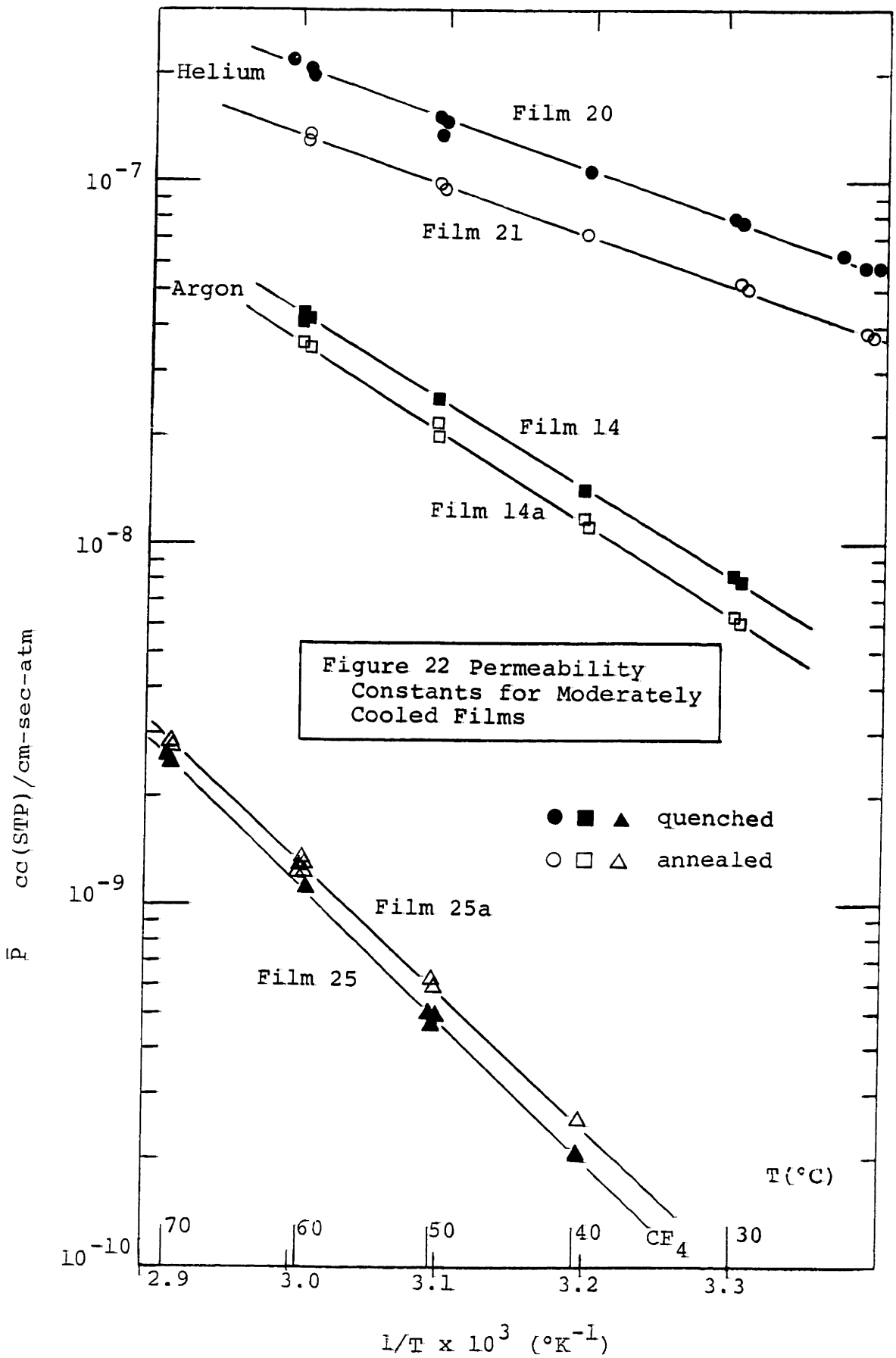
Helium
Film 20
Film 21
Argon
Film 14
Film 14a
Figure 22 Permeability Constants for Moderately Cooled Films
quenched
annealed
Film 25a
Film 25
10^{-7}
10^{-8}
10^{-9}
10^{-10}
$\bar{P}$ cc(STP)/cm-sec-atm
T(°C)
70
60
50
40
30
CF_4
2.9
3.0
3.1
3.2
3.3
$1/T \times 10^3$ ($°K^{-1}$)

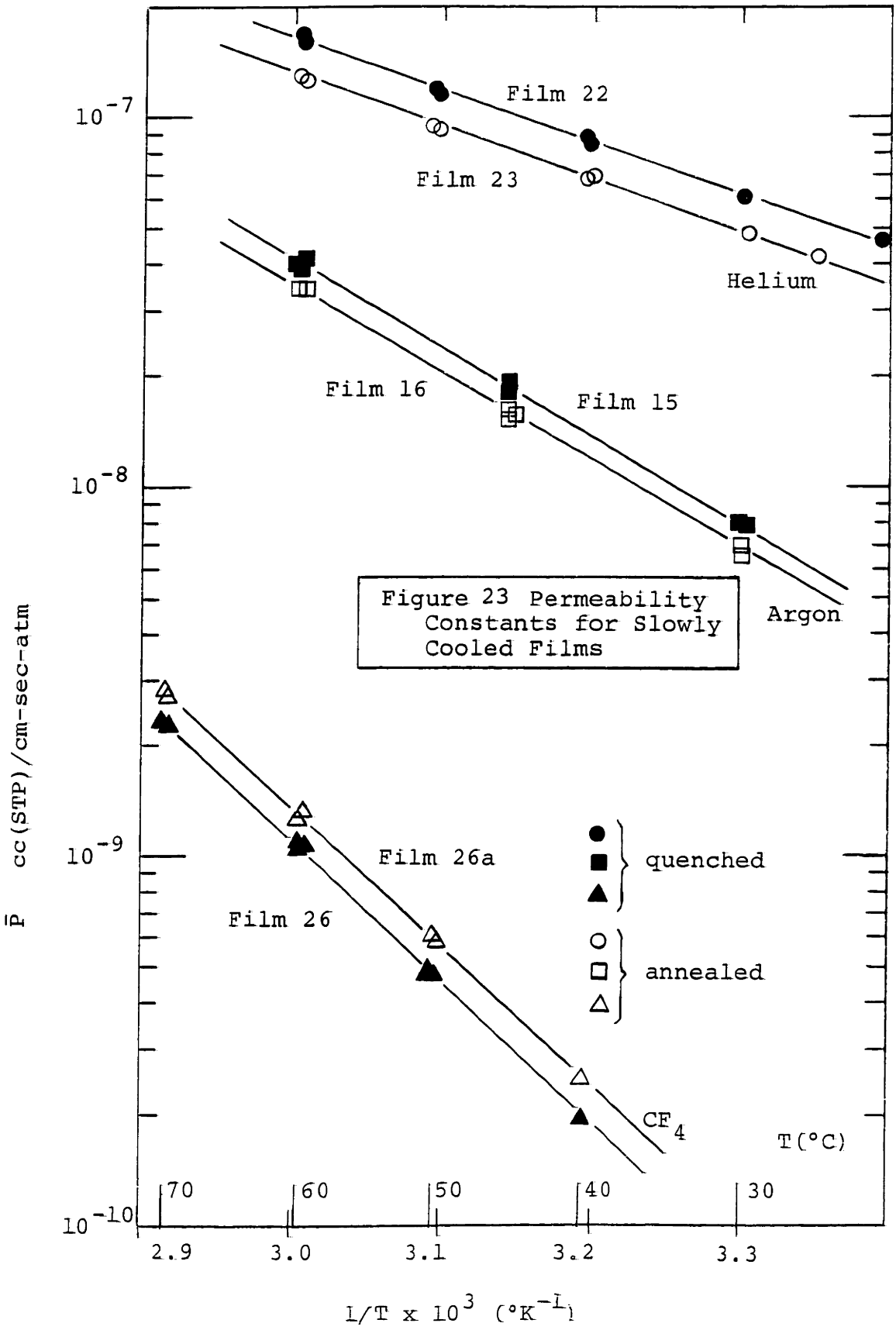

Figure 23 Permeability Constants for Slowly Cooled Films

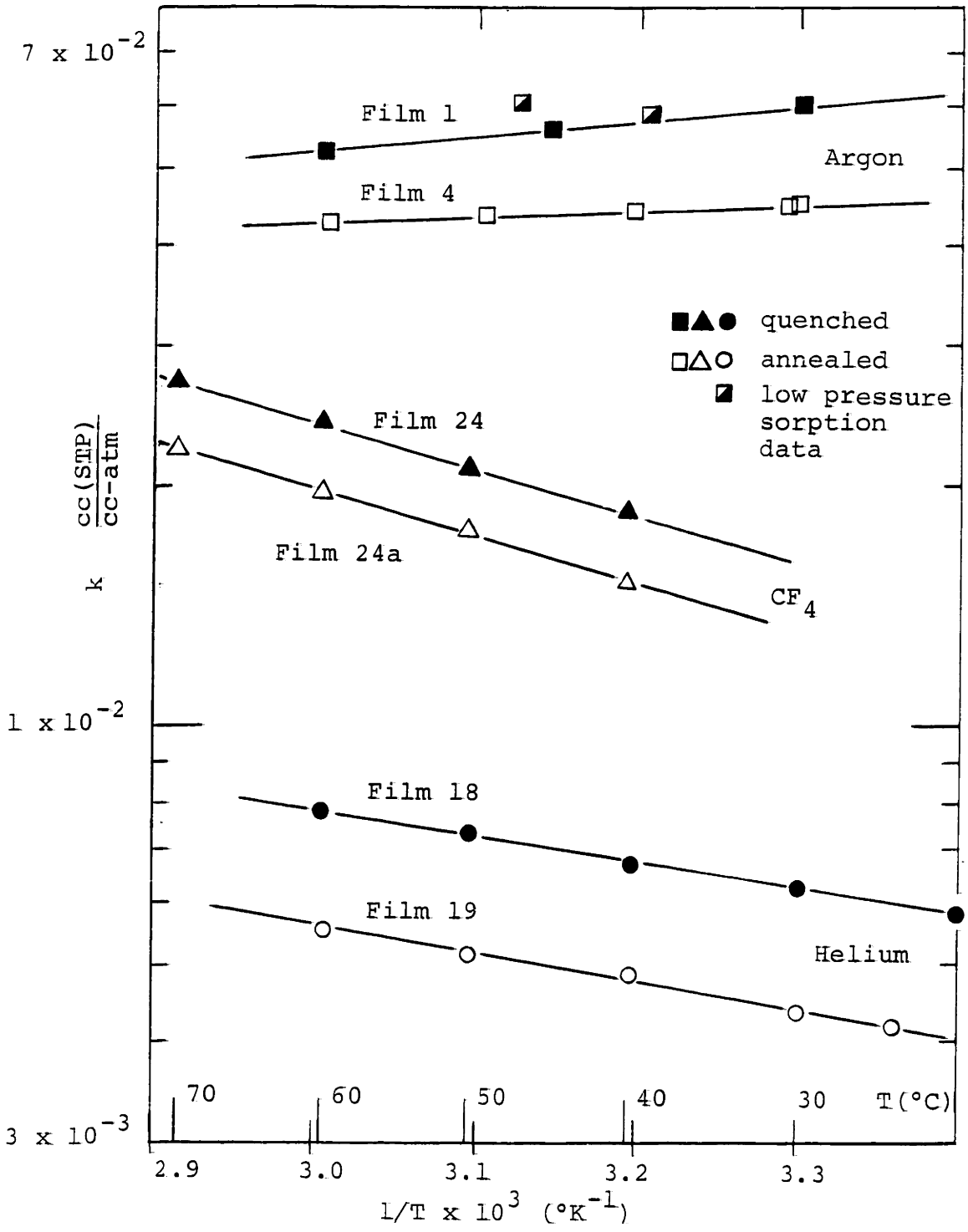

Figure 24 Solubility Constants for Rapidly Cooled Films

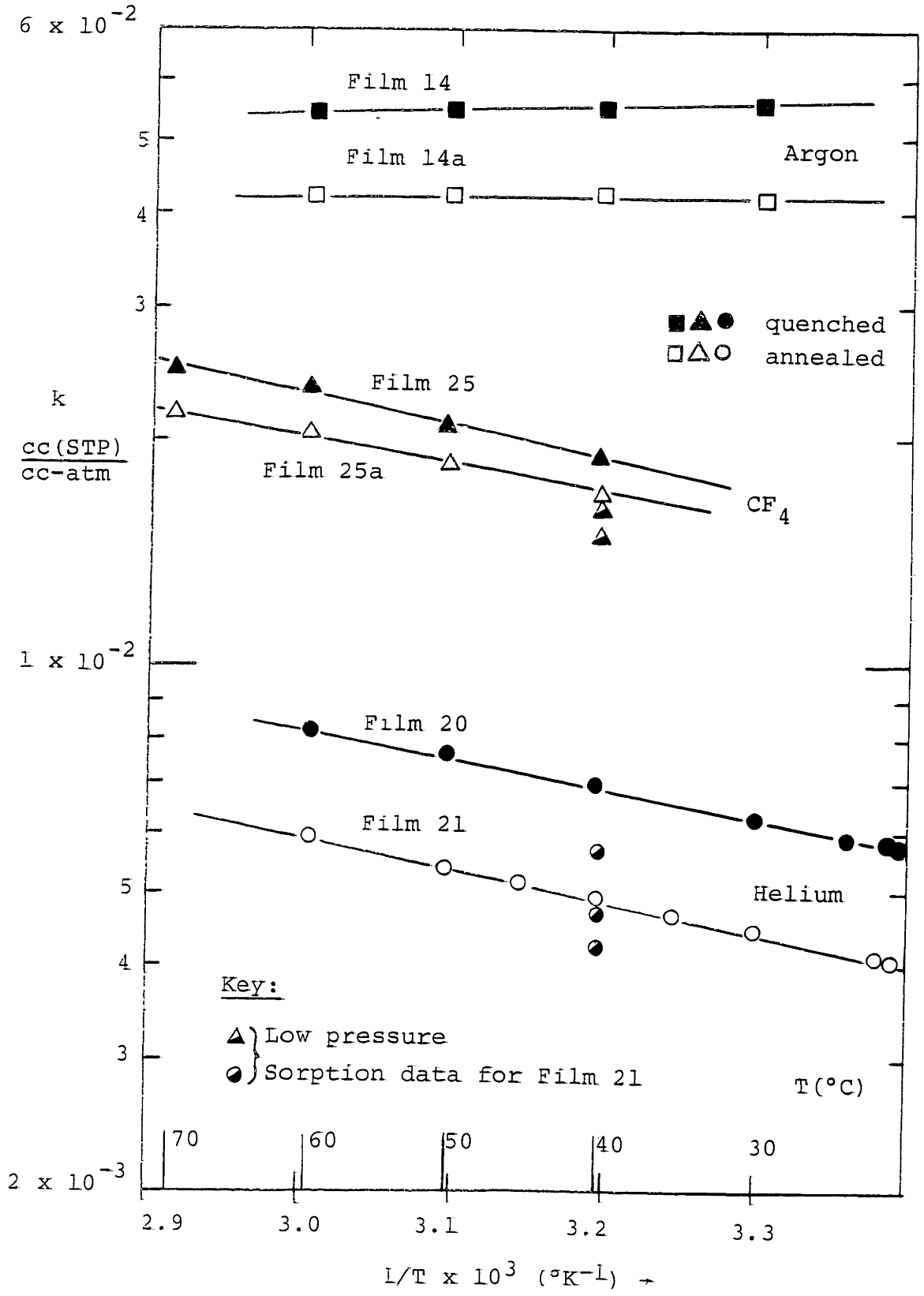

Figure 25 Solubility Constants for Moderately Cooled Films

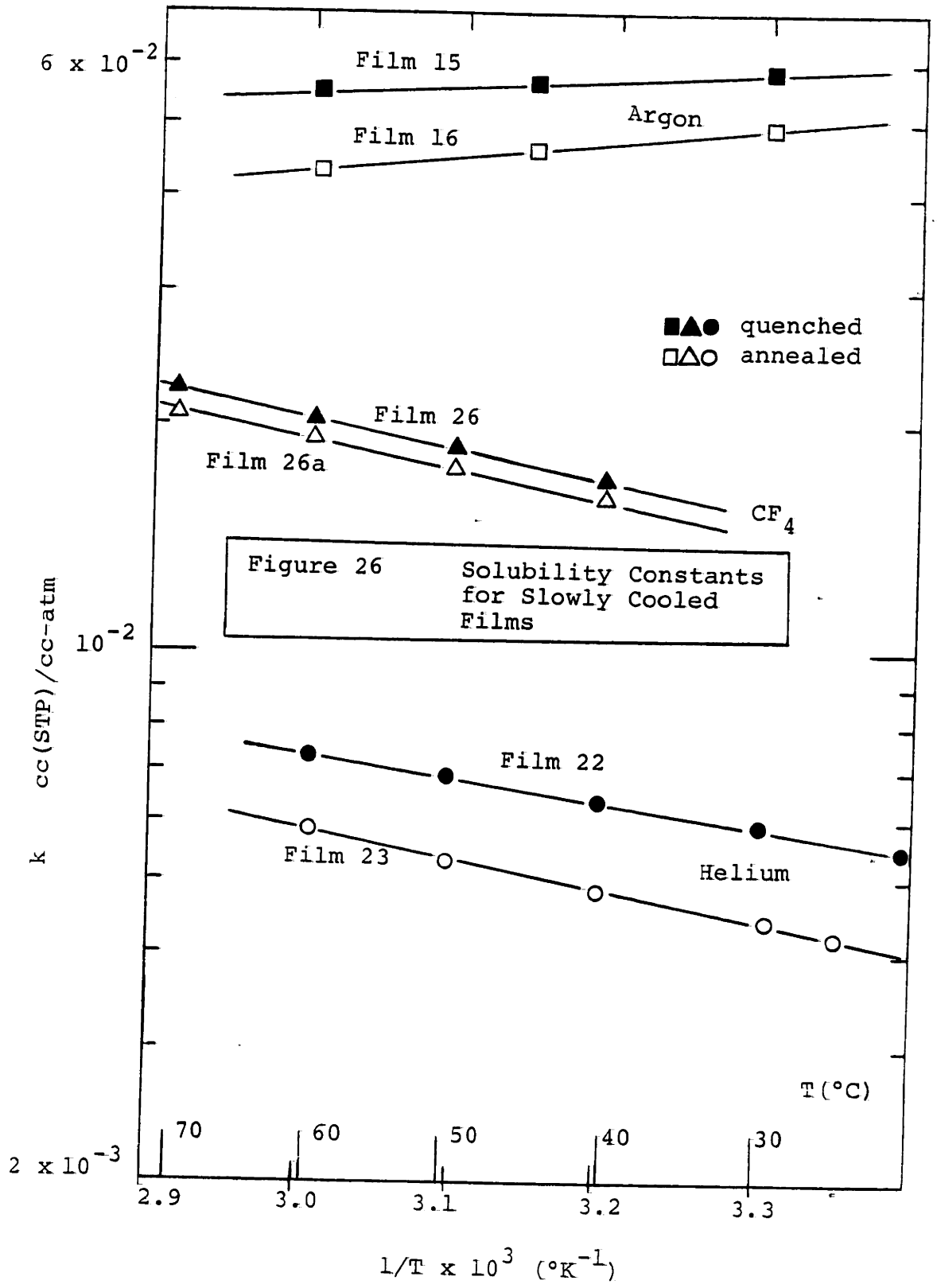

Figure 26 Solubility Constants for Slowly Cooled Films

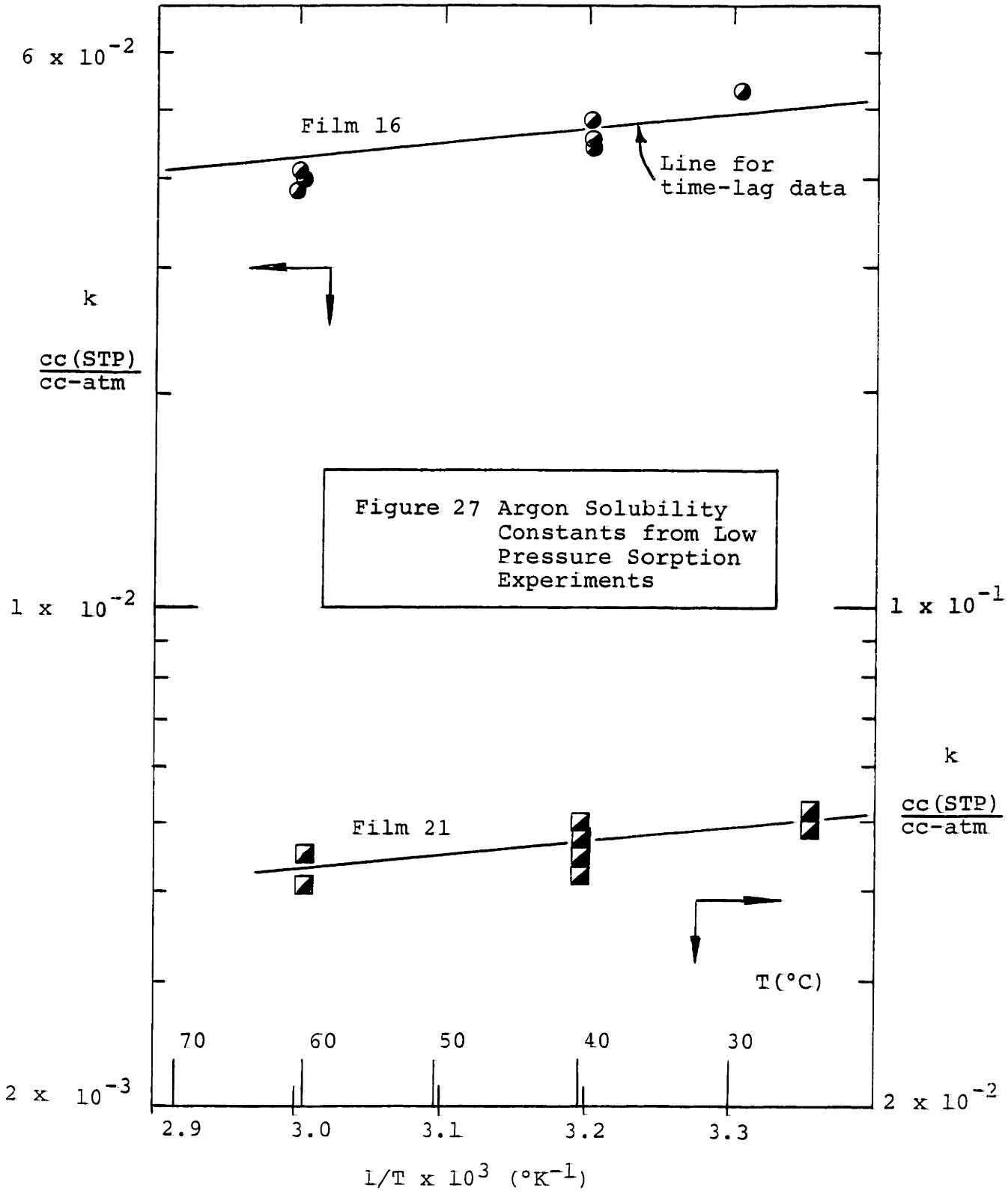

Figure 27 Argon Solubility Constants from Low Pressure Sorption Experiments

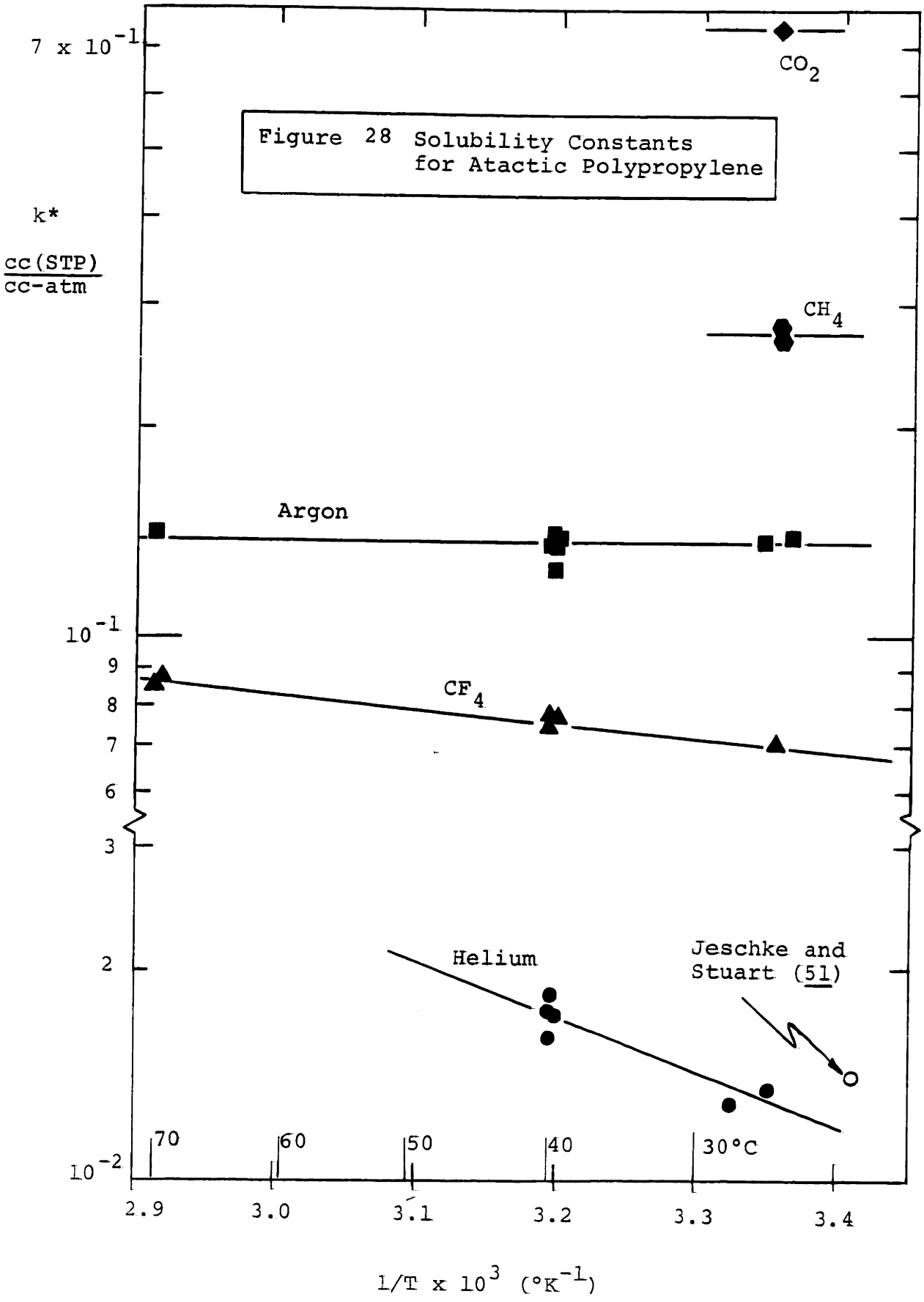

Figure 28 Solubility Constants for Atactic Polypropylene

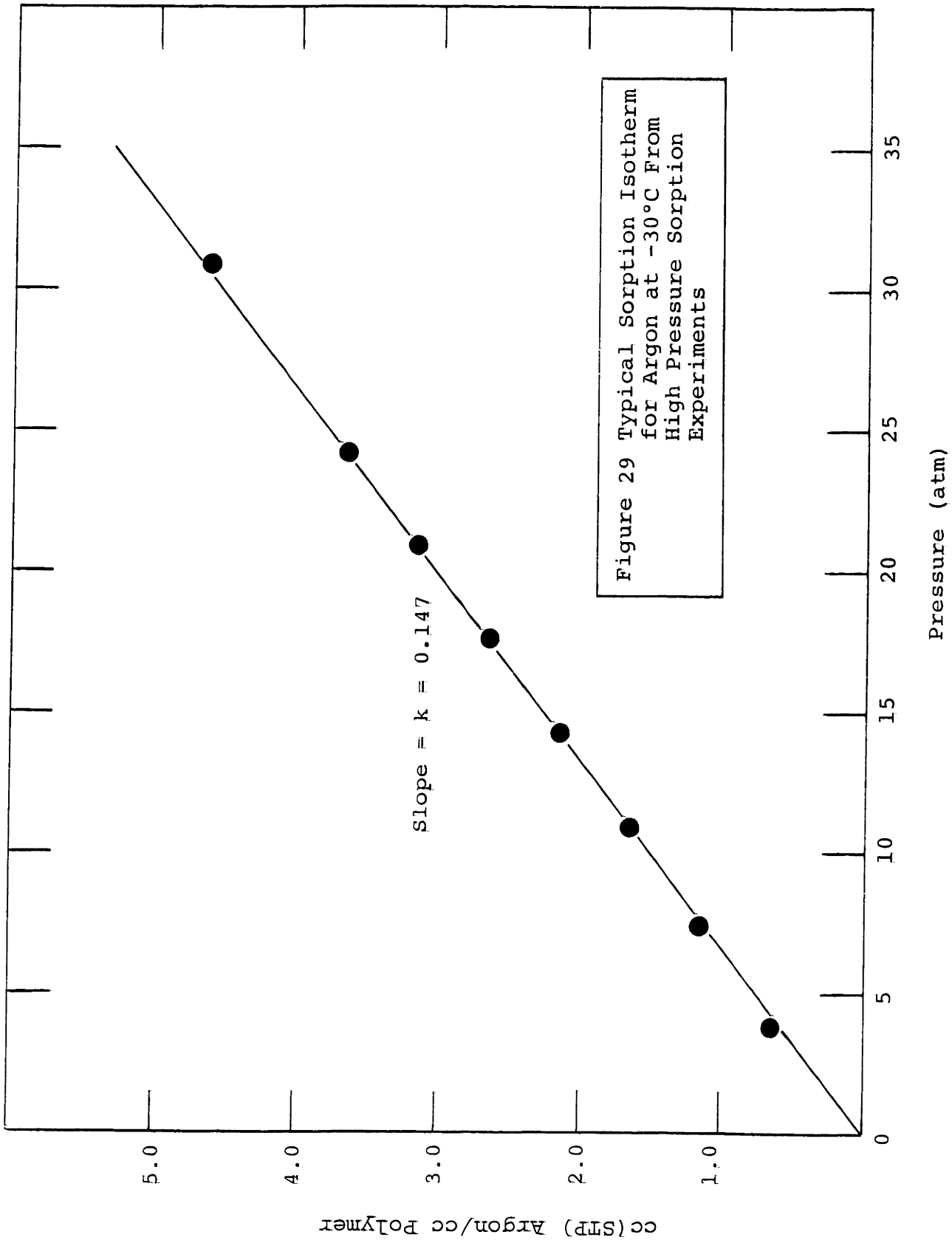

Figure 29 Typical Sorption Isotherm for Argon at -30°C From High Pressure Sorption Experiments

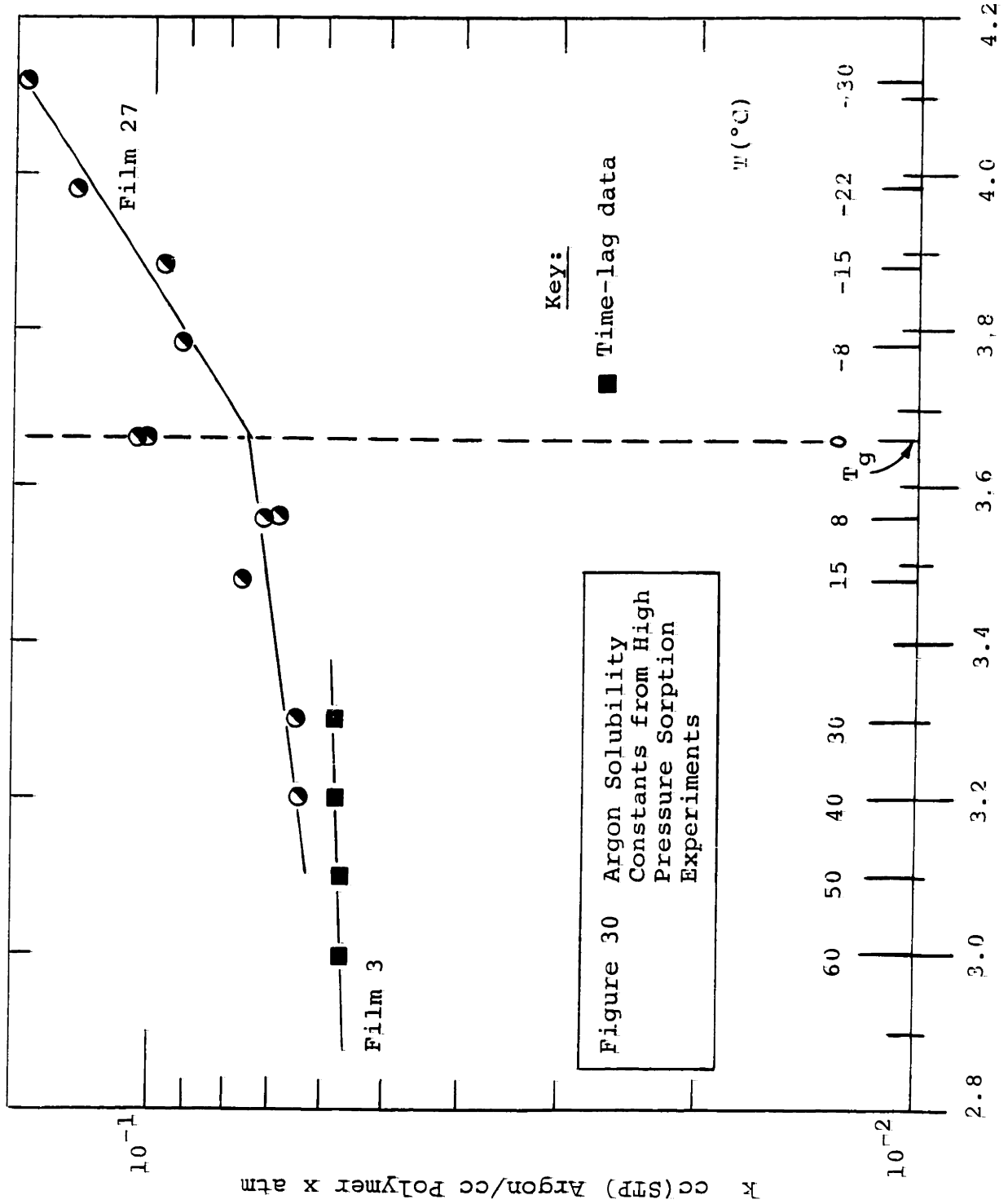

Figure 30 Argon Solubility Constants from High Pressure Sorption Experiments

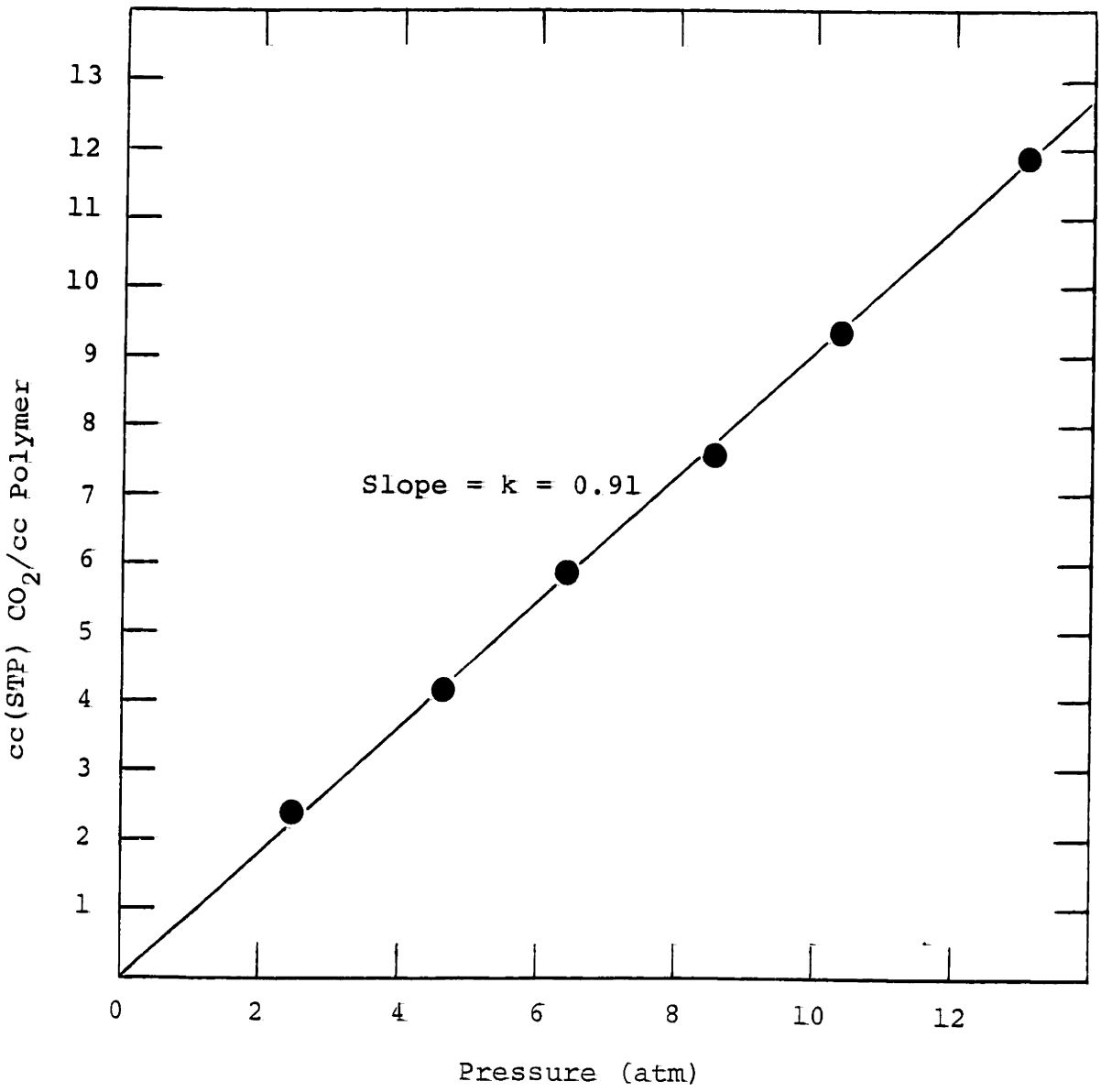

Figure 31 Typical Sorption Isotherm for Carbon Dioxide at -20°C (from high pressure sorption experiments)

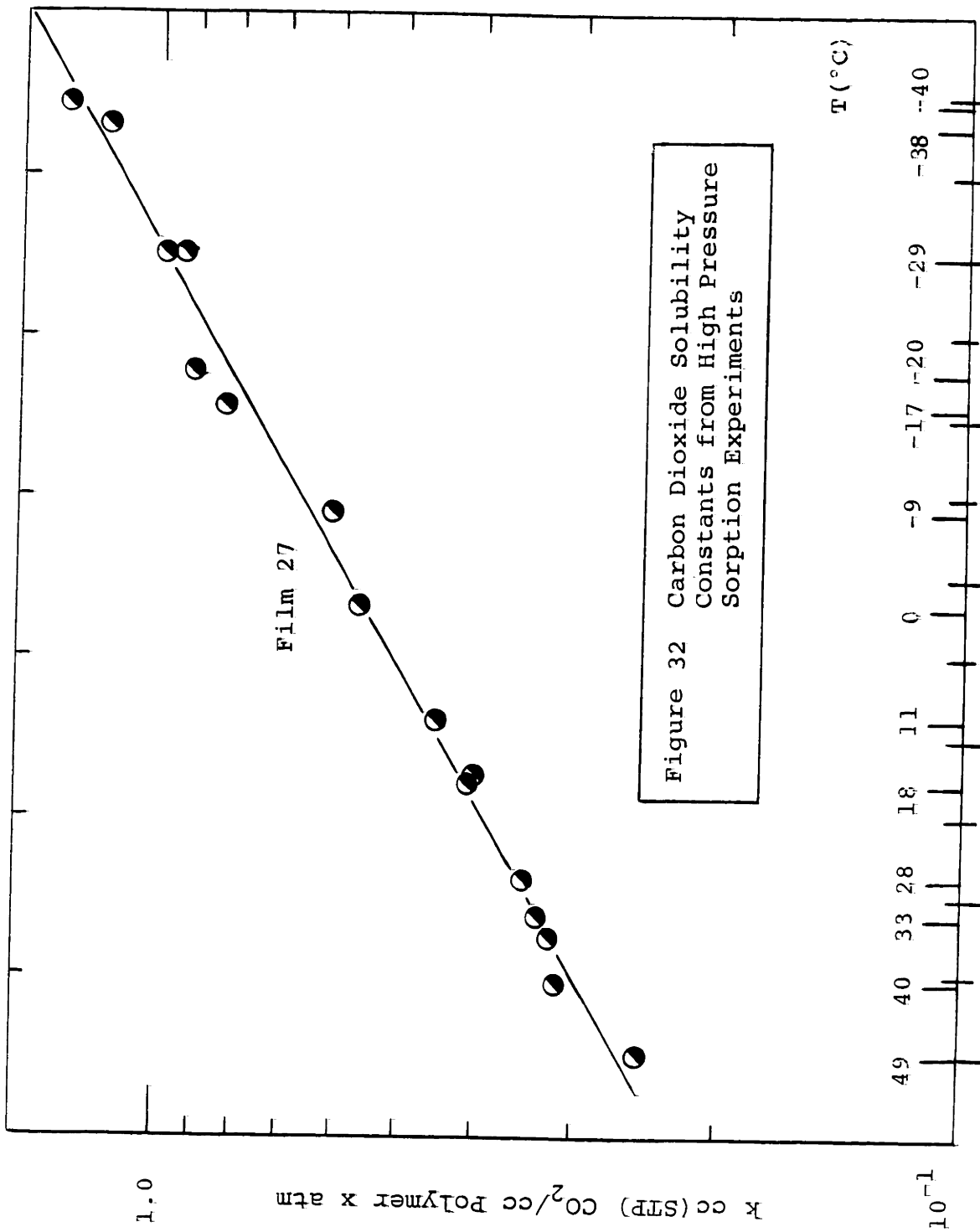

Figure 32 Carbon Dioxide Solubility Constants from High Pressure Sorption Experiments

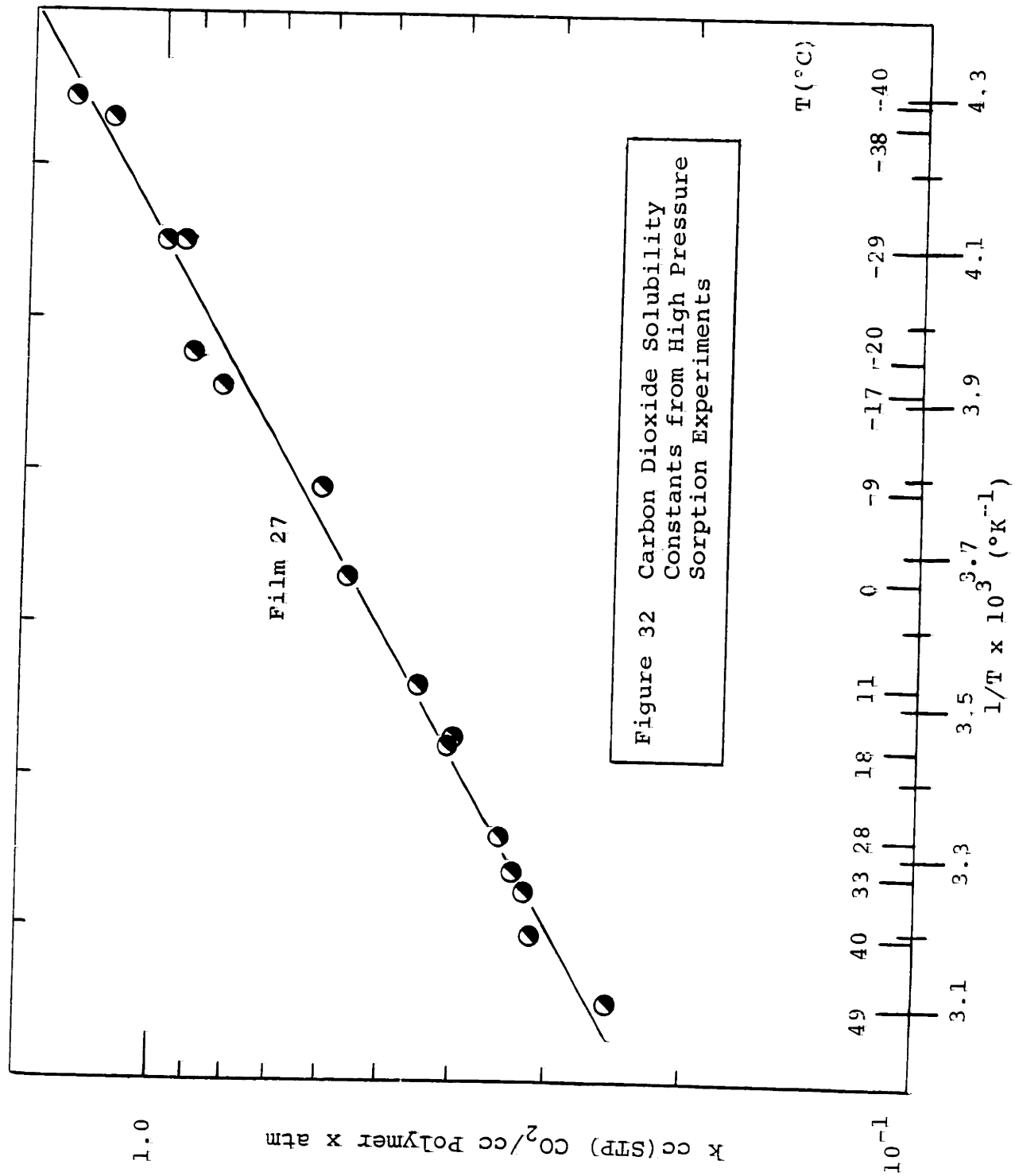

Figure 32 Carbon Dioxide Solubility Constants from High Pressure Sorption Experiments

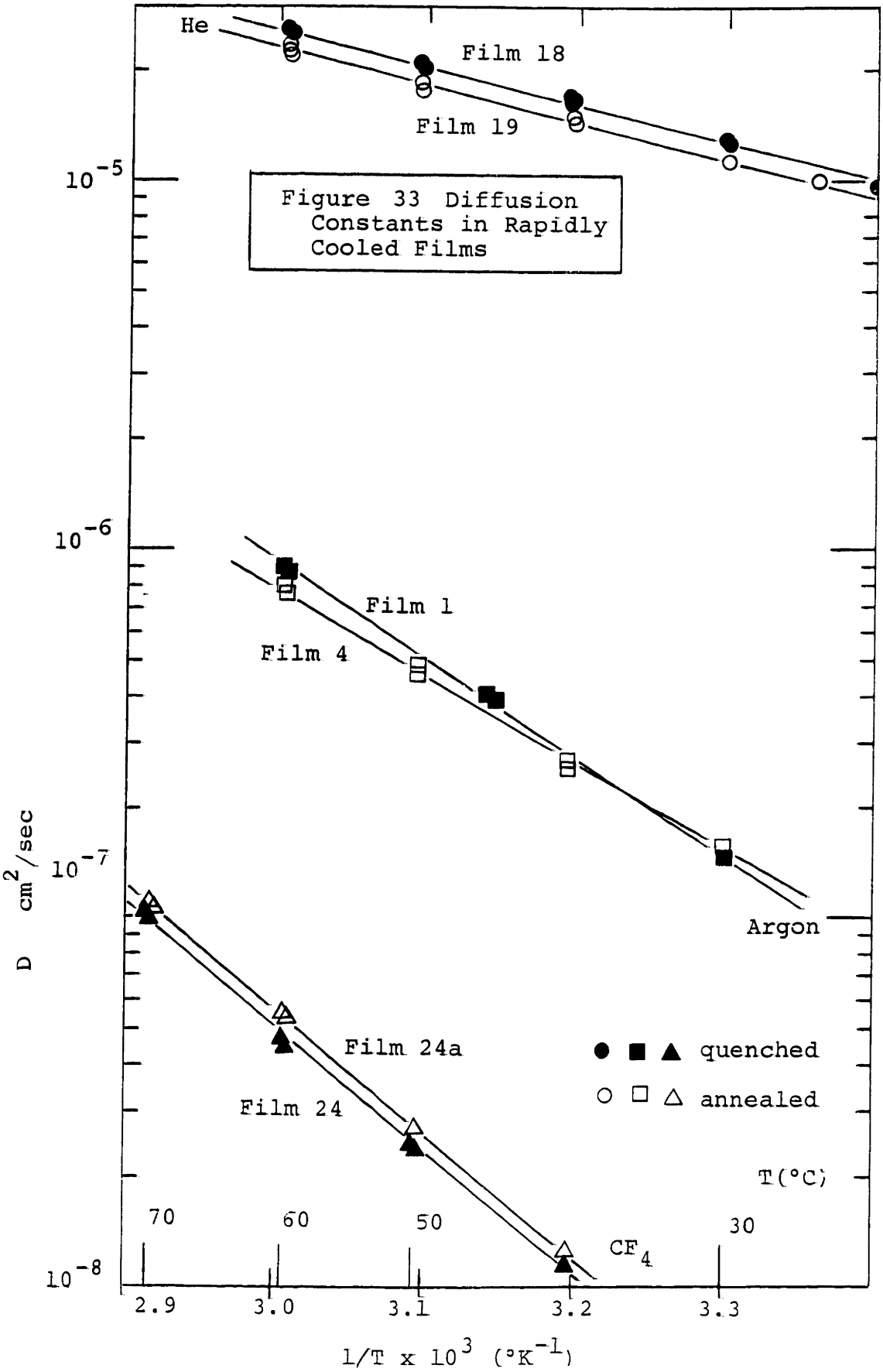

Figure 33 Diffusion Constants in Rapidly Cooled Films

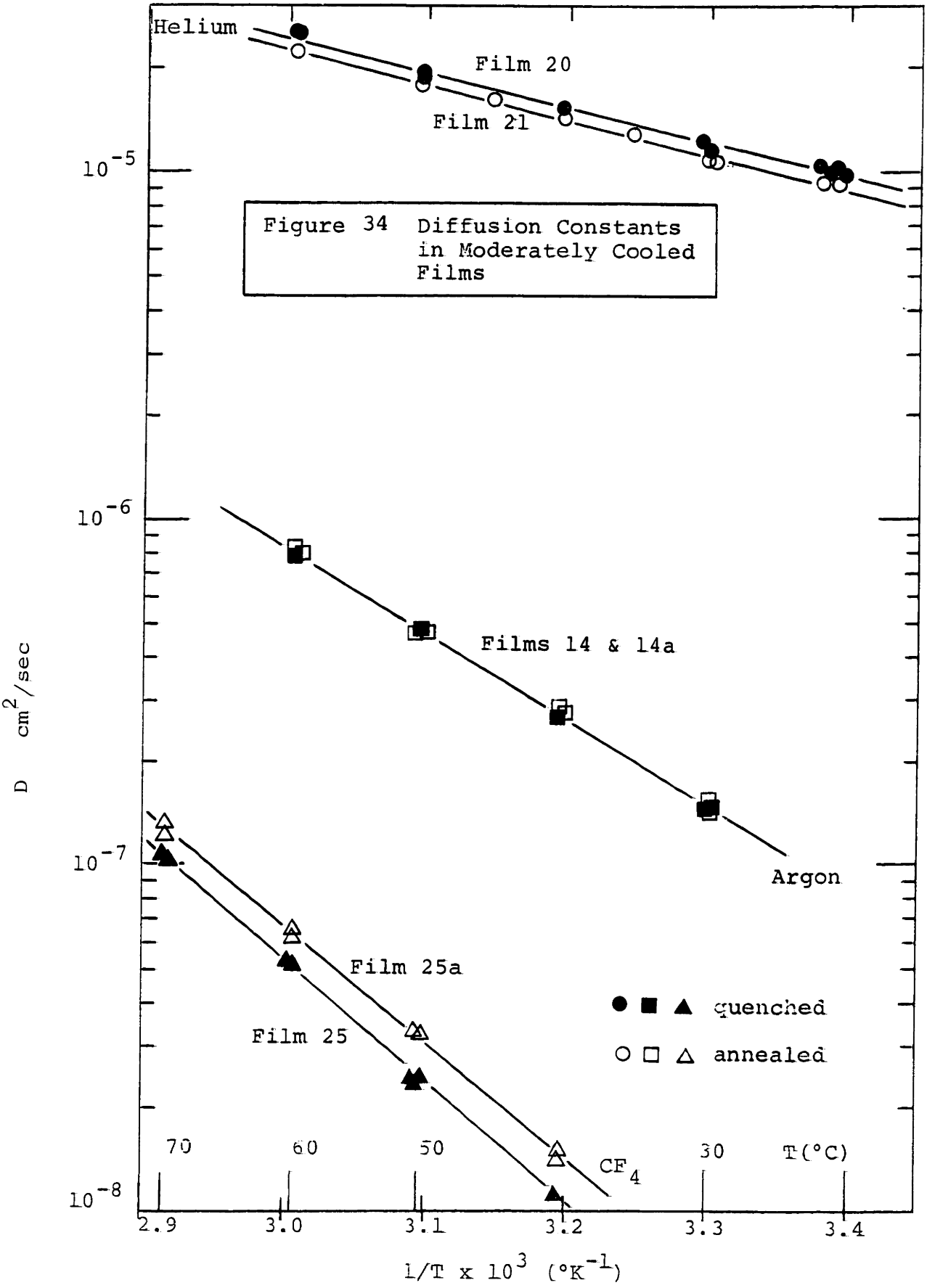

Figure 34 Diffusion Constants in Moderately Cooled Films

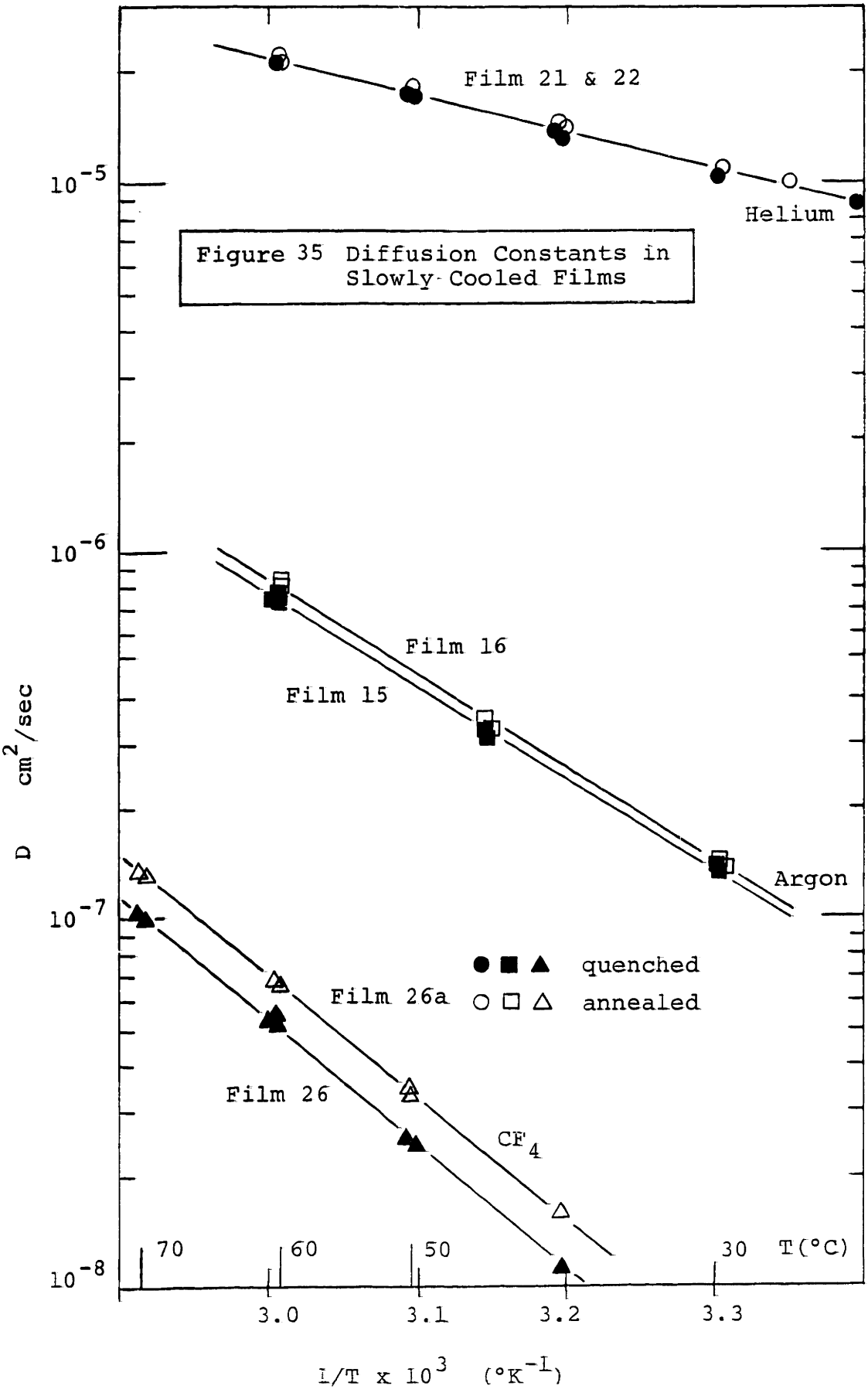

Figure 35 Diffusion Constants in Slowly Cooled Films

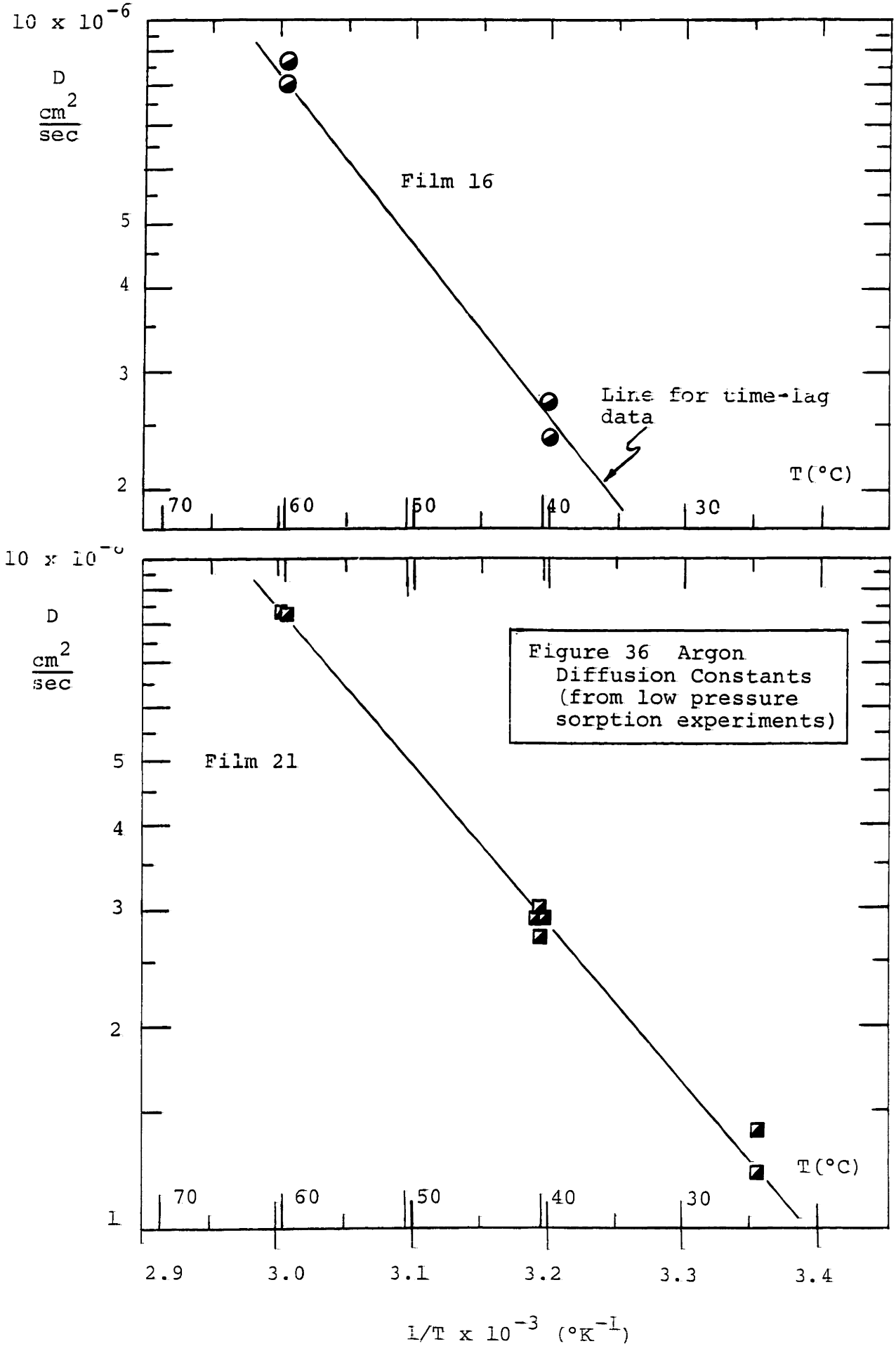

Figure 36 Argon Diffusion Constants (from low pressure sorption experiments)

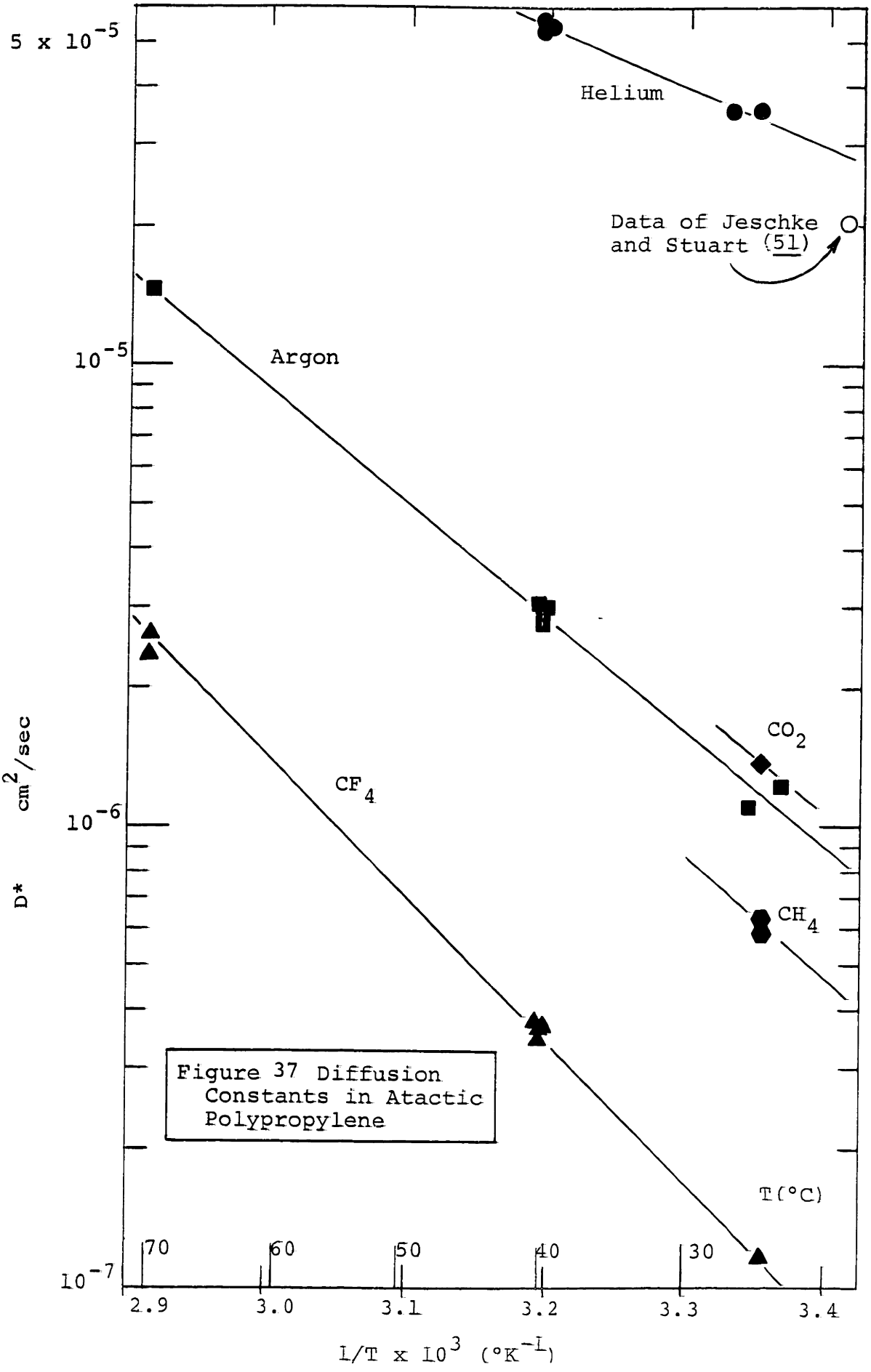

Figure 37 Diffusion Constants in Atactic Polypropylene

TABLE V

ACTIVATION ENERGIES AND ENTHALPIES OF SORPTION

Film	Description	α %	Gas	E_P Kcals. gmol.	E_D Kcals. gmol.	ΔH_S Kcals. gmol.
1	RA	56.5	A	11.4	12.2	-0.8
3	RA	53.0	A	11.9	11.8	-0.1
3a	RA-150	27.5	A	11.1	11.3	-0.3
4	RA-150	29.0	A	10.5	11.4	-0.8
6	MA	44.5	A	11.4	12.2	-0.9
7	MA-80	43.5	A	9.9	11.5	-1.6
8	MA-100	37.8	A	10.2	11.2	-1.1
9	MA-110	37.3	A	10.5	10.8	-0.4
10	MA-130	32.6	A	11.3	12.1	-0.7
11	MA-140	32.7	A	10.8	11.3	-0.5
12	MA-150	28.8	A	10.4	11.2	-0.8
13	MA-150	29.0	A	10.6	10.8	-0.2
14	MA	51.0	A	11.2	11.4	-0.2
14a	MA-150	28.8	A	11.6	11.6	+0.1
15	SA	39.0	A	10.9	11.4	-0.4
16	SA-150	30.5	A	10.8	11.8	-1.0
18	RH	51.0	He	6.4	4.9	+1.6
19	RH-150	31.0	He	6.4	4.8	+1.6
20	MH	50.0	He	6.5	4.8	+1.8
21	MH-150	29.5	He	6.5	4.6	+1.9
22	SH	39.0	He	6.3	4.8	+1.4

TABLE V (Cont'd.)

Film	Description	α %	Gas	E_P Kcals. gmol.	E_D Kcals. gmol.	ΔH_S Kcals. gmol.
23	SH-150	31.0	He	6.4	4.5	+1.9
24	RF	52.2	CF_4	18.3	15.7	+2.7
24a	RF-150	27.0	CF_4	18.3	15.6	+2.7
25	MF	52.4	CF_4	18.3	16.3	+1.9
25a	MF-150	27.5	CF_4	17.2	15.4	+1.8
26	SF	38.2	CF_4	17.7	15.8	+1.9
26a	SF-150	27.4	CF_4	17.2	15.2	+1.9
27	cast	58.0	A	- above Tg -		-0.6
27	cast	58.0	A	- below Tg -		-3.0
27	cast	58.0	CO_2	—	—	-2.6
atactic cubes		100.0	He	—	5.9	+3.7
atactic cubes		100.0	A	—	11.4	~0
atactic cubes		100.0	CF_4	—	14.2	+0.9
Average Values for Films 1 to 26a			He	6.4	4.7	1.7
			A	10.9	11.5	-0.62
			CF_4	17.8	15.7	2.15

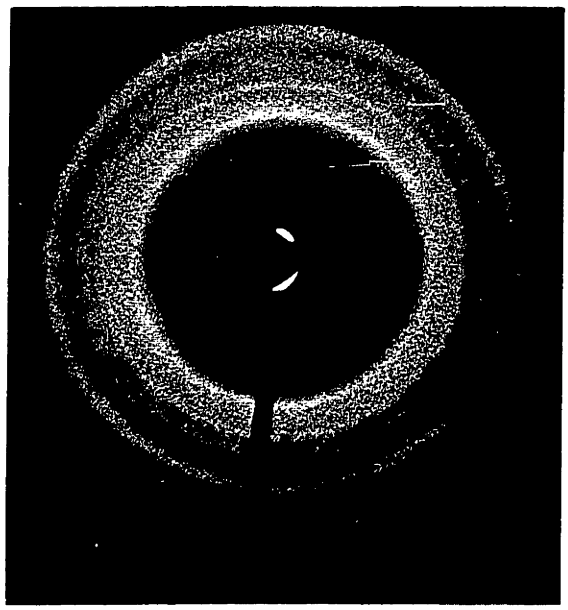

Figure 38

X-ray Diffraction Pattern of Film 2, a "Rapidly Cooled" Film, Unannealed.

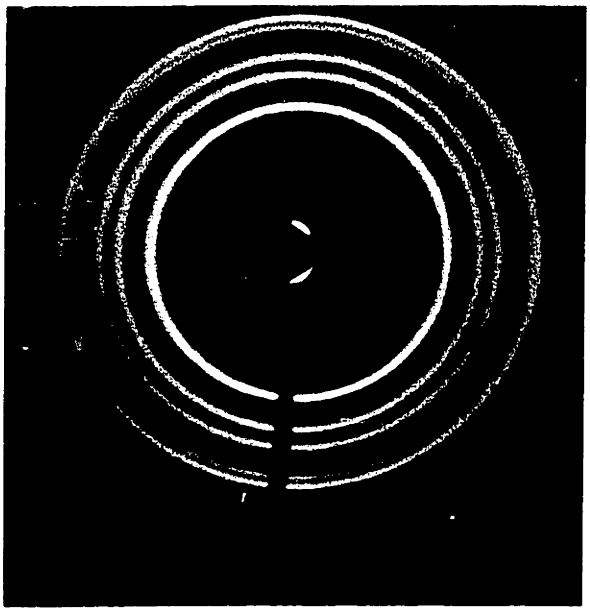

Figure 39

X-ray Diffraction Pattern of Film 5, a "Rapidly Cooled" Film Subsequently Annealed.

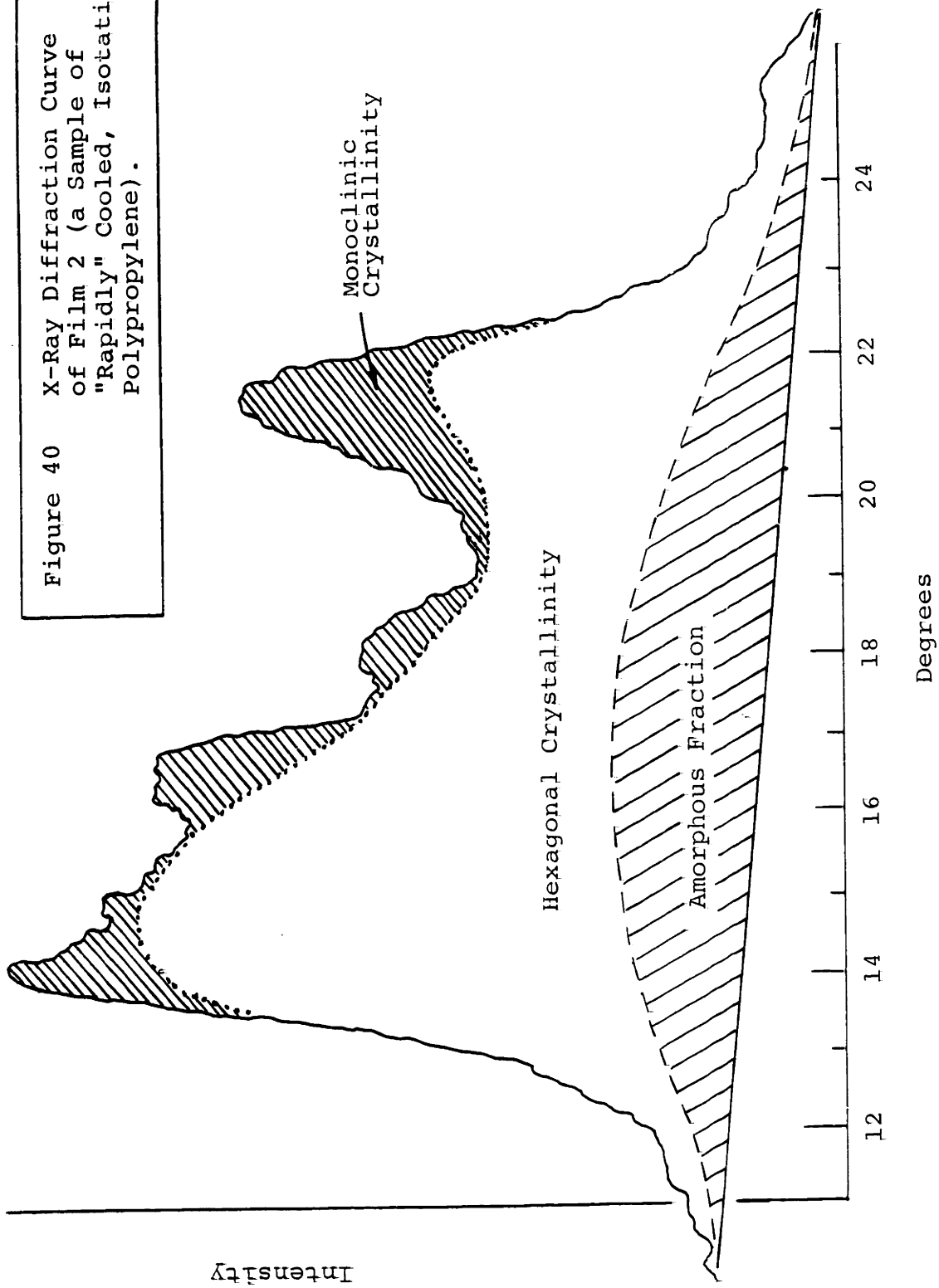

Figure 40 X-Ray Diffraction Curve of Film 2 (a Sample of "Rapidly" Cooled, Isotatic Polypropylene).

Figure 41 X-Ray Diffraction Curve of Film 5, a Sample of "Rapidly" Cooled, Isotactic Polypropylene Subsequently Annealed

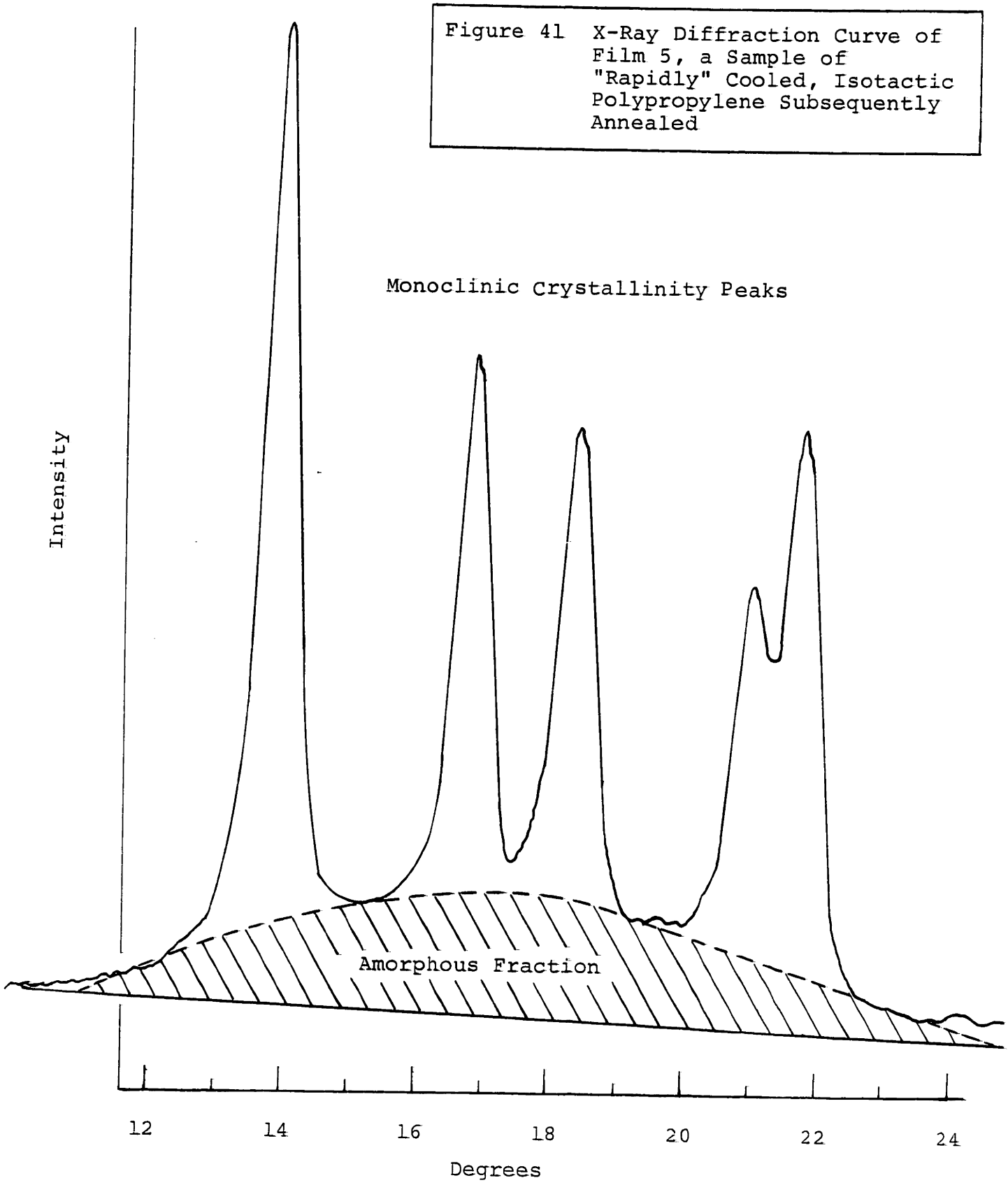

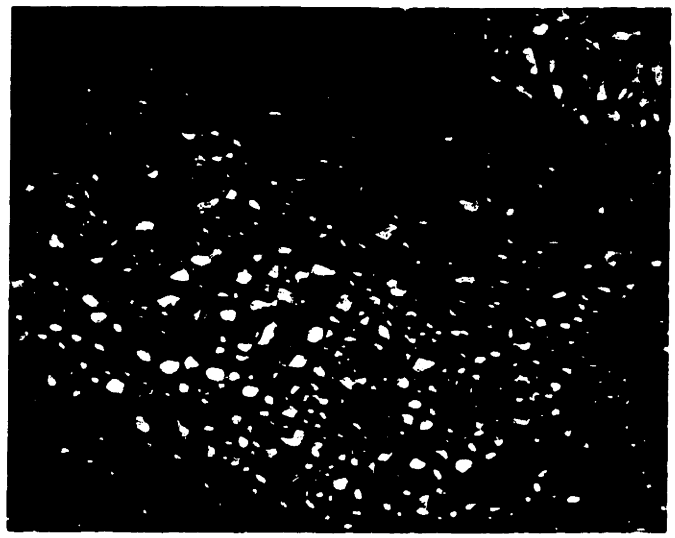

unannealed

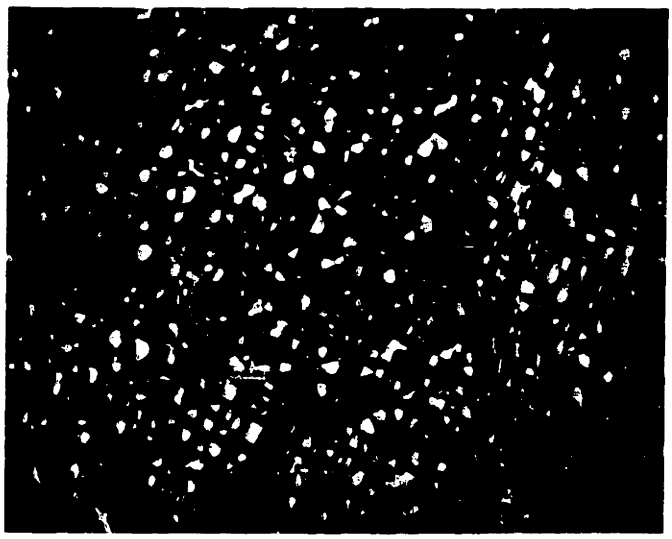

annealed at 150°C for 60 minutes

Fig. 42 -- Optical Micrographs of Spherulites in Films "Rapidly Cooled" from the Melt, Observed Between Crossed Polarizers. 250 X.

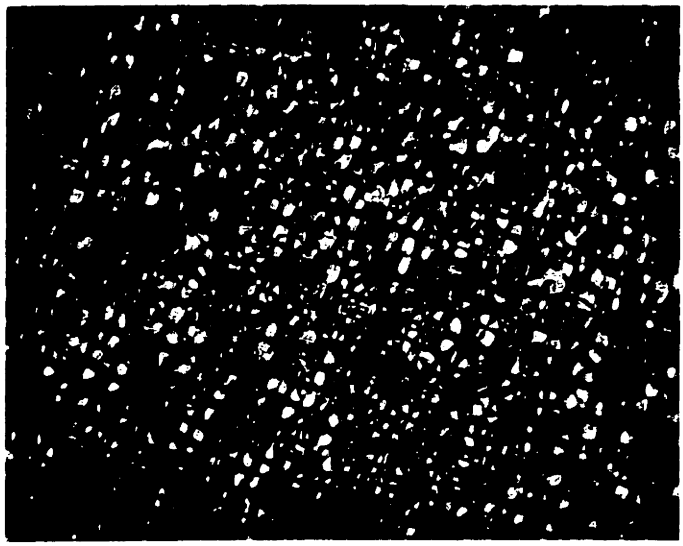

unannealed

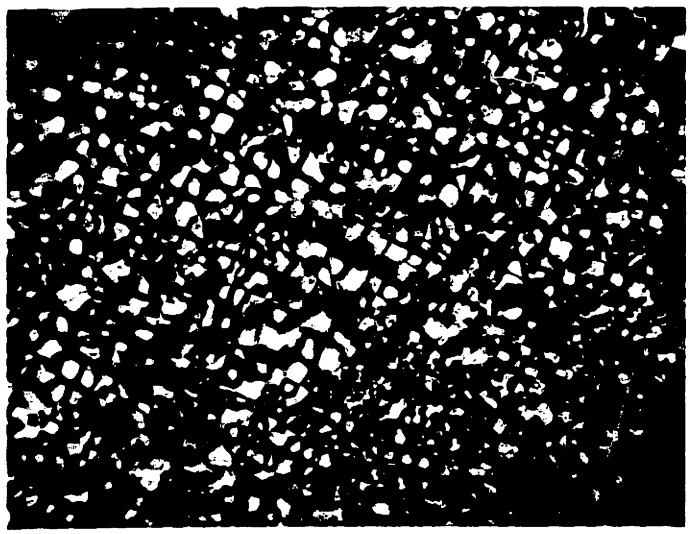

annealed at
150 °C for
60 minutes

Fig. 43 -- Optical Micrographs of Spherulites in Films "Moderately Cooled" from the Melt, Observed Between Crossed Polarizers. 250 X.

unannealed

annealed at
150°C for
60 minutes

Fig. 44 -- Optical Micrographs of Spherulites in Film "Slowly Cooled" from the Melt, Observed Between Crossed Polarizers. 500 X.

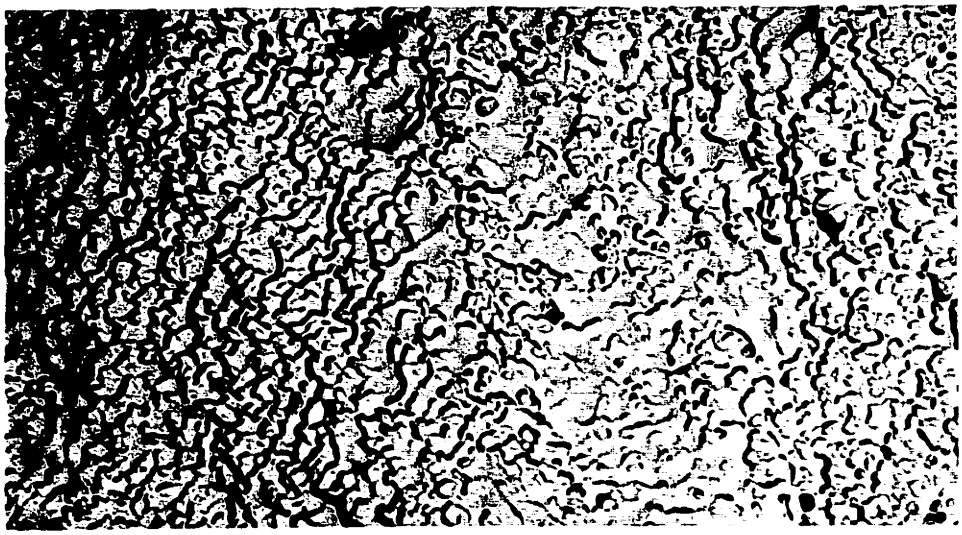

Magnification: 30,000 X

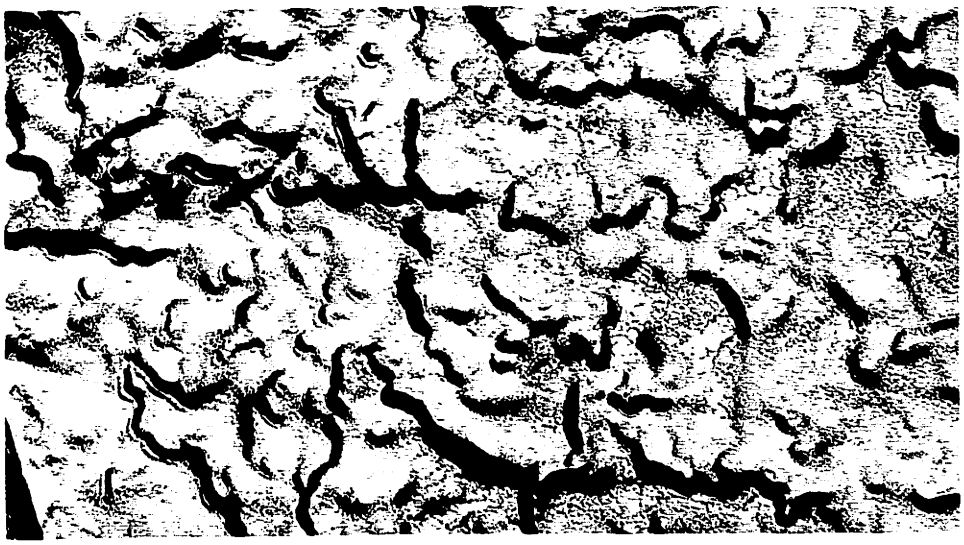

Magnification: 52,000 X

Fig. 45 -- Replicas of Fractured Surfaces of Film 23, a Film "Slowly Cooled" from the Melt, Annealed at 150 °C and Fractured in Liquid Helium. (Electron micrographs)

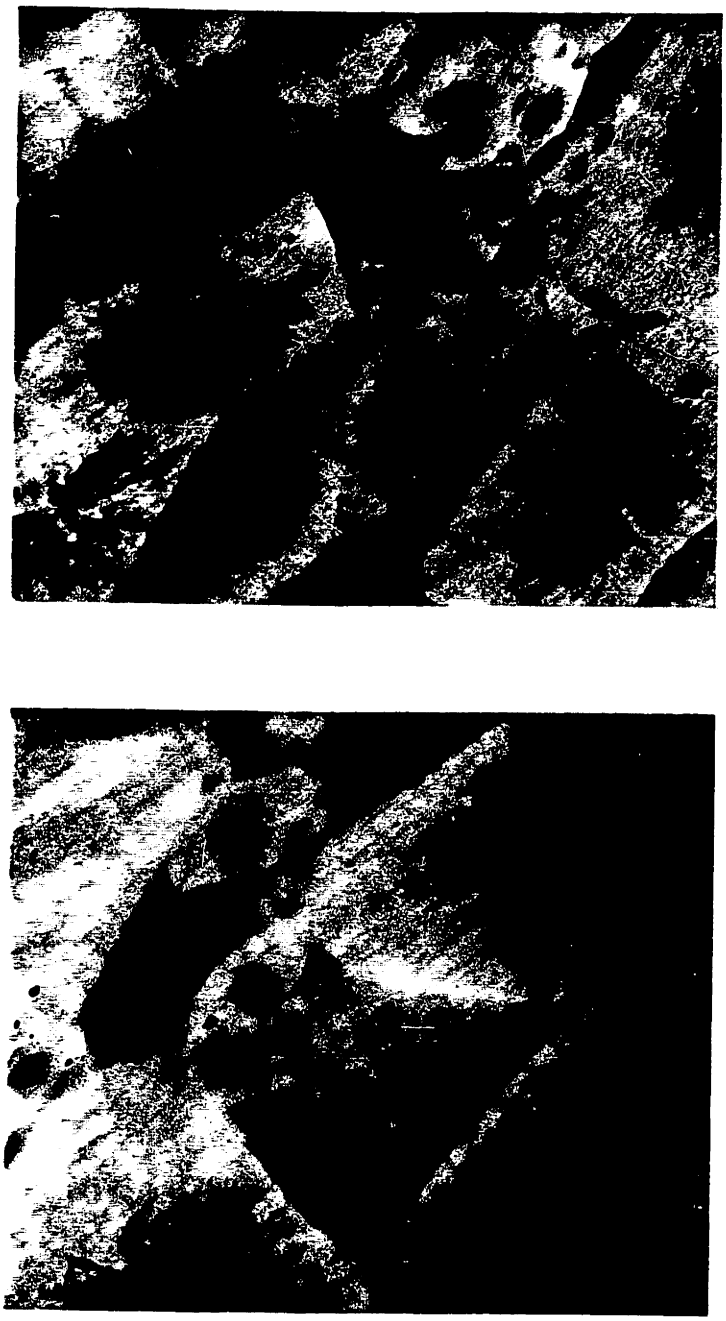

Fig. 46 -- Transmission Micrographs of Ultratomed Sections of Film 23, a Film "Slowly Cooled" from the Melt and Annealed at 150 °C, Showing Spherulites. Electron Microscope. 13,000 X.

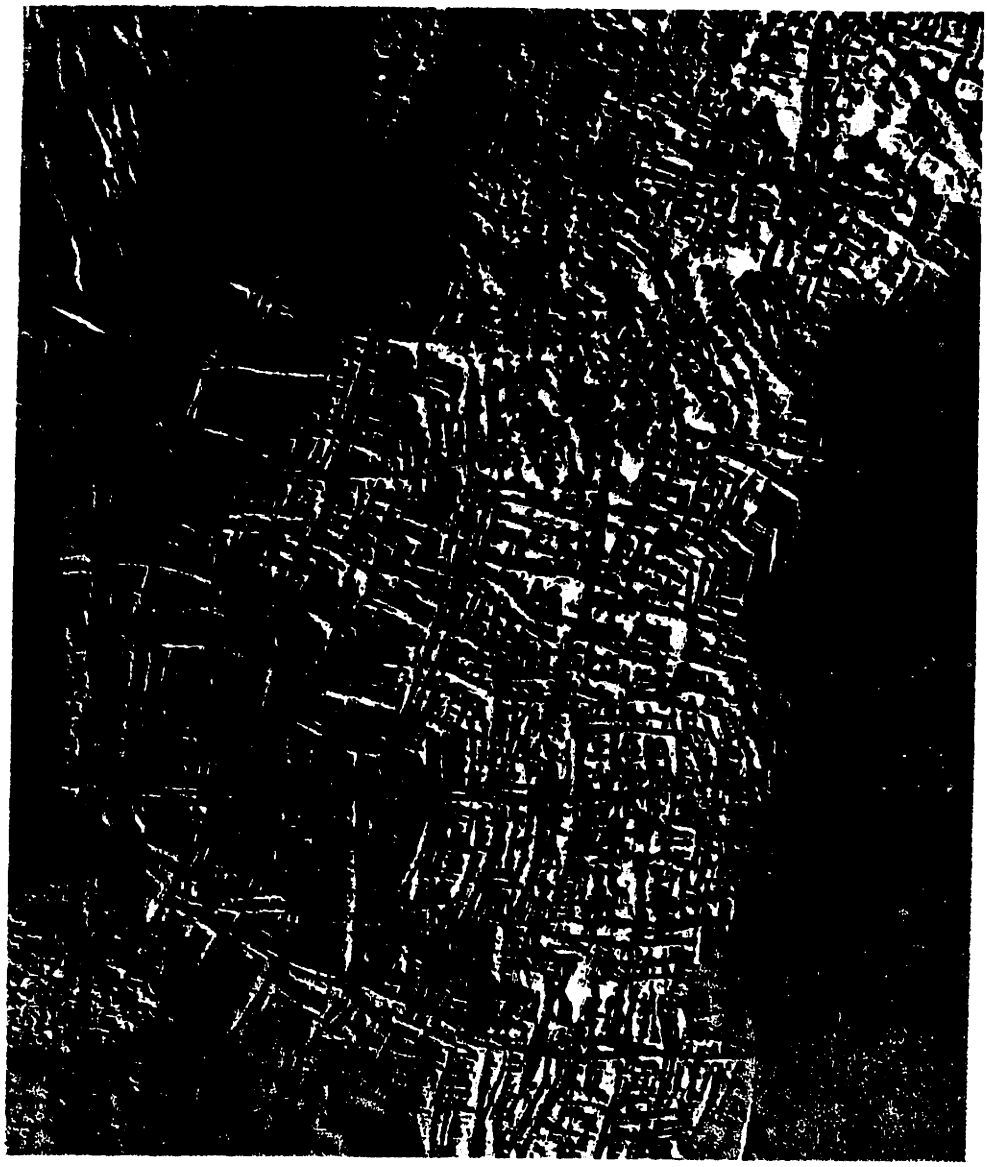

Fig. 47 -- Electron Micrograph of Isotactic Poly(propylene) Crystallized in the Presence of 50% (by weight) Atactic Poly(propylene). Specimen Subsequently Washed in Xylene for 30 Minutes. Magnification 31,000 X.

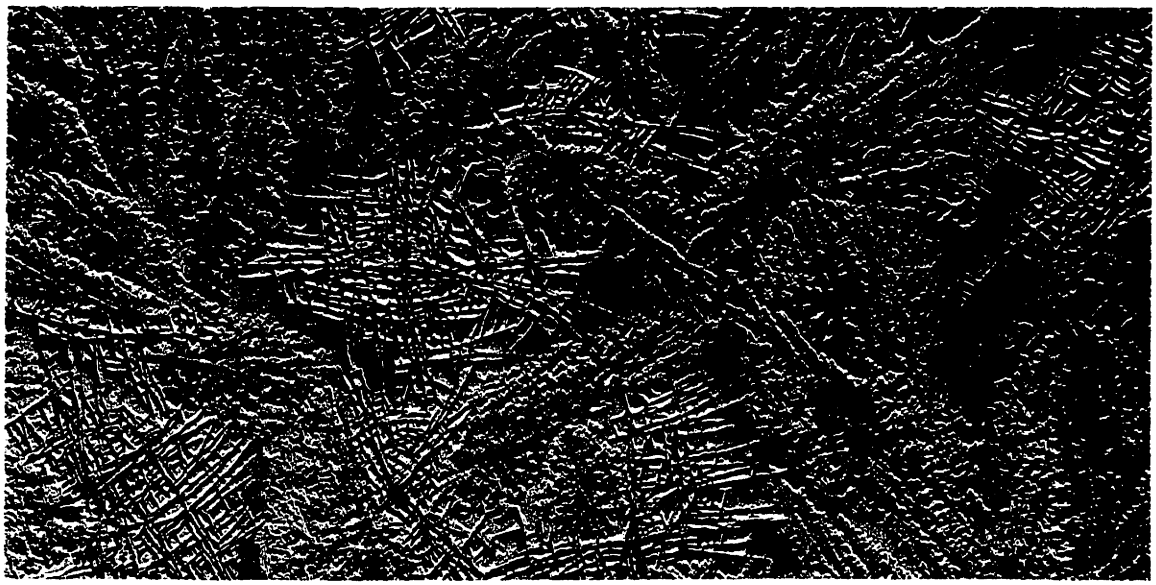

Magnification: 15,000 X

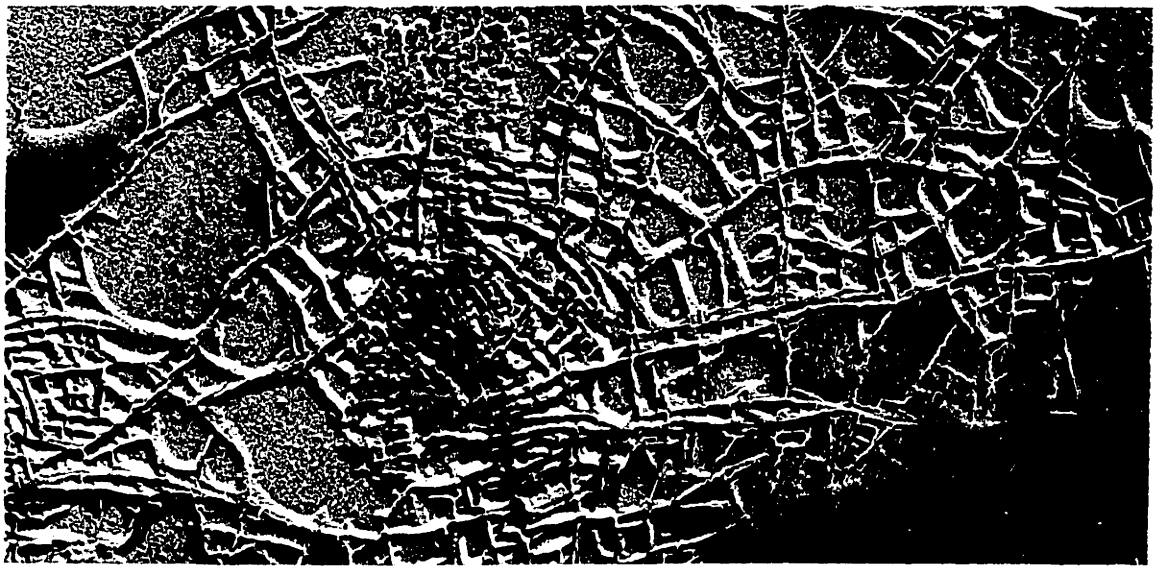

Magnification: 31,000 X

Fig. 48 -- Electron Micrographs of Isotactic Poly(propylene) Crystallized in the Presence of 50% (by weight) Atactic Poly(propylene). Specimen Was Washed 24 Hours in Xylene.

V. DISCUSSION OF RESULTS

A. General Considerations

1. Presentation of Results

The experimental results are summarized graphically by plots of $\bar{P}$ and D versus 1/T in Figures 21 to 26 and 33 to 35 for the time-lag experiments and by plots of D and k versus 1/T in Figures 27, 28, 30, 32, 36 and 37 for the sorption experiment. For clarity's sake, only the most interesting data are presented in these plots; i.e., the data for duplicate films or the films annealed at step-wise higher temperatures (films 7-17) appear only in Table VIII.

The time-lag solubilities shown in Figures 24, 25 and 26 represent the values calculated from equation (9), $\bar{P} = kD$, using averages for the values of $\bar{P}$ and D. It was found that this gave much less scatter in subsequent plots of ℓnk versus 1/T than calculating point values of k for individual runs, and allowed a better estimation of sorption enthalpies.

2. Precision of Data

The inherent error in the determination of $\bar{P}$, D and k by the various experimental methods was estimated by an analysis of variance (see Appendix C). In each case the precision at the 95% confidence limits was determined for a representative run. For the time-lag experiments the precision of $\bar{P}$, D and k for such an "average" run was $\pm$5.2%, 9.6% and 11%, respectively. In the case of the low pressure sorption experiments, the precision was $\pm$1.5%

for k and ±8.4% and ±8.2% for D from sorption and desorption experiments, respectively. Film thickness variations inherent in the molding procedure of the films were, to a high degree, responsible for the magnitude of the estimated error. The diffusion constants calculated from sorption at long times were precise to only ±14.1% due to particle size variations which become especially noticeable at long times. The precision of k from high pressure sorption experiments was estimated at ±8.2%.

As a check on the above estimates of precision, the actually observed precision was estimated from a series of repeat runs made for each method. In all cases, except the solubilities determined from low pressure sorption experiments, the observed precision was considerably better than predicted. This suggests that the error estimates are generally conservative and the precision of the data is probably greater than that suggested by the above analyses.

Since more than one piece of apparatus was used for the time-lag experiments, the equivalence of the data from the two stations was checked with film 13. Several runs (77 through 91, Table XII) were made for argon with film 13 in station 1 and then in station 2. A comparison of the data from the two stations showed no significant differences.

By repeating a series of time-lag experiments with film 4 three months after the initial runs, it was found that no significant changes in film properties occurred on aging of the film.

Analysis of the data for runs 24 through 37, Table XII, shows that the variations in the data are random and well within the estimated precision limits.

B. Permeability Constants

As was indicated earlier in the INTRODUCTION permeability data per se offer little insight into the permeation process and any attempts at correlation must logically be derived from separate analyses of the diffusion and solubility constants. Nevertheless, from an engineering standpoint, permeability data are of prime interest and they probably constitute the greatest, single incentive for continued attempts to understand the morphology of crystalline polymers. Consequently, these data merit some discussion in their own right.

1. Variation with Temperature

Figures 21, 22 and 23, showing the variation of permeability with temperature, point out the generally high level of reproducibility of the experimental data obtained from time-lag studies. It was found that the data were surprisingly well correlated by the empirical relationship, $\bar{P} = P_o e^{-(E_{\bar{P}}/RT)}$, over the range of temperatures studied. The fact that this relationship, originally derived for completely rubbery material, should describe permeation in highly crystalline films is somewhat surprising and points to the rubbery nature of the chain ends and tie-chains between the crystallites through which, presumably, most of the diffusion takes place.

The plots of ℓnP versus 1/T were straight lines yielding constant activation energies, $E_{\bar{P}}$, over the temperature range, 30 - 70°C. The values of $E_{\bar{P}}$ are listed in Table V with average values being 6.4, 10.9 and 17.8 Kcals/gmole for helium, argon and CF_4, respectively. The values of $E_{\bar{P}}$ were virtually independent of thermal history.

2. Effect of Crystallinity on Permeability

In addition, Figures 21, 22 and 23 illustrate the relative permeation rates of the three different gases through crystalline poly(propylene). The unexpected result here is the observation that extensive annealing of the polymer, despite the concomitant increase in crystallinity, may actually result in a net increase in permeability. While this effect is indicated by the data for argon whose decrease in permeability on annealing is less than the change observed for the smaller molecule helium, it is most dramatically illustrated by the plots of $\ell n\bar{P}$ versus 1/T for CF_4, the largest molecule studied. This phenomenon will be examined in more detail later in the light of a model which is based on the concept that annealing enhances diffusion by introducing "row vacancy" defects into the crystalline phase.

Table IV compares the permeability of various gases in crystalline poly(propylene) to that in natural rubber and atactic poly(propylene). Two striking observations evolve from this comparison. Firstly, permeation rates decrease more than one thousand fold in going from helium to CF_4. This dramatically

illustrates the extreme sensitivity of permeation processes to relatively small changes in diameter (2.2 to 4.6Å) of the permeant. Secondly, the effect of crystallinity on permeability is remarkable. Permeability is up to 170 times lower in isotactic poly(propylene) than in its amorphous analogs.

Table VI

Comparison of Permeabilities in Natural Rubber, Atactic, and Isotactic Poly(propylene)

Gas	Natural[1] Rubber	Atactic Poly-(propylene)	Isotactic Poly(propylene) Quenched[2]	Isotactic Poly(propylene) Annealed[3]
He	2.4	4.3	0.64	0.42
A	1.7	1.6	0.058	0.045
CO_2	11.5	10.0	-	-
CH_4	2.4	1.7	-	-
CF_4	-	0.08	0.00046	0.00064

1 Data of Bixler (15)

2 Films 14, 20 and 25 (moderately cooled films)

3 Films 14a, 21 and 25a (moderately cooled films)

The theoretical significance of these observations can best be illustrated by considering the two quantities that comprise permeability, namely solubility and diffusivity. As outlined in the INTRODUCTION, the fundamentally different character of these two quantities makes it easier to correlate them separately than when combined into $\bar{P}$.

C. Solubility Constants

1. Variation with Temperature

The solubility data were collected by three different methods: the time-lag method, the low-pressure sorption method and the high-pressure sorption method. The validity of the solubilities indirectly obtained from the time-lag experiments has been confirmed for this polymer by the runs for films 16 and 21 (shown in Figures 25 and 27) for which solubilities were determined also in the low-pressure sorption apparatus. As found in this work, the equivalence of the k values obtained by either method has also been satisfactorily established by many previous investigators (15, 33, 111).

The high-pressure sorption system was identical in principle to the low-pressure sorption system, the only difference being that it was designed for operation in a pressure range extending well above atmospheric pressure (i.e., up to 33 atm.).

All solubility data are recorded in Tables VIII, IX and X, and are graphically summarized in Figures 24 to 28, 30 and 32 which are plots of ℓnk versus $1/T$. For each run, the solubility constant, k, was obtained by normalizing the solubility at the particular pressure of the run to that at one atmosphere. This assumes the applicability of Henry's Law, $C = kP$, over the range of pressures considered. In the very early low-pressure sorption experiments a non-linear trend was observed at pressures up to one atmosphere. However, this was an artifact later traced to an adiabatic compression effect in the experimental system and was

eliminated by switching to desorption experiments. All later experiments showed no deviation from Henry's Law within the limits of the experimental error.

Plots of ℓnk versus 1/T were linear over the range of temperatures considered, except for the high-pressure sorption data which will be considered in greater detail in a later discussion. Thus solubilities are correlated by the van't Hoff expression, $k = k_o e^{-(\Delta H_S/RT)}$ (13), where ΔH_S, the enthalpy of sorption, is evaluated from the slope of the lines.

2. Effect of Crystallinity on Solubility

As was indicated earlier, it is possible to understand the morphology of crystalline poly(propylene) by interpreting changes in both the solubility and diffusivity in relation to morphological changes introduced into the system. Since isotactic poly(propylene) belongs to the same family of olefin polymers as poly(ethylene), one logically begins to interpret the behavior of poly(propylene) in the light of the model already developed for poly(ethylene).

In the past, investigators studying poly(ethylene) (15, 33, 88) and poly(ethylene terephthalate) (111, 31) have been able to show that for these polymers, above T_g, sorption takes place only in the amorphous regions. In other words, it was concluded that these crystalline polymers are essentially two-phase systems, one phase being completely amorphous and permeable to gases, and the other being crystalline and completely impermeable to gases,

with the possible exception of helium. Together with the observation that Henry's law was obeyed for permanent gases, the data were correlated by the relation $k = \alpha k^*$, where k^* is the solubility constant in the amorphous polymer and α is the amorphous volume fraction. The success of this correlation with these polymers led to attempts to extend the applicability of this two-phase concept to poly(propylene).

As was pointed out in the INTRODUCTION, atactic poly(propylene) was used as an analog for amorphous isotactic poly(propylene), since the latter is not obtainable at room temperature. Since atactic poly(propylene) is simply a stereoisomer of the isotactic form, this substitution seems justified.

Figures 49 and 50 summarize the solubility data for all the films studied in relation to their amorphous content. The amorphous volume fraction of a film was estimated by comparing the film's density with that of 100% crystalline and 100% amorphous poly(propylene). If crystalline poly(propylene) were indeed a simple two-phase system, then one would expect the data to fall on the straight line connecting the origin and the point for 100% amorphous polymer. However, the plots of k versus α show that the solubility in crystalline poly(propylene) does not obey this simple relationship. It appears that all the quenched films have a solubility significantly lower, and apparently independent of amorphous content, in contrast to what one would predict for an idealized situation of two phases. This difference is largest for the largest gas molecule, CF_4, and tends to

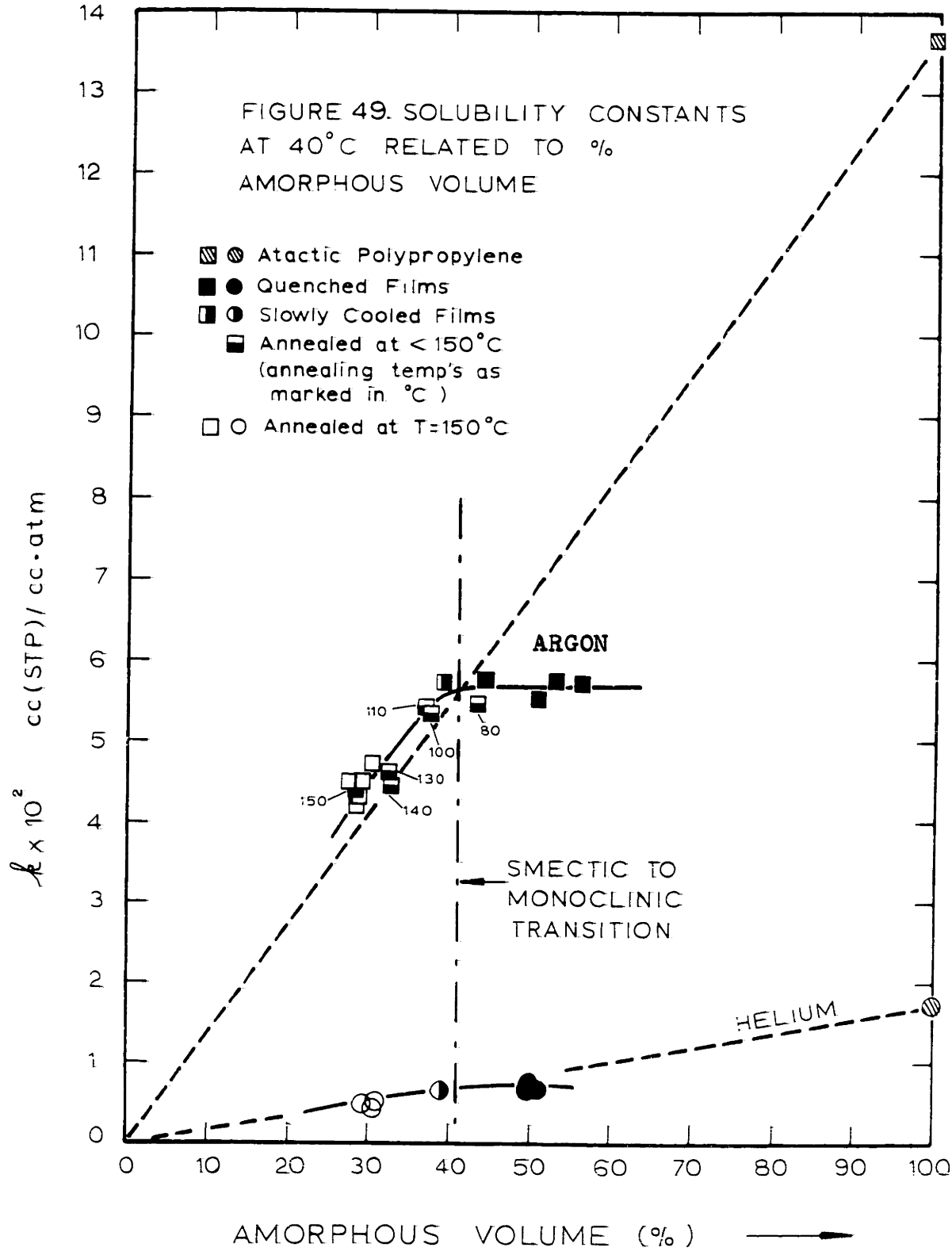
FIGURE 49. SOLUBILITY CONSTANTS AT 40°C RELATED TO % AMORPHOUS VOLUME
Atactic Polypropylene
Quenched Films
Slowly Cooled Films
Annealed at < 150°C (annealing temp's as marked in °C)
Annealed at T=150°C
ARGON
HELIUM
SMECTIC TO MONOCLINIC TRANSITION
110
80
100
130
150
140
$k \times 10^2$ cc(STP)/cc·atm
AMORPHOUS VOLUME (%)
0
1
2
3
4
5
6
7
8
9
10
11
12
13
14
0
10
20
30
40
50
60
70
80
90
100

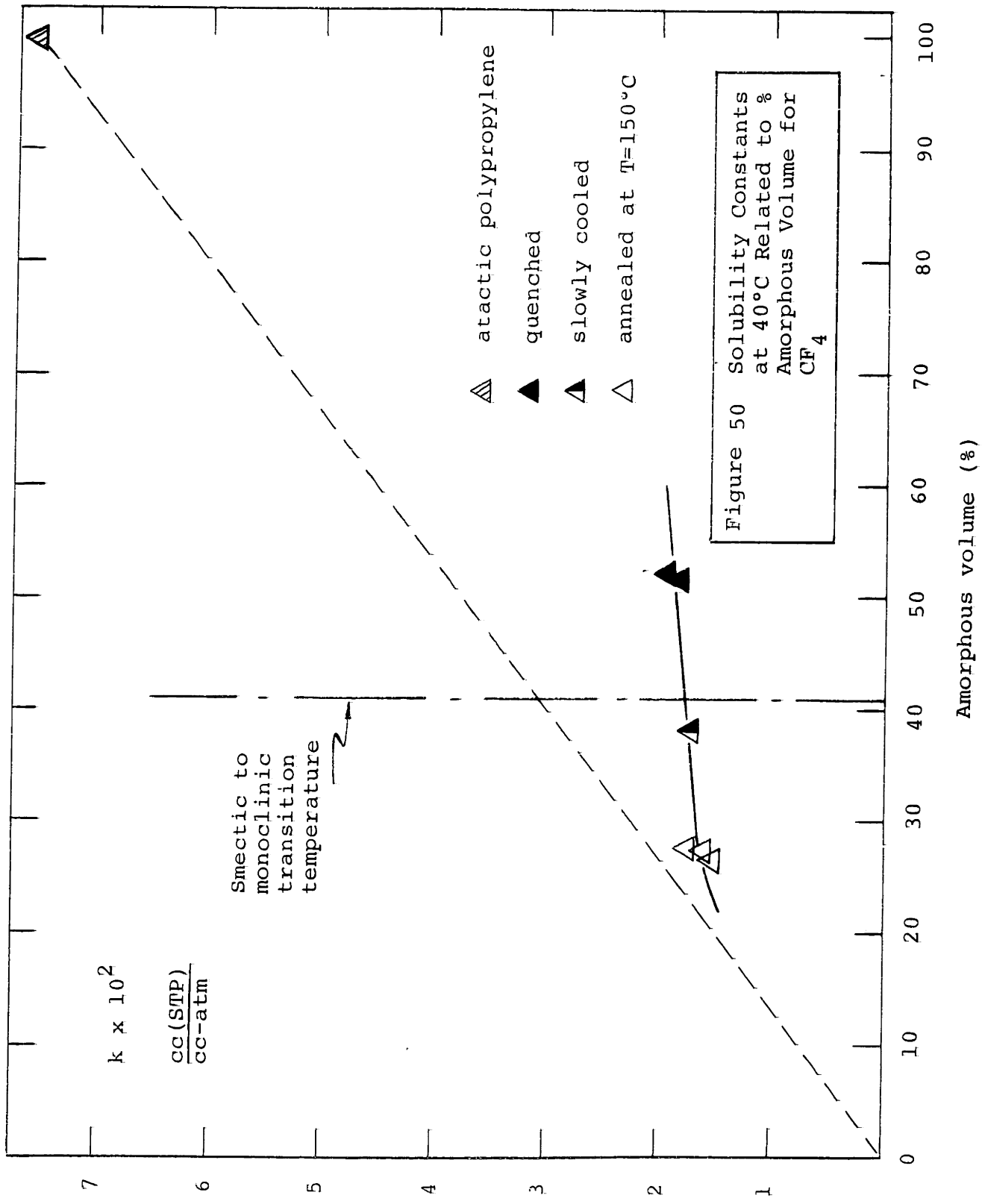

Figure 50 Solubility Constants at 40°C Related to % Amorphous Volume for CF_4

disappear for the annealed films. The solubilities of the "slowly cooled" and annealed films seem to approach the "two-phase solubility curve".

These observations led to the conclusion that the quenched films have a different microstructure than either the annealed films or the amorphous atactic films. In this light the solubility data seem to reflect the observations made by many other authors (53, 73, 98, 81) who using x-ray diffraction, IR-absorption, NMR and dynamic mechanical measurements, have found evidence for a "quenched", "smectic", "paracrystalline" and "non-crystalline" (distinct from "amorphous") structure.

In the case of argon, for which the greatest number of runs were made, the solubility is initially constant and independent of the apparent amorphous content, and appears to drop off rather suddenly, reminiscent of a phase change, as the material is annealed at 100°C and above. This inflection point is in agreement with the results of Gailey and Ralston (36), who in extensive DTA studies observed that the quenched material underwent complete conversion to monoclinic crystallinity if annealed at least 20 minutes at about 90°C. As mentioned previously, the same authors arrived at the conclusion that the quenched poly-(propylene) consists of very small hexagonal crystallites whose intrinsic density is 0.907 gm/cm^3.

The following picture evolves from these observations. On "rapid" or "moderate" cooling a mixture of monoclinic and

hexagonal crystallites are produced, the ratio of the two being a function of the rapidity of the quenching from the melt. The total amount of crystallinity seems to be fixed at approximately 59% by volume. Since both morphological forms are crystalline, it is not unreasonable to assume that both are impermeable to gas, thus accounting for the constant solubility up to the point where films were either "slowly cooled" from the melt (i.e., the quench bath was at 90°C) or annealed at temperatures greater than 90°C. From this point on there is only one crystal form present, namely the monoclinic form, and annealing at temperatures greater than 90°C produces additional crystallinity as well as thickening of the existing crystallites.

Although there is no direct proof that the crystalline phase is impermeable to gas, a careful analysis (see Appendices E and F) of the various dimensions of the unit cell for monoclinic and hexagonal poly(propylene) based on x-ray diffraction suggests that even the largest dimension between polymer chains in a crystalline array is considerably less than the diameter of helium, the smallest molecule considered.

The concept of a distinct "quenched" phase of most probably very small hexagonal crystallites is further supported by the fact that the x-ray diffraction curves (see Figure 40) of film 2, a "rapidly cooled" sample, showed the two typical, broad scattering maxima which many authors (53, 36, 50) have attributed to hexagonal crystals of very small size.

The fact that the argon solubility of the annealed samples is slightly higher than what one would predict on the basis of two, well segregated phases - one crystalline and one amorphous - is most probably due to local variations in the cohesive energy density (C.E.D.) of the intercrystalline, amorphous material. The annealing causes the crystallites to thicken by the incorporation of adjacent, amorphous chain segments which, in turn, leads to decreases in the chain segment density in the remaining amorphous material, as the polymer feeds upon itself (see Figure 51). These changes in morphology result in changes in the cohesive energy density and, as will be shown in a later discussion, are directly responsible for changes in solubility.

The solubility of helium is intrinsically quite low and only slightly lower in the quenched material. Nevertheless, the data for helium does show the same break at the 41% amorphous content. Solubility is slightly lower in the quenched phase while still being equal to that predicted for a "two-phase system" in both the annealed and the "slowly cooled" samples, at the same level of crystallinity.

The data for CF_4, the largest molecule studied, also show the low solubility in the quenched material, explicable by the presence of the hexagonal crystallites. The fact that even the "slowly cooled" samples and the annealed samples show a lower solubility than what one would predict on the basis of discrete crystalline and amorphous phases is probably the result of

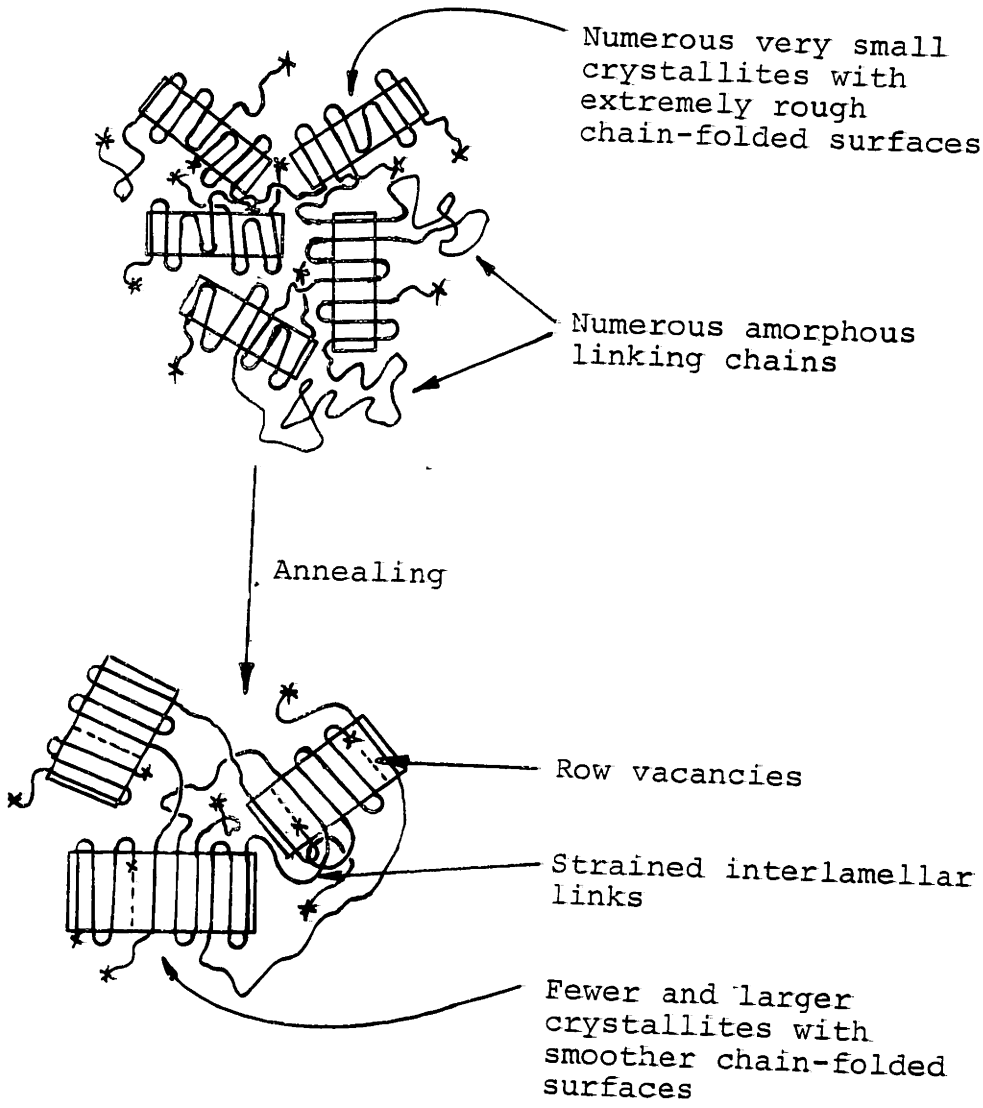

Figure 51 Schematic Diagram Showing Changes in Fine Structure of Isotactic Polypropylene on Annealing.

inaccessibility. To put it differently, because of the large molar volume of the CF_4 molecule, parts of the interlamellar amorphous material may be inaccessible to CF_4 and the solubility never reaches the level commensurate with the volume fraction of amorphous material actually present.

3. Correlation of k*

Ideally one would like to be able to predict the permeability of a given membrane to a given gas from well-known parameters of the membrane and the gas, such as the cohesive energy density of the polymer and the force-constant of the gas. In the case of poly(ethylene) successful steps have been made in this direction by developing a method (15) to predict the solubility of the completely amorphous film, k*, thence estimating the solubility of the partially crystalline film from the relationship $k = \alpha k^*$.

In the case of poly(propylene), the solubility behavior is more complex. However, at least for the annealed and slowly cooled films, the solubility is approximated by the relationship $k = \alpha k^*$. Consequently, the method suggested by Bixler (15) for estimating values of k* from the values of $\varepsilon/\bar{k}$ of the gas will be briefly outlined.

Actually, Jolley and Hildebrand (52) were the first to correlate solubility constants of various non-polar gases in non-polar solvents by means of their force constants, $\varepsilon/\bar{k}$. The force

constant is best defined by the Leonnard-Jones potential field equation:

$$\Phi(r) = 4\varepsilon \left[\left(\frac{\bar{\sigma}}{r} \right)^{12} - \left(\frac{\bar{\sigma}}{r} \right)^{6} \right] \qquad (43)$$

describing the interaction between two like molecules in a condensed state. The parameter $\varepsilon/\bar{k}$ is a measure of the depth of the energy well; the deeper the potential energy well, the more strongly like molecules are attracted to one another. Since one step of gas dissolution in a polymer is pictured as a condensation step, the analysis seems applicable. However, since for the system of gas dissolved in polymer, the interactions are between unlike molecules, it is necessary to turn to a "combining law" wherein the square root of the product of the self-interaction potentials is employed. Although the law holds accurately only in the gas phase, it is probably a satisfactory approximation in the liquid phase if the system is without strong anisometric dipole interactions, large disparity in molecular size and shape and high solute concentrations. Thus if one, considers various gases in the same polymer it becomes obvious how the force constant of each gas reflects the interaction of that gas with segments of the polymer. With this in mind, an empirical correlation of ℓnk^* with $\varepsilon/\bar{k}$ has been attempted and is shown in Figure 52, and it is found that the straight line for atactic poly(propylene) lies parallel to and midway between the lines obtained by Jolley-Hildebrand (52) and Bixler (15) for C_6H_6 and poly(ethylene), respectively.

The theoretical basis for this relationship is readily apparent from the simplified thermodynamic analysis first proposed by Gee (37). The process of dissolution of gas in amorphous poly(propylene) can thermodynamically be considered as a two-step process consisting of, first, condensing the gas and, then, mixing the condensate with the polymer. The total free energy change for the process is zero, since it is assumed that the process occurs at equilibrium.

$$\therefore \Delta F_c + \Delta \bar{F}_m = 0 \tag{44}$$

where ΔF_c is the molar free energy of condensation and $\Delta \bar{F}_m$ is the partial molar free energy of mixing.

Considering the two free energy contributions individually and calling on certain empirical approximations, the following derivation evolves:

$$\Delta F_c = \Delta H_c - T\Delta S_c \tag{45}$$

or

$$\Delta F_c = -\Delta H_v + T\Delta S_v \tag{46}$$

But

$$\Delta S_v = \frac{\Delta H_v}{T_B} \tag{47}$$

and Trouton's Rule states,

$$\Delta H_v \cong 0.020\ T_B \tag{48}$$

$$\therefore \Delta F_c \cong -0.020\ T_B + T\left(\frac{\Delta H_v}{T_B}\right) \tag{49}$$

$$\cong 0.020\ (T - T_B) \tag{50}$$

By the Guldberg-Guye rule,

$$T_B \cong 0.6\ T_c \qquad (51)$$

where

$$T_c \cong 1.3\ \frac{\varepsilon}{\bar{k}} \qquad (52)$$

Thus $$\Delta F_c \cong 0.020\ (T - 0.78\ \frac{\varepsilon}{\bar{k}}) \qquad (53)$$

Using the Flory-Huggins equation, the partial molal free energy of mixing is

$$\Delta\bar{F}_m = RT[\ell n(1 - V_p) + (1 - \frac{1}{m})V_p + \mu V_p^2] \qquad (54)$$

For permanent gases dissolving in poly(propylene),

$$V_p \cong 1.0 \quad \text{and} \quad \frac{1}{m} \to 0$$

Gee (37) has shown that k* can be related to V_p in the following way:

$$k^* = \frac{22{,}400\ (1 - V_p)}{\bar{V}} \qquad (55)$$

$$\therefore \Delta\bar{F}_m = RT[\ell nk^* - \frac{\ell n\ 22{,}400}{\bar{V}} + 1.0 + \mu] \qquad (56)$$

From equation (44) $-\Delta F_c = \Delta\bar{F}_m$ (44a)

$$\therefore 0.020(0.78\ \frac{\varepsilon}{\bar{k}} - T) = RT[\ell nk^* - \frac{\ell n\ 22{,}400}{\bar{V}} + 1.0 + \mu]$$

..... (57)

which at 25°C reduces to

$$\ell nk^*\bar{V} = 0.026 \frac{\varepsilon}{\bar{k}} - (1 + \mu) \qquad (58)$$

where μ is the Flory-Huggins parameter, related to the enthalpy of mixing.

As Bixler has pointed out, attempts to calculate k* directly from equation (58) are generally not very successful because of the difficulty in estimating μ and $\bar{V}$, the partial molar volume of the dissolved gas. Nevertheless, equation (58) suggests a way to correlate k* with available parameters of the dissolving gas. Assuming μ is a constant, a plot of $\ell nk^*\bar{V}$ versus $\varepsilon/\bar{k}$ should yield a straight line. In fact, as shown in Figure 52 good linear correlations were obtained in the case of benzene and poly(ethylene) as well as atactic poly(propylene) for ℓnk^* versus $\varepsilon/\bar{k}$. The solubilities of He, A, CH_4 and CO_2 in atactic poly(propylene) fall on a straight line with a slope identical to that previously observed for amorphous poly(ethylene) and the non-polar solvents. This strongly suggests that the process of dissolution in completely amorphous poly(propylene) occurs by the same mechanism as that of dissolution of permanent gases in either non-polar solvents or amorphous poly(ethylene).

The value of k* for CF_4 seems to fall far below the correlation. This discrepancy parallels the behavior observed by Bixler (15) for SF_6. Now as then, the most plausible explanation for this is probably the appreciably higher partial molar volume of

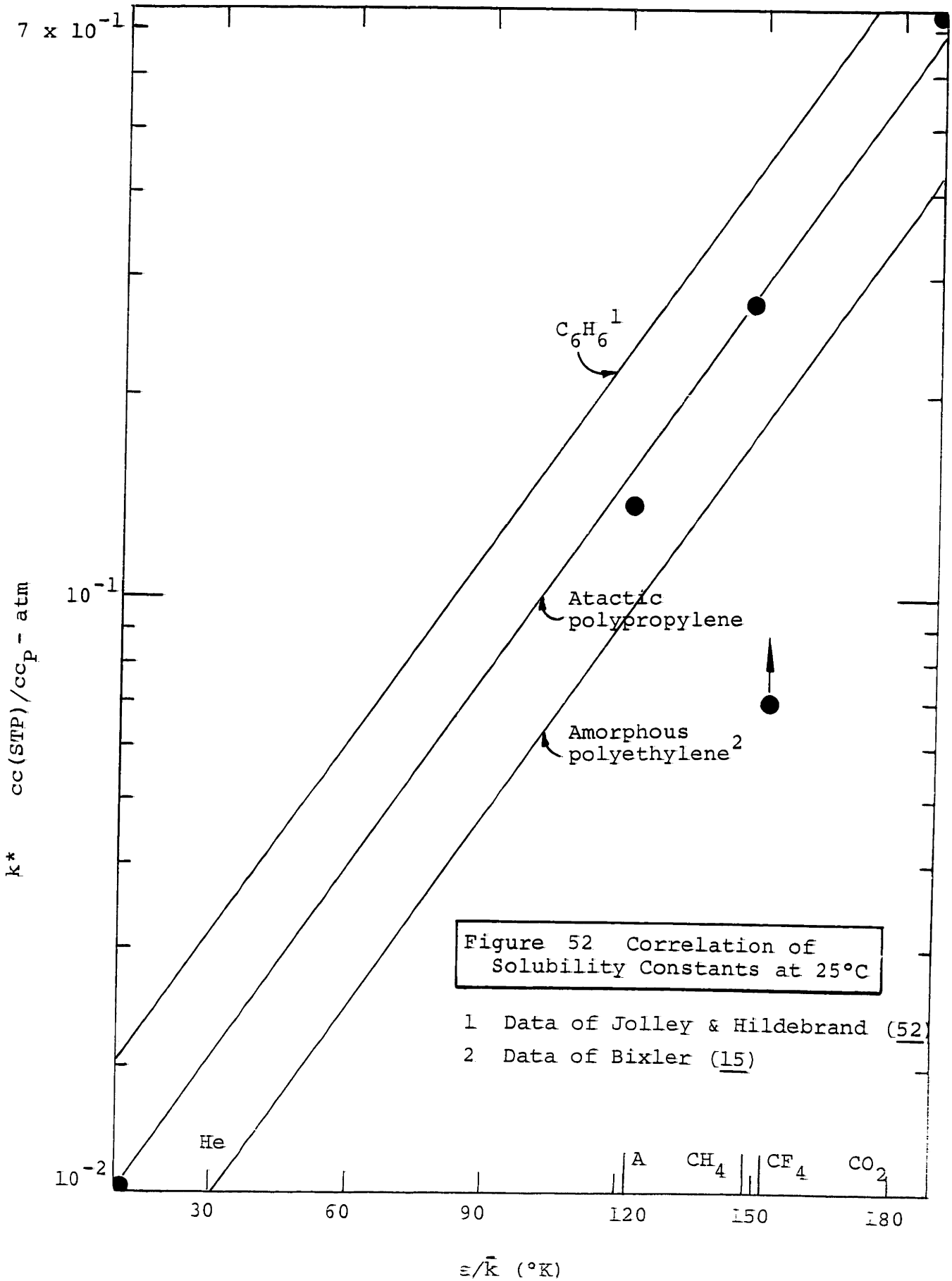

Figure 52 Correlation of Solubility Constants at 25°C

1 Data of Jolley & Hildebrand (52)

2 Data of Bixler (15)

the fluorocarbons compared to that of other molecules of a similar $\varepsilon/\bar{k}$. Thus, if more reliable values of $\bar{V}$ were available, plotting $\ell nk^*\bar{V}$ instead of ℓnk^* would probably improve the correlation.

The value of the slope of the correlation is 0.022 which agrees remarkably well with the value predicted by equation (58). This suggests that either the values of $\bar{V}$ and μ tend to compensate each other from gas to gas or the value of $\bar{V}$ changes only little. The actual values of $\bar{V}$ for He and A in poly(propylene), as estimated from correlations by Prausnitz (90), are 41.3 and 42.7, which suggests that, with the exception of the fluorocarbons, the value of $\bar{V}$ for the different gases does indeed change only very slightly.

4. Solubility in Glassy Poly(propylene)

With the glass transition of crystalline poly(propylene) in the vicinity of zero degrees centigrade (22, 78, 107, 101) it is conceivable that in some of its applications poly(propylene) will be used in this condition. The work of Meares (62) and Vieth (111) has shown that the solubility behavior of the glassy material may be quite different from that of the rubbery material. For this reason, part of this study was devoted to observing the solubility characteristics of poly(propylene) below its glass transition point.

The experiments were performed in the high pressure sorption system over a pressure range of 3 to 31 atmospheres and a

temperature range of -30°C to 40°C. Figures 29 and 31 show the type of isotherms obtained for argon and carbon dioxide, respectively. Within the limits of experimental error, the plots of solubility versus pressure appear to be straight lines. However, a plot of ℓnk versus 1/T for argon, Figure 30, reveals a definite break at the glass transition point, with the solubility in the glassy polymer being considerably higher than what one would predict on the basis of an extrapolation from the rubbery region. This points to the existence of "frozen-in" microvoids, or "holes", much like those observed in poly(ethylene terephthalate). The reason why the high pressure sorption experiments were unable to separate the dissolution and hole-filling components may be the low interaction of the inert argon and the non-polar poly-(propylene). It may be that sorption at pressures greater than 30 atmospheres would have resulted in hole-saturation with any additional sorption after that being due solely to ordinary dissolution, thus allowing a separation of the mechanisms. However, experimental limitations did not permit this point to be checked.

Figure 31 is a typical plot of the isotherms observed for CO_2 sorption. As the force constant $\varepsilon/\bar{k}$ for CO_2 is considerably higher than that for argon (189 versus 122) and as the CO_2 molecule is dipolar, it was thought CO_2 would interact more strongly with the polymer and any hole-filling effect would thus be easily discernible even at moderate pressures. However, it appears that, over the pressure range considered, it was impossible to complete microvoid-filling and separate the two modes of sorption. Owing to

the stronger interaction of CO_2 with the polymer, the level of sorption of CO_2 is almost a factor of 10 higher than for argon. This high level of ordinary dissolution may obscure the contribution to sorption by the process of hole-filling which operates in the glassy state. This may account for the apparently linear relationship in CO_2's plot of ℓnk versus 1/T, Figure 32, over the entire temperature range (-38° to 49°C). Naturally one could argue that no "frozen-in" microvoids exist in glassy poly-(propylene) and what one sees is Henry's Law type of dissolution. However, the discontinuity at the glass transition point for argon as well as a comparison, which is to follow, of the enthalpies of adsorption in glassy poly(propylene) with those observed in poly-(styrene) and PET, leads one to conclude that "frozen-in" voids do exist in poly(propylene) but their effect is less pronounced because of the weak interaction of poly(propylene) and the inert or weakly polar gases studied.

Summary - Gas Solubility

1. The solubility of He, A and CF_4 in crystalline poly-(propylene) obeys Henry's Law up to a pressure of 30 atmospheres.

2. The relationship $k = \alpha k^*$ applies only qualitatively to helium and argon sorption in "slowly-cooled" and annealed films. The quenched films show significantly lower levels of solubility at the same levels of crystallinity.

3. The low level of solubility in quenched poly(propylene) tends to confirm the existence of small hexagonal crystals proposed by several investigators.

4. The somewhat low solubility of CF_4 in annealed films is attributed to the inaccessibility of some of the remaining interstitial amorphous regions to the large CF_4 molecule.

5. The solubilities of He, A, CH_4 and CO_2 in amorphous (atactic) poly(propylene) are well correlated with $\varepsilon/\bar{k}$. The deviation of the CF_4 solubility from this correlation is attributed to its anamolously high partial molar volume and low $\varepsilon/\bar{k}$.

6. The solubility of argon and CO_2 in crystalline poly(propylene) below its glass transition temperature obeys Henry's Law. However, the solubility behavior of argon in the glassy polymer clearly points to the existence of a microvoid-filling process in addition to the ordinary dissolution.

D. Enthalpy of Sorption

1. Above the Glass Transition Temperature

In the previous section, the linear correlations of ℓnk versus $1/T$, shown in Figures 24, 25 and 26 were discussed and it was pointed out that the data obeyed the van't Hoff expression $k = k_o e^{-(\Delta H_S/RT)}$. This equation has been found to apply, within the experimental error, for all films studied here, over the temperature range of 30° - 70°C. The values of ΔH_S, the enthalpies of sorption, are listed in Table V (see "RESULTS"). The time-lag values of ΔH_S were checked by the relationship $\Delta H_S = E_{\bar{P}} - E_D$ (59), and the agreement was found to be excellent.

The enthalpies or "heats" of sorption for argon were negative and usually of the order of 0.5 to 1.0 Kcals/gmole, while the enthalpies of sorption for helium and CF_4 were positive and 1.7 and 2.2 Kcals/gmole, respectively. The values of ΔH_S seemed to fluctuate randomly from film to film with apparently no consistent variation of ΔH_S with percent crystallinity or thermal history.

Since the enthalpy of sorption is a measure of the degree of interaction between the polymer and the dissolving molecule, an attempt was made to correlate ΔH_S with $\varepsilon/\bar{k}$. In the face of the successful correlation of k* with $\varepsilon/\bar{k}$ discussed earlier, and the inherent connection between solubility and the enthalpy of sorption, it was felt that $\varepsilon/\bar{k}$ should correlate ΔH_S just as well. Figure 53 is the resulting plot with the data for linear poly(ethylene) as background. The average values of ΔH_S for helium and argon fit the best line through the poly(ethylene) data very well. This observation reflects the nearly identical values of the cohesive energy densities of the two polymers, namely 62.3 and 65.6 cal/cc for poly(ethylene) (89) and poly(propylene) (1), respectively. For both polymers ΔH_S becomes increasingly negative, or exothermic, with increasing $\varepsilon/\bar{k}$. However, as before, the value for CF_4 is anomalous, in that ΔH_S is endothermic (positive).

Initially, it was felt that the high positive value of ΔH_S for CF_4 may be due to a steric effect. In other words, the large CF_4 molecule may be barred from some of the intercrystalline

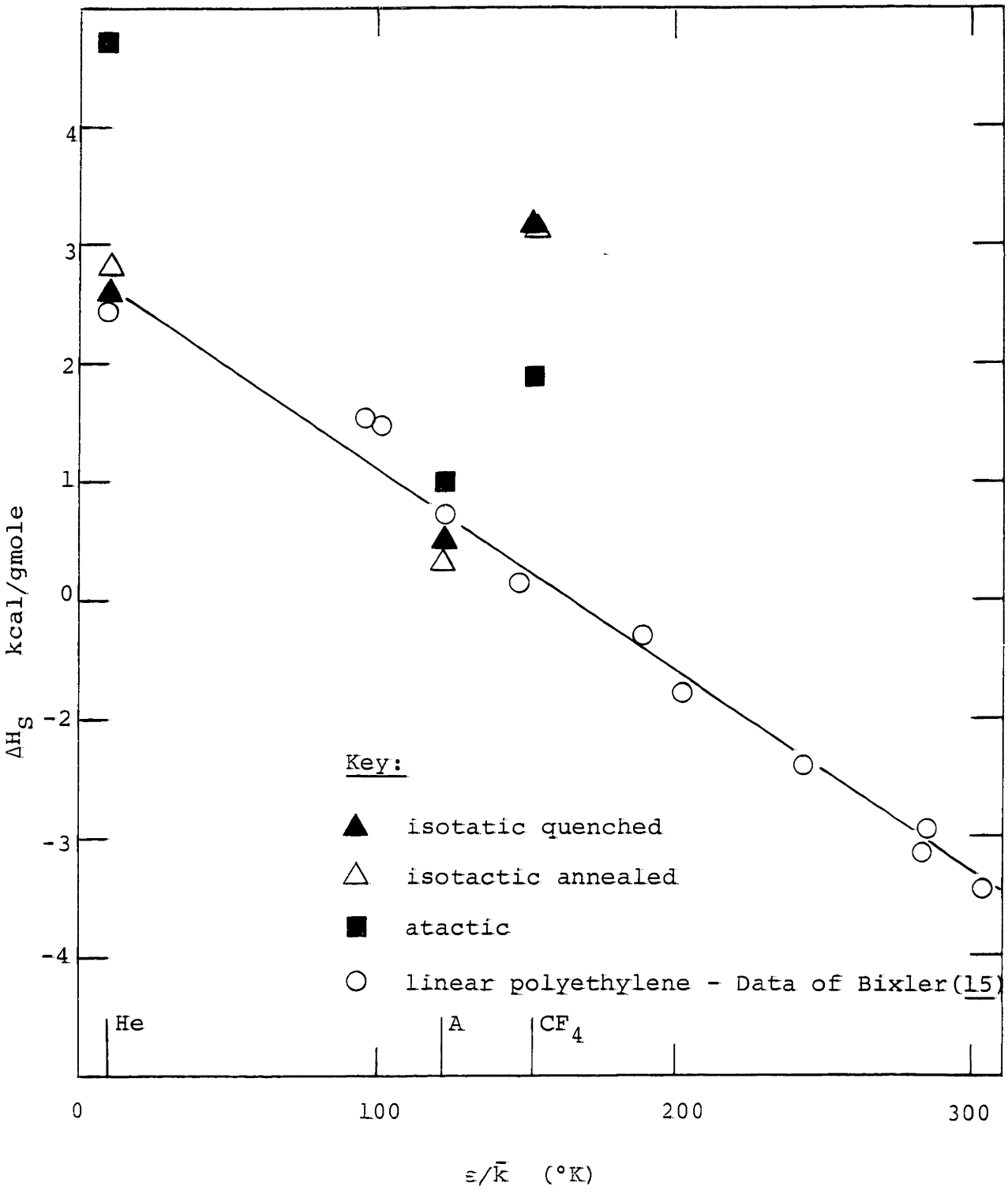

Figure 53 Heat of Sorption Related to Force Constant of Gas

amorphous material due to its size. Then at higher temperatures, these sites may become accessible due to the thermal expansion, giving rise to the large positive heats. However, this possibility was eliminated by the observation that the ΔH_S for the completely amorphous material, i.e., the atactic poly-(propylene), was similarly positive, contrary to other gases of comparable $\varepsilon/\bar{k}$ values. Again, this behavior can be explained on the basis of the high partial molar volume and relatively low $\varepsilon/\bar{k}$ of the CF_4 molecule, namely both tend to reduce the interaction between the polymer and the CF_4 molecule.

The heat of sorption for helium is positive. This is understandable when one considers the low force constant, 10 versus 122 and 158 for argon and CF_4, respectively. The heat of sorption for helium is even more positive in the completely amorphous (atactic) polymer. This may be explained on the basis of variations in the cohesive energy density in the crystalline polymer due to crystal edge effects and intercrystallite stress concentrations which may result in stronger polymer-gas interactions.

2. Below the Glass Transition Temperature

For argon and carbon dioxide sorption studies were made, both above and below the glass transition point. In the case of argon, the heat of sorption in the glassy polymer was considerably more exothermic than in the rubbery polymer. This, together with the higher level of sorption in the glassy polymer, points to the existence of microvoids as a stable phase. The gas

is believed to be adsorbed on the walls of the voids by a Langmuir-type of sorption process (112). This would account for the larger negative heats of sorption.

Although carbon dioxide has a greater force constant and interacts more strongly with the polymer, as indicated by the much higher level of sorption compared to argon, the heats of sorption in the rubbery and glassy polymer were the same within the limits of the experimental error. As suggested earlier, this may be due to the fact that the generally high level of dissolution of CO_2 in the rubbery polymer obscures the contribution to sorption by the microvoid-filling process.

The dual-mode sorption process, ordinary dissolution plus microvoid-filling, has previously been established for poly(ethylene terephthalate), PET (111) and polystyrene, PS (103). In these cases the solubility of the glassy polymer could be expressed as

$$C = C_D + C_H \qquad (60)$$

where C is the overall solubility, C_D is the solubility due to ordinary dissolution and C_H is the solubility due to microvoid-filling. By observing the solubility of these polymers over a range of higher pressures it was possible to separate the hole-filling and ordinary dissolution contribution to solubility. The solubility constant was thus described as

$$C = k_D P + \frac{C'_H bP}{1 + bP} \qquad (61)$$

Table VII

Comparison of Calculated Enthalpies of Adsorption in Glassy Poly(propylene), Poly(styrene) and Poly(ethylene terephthalate)

Gas	Polymer	State	Radius of Micro-Voids	Adsorption Constant, $C'_H b$	U_{OO}	ΔH_{ads} at 25°C
			A°	$\frac{cc(STP)}{cc_p\text{-atm}}$	$\frac{Kcals}{gmole}$	$\frac{Kcals}{gmole}$
A	P.P.	crystalline	32	0.171*	-1.8	-0.9
A	P.S.	unoriented	27	0.191	-2.4	-1.5
A	P.S.	oriented	33	0.159	-2.4	-1.5
CO_2	P.P.	crystalline	32	2.22*	-2.5	-1.6
CO_2	P.S.	unoriented	31	2.85	-3.4	-2.5
CO_2	P.S.	oriented	39	2.42	-3.4	-2.5
CO_2	P.E.T.	amorphous	44	2.33	-3.5	-2.6
CO_2	P.E.T.	crystalline	32	3.33*	-3.2	-2.3
CO_2	P.E.T.	oriented	22	5.51*	-3.2	-2.3
CH_4	P.S.	unoriented	25	0.80	-2.6	-1.7
CH_4	P.S.	oriented	31	0.47	-2.5	-1.6

---

* Normalized to $\alpha = 1.0$

U_{OO} = the potential energy at the minimum in $U_O(z,y)$

$\Delta H_{ads} = U_{OO} + \frac{h\nu_z}{2} + \frac{3}{2}\bar{k}T$

P.P. = poly(propylene)

P.S. = poly(styrene), data of Vieth, Tam and Michaels (112)

P.E.T. = poly(ethylene terephthalate), data of Vieth, Alcalay and Frabetti (114)

where C'_H is the hole-saturation constant and b is the hole-affinity constant. The first term on the right hand side of equation (61) describes the ordinary dissolution and the second term the hole-filling contribution. This later process is pictured as a Langmuir-type or physical adsorption of gas molecules on the surface of the "frozen-in" microvoids. Thus the parameter b is a measure of the interaction of the gas and the polymer, and C'_H, the microvoid saturation limit, is related to the number of gas molecules that can be accomodated on the walls of the microvoids.

For PET and PS a plot of solubility versus pressure showed an initial curvature towards the x-axis followed by a straight line of constant slope. This meant that, at low pressures, one was observing the sum of both sorption processes, while, at higher pressure, the microvoids were saturated with gas, and any additional solubility was due simply to Henry's Law-type dissolution.

Table VII is the result of an analysis and comparison of the data for glassy poly(propylene) with the data of Vieth (111), and Vieth and Tam (112) for PET and PS, respectively. Although the main points of the analysis will only be summarized here, a detailed evaluation can be found under "Sample Calculations" in Appendix B.

The fourth column in Table VII represents the apparent radius of the "frozen-in" microvoids. One arrives at this

hole-size by making the assumptions that firstly, the total volume of voids present is equivalent to the WLF free volume of 0.025 cc/cc of polymer and secondly, the voids are spherical and all of the same size. Although these assumptions are approximations at best, they seem to lead to values which appear to be quite reasonable.

As mentioned above for PET and PS, it was possible to evaluate the contribution made by the hole-filling process. Thus, by knowing C_H', the saturation constant, it was possible to determine the average hole-size. The values ranged from 25 to 39Å for poly(styrene), with the unoriented polymer having the smaller microvoids and the oriented polymer having the larger microvoids. This is exactly what would be predicted on the basis of experience with stretched polymers.

The hole size calculated for PET is in the same range. The largest holes (44Å in radius) were observed for the amorphous material with the holes in the crystalline material being 32Å in radius. It was surprising that the holes were smaller (R = 22Å) in the drawn samples. However, recent work by Vieth et al. (113) has shown that the curve of permeability versus orientation goes through a maximum which may be indicative of competing processes of hole-formation and hole-closing, reminiscent of stretching a fish net (61).

As was pointed out earlier, it was not possible to establish values of C_H' for glassy poly(propylene). Nevertheless, since the

hole size in PET was not much different from PS it was felt that the hole size in crystalline PET would be a good approximation of that in crystalline poly(propylene). With the estimate of the hole size it became possible to calculate an adsorption constant, bC'_H, which is a measure of the strength of sorption due to hole-filling.

The adsorption constants for argon and CO_2 in poly(propylene) compare in magnitude with those for the same gases in poly(styrene) and poly(ethylene terephthalate), although for the latter, the values are slightly higher. That, however, is attributable to the polar nature of PET. In the case of PS, data for three different gases are reported and it appears that the magnitude of C'_Hb increases with increasing force constant.

Under column 6 of Table VII are listed the values of U_{OO}, the potential energy of an adsorbed molecule at its point of closest approach to the adsorbing surface. This quantity could be evaluated using statistical mechanics and assuming the adsorbed gas is in the state of a dilute, mobile adsorbed phase. According to Hill (43) the adsorbed phase is "mobile" if $\bar{k}T >> V_o$, where V_o is the potential energy barrier to movement of an adsorbed molecule along the surface. With van der Waal forces, these barriers are of the order of 0.3 to 1 Kcal/gmole. A quick calculation shows that this is the condition applicable to this study.

Accounting for the vibrational and thermal energy of the molecule at the temperature under consideration one obtains from U_{OO} the enthalpy of adsorption, ΔH_{ads}. The values of ΔH_{ads} for the three polymers were in the range of -0.9 to -2.6 Kcals/gmole - an energy level characteristic of physical adsorption. Again the heats of adsorption reflect the force constant of the gas in that the ΔH_{ads} increases with increasing $\varepsilon/\bar{k}$ of the gas. The values of ΔH_{ads} for poly(propylene) are slightly lower than for poly(styrene). The polarizable benzene rings in poly(styrene) are probably responsible for this.

Summary - ΔH_S

1. The level of the enthalpies of sorption for He, A and CF_4 in the rubbery, crystalline polymer is characteristic of dissolution. The enthalpies of sorption for helium and CF_4 are positive, those for argon, negative. While the behavior of He and A is as expected, based on previous experience with poly-(ethylene), the positive enthalpy of sorption for CF_4 is somewhat anomalous. It can, however, be explained on the basis of the relatively high partial molar volume and the low $\varepsilon/\bar{k}$ of CF_4. One would expect ΔH_S to become increasingly more negative with increasing $\varepsilon/\bar{k}$.

2. The enthalpy of sorption is constant over the range of temperatures considered, in both the rubbery and glassy region.

3. For argon, ΔH_S is significantly more exothermic in the glassy polymer, pointing to additional sorption by micrvoid-filling. The enthalpy of sorption for CO_2, on the other hand, is already quite high in the rubbery state, and any incremental contribution to sorption by microvoid-filling in the glassy state is most likely obscured by it.

4. The data for argon suggested a definite break at the glass transition point which appears to be approximately zero degrees centigrade, a value most generally quoted as the T_g of crystalline poly(propylene).

5. The average size of the "frozen-in" microvoids in glassy poly(propylene) appears to be 32Å in radius. The enthalpy of adsorption is slightly lower than that in poly(styrene) and poly-(ethylene terephthalate), but the magnitude of the calculated ΔH_{ads} is characteristic of physical adsorption and in rather good agreement with the measured value for ΔH_S.

E. Entropy of Solution

An additional attempt toward better understanding of the solution of gases in a polymer consisted of an evaluation of the entropies of solution. Jolley and Hildebrand (52) found a remarkably close correlation of different gases in the same solvent by plotting the entropy of solution, $(\bar{S}_2 - S_2^g)$, versus $R\ell nx_2$, the molefraction of the gas in solution. A similar plot, Figure 54, shows that the entropies of solution for He, A and

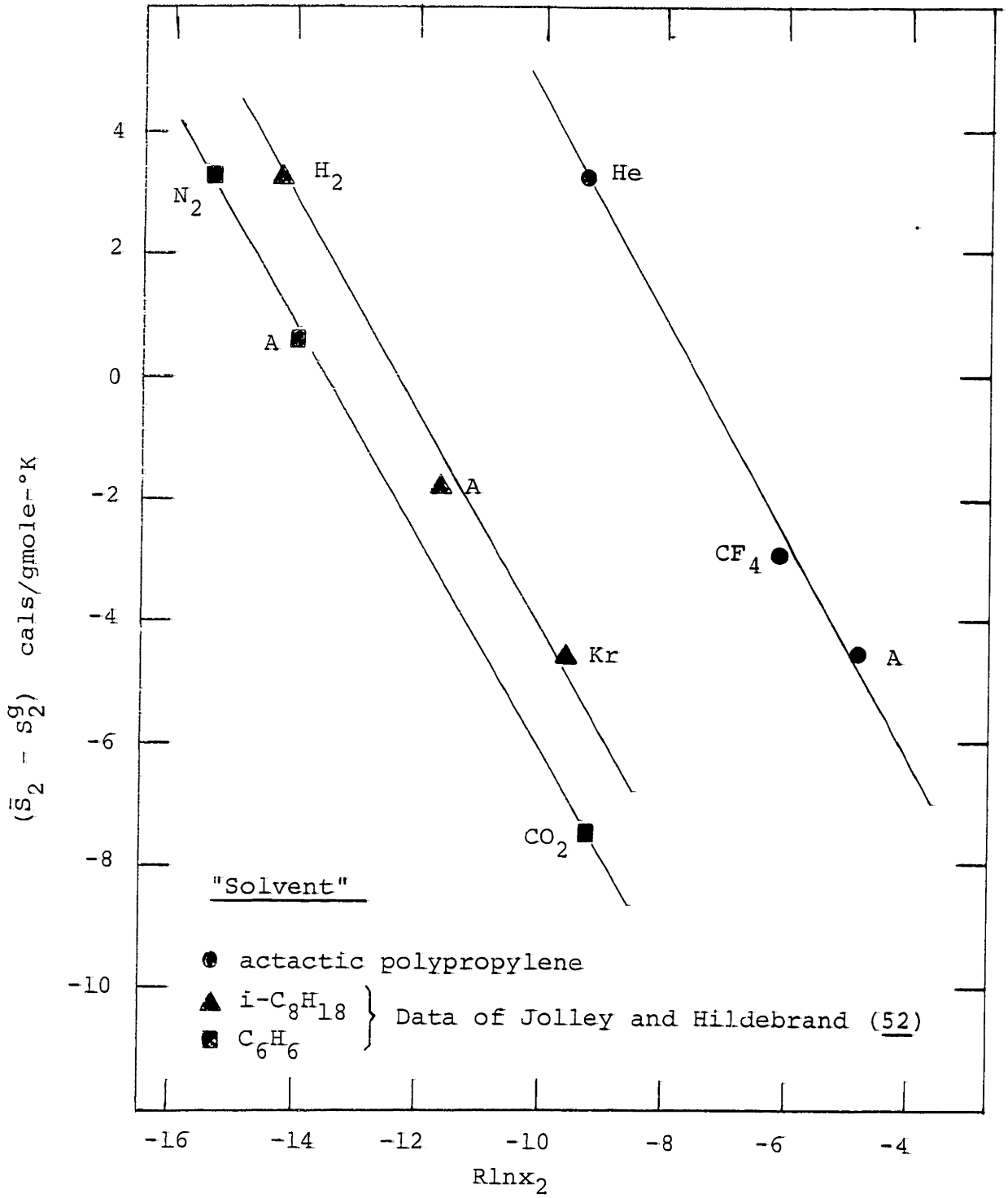

Figure 54 Entropy of Solution Related to Mole Fraction in Solution

CF_4 correlate well with their mole fraction in the polymer. In fact, the line of the data for poly(propylene) was parallel to the lines for various hydrocarbon solvents, as shown by Jolley and Hildebrand (52).

Table VIII

Isosteric Heats and Entropies of Solution

Gas	Polymer	q_s $\frac{cals}{gmole}$	$(\bar{S}_2 - S_2^g)$ $\frac{cals}{gmole-°K}$	$R\ell nx_2$ $\frac{cals}{gmole-°K}$
He	atactic	-3720	+3.25	-9.25
A	atactic	-68	-4.57	-4.80
CF_4	atactic	-930	-2.96	-6.09

Table VIII lists the values of $(\bar{S}_2 - S_2^g)$ as well as q_s (see below) and $R\ell nx$, both associated with the calculation of the entropies of solution. $(\bar{S}_2 - S_2^g)$ was calculated from the expression

$$(\bar{S}_2 - S_2^g) = R\ell nx - \frac{q_s}{T} \qquad (62)$$

derived from a thermodynamic analysis of the sorption process. The isosteric heat of sorption, q_s, was obtained from the relationship

$$q_s = -R \left(\frac{d\ell nP}{d\frac{1}{T}} \right)_c \qquad (63)$$

Detailed calculations are presented in Appendix B.

Although the values of $(\bar{S}_2 - S_2^g)$ and $R\ell nx$ appear reasonable and are in line with the data presented by Jolley and Hildebrand (52) the values of q_s appear somewhat anomalous. No satisfactory explanation is presently available for this discrepancy.

F. Diffusion Constants

1. Variation with Temperature

Figures 33, 34 and 35 show plots of ℓnD versus 1/T for the three gases in the various films studied. Without exception, the data are well correlated by straight lines described by the Arrhenius-type expression,

$$D = D_o e^{-E_D/RT} \qquad (12)$$

Theoretically, E_D should be a slight function of temperature, but for all practical purposes E_D appears constant over the temperature range of 30 - 70°C, the range under consideration in this study.

The plots of ℓnD versus 1/T point out the considerable difference between the diffusion levels of helium, argon and CF_4. In other words, diffusivity is a strong function of the size of the diffusing molecule. Furthermore, the pronounced increase in the slope of the lines with increase in penetrant size is convincing evidence that the diffusion process is indeed a size-dependent, activated one.

As was the case with permeability, the differences in individual gas diffusivity for films with different thermal histories were not very large. Nevertheless, these differences were significant and contributed in large measure to the understanding of polymer morphology as will be shown in a later discussion.

In Figure 36 the time-lag data for film 16 was compared with the data obtained for the same film on the low pressure sorption equipment. The agreement was excellent. The same plot also shows another comparison of the data obtained by the "dynamic" method and the "static" method. In this case film 21 was first studied on the time-lag equipment using helium and then on the low pressure sorption equipment using argon. The resulting plot of ℓnD versus $1/T$ compared well with the data of a similar film, film 15, studied in the time-lag apparatus. This gives one confidence that the data obtained by the two different methods is without experimental artifacts and that the two methods are interchangeable. Furthermore, it strongly suggests that the diffusion medium is isotropic.

The diffusion constants for the atactic poly(propylene), the analog for amorphous isotactic poly(propylene), are shown in Figure 37. The diffusivity values in the atactic poly(propylene) were all determined in the low pressure sorption system because the atactic polymer is too tacky and structurally unsound for time-lag studies. However, based on the above discussion of the complete equivalence of diffusion data obtained by either the

time-lag or the static sorption methods, the data should be reliable in describing an amorphous analog with which to compare diffusion constants in the semi-crystalline films.

2. Effect of Crystallinity on Diffusivity

In the following discussion of diffusion constants in semi-crystalline films, frequent reference will be made to a relationship first presented by Parker (88) and later successfully used by Bixler (15). The relationship is $D = (D^*/\tau\beta)$. To aid in the interpretation of the experimental data in the light of this equation, a brief review of its parameters seems advisable at this point.

Strictly speading, D^* would be the diffusivity of the gas in isotactic poly(propylene) in the absence of crystallinity, that is, in completely amorphous, isotactic poly(propylene). As the latter is not obtainable, irrespective of the rate of quenching from the melt, atactic poly(propylene) was chosen as the analog for completely amorphous isotactic poly(propylene). Since isotactic and atactic poly(propylene) are mere stereo-isomers of each other, this approximation is believed to be quite sound. Jeschke and Stuart (51) have used this same substitution and justified it on the basis of the observation that the refractive indices of molten isotactic poly(propylene) - presumably entirely amorphous at this point - and atactic poly(propylene) are identical, within the limits of the experimental error.

The parameter τ, referred to as the geometric impedance factor, was proposed to account for the local reduction in the area available for diffusion and the increased effective path length due to the presence of crystallites. In other words, in the crystalline polymer the gas molecule, in diffusing from one side of the membrane to the other, has neither the total cross-section of the film available for flow nor can it take the most direct path, but must circumvent crystallites. In short, τ is a function of the total amount of crystallinity, the shape of the crystals, and their size and size distribution. Naturally, τ is also a function of temperature, insofar as temperature affects the former variables.

The parameter β was introduced to account for the impedance to diffusion resulting from decreased chain mobility imposed by the presence of crystallites. Since the crystallites act much like cross-links in restraining the movement of the amorphous polymer chain segments, the parameter β will vary with the percent crystallinity, the shape of the crystallites and the size distribution of the crystallites.

Having thus reviewed the current concept of how crystallinity affects diffusivity in semi-crystalline polymers, the discussion will now focus on the experimental observations made for poly(propylene). In Figures 55,56 and 57 are presented plots of diffusivity as a function of the percent amorphous volume. On the basis of the behavior of poly(ethylene) (15) and in the light of the above interpretation of τ and β, one would

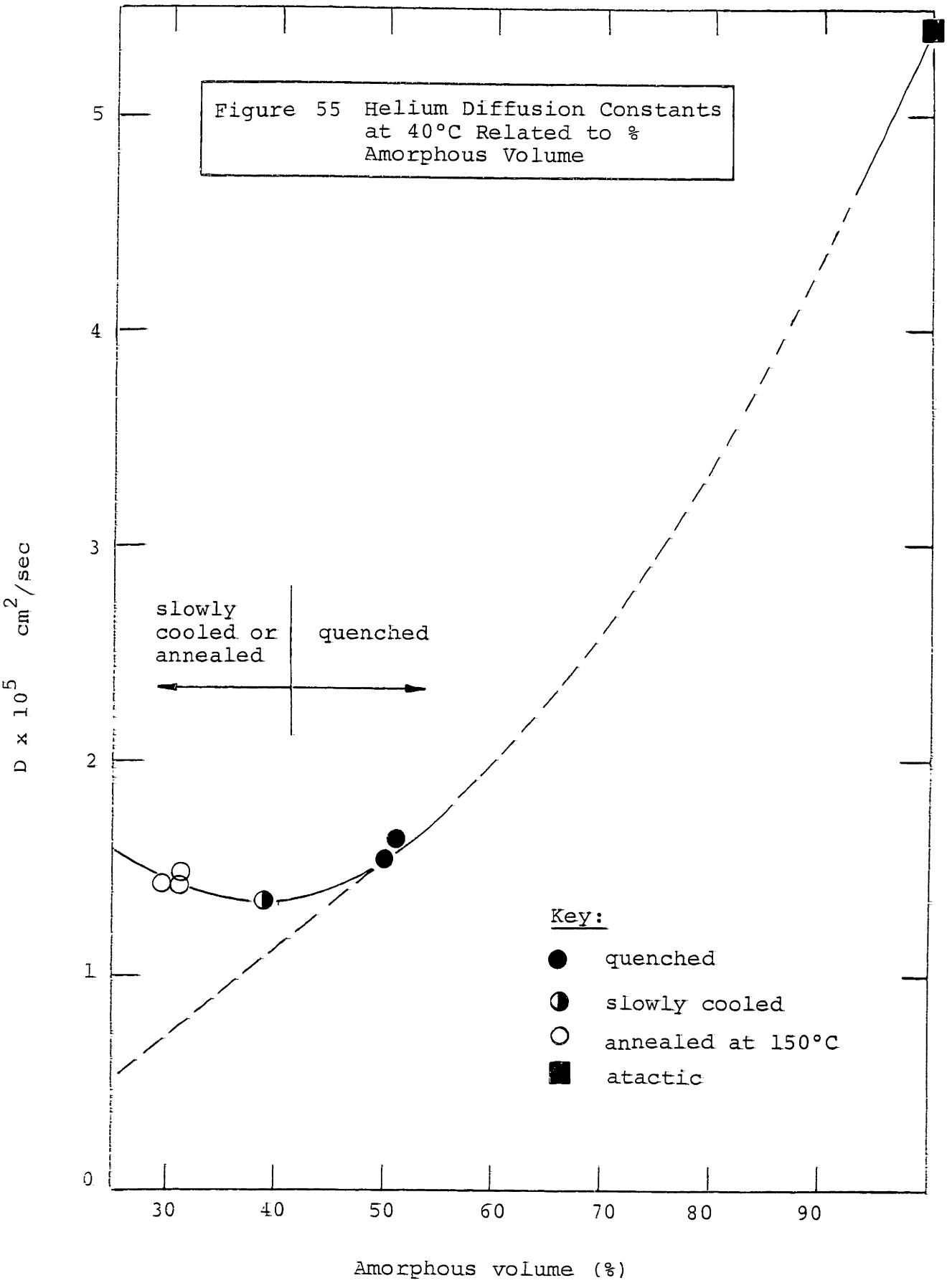
Figure 55 Helium Diffusion Constants at 40°C Related to % Amorphous Volume
slowly cooled or annealed
quenched
Key:
quenched
slowly cooled
annealed at 150°C
atactic
D x 10^5 cm^2/sec
Amorphous volume (%)
0
1
2
3
4
5
30
40
50
60
70
80
90

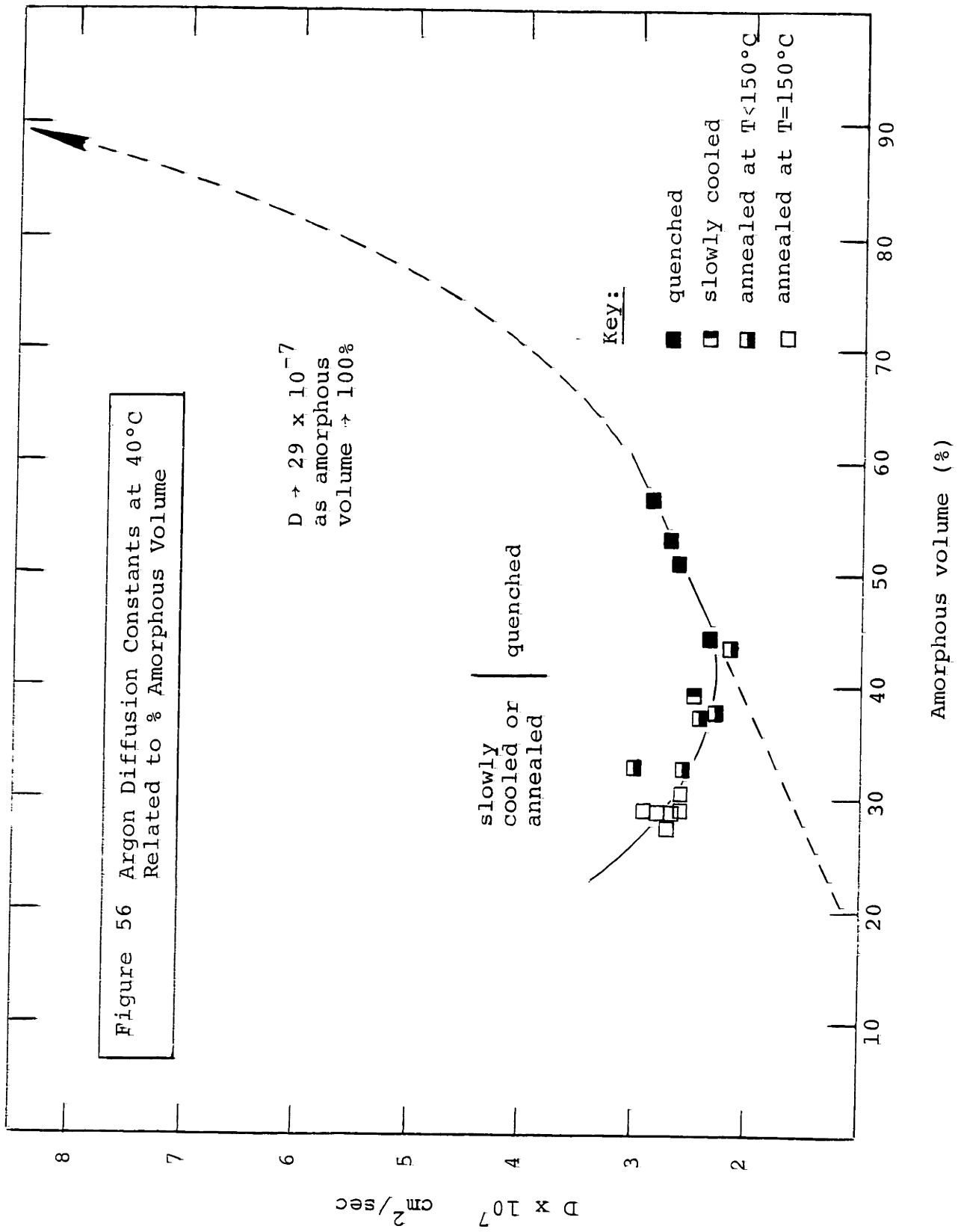
Figure 56 Argon Diffusion Constants at 40°C
Related to % Amorphous Volume
D → 29 x 10⁻⁷
as amorphous
volume → 100%
slowly
cooled or
annealed
quenched
Key:
quenched
slowly cooled
annealed at T<150°C
annealed at T=150°C
D x 10⁷ cm²/sec
Amorphous volume (%)

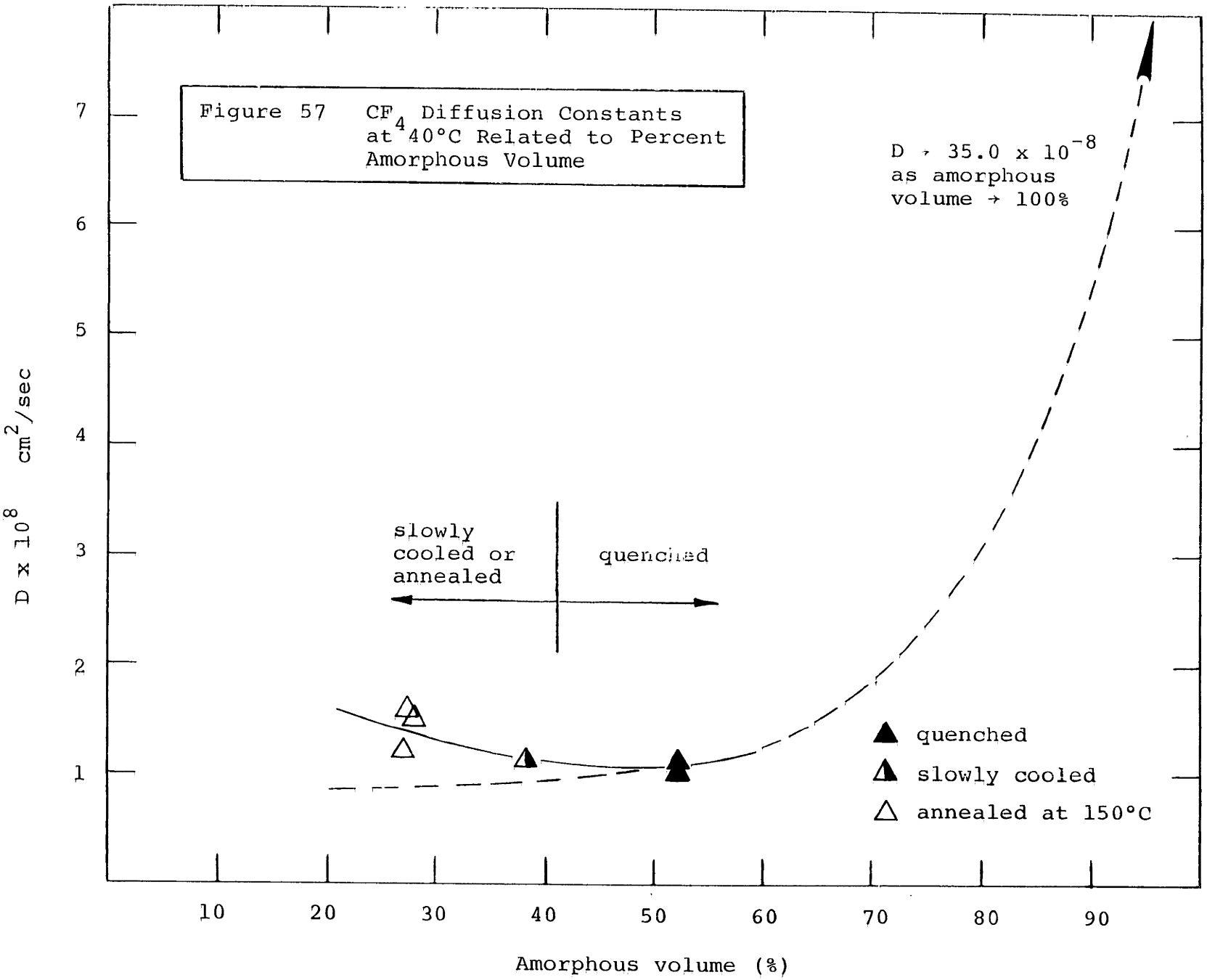
Figure 57 CF_4 Diffusion Constants at 40°C Related to Percent Amorphous Volume
D → 35.0 x 10^{-8} as amorphous volume → 100%
slowly cooled or annealed
quenched
quenched
slowly cooled
annealed at 150°C
D x 10^8 cm^2/sec
Amorphous volume (%)
1
2
3
4
5
6
7
10
20
30
40
50
60
70
80
90

expect the diffusivity to decrease as the percent amorphous volume decreases, i.e., as crystallinity goes up. However, instead of observing this behavior, the curve of diffusivity versus percent amorphous volume appears to pass through a minimum. Initially, diffusivity decreases rapidly but then, as the films are annealed above 80°C, the diffusivity curve flattens and eventually increases. Thus the effect of annealing, with its concomitant increase in crystallinity, does not seem to be simply one of increasing geometric and chain impedance.

In the light of the morphological changes suggested earlier by the solubility data, the following explanation for the diffusion behavior in poly(propylene) evolves. Recalling the conclusion that the change in amorphous content of the films from approximately 60 to 41% (by volume) is not the result of additional crystallization but rather the consequence of the transformation of the smectic to the monoclinic crystal structure aids in this pursuit. Since it is now widely believed (see INTRODUCTION) that the smectic form consists of very small hexagonal crystals, it is reasonable to suggest that the crystal transformation is accompanied by an association of many minute hexagonal crystals into larger, but fewer monoclinic crystals. This would certainly be favored thermodynamically and would become kinetically possible as the thermal motion increases. Most probably, the resulting crystals are more anisometric and offer more diffusional impedance.

Hoffman et al. (45) point out that in the process of quenching a polymer from the melt the supercooled liquid simply collapses into a highly disorganized mass of microcrystallites. This clearly implies that these microcrystallites are connected to one another on a massive scale by intercrystalline links. If it is conceded that the crystals act like chemical cross-links on the movement of the chains, then one would expect the chain impedance, β, to be considerable in the quenched material. Similarly, after the crystal transformation one would expect much fewer restraints on the chain segments due to the reduction in the number of crystals, and subsequently "cross-links", as is illustrated in Figure 51.

Thus the effect of the crystal transformation on diffusivity is two-fold: firstly, it decreases diffusivity by making the diffusion path more tortuous, and secondly, it tends to increase diffusivity by enhancing chain mobility. Since the first phenomenon predominates, the net result is a decrease in diffusivity.

On annealing, two more effects come into play: namely, additional crystallization and thickening of existing crystals without new growth. Due to the chain-folded nature of the lamellae, the crystal grows by adding material to its edges with an inevitable increase in lateral dimensions. This tends to make the diffusional path more tortuous and to lower diffusivity.

Thickening of the crystal, on the other hand, tends to make them more isometric and tends to remove interlamellar links. As discussed in the INTRODUCTION, Hoffman and coworkers (45) picture the thickening process as one of pulling chain ends into the crystal surface and lengthening of the fold period by self-diffusion of the molecules along their own backbones and/or by partial melting and recrystallization with a larger fold-period. As the thickening process proceeds, chains may actually be pulled right through the lamella, leaving behind a vacant row. A series of such row vacancies would greatly enhance diffusion, because diffusion through them would presumably no longer have to be activated but could proceed by a non-activated diffusion mechanism. The increase in D due to such row vacancy defects overshadows the effect of increased tortuosity completely, with the net effect of causing an actual upswing of D in spite of the increasing crystallinity of the film.

An analysis of this process of row vacancy defect formation on the basis of a rate expression for lamellar thickening (see Appendix G) reveals that, for a given annealing time, the process is directly related to the annealing temperature. In other words, at a high annealing temperature more thickening occurs with consequently greater propensity for defect formation.

As mentioned before, the thickening of the lamellae is accompanied by a reduction in the number of interlamellar links. Consequently, the diffusing molecule encounters fewer chains as it

meanders through the remaining amorphous regions. This too, contributes to the diffusion enhancement, yet to a minor extent.

These results are summarized in Figure 58, which shows qualitatively the variation of D, and the factors influencing D, with the amorphous content of the film. For the films quenched to various amorphous levels, the slight decrease in chain impedance counteracts the effect of increasing tortuosity somewhat with the result that the diffusivity is slightly enhanced. On annealing, row vacancy defect formation and reduction in the number of interlamellar links predominate and overshadow the effect of increasing geometric impedance to such an extent that diffusivity actually increases in spite of the increasing crystallinity.

The conclusion that crystalline defects rather than changes in the amorphous phase are responsible for the observed diffusional enhancement was reached on the basis of the following analysis. A change in the properties of the amorphous phase, on annealing, should be reflected by a change in the values of E_D and ΔH_S, a change which would be greatest for the largest molecule, CF_4. Neither was observed - the values of E_D and ΔH_S did not change on annealing and CF_4 showed the smallest diffusional enhancement. Thus, the increase in diffusivity in spite of the increased crystallinity must be due to a decrease in the tortuosity of the diffusional path. This, in turn, could occur either by the crystals becoming more isometric or by the formation of crystalline defects large enough to allow passage of the

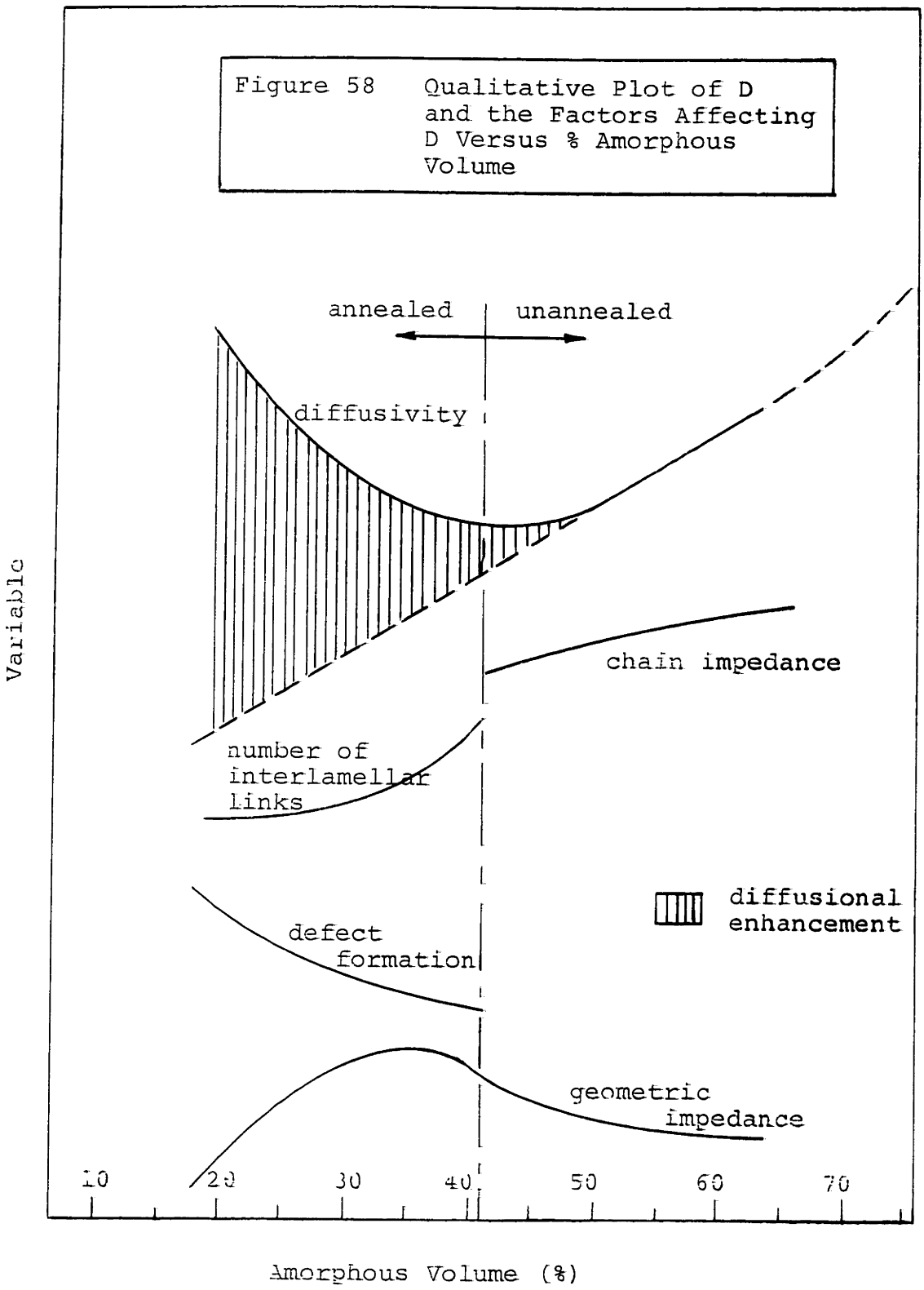

Figure 58 Qualitative Plot of D and the Factors Affecting D Versus % Amorphous Volume

diffusing molecule. The first possibility is unlikely because the crystals are chain-folded lamellae with additional growth at the crystal edges preferred over growth at the crystal faces. Furthermore, observations with single-crystal lamellae of poly-(ethylene) have shown that lamellar thickening produced no decrease in the lateral dimensions of the lamella. This strongly suggests the formation of crystal defects, i.e., vacant micro-pores through the lamella.

The mechanism of diffusion in the defects if probably non-activated and analogous to gas diffusing in very small pores, i.e., Knudsen diffusion, where the diffusion coefficient is a factor of several hundred-fold larger than those measured in this work. However, in annealed films activation energies equal to those in the unannealed films were observed. This militates against the possibility that there exist interconnected defect pathways through the entire film, but still allows for the existence of non-interconnected defects passing through individual lamellae. This leads to a picture of diffusion through an amorphous phase containing a suspension of partially permeable crystallites, where the diffusing molecule spends most of its time in the amorphous phase and only occasionally passes through a lamellar defect.

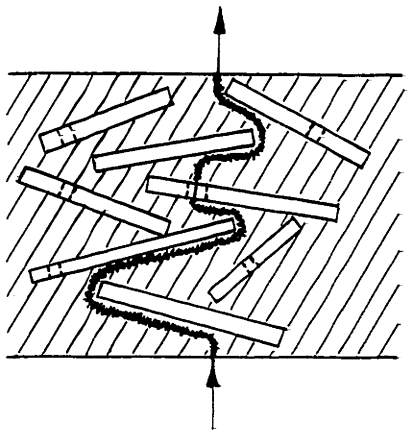

Since diffusion through defects is so much easier than through the amorphous phase, the number of defects necessary to

account for the observed diffusion enhancement is governed primarily by the ability of the diffusing molecule to find defects. Unfortunately, it is impossible to establish a realistic two-dimensional model for the size, shape, and orientation of the crystals in an isotropic sample of poly(propylene). Therefore, it is difficult to accurately estimate the volume fraction of defects necessary so that, on the average, a diffusing molecule finds enough defects to reduce its diffusion path length through the membrane by 97%, in the case of helium for example.

However, one can obtain some indication of the volume fraction of defects present from the following analysis. From entropy considerations, one finds that for the gases studied the length of an average diffusion step in the amorphous phase is on the order of 30Å, a value which compares well with the value of 27Å observed by Meares (63) for similar gases in poly(vinyl acetate).

For a molecule to be never more than one diffusion step length away from a defect, it would require 0.6% defects based on total sample volume (Appendix G). This estimate implies defects of uniform size (4.5Å in diameter), homogeneously distributed. This is an admittedly oversimplified picture. Nevertheless, this calculation tends to over-estimate the volume fraction of defects actually present because the crystalline phase does not act like a sieve as is apparent from the observation that τ is still approximately four for the annealed films.

Another estimate of required defect-fraction may be obtained from an application of a series resistance law for transport in an amorphous phase containing a suspension of partially permeable

crystallites. The simplest assumption would be that the defective crystallites are homogeneously distributed. This, however, is again an over-simplification, as accepted models of the crystallization process show that it is the older, more highly annealed crystals which will be defective. Consequently, the distribution of defects will be spatially non-randomized, and one again would require only a very small volume fraction of defects to account for the observed diffusional enhancement.

Finally, considering especially the presence of only minor differences (1.9%) between X-ray diffraction and density gradient-method estimates of crystallinity in annealed samples, one is led to the conclusion that a very small fraction of the sample (ca. a few percent) would have to be defective to account for the observed diffusional enhancement.

The discussion will now briefly focus on the concept of row vacancy defects in relation to penetrant size. It was postulated that on thickening of the lamella, rows become vacant in the crystal lattice. The chance, however, that two or more adjacent rows are vacated concurrently becomes less and less probable, so that there must exist a size distribution of row vacancies. In other words, diffusional enhancement should depend on the penetrant size and should be smaller for the larger molecules.

Indeed, this is what one observes experimentally for the annealed films. The increase in diffusivity over what one would predict from equation (18) at the 30% amorphous level,

for example, is 97%, 66% and 44% for helium, argon and CF_4, respectively. The diffusivity of the smallest molecule, helium, is enhanced much more than that of CF_4, the largest molecule studied. If one assumes that the mode of transport in the defects is non-activated and that, thus, the diffusional resistance in the defects is negligible compared to that in the amorphous regions, it becomes possible to estimate a size distribution for the accessible defects, i.e., defects large enough to accommodate the helium molecule. From the diffusional enhancement for each gas one calculates the reduction in sinuosity of the diffusion path, τ_{eff}/τ, due to the defects and determines the fraction of all defects accessible to each gas (see Appendix H). This leads to the cumulative plot, shown in Figure 59. From this plot, in turn, it is possible to construct Figure 60, showing the size distribution of the accessible defects.

The size of the most common defect appears to be 4.2Å in diameter, with defects of either size distributed almost symmetrically around this value. From an analysis of the monoclinic crystal lattice (see Appendix F) one can conclude that the largest uniform cavity left by the removal of one chain from the lattice is approximately 4.5Å. Thus the size of the most common defect compares well with the size of a vacant lattice site and strongly suggests that, indeed a large percentage of the lamellar defects are single, vacant rows in the crystal lattice.

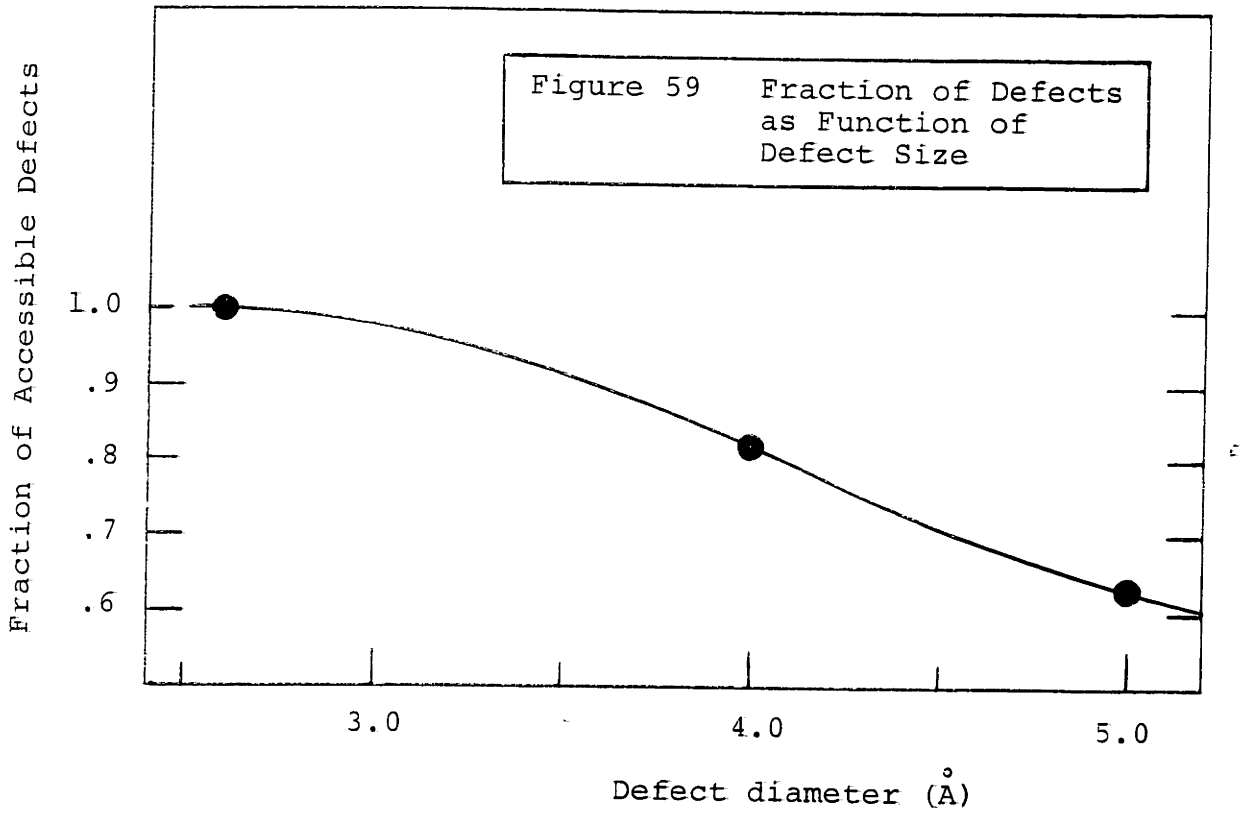

Figure 59 Fraction of Defects as Function of Defect Size

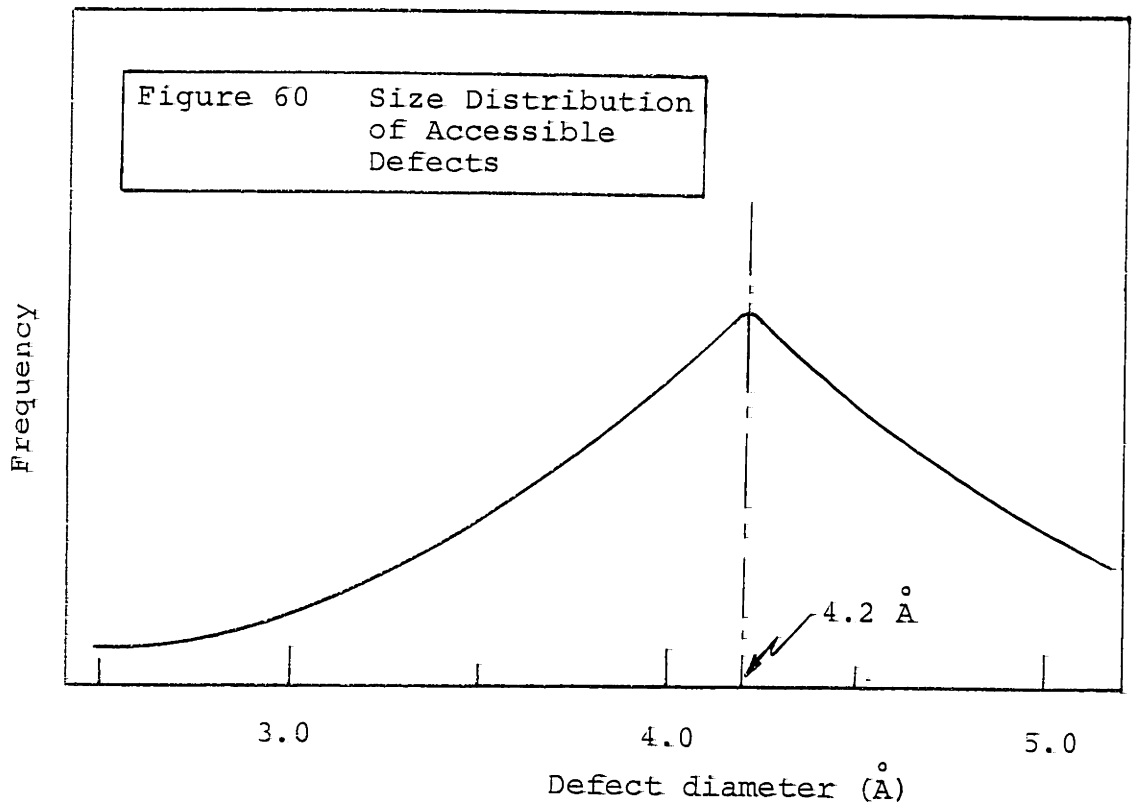

Figure 60 Size Distribution of Accessible Defects

3. Variation of τ with α

To recapitulate briefly, in going from rapidly quenched to fully annealed films, τ increases initially due to the reduction of the area available for flow and the formation of large, more anisometric crystallites and then decreases due to defect formation during annealing. In turn, the diffusivity passes through a minimum as the amorphous volume fraction decreases. Furthermore, the changes in τ are not of the same magnitude for the three gases. It appears that the larger molecules have difficulty in availing themselves of all newly formed channels because of their size. Therefore the increase in diffusivity, over what one would predict for a system without defects, is in the ratio of 1:1.4:2.1 for CF_4, argon and helium respectively. This is approximately the same ratio as the molecular diameters of these gases, namely 1:1.6:2.1 for helium, argon and CF_4, respectively.

In previous investigations (15, 33) it was assumed that the tortuosity is the same for all gases and identical to that of helium. It was further assumed that the helium gas molecule was so small that it was insensitive to any restraints on chain mobility due to crystallinity; consequently, $\beta = 1$ for helium. From that it was possible to calculate τ for any gas by rearranging equation (18) to

$$\tau = \frac{D^*}{D\beta} \qquad (18a)$$

Table IX

Geometric Impedance and Chain Immobilization Factors

Film	Description	Gas	α (%)	τ	β	$\tau\beta$
18	RH	He	51.0	3.31	1.00	3.31
19	RH-150	He	31.0	3.67	1.00	3.67
20	MH	He	50.0	3.48	1.00	3.48
21	MH-150	He	29.5	3.78	1.00	3.78
22	SH	He	39.0	4.00	1.00	4.00
23	SH-150	He	31.0	3.78	1.00	3.78
1	RA	A	56.5	2.55*	4.03	10.28
3	RA	A	53.0	2.82*	3.81	10.74
6	MA	A	44.5	3.75*	3.30	12.40
7	MA-80	A	43.5	3.93*	3.42	13.40
14	MA	A	51.0	3.00*	3.72	11.16
24	RF	CF_4	52.2	2.88*	11.05	31.82
25	MF	CF_4	52.4	2.87*	11.29	32.40

* Estimated from Figure 61 at the values of α shown.

The values of τ for helium in poly(propylene) evaluated in this way, are tabulated in Table IX and correlated against the percent amorphous volume in a log-log plot as shown in Figure 61. The diagonal lines represent the geometric impedance to be expected in unannealed films. For comparison the lines for τ in linear and branched poly(ethylene) are also shown. The more horizontal line represents the tortuosity experienced by helium in the annealed films and clearly illustrates that the geometric impedance in annealed films is much lower than what one would predict from the line for the unannealed films at the same level of crystallinity (see shaded area, Figure 61). In fact, at the 30% amorphous level the τ is approximately one half (i.e., 51%) of what one would predict for the unannealed film. Thus the reduction of τ by a factor of two explains the 97% increase of the helium diffusivity in annealed films at α = 30%.

The fact that, in annealed films, the diffusivity does not increase by an equal percentage for all three gases must mean that argon and CF_4, being larger molecules, do no longer encounter the same tortuosity as the small helium molecule. However, as in the previous investigations, it is believed that the geometric impedance factor for helium represents the tortuosity for all gases in the unannealed films.

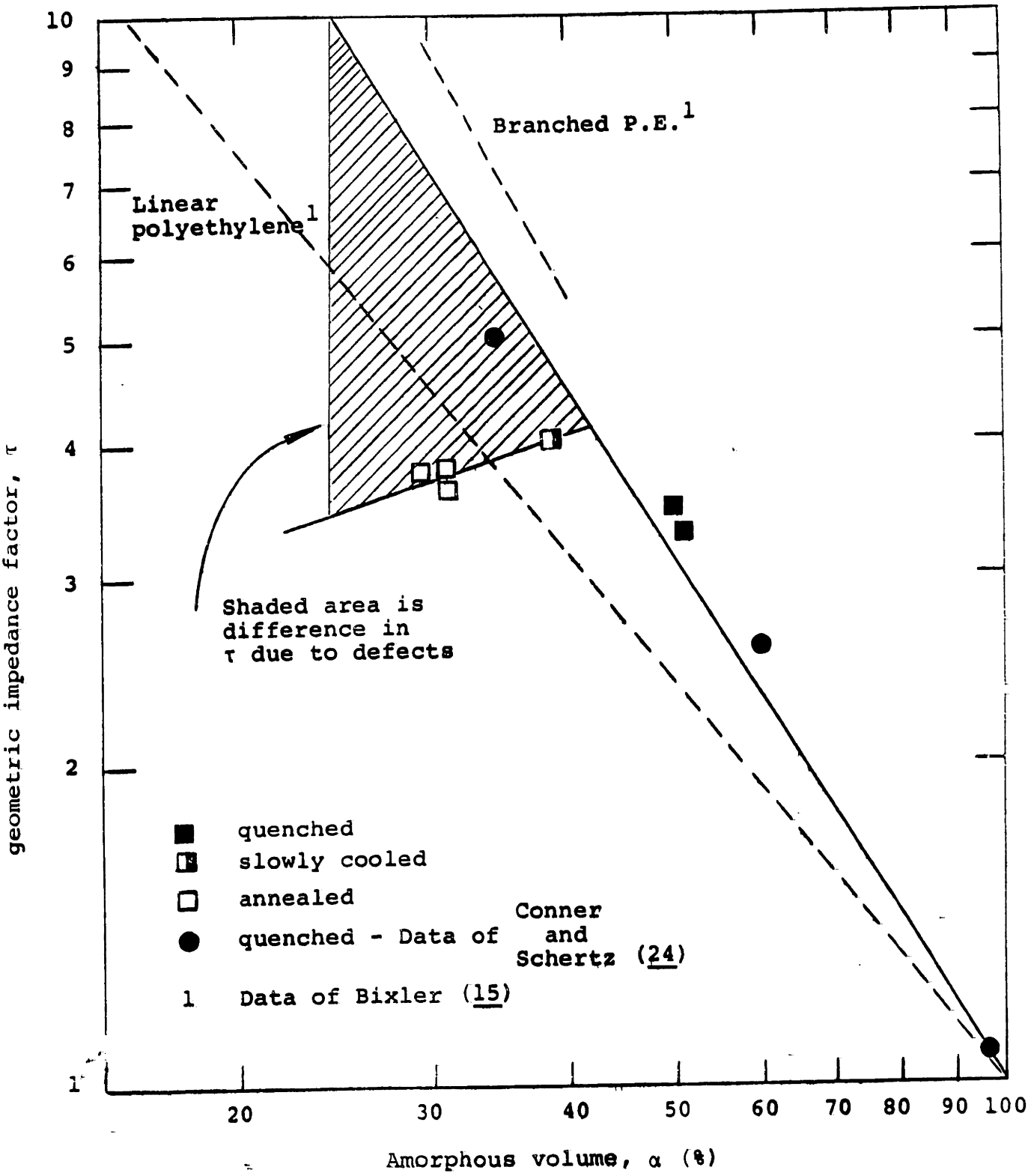

Figure 61 Variation of τ with α for Helium

The same type of variation of τ with thermal history was observed by Fein (33) in annealed films of poly(ethylene). Fein found that the tortuosity of his annealed films fell far below what one would predict from the values observed for various quenched films. Although he offers no explanation for these observations, he explains the marked drop in mean axial ratio of the crystallites in his annealed films by proposing a hole-formation mechanism similar to that observed in single crystals of poly(ethylene).

4. Chain Immobilization Factor, β

In the previous discussion it was pointed out how, with the assumption that $\beta = 1.0$ for helium and the equation (18a), it was possible to evaluate τ for helium. Assuming further that τ is the same for all three gases at least in the unannealed films, it is possible to estimate values of τ for argon and CF_4 in the quenched films (see Table IX). Figure 62 shows that $\ln\beta$ is correlated well by d^2, the square of the molecular diameter. Although this correlation is entirely empirical, some significance can be attached to it. Since the mechanism of activated diffusion is pictured as the passage of the activated molecule from hole to hole in the amorphous matrix via a temporary tunnel, it becomes obvious that prying apart chains to allow a molecule to pass is a necessary step in diffusion. The extent of chain separation should, in turn, be a function of the cross-sectional area of the diffusing molecule. Therefore it is not unreasonable to find that β correlates well with d^2.

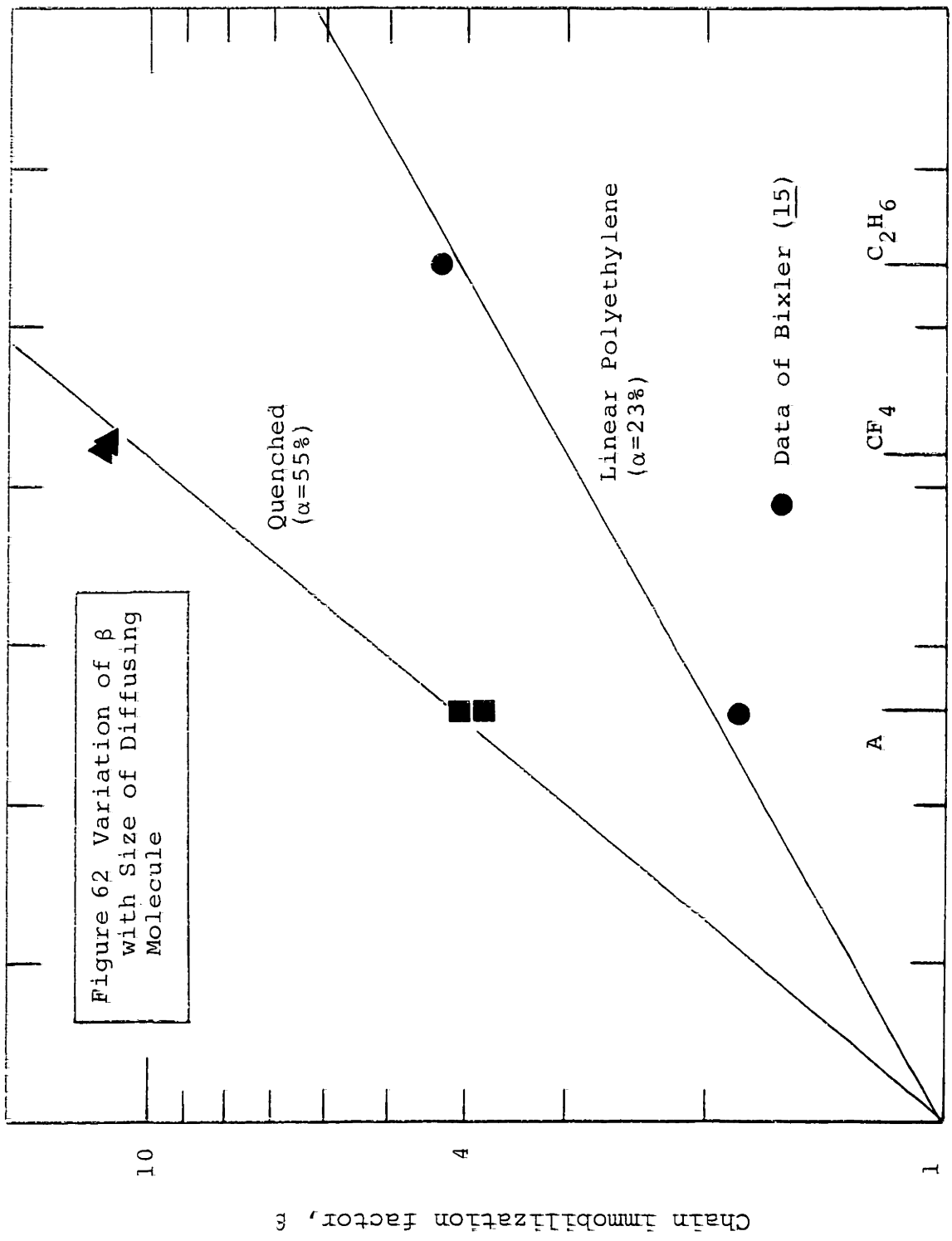

Figure 62 Variation of β with Size of Diffusing Molecule

A similar line for the data of linear poly(ethylene) is shown for comparison. The fact that the line for poly-(propylene) lies above that for poly(ethylene) may be attributed to the fact that the chain of the former is stiffer with chain rotations hindered by the bulky $\dot{C}H_3$ groups. In addition, the diffusing molecule may occasionally encounter the chain in its helical conformation, giving even greater rigidity to the chain.

On one occasion, the assumption was made that the tortuosity observed for helium in annealed as well as unannealed films is the same for the three gases, an acceptable assumption in the absence of crystalline defects. From the subsequent plot of $\ell n\beta$ versus d^2 (not shown) one finds that the line for the annealed poly(propylene) films lies below that for the quenched films. According to the definition of β this would mean that, after annealing, chains are less restrained and freer to move in spite of increased crystallinity. If so, this effect should also be reflected in the activation energies for diffusion. However, no significant changes in E_D's from quenched to annealed films were observed. Thus, also in the light of this discussion, the concept of row-vacancy defect formation, with the concomitant decrease in τ, explains the marked change in diffusivity on annealing much more convincingly.

Figure 63 is a plot which relates the product of the two impedances, τ and β, in the quenched films to the cross-sectional area of the diffusing molecule. The fact that the plot of $\ell n\beta\tau$

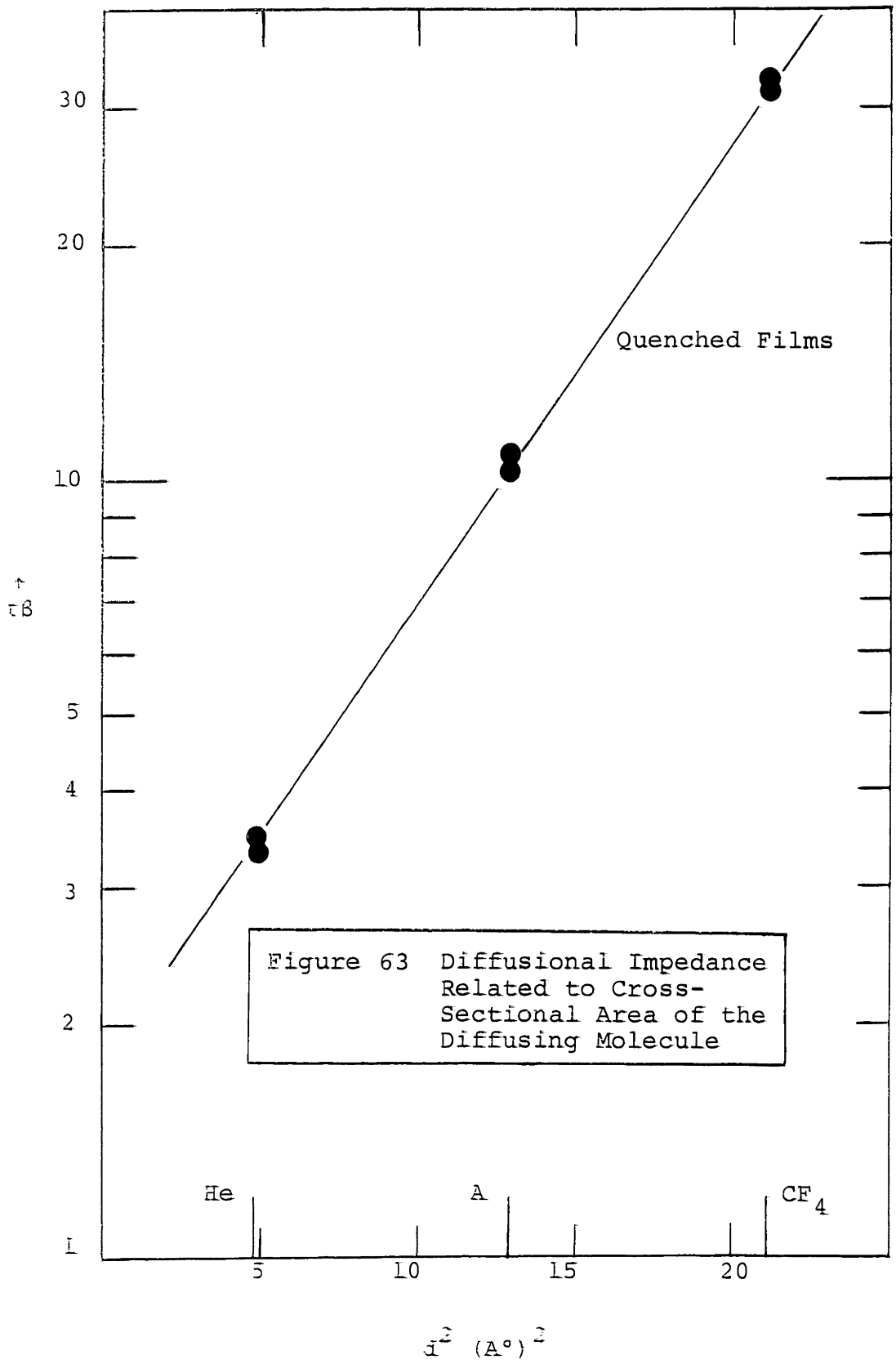

Figure 63 Diffusional Impedance Related to Cross-Sectional Area of the Diffusing Molecule

versus d^2 is an excellent straight line is not in itself of added significance because $\ell n\beta$ versus d^2 was already a linear relationship and it was assumed at the outset that τ remains constant for all three gases. Nevertheless, the plot is valuable in illustrating the magnitude of the total impedance to gas diffusion in crystalline poly(propylene). It also points out how strongly dependent the impedance is on the size of the diffusing molecule. This will be further emphasized in the immediately following discussion of activation energies of diffusion.

5. Summary

1. The diffusion constants are well correlated by the expression $D = D_o e^{-E_D/RT}$.

2. The effect of crystallinity on diffusivity is a function of the thermal history of the film. For the unannealed films the change in diffusivity with changes in the amorphous volume fraction follows the relationship $D = D^*/\tau\beta$, while for the annealed films the diffusivity is markedly enhanced by introduction of crystalline, row-vacancy defects which tend to reduce the geometric impedance.

3. The diffusional enhancement on annealing is greatest for the smallest molecule, helium, and least for CF_4.

4. The most common defect size is 4.2Å which is in good agreement with the size of a vacant site in the monoclinic crystal lattice.

5. For the unannealed films τ seems to correlate quite well with α, the data falling between linear and branched poly(ethylene).

6. β correlates well with cross-sectional area of the diffusing molecule. The observation that the β factors in poly(propylene) are higher than those for poly(ethylene) most probably reflects the greater rigidity of the poly(propylene) chain.

G. Activation Energies for Diffusion

1. Activation Energy Related to Molecular Size

The activation energies for diffusion were calculated according to the relationship $D = D_o e^{-E_D/RT}$. In Figure 64, the resulting activation energies are correlated with the diameter of the diffusing gas molecule for both quenched and annealed isotactic poly(propylene), as well as atactic poly(propylene). Surprisingly enough, a single straight line fits all data equally well, at least to a good approximation. One would have expected lower activation energies for the amorphous and less crystalline films. Jeschke and Stuart (51) have encountered a similar situation in their studies of diffusion in crystalline poly(ethylene terephthalate) and poly(propylene). They offer the following explanation, starting with the premise that the activation energy of diffusion is related to λ, the length of an individual diffusion jump. They go on to suggest that, in a crystalline film, the regions in which diffusion occurs,

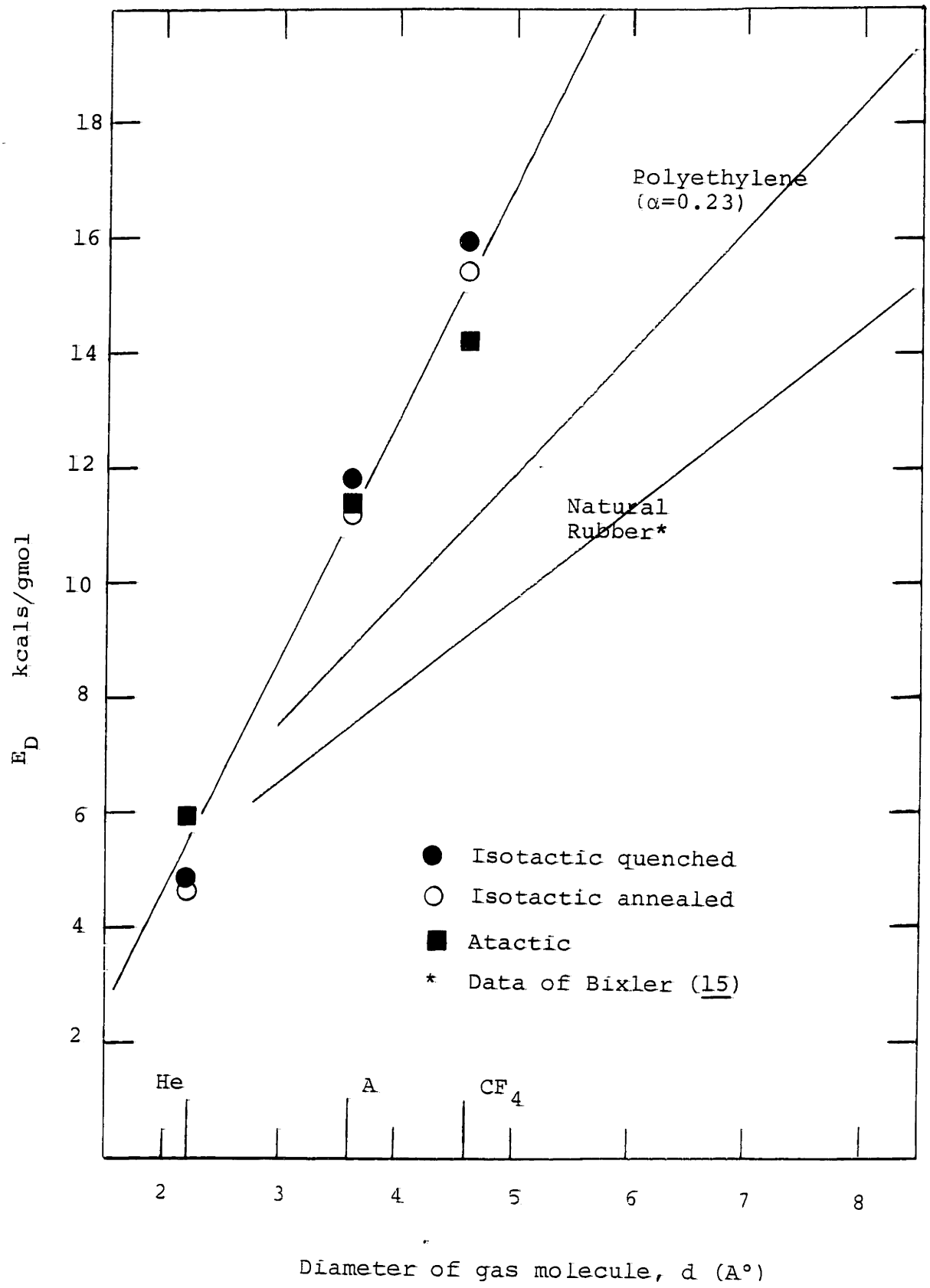

Figure 64 Activation Energy for Diffusion Related to the Size of Diffusing Molecule

may become shorter than the length of λ in the completely amorphous polymer. This must, out of necessity, lead to a reduction in the average length of a diffusion jump. Then, if λ is smaller, the activation energy of diffusion may be the same or even lower than in a less crystalline system with fewer restraints on segmental mobility.

Figure 64, furthermore, points out the pronounced increase of E_D with increasing molecular diameter of the diffusing gas. The data for poly(propylene) is presented in conjunction with plots for poly(ethylene) and natural rubber; both of these curves lie lower and show a less pronounced dependence on the molecular diameter of the gas. The bulky $\overset{|}{C}H_3$ side group plus the propensity of the poly(propylene) chain to coil must make movement of the chain, or even just a few segments along the chain, increasingly difficult.

2. Diffusivity Related to Molecular Size

Since equation (18), $D = D^*/\tau\beta$, could be used to estimate the diffusivity of a gas not already studied in crystalline poly(propylene), a correlation of D^* with some readily available parameter such as the diameter of the diffusing molecule was attempted. Figure 65 is such a plot and shows that $\ln D^*$ versus d results in a conveniently linear relationship. As one would expect, diffusivity decreases with increasing diameter of the gas molecule. CF_4, the gas which showed such abnormal behavior in all solubility plots seems, however, to be completely normal in this case.

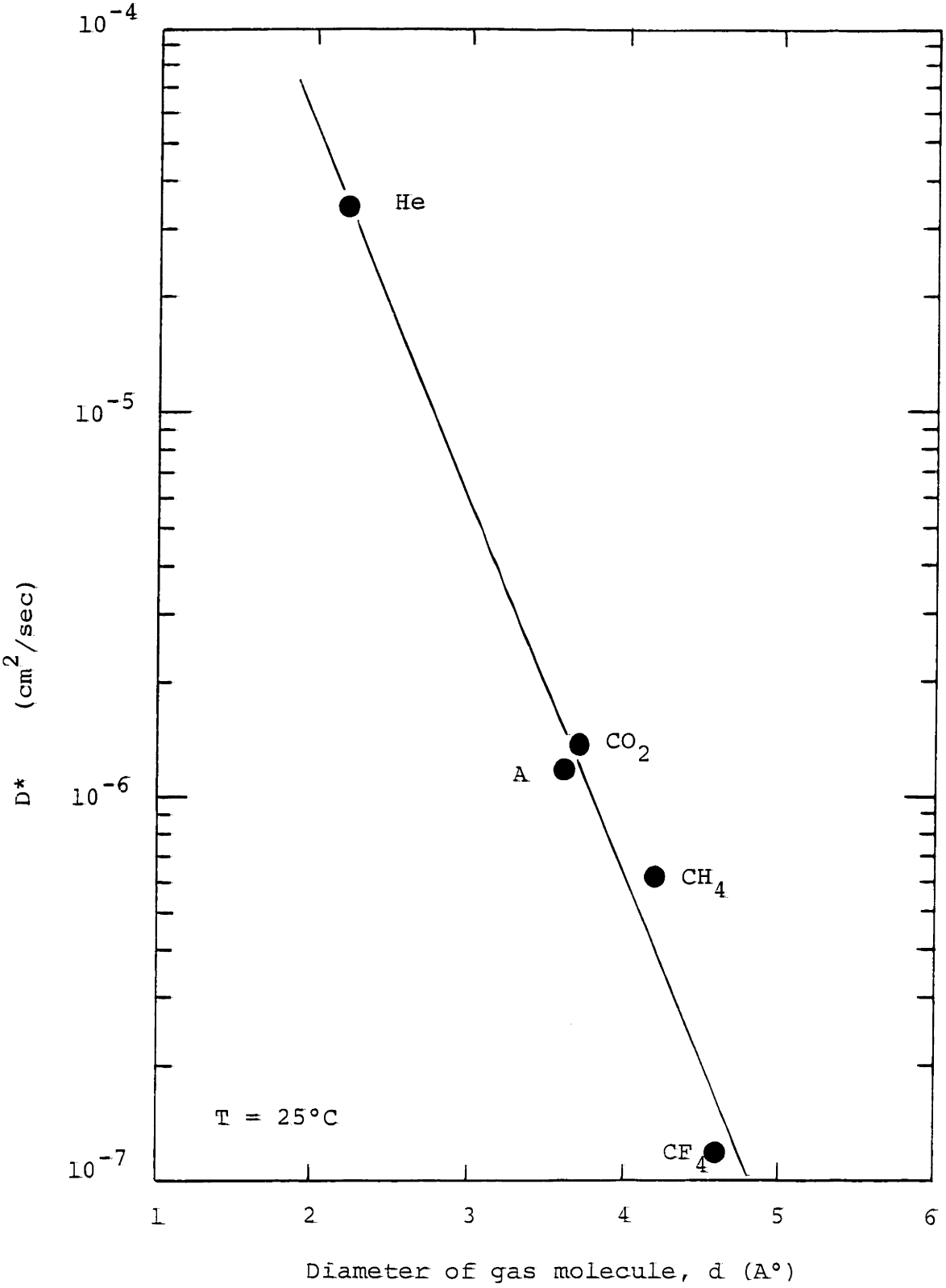

Figure 65 Diffusivity in Atactic Polypropylene Related to Molecular Size

3. Summary

1. The energies of activation for diffusion do not vary significantly from completely amorphous to quenched to annealed poly(propylene).

2. The values of E_D are significantly higher than those for poly(ethylene) and natural rubber reflecting the greater rigidity and helical nature of the poly(propylene) chain.

3. The activation energies for diffusion correlate well with the diameter of the diffusant. It is concluded that the diffusion step in crystalline poly(propylene) involves the movement of chains to open a diffusion passage just as in the completely amorphous polymer.

H. Entropies of Activation for Diffusion

The observation that ℓnD is a linear function of $1/T$ over the temperature range considered has led to the conclusion that diffusion may be regarded as a thermally activated process with the relation between D and T expressed by the Arrhenius-type equation

$$D = D_o e^{-E_D/RT} \qquad (12)$$

where E_D and D_o are constants, characteristic of the gas and the polymer. The activation energy of diffusion has been the subject of an earlier discussion and attention will now be focused on the parameter D_o.

Applying Eyring's (42) theory of absolute reaction rates to diffusion one finds that diffusion can be expressed by

$$D = e\lambda^2 \frac{\bar{k}T}{h} e^{\Delta S^*/R} e^{-E_D/RT} \qquad (15)$$

and by comparison with equation (12),

$$D_o = e\lambda^2 \frac{\bar{k}T}{h} e^{\Delta S^*/R} \qquad (65)$$

where λ is the average length of a unit diffusion jump, e is the base of the natural log, $\bar{k}$ is Boltzmann's constant, h is Planck's constant and ΔS^* is the entropy of activation for a diffusion jump.

Meares (63) pictures the activation process as "the breaking of van der Waal bonds between polymer segments which separate by synchronized rotation and torsional oscillation about -C-C- bonds to produce a cylindrical void along which the diffusing molecule can travel". If one assumes that all the observed activation energy goes into the breaking of bonds to provide such a cylindrical cavity, one can calculate the average length of the diffusion jump. The cavity needed to permit passage of a molecule would have to have a cross-section of $\pi d^2/4$. If the cavity length is λ, the volume of the void would be $1/4(\pi d^2 \lambda)$. Then, knowing the cohesive energy density (C.E.D.) of the rubbery polymer λ can be evaluated by equating the observed energy of activation for diffusion to the energy represented by a mole of such cavities, i.e.,

Table X

Entropies of Activation for Diffusion

Film	Description	λ Å	ΔS^*_G cals/gmole-°K	ΔS^*_P cals/gmole-°K	ΔS^* cals/gmole-°K
14	MA	29	-7.9	13.6	5.7
14a	MA-150	29	-7.9	14.3	6.4
20	MH	33	-2.7	-5.1	-7.8
21	MH-150	32	-2.8	-5.6	-8.4
25	MF	25	-10.4	25.9	15.5
25a	MF-150	23	-10.5	24.0	13.5

$$E_D = \frac{\pi d^2}{4} N\lambda \text{ (C.E.D.)} \qquad (66)$$

In this way it was possible to estimate the values of λ listed in Table X. The values of λ ranged from 23 to 33Å with an average of 30Å, a value which compares very favorably with the value of 27Å quoted by Meares (63) for poly(vinyl acetate).

From the value of λ, the entropy of activation can be calculated. The values of ΔS^* are again tabulated in Table X. As one would expect the overall entropy change is greatest for the largest molecule, CF_4. However, even more insight can be gained by considering the individual contributions to the entropy change from the diffusing gas molecule and from the medium.

The entropy of activation for the gas molecule can be determined by focusing on the state of the sorbed gas molecule. A sorbed gas molecule, occupying an equilibrium site, behaves as an isotropic three-dimensional harmonic oscillator. During a diffusion step one vibrational freedom is exchanged for one degree translational freedom. Meares (63) and Hill (43) quote values of the vibrational frequencies which make it possible to calculate the change in entropy for the gas. The translational energy for one degree of freedom is

$$S_{trans} = R\ell n \left[\frac{(2\pi m\bar{k}T)^{1/2}\lambda}{h} \right] + \frac{1}{2} R \qquad (67)$$

and the vibrational entropy in three dimensions is

$$S_{vib} = 3\left[\frac{Nh\nu}{T(e^{h\nu/\bar{k}T} - 1)} - R\ell n \left(e^{h\nu/\bar{k}T} - 1\right)\right] \qquad .... (68)$$

The entropy of activation for the diffusing molecule is then

$$\Delta S_G^* = S_{trans} - S_{vib} \qquad (69)$$

Thus knowing ΔS_G^*, the entropy of activation for the medium is

$$\Delta S_P^* = \Delta S^* - \Delta S_G \qquad (70)$$

These values are again tabulated in Table X and graphically illustrated in Figure 66, which is a plot of ΔS_P^* and ΔS_G^* versus d, the diameter of the diffusant.

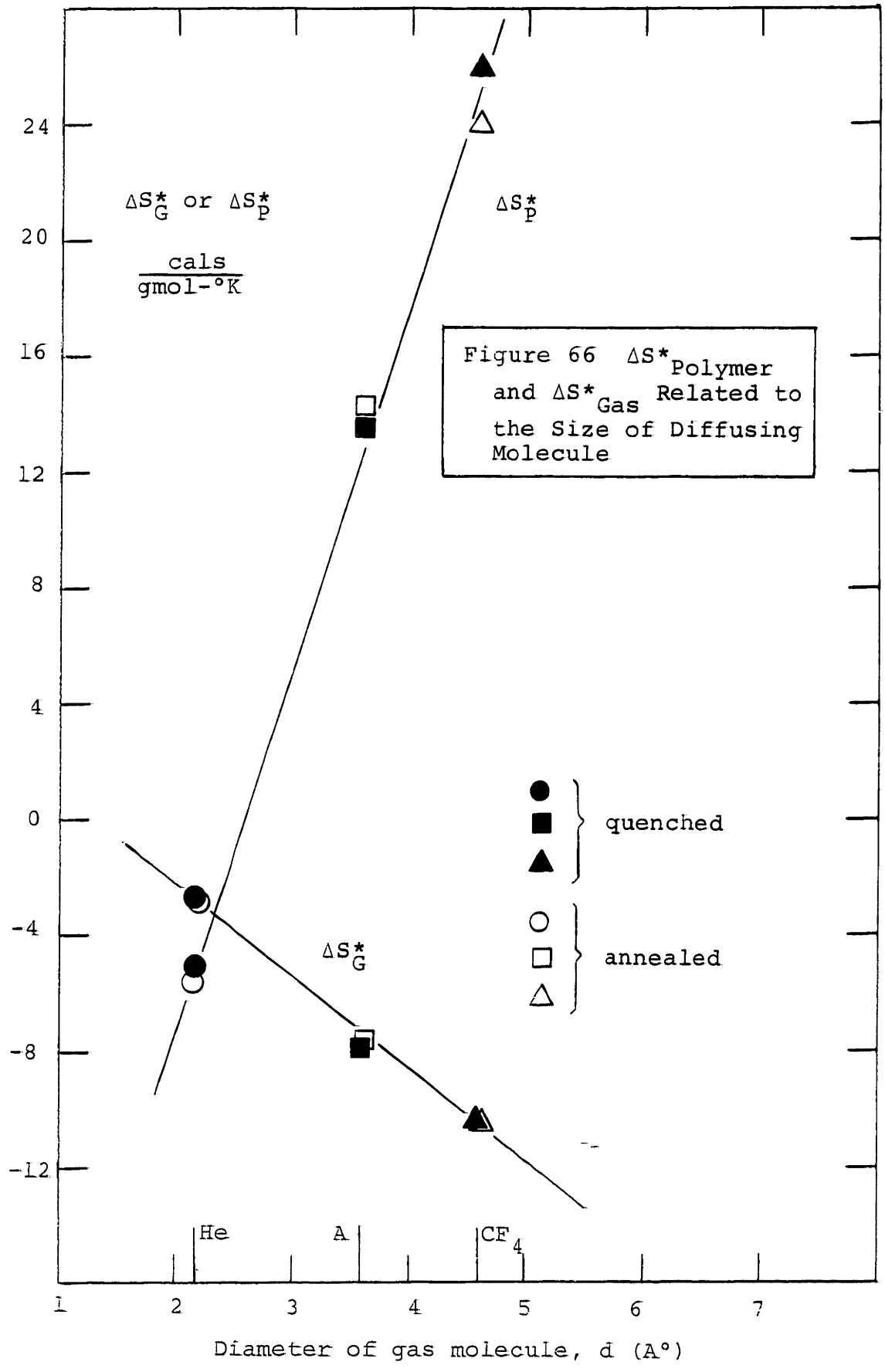

Figure 66 $\Delta S^*_{Polymer}$ and ΔS^*_{Gas} Related to the Size of Diffusing Molecule

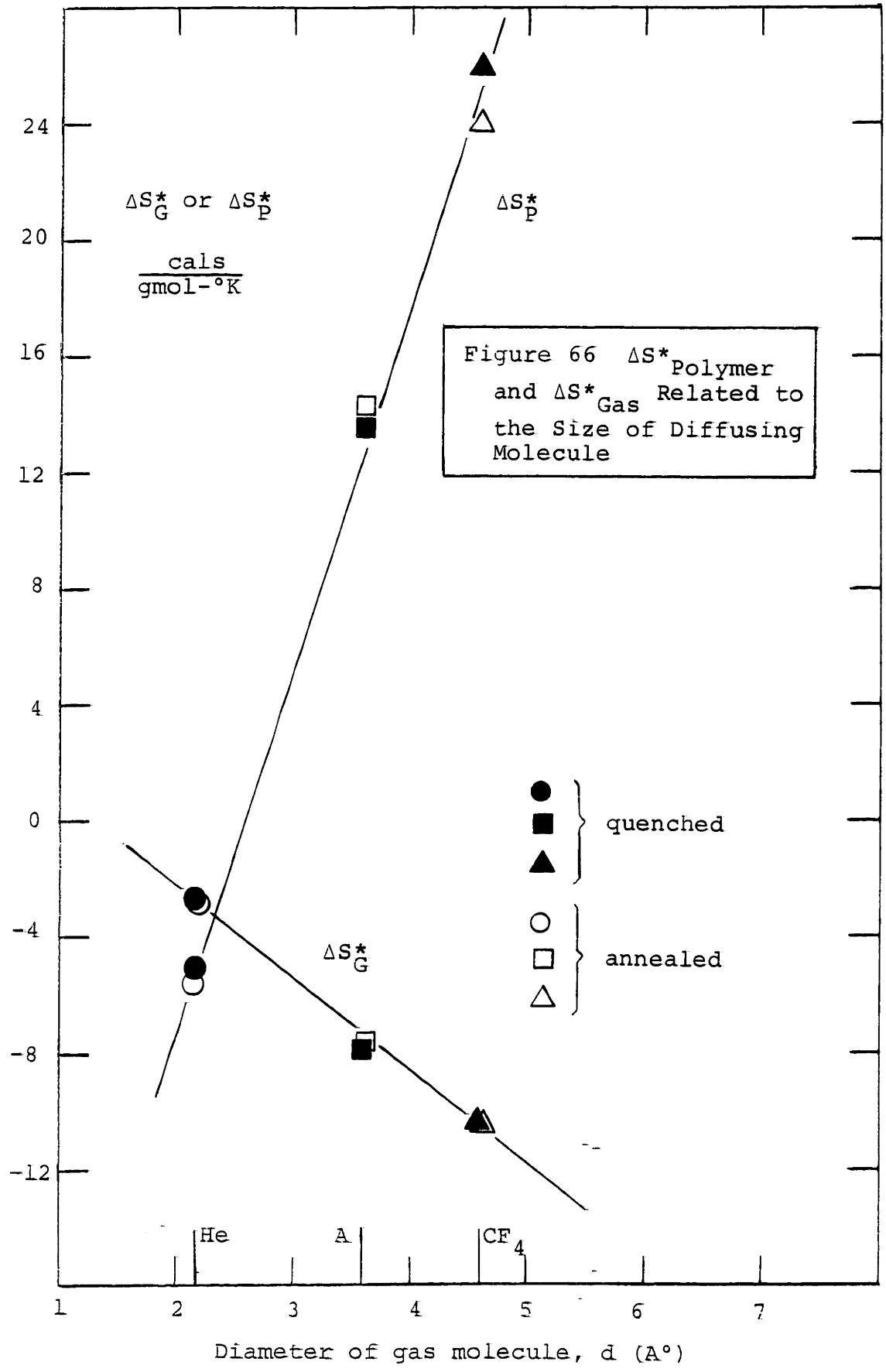

Figure 66 $\Delta S^*_{Polymer}$ and ΔS^*_{Gas} Related to the Size of Diffusing Molecule

During the translation of a gas molecule in the diffusional tunnel, the remaining two vibrational modes of the gas are restrained and a finite zone within the polymer has to be activated to produce a cavity of the required size. Thus, as expected, CF_4, the largest molecule studied, experienced the greatest entropy decrease and induced the greatest entropy increase in the polymer, i.e., $\Delta S_G^* = -10.5$ and $\Delta S_P^* = 15.5$ cals/gmol-°K. The diffusion of A and CF_4 represent the disruption of a considerable zone of the polymer matrix. In fact, A and CF_4 require complete separation of adjacent chains beyond the limit of van der Waals interaction. The helium molecule, on the other hand, is so small that its diffusion does not involve breaking existing contacts or van der Waal's forces between chains but rather promotes even closer approach of the chains after passage of the diffusant. This would explain the negative ΔS_P^* for helium, suggesting greater order of the polymer matrix <u>after</u> the diffusional jump.

Figure 66 clearly illustrates the marked dependency of the entropies of activation on the size of the diffusing molecule. ΔS_P^* <u>increases</u> linearly and ΔS_G^* <u>decreases</u> linearly with the size of the diffusant.

Barrer (<u>7</u>) predicts that for a process in which the activation energy is shared between a number of degrees of freedom in a zone of activation, ΔS^* versus E_D should give a linear correlation. Barrer further pointed out that this condition should hold for viscous flow in liquids or diffusion

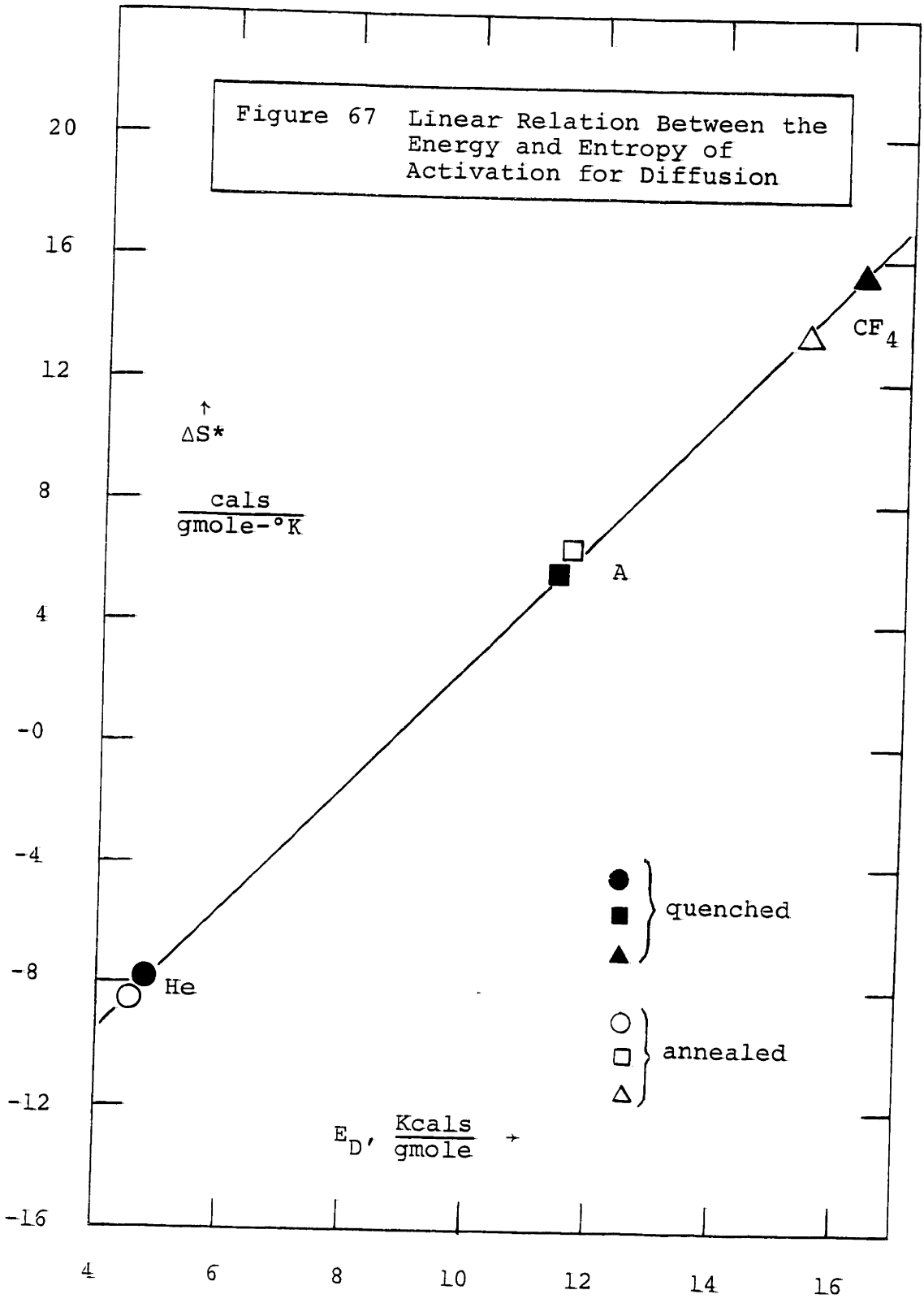

Figure 67 Linear Relation Between the Energy and Entropy of Activation for Diffusion

in rubbers. A plot of ΔS^* versus E_D (Figure 67) for crystalline poly(propylene) does indeed result in a good straight line. This emphasizes the fact that the inter-crystalline amorphous material is surprisingly rubbery in nature.

Summary

1. The average length of a diffusion jump is 28Å.

2. The overall change in the entropy of activation for diffusion is greatest for the largest molecule.

3. The entropies of activation for diffusion show a marked dependency on the size of the diffusing molecule. ΔS_P^* increases linearly and ΔS_G^* decreases linearly with the size of the diffusant.

I. Characterization of the Polymer

1. Density Determinations

To relate the effect of thermal history to changes in the microstructure of the polymer it becomes imperative to find a convenient way to characterize the polymer. Determination of the crystalline/amorphous ratio is one way to observe changes in the polymer. Since there are easily measurable density differences associated with the crystalline and amorphous form of the polymer, crystallinity determinations for a system with a distinct crystalline phase appear ideal. However, a problem arises because the crystallites in isotactic poly(propylene), as

well as all the other crystalline polymers, are not definite entities with sharp boundaries or crystal faces separating them from the surrounding amorphous material. Rather than a sharp discontinuity, there is most probably a gradual transition in density from the crystallites to the completely amorphous regions via the chains and chain loops that connect the two phases. As well as that, the crystallites themselves must contain many defects and dislocations (46) arising from the extensive entanglement of the molecules in the melt just prior to crystallization.

Nevertheless, density determinations have proved to be reproducible, reliable and, at least for the annealed poly(propylene) samples, comparable to the values obtained from x-ray diffraction and calorimetric determinations. It appears that, for the well annealed samples, the ideal of a two-phase system is approached and the percent amorphous volume calculated from density determinations is representative of the fraction of the polymer that is actually available to flow and sorption.

Table III shows the density measurements and the percent amorphous volume, calculated on the basis of these values. The density of the crystalline films ranged between 0.8907 and 0.9148 gm/cc, measured in iso-propyl alcohol-water density gradient columns at 23°C. The density of completely crystalline material (i.e., the monoclinic modification of poly(propylene)) was taken as 0.936 gm/cc (94) and that of completely amorphous polymer as 0.858 gm/cc (94). The latter value was identical to the density of the atactic material, whose density was determined by weighing

a sample in air and immersed in water (Archimedes' principle). This observation further justified the substitution of atactic poly(propylene) for amorphous, isotactic poly(propylene).

In previous discussions it was concluded that the quenched polymer contains hexagonal crystals or a mixture of hexagonal and monoclinic crystals, the ratio of the two being a function of the rate of quenching. Thus, the apparent amorphous content of the quenched films, calculated on the assumption that all crystallinity is present in the form of monoclinic crystals, does not really reflect the actual situation. The experimental evidence suggests that annealing of quenched films below 100°C results in very little additional crystallization, and that changes in density and apparent amorphous content are due to the conversion of hexagonal to monoclinic crystals. The conversion is accompanied by a density change from 0.907 gm/cc for the hexagonal form (36) to 0.936 gm/cc for the monoclinic form.

Alcalay (1) in his study of fluid transport in poly(propylene) analyzed his density data solely on the basis of the two-phase model of completely amorphous and completely monoclinic, crystalline phases and found that "there appears to be no correlation between the liquid permeation fluxes and the amorphous fraction for the systems used in this study". Since he studied quenched films as well as films subsequently annealed at various temperatures and in various solvents, it is very likely that some of the confusion resulted from a failure to recognize the existence of the second

crystalline form and its transformation to the more stable, monoclinic form with an apparent change in density.

Thus one can conclude that density determinations are valuable in characterizing annealed films of poly(propylene) by providing a measure of the amorphous/crystalline ratio. However, for quenched films the amorphous content based on a two-phase model is due solely to the conversion of hexagonal crystals to monoclinic crystals. Therefore, in addition to the oversimplification of two well segregated phases - amorphous and crystalline - one must be aware of the presence of two crystal modifications of different densities in the determinations of crystallinity or amorphous content in poly(propylene).

2. X-Ray Diffraction

(a) Crystallinity.

Another method frequently used to determine the crystalline content of a polymer sample is x-ray diffraction. A typical x-ray diffraction pattern from a crystalline polymer consists of sharp, crystalline rings superimposed upon a diffuse, amorphous halo. Appropriate integration of the intensities of these separate contributions to the total x-ray pattern allows one to estimate the amorphous and crystalline content of the sample.

Two samples of isotactic film were characterized using this x-ray diffraction technique. One sample was film 2, a "rapidly cooled" film, the other was film 5, a "rapidly cooled" film subsequently annealed for 60 minutes at 150°C. The results are shown in Figures 38 through 41.

Figures 38 and 39 show the x-ray diffraction patterns from which the x-ray diffraction curves in Figures 40 and 41 were constructed. For film 5, the annealed sample, the four major peaks and one minor peak, characteristic of monoclinic crystallinity, were clearly visible. The absolute crystallinity for this film, as calculated from this x-ray diffraction pattern, was 69.4%. This value compared favorably with the density gradient column value of 71.3%. The slightly lower value for the x-ray determination is due to the fact that this method "sees" only the perfect crystals and treats any material of intermediate order as amorphous.

Figure 40, on the other hand, represents the picture obtained for film 2, the quenched sample. The curve clearly indicates the beginnings of the sharp peaks associated with the monoclinic crystallinity. However, closer analysis also reveals the presence of the two broad scattering maxima reported by many investigators (36, 73, 82, 4, 110) for the quenched form of poly-(propylene). The fact that these broad maxima coincide with the two peaks reported for a rare type of poly(propylene) spherulite of known hexagonal crystal structure has led some investigators (36, 50) to the conclusion that the quenched material must have hexagonal crystal structure. The small size of the individual crystals would account for the broad scattering and absence of the typical crystalline diffraction peaks.

A detailed analysis of the x-ray diffraction curve led to the following estimate of crystallinities: monoclinic crystallinity = 10.2%, hexagonal crystallinity = 71.2%, amorphous volume = 18.6%. Thus the x-ray findings clearly confirm the conclusions reached on the basis of the sorption work, namely the presence of three phases in quenched films of isotactic poly(propylene) films.

(b) Crystallite orientation.

If the x-ray diffraction pattern of a sample of crystalline polymer shows small spots or arcs it means that the crystallites are quite perfect and more or less aligned in some definite direction (e.g., drawn poly(ethylene)). On the other hand, if the spots are long arcs, alignment is poor. Thus x-ray diffraction patterns can provide evidence for the presence of crystallite orientation.

The flat-plate x-ray diffraction photos presented in Figures 38 and 39 show no crystallite orientation for either sample. For film 2, a second photo was taken with the sample turned 90° from its first photo position to check for possible two dimensional ordering. Again absolutely no ordering was evident. These observations support the belief held throughout this study that the molded films are essentially isotropic and unoriented.

(c) Crystallite size.

Crystallite size was determined from line-broadening according to a method described in "X-Ray Diffraction Procedures"

by Klug and Alexander (56), using angular width at half maximum intensity.

Measurements were made on the five crystalline peaks found for film 5, and the average crystallite size was found to be 176Å. The value represents an average over all directions with no specific crystallite shape assumed. Since this indicates that the crystallites are still relatively small, even after extensive annealing of the film, it is not difficult to see how the hexagonal crystals formed during quenching may, indeed, be very small, which, in turn, leads to the broad x-ray scattering maxima. The small size of the hexagonal crystals is further suggested by the initial decrease of diffusivity with the apparent decrease in amorphous content of the quenched films, a phenomenon which is probably due to the increased tortuosity resulting from the combining of small hexagonal crystals into larger monoclinic units.

3. Thermal Analysis

Calorimetric measurements provided another avenue for characterizing the crystalline and atactic poly(propylene). Using both a Differential Scanning Calorimeter (DSC) and a Differential Thermal Analyzer (DTA) it was possible to determine glass transition temperatures, melting points, and heats of fusion.

The DTA was valuable in detecting the glass transition point of the atactic material which was used as analog for the amorphous

isotactic poly(propylene). The value was -12 ±2°C. Although repeated tests were made for the isotactic material (in the form of finely cut-up film) as well, no T_g could be detected for it. Nevertheless, the value of -12°C for the atactic material suggests that the value of 0°C, widely quoted for the T_g of crystalline poly(propylene) (13, 101, 22) is not unreasonable. Thus, one can conclude that the crystalline polymer was above T_g and in its rubbery state for the experiments performed on the time-lag and low pressure sorption apparatus.

The DTA equipment is best suited for work with powders, liquids and gels, because for proper functioning of the thermocouple, which detects the changes in the temperature of the sample, it must always be in intimate contact with the sample. With this in mind, further tests were made on pulverized, isotactic poly(propylene), but again not a trace of a T_g was found.

The average value of T_m determined on the DTA for crystalline poly(propylene) was 163°C, in line with the value of 165°C quoted by Billmeyer (13).

The DSC work was aimed specifically at estimating the crystalline/amorphous ratio of a sample by comparing the enthalpy of fusion measured for it with the enthalpy of fusion for a perfectly crystalline specimen. Since there is some disagreement as to what the true value of ΔH_F for 100% crystalline material is, an internally-derived value of 32.5 cals/gm was used. This value

was based on the crystallinity determined for film 5, a well annealed sample, by x-ray diffraction and is in good agreement with the most commonly used, published value of 35 cal/gm (109). No value of the enthalpy of fusion for the hexagonal crystal modification was available so that the heats determined for the quenched films are at best qualitative.

Table XI is a comparison of the crystallinities determined by DSC and density gradient column. The agreement is at best qualitative. The DSC values shown in Table XI were the average values for two to three separate samples, the reproducibility between samples being better than $\pm 3\%$. On closer analysis of the table one finds that, for the annealed samples, the crystallinities determined by density measurements are consistently higher. This is due to the fact that the density method "sees" intermediate changes in density while the DSC can only detect actual crystals.

The higher DSC values for the quenched samples, on the other hand, may provide further evidence for the existence of an hexagonal phase which, due to its lower density and yet probably comparable ΔH_f, would result in a high DSC value and a low "density gradient column" value.

The values for T_m, as determined by the DSC, ranged between 157°C and 166°C. The true melting point for perfectly crystalline (monoclinic) poly(propylene) is 168°C. Since all films were originally cooled from the melt by quenching of some fashion, one would expect, even after annealing, a preponderance of small,

Table XI

Comparison of Crystallinities Determined by DSC and Density Gradient Columns

Film	Description	% Crystallinity		T_M
		DSC	Density Grad. Col.	(°C)
2	RA	56.4	44.0	159
3	RA	58.1	47.0	160
5	RA-150	69.4	71.3	162
6	MA	49.5	55.5	161
12	MA-150	65.6	71.2	162
13	MA-150	65.3	71.0	161
14	MA	57.8	49.0	160
15	SA	47.7	61.0	161
16	SA-150	66.7	69.5	161
18	RH	53.5	49.0	166
19	RH-150	63.9	69.0	164
20	MH	44.3	50.0	163
21	MH-150	61.2	70.5	165
22	SH	40.5	61.0	165
23	SH-150	61.5	69.0	166

imperfect crystallites, giving rise to the lowered melting points. Furthermore, it was noted that, in every case but one, the value of T_m increased slightly on annealing, definitely suggesting thickening of crystals, with concomitant defect formation.

Again numerous traces were made in an attempt to locate T_g for the isotactic samples, but again none was found over the temperature range of -100 to 190°C.

4. Optical Microscopy

The spherulitic structure of isotactic poly(propylene) is readily visible in the polarizing microscope. The spherulites are characteristic in appearance and are seen as circular birefringent areas possessing the dark Maltese cross pattern. However, the ring structure observed for poly(ethylene) and associated with a periodic twisting of the lamellae is absent.

It was hoped that close observation of film samples under cross-polarizers would make it possible to observe changes in spherulite size and spherulite texture and to relate these changes to the thermal history of the films. For this purpose, film samples were ultratomed and viewed, in cross-section, under the polarizing microscope (see Figures 42, 43 and 44). However, in support of the argument that the transport properties of poly-(propylene) are controlled at a level of microstructure well below the characteristic dimensions of spherulites, it was observed that bulk-crystallized poly(propylene) has a spherulitic

structure whose size and texture do not change on annealing. Since, at the level of magnification possible with the optical microscope, the fine details of the microstructure cannot be resolved, studies with the electron microscope were attempted next.

5. Electron Microscopy

The value of the electron microscope lies in its ability to greatly extend the range of magnification possible with the optical microscope. However, as a result of the relatively low atomic weight of the atoms comprising the polymer molecule, the crystal images are generally of low contrast with respect to the background image. Nevertheless, electron microscopy has provided additional clues and corroborating evidence in the attempt to elucidate the complex crystalline microstructure of poly(propylene).

The replicas of the fracture surface of film 23 (Figure 45) indicate that the crystalline microstructure of poly(propylene) is much more rod-like than lamellar. The fracture surfaces appear to be very rough and pebbly. The many small protrusions seen on the micrographs appear to be the broken-off ends of pencil-like rods rather than flat lamellae such as associated with the structure of poly(ethylene).

The transmission micrographs of ultratomed sections of the same film are shown in Figure 46. They show a prominent structural organization on a scale larger than the before-mentioned "rods", namely that of spherulites. The spherulites

range in size up to 10 μ. Although there is not enough definition to distinguish the rod or ribbon-like substructure, the spherulitic growth appears to radiate from a well-defined center. However, the lack of definition has again frustrated attempts at correlating spherulite texture with thermal history.

Figures 47 and 48 represent the observations made on thin films crystallized from the melt and with the "diluent" of atactic poly(propylene) partially removed, a technique suggested by Padden and Keith (85). By crystallizing the poly(propylene) in the presence of a diluent, which is subsequently washed away, one is able to reveal a more or less skeletal form of poly-(propylene) spherulites. One sees that the crystal habit is quite unique; it appears to be highly interwoven and branched with readily identifiable structural members. Padden and Keith (85) have estimated the dimensions of these ribbons to be about 150Å thick, about 800Å wide, and up to 20,000Å long. Although these micrographs show only a two-dimensional network, it is obvious that in a bulk sample this structure must exist throughout. It is the densely woven character of these branching structures that has made detailed morphological studies using optical and electron microscopy so difficult.

Summary

1. For the annealed samples, the crystalline and amorphous regions appear to be well segregated and density is good measure of crystallinity.

2. For the quenched films, density measurements are deceiving because both monoclinic and hexagonal crystals are present.

3. X-ray diffraction analysis of two samples indicates (i) the presence of two crystal modes in the quenched sample, (ii) the complete randomness of crystallite orientation, and (iii) an average crystal size of 176Å.

4. Calorimetric measurements could detect no glass transition temperature for the crystalline polymer.

5. Poly(propylene) has a spherulitic structure; however, the size and texture of the spherulites does not change with changes in thermal history.

6. The crystallite structure inside the spherulite appears to be rod-like rather than lamellar.

VI. CONCLUSIONS AND RECOMMENDATIONS

A. Conclusions

1. The applicability of Henry's law to the solution of He, A and CF_4 in poly(propylene) was checked up to one atmosphere, and up to 30 atmospheres in the case of A and CO_2, and found to be valid over the range of temperatures considered.

2. The solubility constants of He, A and CF_4 in quenched samples of poly(propylene) are all anomalously lower than what one would predict from the relationship $k = \alpha k^*$. All quenched films appear to have the same amorphous content (ca. 41%), independent of the rate of cooling from the melt, with the remaining material being a mixture of monoclinic and hexagonal crystallinity. The diffusing gas is not soluble in either crystalline phase. The strongest evidence for the presence of the hexagonal crystal mode are x-ray diffraction patterns of the quenched film.

3. The ratio of monoclinic to hexagonal crystallinity in unannealed films is a function of the rate of quenching and changes, on annealing, in favor of the more stable, monoclinic form; the transition occurring rather sharply at 90°C as evident in the gas sorption behavior.

4. The solubility constants of argon and helium in the annealed samples are more normal, varying linearly with the amorphous volume fraction.

For CF_4, even the solubility in the annealed films is low, suggesting exclusion of the large molecules from some of the interlamellar amorphous regions. Thus, the concept of a distinct amorphous phase and a distinct crystalline phase fails to adequately describe the situation in crystalline poly(propylene).

5. The solubility of He, A, CH_4 and CO_2 in amorphous (atactic) poly(propylene) is well correlated by the gas force constant, $\varepsilon/\bar{k}$, in the Lennard-Jones potential energy function. The correlation is parallel to - and of the same magnitude as - other such correlations for non-polar gases in natural rubber and hydro-carbon liquids. This provides a means for estimating a value of k* for a number of gases on the basis of one measurement. Then, knowing α for the particular annealed film, k could be estimated from $k = \alpha k^*$. The deviation of CF_4 from this correlation is attributed to its anomalously high partial molar volume and low $\varepsilon/\bar{k}$.

6. Below the glass transition temperature, the solubility of argon is greater than what one would predict from solubility behavior above T_g. The enhanced solubility and relatively large enthalpy of sorption of argon in glassy poly(propylene) point to the presence of microvoids and sorption by microvoid-filling in addition to ordinary dissolution.

7. The solubility data for argon show a definite break at approximately zero degrees centigrade, a value generally quoted as the T_g of crystalline poly(propylene).

8. The level of the enthalpies of sorption for helium, argon and CF_4 in crystalline poly(propylene) is characteristic of dissolution. In similarity to the finding in the solution behavior of SF_6 in poly(ethylene), the enthalpy of sorption for CF_4 is anomalously high and explained by its relatively high molar volume and low $\varepsilon/\bar{k}$.

9. In the glassy region, the ΔH_S for argon is significantly more exothermic than above T_g, which points to a Langmuir-type adsorption process in microvoids.

10. The size of the microvoids in glassy poly(propylene) appears to be on the order of 32Å in radius. The enthalpy of adsorption is slightly lower than that in glassy poly(styrene) and poly(ethylene terephthalate), but the magnitude of ΔH_{ads} is characteristic of physical adsorption and agrees rather well with the measured value of ΔH_S.

11. Diffusion of He, A and CF_4 in crystalline and amorphous poly(propylene) is normal and Fickian, and variations with temperature are independent of thermal history and level of crystallinity.

12. However, the diffusivity of He, A and CF_4 is a function of the level of crystallinity and dependent on the film's thermal history. In the quenched films, the diffusion constants decrease, up to the point of complete conversion of hexagonal to monoclinic crystallinity. This is attributed to an increase in the geometric

diffusional impedance with the consolidation of very small hexagonal crystals into fewer - but larger - monoclinic crystals.

13. On annealing, diffusivity increases significantly in spite of increasing crystallinity. This suggests a marked decrease in diffusional impedance with increasing crystallinity, resulting from the formation of defects in the existing crystallites as the lamellae thicken, which is also observed on annealing of poly(ethylene) single crystals.

14. The diffusional enhancement in the annealed films is a function of the penetrant size, being greatest for the smallest molecule.

15. The diameter of the most common defect is approximately 4.2Å. This dimension is in excellent agreement with the estimated diameter of a vacant site in the monoclinic crystal lattice of poly(propylene).

16. The chain immobilization factor for the quenched films correlates well with the cross-sectional area of the diffusing molecule. However, the fact that the apparent activation energies for diffusion were essentially constant irrespective of thermal history casts doubt on the significance of this factor.

17. The activation energies for diffusion for He, A, and CF_4 are essentially constant and independent of the level of crystallinity and thermal history. This confirms conclusion (16) and strongly suggests that, in a highly crystalline polymer,

diffusion is not so much impeded by the restricted mobility of chain-segments but rather by the extremely small dimensions of the amorphous, diffusional paths. This, in turn, gives meaning to the concept of a one-phase, crystalline aggregate with numerous defects and lamellae borders in which diffusion and sorption take place.

18. The activation energies for poly(propylene) are higher than those for poly(ethylene) and natural rubber, which suggests greater chain rigidity and may support the contention that the poly(propylene) chain is coiled in the amorphous phase.

19. The activation energies for diffusion, as well as the entropies of activation for diffusion, correlate well with the diameter of the penetrant. This leads to the unexpected conclusion that the diffusion process in highly crystalline polymer, just as in natural rubber, involves the movement of polymer chains to accommodate the diffusing molecule.

20. The average length of an activated diffusion step seems to be 30 Å. This value decreases with the size of the gas molecule but varies only little with the level of crystallinity or thermal history.

21. For the annealed samples, the distinction between crystalline and amorphous regions appears to be sufficient to make density a good measure of crystallinity. For annealed films, crystallinities calculated from density, DSC and x-ray diffraction measurements were comparable.

22. X-ray diffraction measurements for a quenched film definitely indicate the presence of an hexagonal crystal phase.

23. Poly(propylene) has a spherulitic structure which is more fully developed for films cooled slowly from the melt. However, no change in the size or texture of the spherulites was observed on annealing.

24. The morphology within the spherulite appears to be highly branched and interwoven.

B. Recommendations

1. The concept of row vacancy defect formation should be investigated more fully by further diffusion studies in samples of poly(propylene) film annealed at progressively higher temperatures. At least five different gases of widely different molecular size should be used to allow accurate determination of defect size distribution as a function of the extent of annealing. This may open the way to the design of membranes with defects of just the right size to give high selectivity as well as high flux for such promising gas separations as helium separation from natural gas mixtures.

2. The extensive diffusion data for annealed samples of other highly crystalline polymers such as poly(ethylene) and poly(ethylene terephthalate) should be re-evaluated in the light of the proposed mechanism of defect formation by row vacancies in the crystal lattice.

3. Since films of commercial, isotactic poly(propylene) (~95% isotactic) crack excessively when crystallized by slow-cooling from the melt, it is suggested that well-blended mixtures of atactic and isotactic material be used to extend the presently accessible range of crystallinities. Both solution and diffusion data at high (>41%) and low (<25%) amorphous content are certainly needed to confirm and enlarge upon the observations of the present study.

4. The precision of $\bar{P}$ and D measurements in molded film samples could be greatly enhanced if thickness variations across a film sample could be reduced. Since films of a wide range of thicknesses are required for a time-lag study with gases of widely different molecular diameters, some efforts should be directed toward developing either a better molding technique or an entirely new method of laboratory film preparation.

VII. APPENDIX

Appendix A

Summary of Experimental Data

TABLE XII

SUMMARY OF TIME - LAG DATA

Run	Film	Description	α %	Gas	P_1 mmHg	T °C	$\bar{P}$ $\times 10^9$ cc(STP) / cm-sec-atm	D $\times 10^7$ cm^2 / sec	k $\times 10^2$ cc(STP) / cc-atm
1	1	RA	56.5	A	643	30	8.66	1.47	5.95
2	1	RA	56.5	A	400	45	21.80	3.94	5.61
3	1	RA	56.5	A	568	45	22.09	3.95	5.61
4	1	RA	56.5	A	332	60	47.40	8.99	5.28
5	1	RA	56.5	A	473	60	47.60	8.99	5.28
6	1	RA	56.5	A	457	60	47.90	8.71	5.28
7	3	RA	53.0	A	539	30	8.29	1.46	5.76
8	3	RA	53.0	A	556	40	16.03	2.68	5.74
9	3	RA	53.0	A	516	40	16.10	2.71	5.74
10	3	RA	53.0	A	517	40	15.58	2.72	5.74
11	3	RA	53.0	A	529	50	27.20	5.45	5.60
12	3	RA	53.0	A	492	50	26.60	5.13	5.60
13	3	RA	53.0	A	529	60	49.3	8.78	5.64
14	3	RA	53.0	A	360	60	49.5	8.78	5.64
15	3	RA	53.0	A	542	60	48.7	8.62	5.64
16	3a	RA-150	27.5	A	538	30	6.83	1.51	4.53
17	3a	RA-150	27.5	A	528	30	6.58	1.55	4.53
18	3a	RA-150	27.5	A	548	40	12.08	2.68	4.44
19	3a	RA-150	27.5	A	502	40	12.15	2.62	4.44
20	3a	RA-150	27.5	A	367	50	20.96	4.87	4.38
21	3a	RA-150	27.5	A	555	50	21.75	4.56	4.38

TABLE XII (Cont'd.)

Run	Film	Description	α	Gas	P_1	T	$\bar{P}$	D	k
			%		mmHg	°C	$\times 10^9$ cc(STP) / cm-sec-atm	$\times 10^7$ cm^2 / sec	$\times 10^2$ cc(STP) / cc-atm
22	3a	RA-150	27.5	A	548	60	34.80	8.29	4.32
23	3a	RA-150	27.5	A	371	60	34.42	8.29	4.32
24	4	RA-150	29.0	A	353	30	7.16	1.48	4.54
25	4	RA-150	29.0	A	388	30	7.10	1.43	4.54
26	4	RA-150*	29.0	A	283	30	7.10	1.57	4.54
27	4	RA-150*	29.0	A	555	31	7.15	1.54	4.51
28	4	RA-150*	29.0	A	408	40	12.20	2.67	4.46
29	4	RA-150*	29.0	A	581	40	11.70	2.55	4.46
30	4	RA-150	29.0	A	280	45	16.70	4.09	4.40
31	4	RA-150*	29.0	A	578	50	21.0	4.64	4.38
32	4	RA-150*	29.0	A	567	50	20.5	4.82	4.38
33	4	RA-150	29.0	A	572	60	34.8	—	4.29
34	4	RA-150	29.0	A	403	60	35.0	8.10	4.29
35	4	RA-150*	29.0	A	520	60	33.6	7.76	4.29
36	4	RA-150*	29.0	A	364	60	34.6	8.04	4.29
37	4	RA-150*	29.0	A	412	60	33.5	7.93	4.23

*Film 4 aged 3 months

TABLE XII (Cont'd.)

Run	Film	Description	α	Gas	P_1	T	$\bar{P}$	D	k
			%		mmHg	°C	$\times 10^9$ cc(STP) / cm-sec-atm	$\times 10^7$ cm^2 / sec	$\times 10^2$ cc(STP) / cc-atm
38	6	MA	44.5	A	564	30	7.48	1.23	6.00
39	6	MA	44.5	A	544	40	13.40	2.34	5.74
40	6	MA	44.5	A	341	50	24.20	4.11	5.61
41	6	MA	44.5	A	467	60	39.60	7.52	5.27
42	6	MA	44.5	A	510	60	41.60	7.81	5.27
43	7	MA-80	43.5	A	401	30	6.38	1.14	5.85
44	7	MA-80	43.5	A	575	40	11.70	2.21	5.46
45	7	MA-80	43.5	A	391	50	20.13	3.67	4.99
46	7	MA-80	43.5	A	346	60	29.20	—	4.61
47	7	MA-80	43.5	A	593	60	30.98	6.53	4.61
48	8	MA-100	37.8	A	260	30	6.78	1.28	5.63
49	8	MA-100	37.8	A	393	40	12.25	2.08	5.35
50	8	MA-100	37.8	A	580	50	19.85	4.19	5.01
51	8	MA-100	37.8	A	580	50	18.60	4.19	5.01
52	8	MA-100	37.8	A	249	60	32.10	6.75	4.81
53	8	MA-100	37.8	A	168	60	32.70	6.66	4.81

TABLE XII (Cont'd.)

Run	Film	Description	α	Gas	P_1	T	$\bar{P}$	D	k
			%		mmHg	°C	x10^9 cc(STP) / cm-sec-atm	x10^7 cm^2 / sec	x10^2 cc(STP) / cc-atm
54	9	MA-110	37.3	A	367	30	7.65	1.50	5.51
55	9	MA-110	37.3	A	545	40	13.06	2.38	5.41
56	9	MA-110	37.3	A	243	50	22.10	4.08	5.26
57	9	MA-110	37.3	A	527	60	36.10	7.65	5.22
58	9	MA-110	37.3	A	360	60	35.70	6.93	5.22
59	10	MA-130	32.6	A	347	30	6.43	—	4.71
60	10	MA-130	32.6	A	513	38	9.57	2.27	4.59
61	10	MA-130	32.6	A	520	45	15.41	3.30	4.48
62	10	MA-130	32.6	A	515	45	15.40	3.24	4.48
63	10	MA-130	32.6	A	348	60	34.49	8.12	4.27
64	10	MA-130	32.6	A	366	60	35.37	8.49	4.27
65	10	MA-130	32.6	A	452	60	34.30	7.71	4.27
66	10	MA-130	32.6	A	306	60	34.83	8.19	4.27
67	10	MA-130	32.6	A	511	60	34.37	8.12	4.27
68	11	MA-140	32.7	A	516	32	7.64	1.75	4.52
69	11	MA-140	32.7	A	371	40	13.15	2.83	4.43
70	11	MA-140	32.7	A	552	50	21.95	5.08	4.38
71	11	MA-140	32.7	A	527	60	37.02	8.95	4.24
72	11	MA-140	32.7	A	359	60	37.70	8.59	4.24
73	12	MA-150	28.8	A	363	30	6.76	1.49	4.53
74	12	MA-150	28.8	A	542	40	11.80	2.74	4.40

TABLE XII (Cont'd.)

Run	Film	Description	α	Gas	P_1	T	$\bar{P}$	D	k
			%		mmHg	°C	$\times 10^9$ cc(STP)/cm-sec-atm	$\times 10^7$ cm^2/sec	$\times 10^2$ cc(STP)/cc-atm
75	12	MA-150	28.8	A	471	50	20.30	4.86	4.21
76	12	MA-150	28.8	A	546	60	31.40	7.74	4.04
77	13	MA-150[2]	29.0	A	478	30	7.25	1.63	4.41
78	13	MA-150[1]	29.0	A	371	30	7.03	1.56	4.00
79	13	MA-150[2]	29.0	A	358	40	11.70	3.30	4.25
80	13	MA-150[2]	29.0	A	506	40	12.50	3.03	4.25
81	13	MA-150[2]	29.0	A	306	40	12.84	2.84	4.25
82	13	MA-150[1]	29.0	A	358	40	12.30	3.03	4.10
83	13	MA-150[2]	29.0	A	497	50	22.00	5.12	4.12
84	13	MA-150[2]	29.0	A	486	50	20.15	5.07	4.12
85	13	MA-150[1]	29.0	A	545	50	21.00	4.80	4.20
86	13	MA-150[1]	29.0	A	505	50	21.00	4.95	4.20
87	13	MA-150[2]	29.0	A	302	60	34.20	8.62	3.96
88	13	MA-150[2]	29.0	A	494	60	33.80	8.59	3.96
89	13	MA-150[1]	29.0	A	555	60	34.3	7.95	4.33
90	13	MA-150[1]	29.0	A	543	60	34.2	8.12	4.33
91	13	MA-150[1]	29.0	A	544	60	—	8.05	4.33
92	14	MA	51.0	A	500	30	8.04	1.44	5.59
93	14	MA	51.0	A	303	30	8.00	1.43	5.59
94	14	MA	51.0	A	468	40	14.10	2.58	5.50

1=Station 1, 2=Station 2

TABLE XII (Cont'd.)

Run	Film	Description	α %	Gas	P_1 mmHg	T °C	$\bar{P}$ $\times 10^9$ cc(STP)/cm-sec-atm	D $\times 10^7$ cm^2/sec	k $\times 10^2$ cc(STP)/cc-atm
95	14	MA	51.0	A	440	50	25.3	4.76	5.48
96	14	MA	51.0	A	453	60	43.1	7.72	5.42
97	14	MA	51.0	A	490	60	43.0	7.90	5.42
98	14	MA	51.0	A	283	60	43.6	7.86	5.42
99	14	MA	51.0	A	463	60	41.9	7.90	5.42
100	14a	MA-150	28.8	A	470	30	6.35	1.50	4.14
101	14a	MA-150	28.8	A	467	30	6.33	1.44	4.14
102	14a	MA-150	28.8	A	478	40	11.80	2.84	4.21
103	14a	MA-150	28.8	A	457	40	11.60	2.76	4.21
104	14a	MA-150	28.8	A	290	50	21.92	4.75	4.20
105	14a	MA-150	28.8	A	496	50	20.03	4.77	4.20
106	14a	MA-150	28.8	A	476	60	35.34	8.24	4.18
107	14a	MA-150	28.8	A	476	60	35.19	8.22	4.18
108	14a	MA-150	28.8	A	278	60	34.70	7.83	4.18
109	15	SA	39.0	A	289	30	7.93	1.38	5.85
110	15	SA	39.0	A	551	30	7.93	1.34	5.85
111	15	SA	39.0	A	502	45	18.0	3.11	5.61
112	15	SA	39.0	A	312	45	19.2	3.24	5.61
113	15	SA	39.0	A	184	60	40.9	7.35	5.48
114	15	SA	39.0	A	451	60	39.2	7.78	5.48
115	15	SA	39.0	A	282	60	40.1	7.63	5.48

TABLE XII (Cont'd.)

Run	Film	Description	α %	Gas	P_1 mmHg	T °C	$\bar{P}$ x10⁹ cc(STP)/cm-sec-atm	D x10⁷ cm²/sec	k x10² cc(STP)/cc-atm
116	15	SA	39.0	A	437	60	39.4	7.30	5.48
117	16	SA-150	30.5	A	253	30	6.76	1.36	4.96
118	16	SA-150	30.5	A	166	30	7.04	1.41	4.96
119	16	SA-150	30.5	A	250	45	16.25	3.49	4.62
120	16	SA-150	30.5	A	569	45	15.65	3.21	4.62
121	16	SA-150	30.5	A	383	45	16.10	3.36	4.62
122	16	SA-150	30.5	A	567	60	34.90	8.00	4.31
123	16	SA-150	30.5	A	378	60	—	8.18	4.31
124	16	SA-150	30.5	A	491	60	35.0	7.93	4.31
							$\bar{P}$ x 10^7	D x 10^5	k x 10^2
125	18	RH	51.0	He	513	21	0.565	0.945	.580
126	18	RH	51.0	He	353	30	0.77	1.29	.624
127	18	RH	51.0	He	360	30	0.77	1.28	.624
128	18	RH	51.0	He	533	40	1.09	1.62	.669
129	18	RH	51.0	He	345	40	1.08	1.65	.669
130	18	RH	51.0	He	569	40	1.07	1.72	.669
131	18	RH	51.0	He	515	50	1.50	2.06	.737
132	18	RH	51.0	He	342	50	1.51	2.10	.737
133	18	RH	51.0	He	539	60	2.04	2.59	.787
134	18	RH	51.0	He	381	60	2.07	2.55	.787

TABLE XII (Cont'd.)

Run	Film	Description	α	Gas	P_1	T	$\bar{P}$	D	k
			%		mmHg	°C	x10^7 cc(STP) / cm-sec-atm	x10^5 cm^2 / sec	x10^2 cc(STP) / cc-atm
135	19	RH-150	31.0	He	495	24.5	0.411	0.996	.418
136	19	RH-150	31.0	He	352	30	0.512	1.12	.435
137	19	RH-150	31.0	He	540	40	0.704	1.48	.483
138	19	RH-150	31.0	He	325	40	0.657	1.59	.483
139	19	RH-150	31.0	He	508	40	0.675	1.46	.483
140	19	RH-150	31.0	He	515	50	0.980	1.79	.513
141	19	RH-150	31.0	He	335	50	0.985	1.86	.513
142	19	RH-150	31.0	He	330	60	1.33	2.26	.551
143	19	RH-150	31.0	He	216	60	1.32	2.24	.551
144	19	RH-150	31.0	He	526	60	1.30	2.38	.551
145	20	MH	50.0	He	536	0	0.271	0.523	—
146	20	MH	50.0	He	352	0	0.279	0.513	—
147	20	MH	50.0	He	544	21.4	0.580	0.965	.577
148	20	MH	50.0	He	319	21.9	—	1.04	.580
149	20	MH	50.0	He	363	22.6	0.578	1.00	.583
150	20	MH	50.0	He	524	23.5	0.622	1.03	.590
151	20	MH	50.0	He	482	30.0	0.776	1.12	.628
152	20	MH	50.0	He	364	30.5	0.785	1.25	.630
153	20	MH	50.0	He	550	40	1.075	1.52	.695
154	20	MH	50.0	He	530	50	1.37	—	.765
155	20	MH	50.0	He	353	50	1.49	—	.765

TABLE XII (Cont'd.)

Run	Film	Description	α	Gas	P_1	T	$\bar{P}$	D	k
			%		mmHg	°C	$\times 10^7$ cc(STP) / cm-sec-atm	$\times 10^5$ cm^2 / sec	$\times 10^2$ cc(STP) / cc-atm
156	20	MH	50.0	He	506	50	1.49	1.91	.765
157	20	MH	50.0	He	338	50	1.50	1.88	.765
158	20	MH	50.0	He	512	60	2.06	2.48	.816
159	20	MH	50.0	He	343	60	2.03	2.53	.816
160	21	MH-150	29.5	He	504	0	0.181	0.523	—
161	21	MH-150	29.5	He	335	0	0.172	0.521	—
162	21	MH-150	29.5	He	283	21.8	0.376	0.925	.408
163	21	MH-150	29.5	He	437	22	0.381	0.930	.410
164	21	MH-150	29.5	He	344	29.6	0.506	1.09	.443
165	21	MH-150	29.5	He	511	30	0.522	1.09	.447
166	21	MH-150	29.5	He	419	35	—	1.31	.465
167	21	MH-150	29.5	He	531	40	0.726	1.45	.490
168	21	MH-150	29.5	He	544	45	—	1.64	.515
169	21	MH-150	29.5	He	320	50	0.958	1.87	.538
170	21	MH-150	29.5	He	473	50	0.980	1.81	.538
171	21	MH-150	29.5	He	471	50	—	1.79	.538
172	21	MH-150	29.5	He	508	60	1.31	2.52	.591
173	21	MH-150	29.5	He	332	60	1.35	2.26	.591
174	22	SH	39.0	He	552	21.5	0.466	0.88	.550
175	22	SH	39.0	He	542	30	0.610	1.03	.590
176	22	SH	39.0	He	533	40	0.873	1.38	.637

TABLE XII (Cont'd.)

Run	Film	Description	α %	Gas	P_1 mmHg	T °C	$\bar{P}$ x10^7 cc(STP)/cm-sec-atm	D x10^5 cm^2/sec	k x10^2 cc(STP)/cc-atm
177	22	SH	39.0	He	547	40	0.863	1.34	.637
178	22	SH	39.0	He	538	50	1.185	1.75	.690
179	22	SH	39.0	He	360	50	1.19	1.73	.690
180	22	SH	39.0	He	532	60	1.615	2.17	.730
181	22	SH	39.0	He	552	60	1.62	2.17	.730
182	23	SH-150	31.0	He	546	25.4	0.422	1.01	.420
183	23	SH-150	31.0	He	530	29.5	0.484	1.10	.440
184	23	SH-150	31.0	He	521	40	0.694	1.41	.486
185	23	SH-150	31.0	He	513	40	0.683	1.44	.486
186	23	SH-150	31.0	He	533	50	0.934	1.84	.531
187	23	SH-150	31.0	He	349	50	0.949	1.77	.531
188	23	SH-150	31.0	He	336	60	1.30	2.15	.584
189	23	SH-150	31.0	He	503	60	1.29	2.22	.584
							$\bar{P}$ x10^{10}	D x10^8	k x10^2
190	24	RF	52.2	CF_4	546	40	2.07	1.14	1.86
191	24	RF	52.2	CF_4	530	50	5.16	2.38	2.10
192	24	RF	52.2	CF_4	528	50	5.14	2.42	2.10
193	24	RF	52.2	CF_4	565	60	12.45	5.06	2.40
194	24	RF	52.2	CF_4	516	60	12.00	4.71	2.40
195	24	RF	52.2	CF_4	538	60	12.00	4.64	2.40

TABLE XII (Cont'd.)

Run	Film	Description	α %	Gas	P$_1$ mmHg	T °C	$\bar{P}$ x10^{10} cc(STP) cm-sec-atm	D x10^8 cm^2 sec	k x10^2 cc(STP) cc-atm
196	24	RF	52.2	CF_4	536	70	27.5	10.2	2.70
197	24	RF	52.2	CF_4	546	70	26.0	10.0	2.70
198	24a	RF-150	27.0	CF_4	550	40	1.94	1.25	1.52
199	24a	RF-150	27.0	CF_4	500	50	4.79	—	1.75
200	24a	RF-150	27.0	CF_4	549	50	4.68	2.67	1.75
201	24a	RF-150	27.0	CF_4	531	60	—	5.55	1.96
202	24a	RF-150	27.0	CF_4	550	60	11.20	5.46	1.96
203	24a	RF-150	27.0	CF_4	579	70	24.2	10.52	2.22
204	24a	RF-150	27.0	CF_4	504	70	24.2	10.70	2.22
205	25	MF	52.4	CF_4	539	40	2.03	1.10	1.90
206	25	MF	52.4	CF_4	552	50	4.73	2.31	2.08
207	25	MF	52.4	CF_4	371	50	4.99	2.43	2.08
208	25	MF	52.4	CF_4	541	50	4.98	2.44	2.08
209	25	MF	52.4	CF_4	538	60	12.30	5.17	2.31
210	25	MF	52.4	CF_4	540	60	12.10	5.14	2.31
211	25	MF	52.4	CF_4	364	60	12.50	5.08	2.31
212	25	MF	52.4	CF_4	490	70	25.6	10.6	2.47
213	25	MF	52.4	CF_4	502	70	25.5	10.8	2.47
214	25a	MF-150	27.5	CF_4	528	40	2.39	1.50	1.69
215	25a	MF-150	27.5	CF_4	552	40	2.55	1.47	1.69
216	25a	MF-150	27.5	CF_4	530	50	6.25	3.23	1.85

TABLE XII (Cont'd.)

Run	Film	Description	α %	Gas	P_1 mmHg	T °C	$\bar{P}$ $\times 10^{10}$ cc(STP) cm-sec-atm	D $\times 10^{8}$ cm^2 sec	k $\times 10^{2}$ cc(STP) cc-atm
217	25a	MF-150	27.5	CF_4	498	50	6.06	3.30	1.85
218	25a	MF-150	27.5	CF_4	524	60	13.4	6.51	2.03
219	25a	MF-150	27.5	CF_4	526	60	12.9	6.29	2.03
220	25a	MF-150	27.5	CF_4	531	70	27.2	13.1	2.17
221	25a	MF-150	27.5	CF_4	554	70	27.2	12.2	2.17
222	26	SF	38.2	CF_4	489	40	1.94	1.15	1.69
223	26	SF	38.2	CF_4	480	50	4.70	2.51	1.86
224	26	SF	38.2	CF_4	481	50	4.81	2.55	1.86
225	26	SF	38.2	CF_4	501	60	1.04	5.20	2.03
226	26	SF	38.2	CF_4	495	60	1.07	5.32	2.03
227	26	SF	38.2	CF_4	514	60	1.06	5.41	2.03
228	26	SF	38.2	CF_4	505	70	23.0	10.40	2.22
229	26	SF	38.2	CF_4	526	70	22.9	10.22	2.22
230	26a	SF-150	27.4	CF_4	505	40	2.51	1.58	1.59
231	26a	SF-150	27.4	CF_4	475	50	6.10	3.30	1.76
232	26a	SF-150	27.4	CF_4	501	50	5.98	3.48	1.76
233	26a	SF-150	27.4	CF_4	509	60	12.8	6.70	1.93
234	26a	SF-150	27.4	CF_4	527	60	13.0	6.76	1.93
235	26a	SF-150	27.4	CF_4	503	70	27.9	13.5	2.09
236	26a	SF-150	27.4	CF_4	486	70	27.3	13.1	2.09

TABLE XIII

SUMMARY OF LOW PRESSURE SORPTION DATA

Run*	Film	Description	α %	Gas	T °C	P mmHg	D $\times 10^7$ $\frac{cm^2}{sec}$	k $\times 10^2$ $\frac{cc(STP)}{cc\text{-}atm}$
1	1	RA	56.5	A	39	536	—	5.88
2	1	RA	56.5	A	47	598	—	6.06
3	16	SA-150	30.5	A	29.6	179	—	5.3
4	16	SA-150	30.5	A	39.5	173	2.4	4.5
5	16	SA-150	30.5	A	39.5	240	2.6	4.4
6	16	SA-150	30.5	A	39.5	203	—	4.8
7	16	SA-150	30.5	A	60.6	174	8.7	4.1
8	16	SA-150	30.5	A	60.7	224	8.1	3.8
9	16	SA-150	30.5	A	60.5	205	—	4.0
10	17	RH	50.0	He	40	718	—	0.68
11	17	RH	50.0	He	40	703	—	0.74
12	17	RH	50.0	A	40	642	—	6.13
13	17	RH	50.0	A	40	613	—	6.30
14	21	MH-150	29.5	He	39.9	204	—	0.4
15	21	MH-150	29.5	He	39.9	208	—	0.4
16	21	MH-150	29.5	He	40	201	—	0.4
17	21	MH-150	29.5	He	40	209	—	0.58
18	21	MH-150	29.5	He	40	541	—	0.47
19	21	MH-150	29.5	He	40	548	—	0.42
20	21	MH-150	29.5	A	25	202	1.4	4.9
21	21	MH-150	29.5	A	25	198	1.2	5.2

TABLE XIII (Cont'd.)

Run*	Film	Description	α %	Gas	T °C	P mmHg	D $\times 10^7$ $\frac{cm^2}{sec}$	k $\times 10^2$ $\frac{cc(STP)}{cc\text{-}atm}$
22	21	MH-150	29.5	A	40	198	2.7	4.2
23	21	MH-150	29.5	A	40	197	2.9	5.0
24	21	MH-150	29.5	A	40	204	2.91	4.76
25	21	MH-150	29.5	A	40.1	201	3.02	4.72
26	21	MH-150	29.5	A	40	200	—	4.48
27	21	MH-150	29.5	A	40	215	—	4.10
28	21	MH-150	29.5	A	40	196	—	4.08
29	21	MH-150	29.5	A	40	209	—	5.13
30	21	MH-150	29.5	A	40	196	—	5.49
31	21	MH-150	29.5	A	60	196	8.3	4.10
32	21	MH-150	29.5	A	60	204	8.3	4.50
33	21	MH-150	29.5	CF_4	40	537	—	1.63
34	21	MH-150	29.5	CF_4	40	486	—	1.49
35	—	atactic	100	He	25.5	493	355	1.35
36	—	atactic	100	He	27.5	537	355	1.34
37	—	atactic	100	He	40	377	535	1.84
38	—	atactic	100	He	40	382	555	1.73
39	—	atactic	100	He	40	403	549	1.74
40	—	atactic	100	He	40	540	555	1.60
41	—	atactic	100	A	24.2	535	12.2	13.94
42	—	atactic	100	A	26.0	437	11.0	13.62

TABLE XIII (Cont'd.)

Run*	Film	Description	α %	Gas	T °C	P mmHg	D $\times 10^7$ $\frac{cm^2}{sec}$	k $\times 10^2$ $\frac{cc(STP)}{cc\text{-}atm}$
43	—	atactic	100	A	40	472	29.5	13.60
44	—	atactic	100	A	40	490	29.9	12.45
45	—	atactic	100	A	40	493	29.5	14.00
46	—	atactic	100	A	40	571	29.5	13.50
47	—	atactic	100	A	40	473	29.5	13.58
48	—	atactic	100	A	40	—	27.3	—
49	—	atactic	100	A	40	396	29.1	13.64
50	—	atactic	100	A	70	461	146	14.11
51	—	atactic	100	CF_4	25	555	1.17	7.05
52	—	atactic	100	CF_4	40	427	3.72	7.42
53	—	atactic	100	CF_4	40	472	3.47	—
54	—	atactic	100	CF_4	40	507	3.72	7.68
55	—	atactic	100	CF_4	40	574	3.71	7.83
56	—	atactic	100	CF_4	70	680	26.4	8.51
57	—	atactic	100	CF_4	70	701	23.3	8.65
58	—	atactic	100	CH_4	25	367	6.37	27.58
59	—	atactic	100	CH_4	25	97	5.92	27.58
60	—	atactic	100	CO_2	25.2	163	13.8	74.15

*NOTE: Runs 1-34 are sorption experiments;
Runs 35-60 are desorption experiments.

TABLE XIV

SUMMARY OF HIGH PRESSURE SORPTION DATA

Run	Gas	T °C	Pressure Range atm	k cc(STP) / cc-atm
1	A	-30	3.9 - 30.9	0.147
2	A	-22	4.0 - 10.5	0.125
3	A	-15	4.1 - 27.5	0.097
4	A	-8.0	3.9 - 25.9	0.092
5	A	-0.5	3.7 - 20.1	0.101
6	A	0	4.1 - 27.7	0.104
7	A	7.8	3.5 - 17.8	0.068
8	A	8.0	4.0 - 19.1	0.072
9	A	15	4.2 - 30.7	0.076
10	A	30	4.0 - 21.1	0.064
11	A	39	4.1 - 21.3	0.064
12	CO_2	-40	2.0 - 10.7	1.31
13	CO_2	-38	1.2 - 10.3	1.170
14	CO_2	-29	2.9 - 12.3	0.942
15	CO_2	-28.5	2.7 - 11.6	0.990
16	CO_2	-20	2.5 - 13.1	0.910
17	CO_2	-17	3.6 - 21.3	0.828
18	CO_2	-8.5	2.6 - 13.9	0.610
19	CO_2	0	3.2 - 20.2	0.560
20	CO_2	11	3.5 - 16.9	0.450
21	CO_2	17	3.6 - 21.3	0.402
23	CO_2	18	3.2 - 20.6	0.410

TABLE XIV (Cont'd.)

Run	Gas	T	Pressure Range	k
		°C	atm	$\frac{cc(STP)}{cc\text{-}atm}$
24	CO_2	28	3.5 - 20.5	0.350
25	CO_2	33	3.3 - 23.0	0.331
26	CO_2	34.8	3.5 - 21.6	0.325
27	CO_2	40	3.4 - 21.3	0.316
28	CO_2	49	3.7 - 20.6	0.250

TABLES XV and XVI

DATA FOR SORPTION ISOTHERMS SHOWN IN FIGURES 29 and 31

Run	Film	Gas	T	T_{a_i}	P_i	T_{a_f}	P_f	ΔP	ΔC	C_T
			°C	°K	atm	°K	atm	atm	$\frac{cc(STP)}{cc_P}$	$\frac{cc(STP)}{cc_P}$
Table XV - Fig. 29										
1	27	A	-30	293.4	4.42	296.4	3.89	.527	0.654	0.654
1	27	A	-30	296.4	7.81	294.9	7.38	.426	0.515	1.169
1	27	A	-30	294.9	11.27	296.0	10.85	.406	0.503	1.672
1	27	A	-30	296.2	14.54	293.7	14.18	.392	0.458	2.130
1	27	A	-30	293.7	17.95	293.0	17.52	.416	0.514	2.644
1	27	A	-30	293.0	21.40	292.0	20.93	.442	0.538	3.182
1	27	A	-30	292.4	24.53	291.7	24.13	.408	0.486	3.668
1	27	A	-30	291.7	31.60	293.0	30.85	.748	0.936	4.604
Table XVI - Fig. 31										
16	27	CO_2	-20	280	4.36	280	2.48	1.88	2.38	2.38
16	27	CO_2	-20	280	6.00	278	4.65	1.35	1.77	4.15
16	27	CO_2	-20	278	7.65	278	6.40	1.25	1.70	5.85
16	27	CO_2	-20	278	9.70	278	8.52	1.18	1.68	7.53
16	27	CO_2	-20	278	11.60	278	10.37	1.23	1.79	9.32
16	27	CO_2	-20	278	14.70	276	13.05	1.65	2.55	11.87

Appendix B

Sample Calculations

1. Time-Lag Data

a. Diffusion Constants.

To illustrate the calculation of D, k and $\bar{P}$ from the time-lag data, run number 94, Table XII, will be used.

Referring to equation (23)

$$D = \frac{\ell^2}{360\theta} \qquad (23)$$

Figure 8 is a plot of the experimentally observed pressure change with time; from it one obtains θ = 14.9 mins. For the film used in run 94, $\ell = 37.2 \times 10^{-3}$ cm (see Table III), where ℓ is the film thickness.

$$\therefore D = \frac{(37.2 \times 10^{-3})}{(360)\ (14.9)} = 2.58 \times 10^{-7}\ \frac{cm^2}{sec}$$

b. Permeability Constants.

$\bar{P}$ is calculated from equation (24)

$$\bar{P} = \frac{(dP/dt)\,(10^{-3})\,(\ell)\,(V_s)\,(273)}{(A)\,(P_1)\,(60)\,(T_a + 273)} \qquad (24)$$

Again from Figure 8, the slope (dP/dt) = 3.55 μ/min and correcting for the leak rate, determined immediately prior to run 94, (dP/dt) = 3.49 μ/min. V_s = 107.55 cc and A = 32.2 cm^2.

The ambient temperature, T_a, was 25.8°C and the upstream pressure, P_1, was 468 mm Hg

$$\therefore \bar{P} = \frac{(3.49 \times 10^{-3})(37.2 \times 10^{-3})(107.5)(273)}{(32.2)(468)(60)(25.8 + 273)}$$

$$= 14.1 \times 10^{-9} \frac{cc(STP)}{cm\text{-}sec\text{-}atm}$$

c. Solubility Constant.

From equation (25), $k = \bar{P}/D$

then, from above

$$k = \frac{14.1 \times 10^{-9}}{2.58 \times 10^{-7}}$$

$$= 5.50 \times 10^{-2} \frac{cc(STP)}{cc\text{-}atm}$$

2. Low Pressure Sorption Data

a. Solubility Constants.

(i) From Sorption Experiments

The following calculations will be illustrated using the data of run 26, Table XIII, and equation (27).

$$k = \frac{V_V}{V_P} \cdot \frac{273}{T} \cdot \frac{P_i - P_e}{P_e} \qquad (27)$$

$V_V = V_T - V_P = 29.20 - 6.65 = 22.55$ cc. The temperature inside the constant temperature enclosure was 40°C. The initial pressure, P_i, was 203 mm Hg. The pressure drop due to sorption, $P_i - P_e$, was 3.42 mm Hg. The correction for the blank sorption

effect was 0.394 mm Hg. Thus the $(P_i - P_e)_{net} = 3.03$ and the equilibrium pressure = 200 mm Hg.

$$\therefore k = \left(\frac{22.55}{6.65}\right) \cdot \left(\frac{273}{313}\right) \cdot \left(\frac{3.03}{200}\right)$$

$$= 4.48 \times 10^{-2} \ \frac{cc(STP)}{cc\text{-}atm}$$

(ii) From Desorption Experiments

The calculation of solubilities from desorption data will be illustrated with run 42, Table XIII.

From equation (28)

$$k = \frac{V_V}{V_P} \cdot \frac{273}{T} \cdot \frac{P_e}{[(1 - f)P_i - P_e]} \qquad (28)$$

where f is the fraction of gas lost from the sample during the pump-down and is estimated from equation (32)

$$(1 - f) = \left[1 - 2\left(\frac{Dt}{\pi \ell^2}\right)^{1/2}\right]^3 \qquad (32)$$

For run 42, the half-thickness of the polymer cubes was 0.3 cm; the pump-down time, t, was 15 sec; the diffusivity of Argon at 40°C = 11.0×10^{-7} cm^2/sec.

$$\therefore (1 - f) = \left\{1 - 2\left[\frac{(11.0 \times 10^{-7})(15)}{(3.14)(0.3)^2}\right]^{1/2}\right\}^3$$

$$= 0.955$$

The P listed in Table XIII is equivalent to

$$(1 - f)P_i = 437 \text{ mm Hg}$$

Thus, with $V_V = 81.5$ cc

$V_P = 46.0$ cc

$T = 26°C = 299°K$

and $P'_e = 34.4$ mm Hg,

with the correction for residual pressure after pump-down,

$$P_e = (P'_e - P')$$

$$= 34.4 - 0.4 = 34.0 \text{ mm Hg}$$

$$\therefore k = \frac{81.5}{46.0} \cdot \frac{273}{299} \cdot \frac{34.0}{437 - 34.0}$$

$$= 13.62 \times 10^{-2} \frac{\text{cc(STP)}}{\text{cc-atm}}$$

b. Diffusion Constants.

As pointed out in the "PROCEDURE" several methods were used to determine diffusion constants from low pressure sorption experiments.

(i) For runs 1 to 34, equation (30) was used to determine values of D.

$$\frac{M_t}{M_\infty} = 2 \left(\frac{Dt}{\ell^2 \pi} \right)^{1/2} \qquad (30)$$

In this case, P/P_e is a measure of M_t/M_∞. Therefore, at short times, a plot of P/P_e versus $t^{1/2}$ yields a straight line with a slope equal to $2(D/\pi\ell^2)^{1/2}$. The calculation for this case will be illustrated for run 24, Table XIII.

From Figure 13,

$$\text{Slope} = 2\left(\frac{D}{\pi\ell^2}\right)^{1/2} = 0.105 \quad (\text{min})^{-1/2}$$

$$= 1.355 \times 10^{-2} \quad (\text{sec})^{-1/2}$$

From Table III, "ℓ" = 89.9×10^{-3} cm

then, the <u>half</u>-thickness = 44.9×10^{-3} cm

and $$D = \frac{(1.355 \times 10^{-2})^2(\pi)(\ell^2)}{(4)} = 2.91 \times 10^{-7} \ \frac{\text{cm}^2}{\text{sec}}$$

(ii) Diffusion constants obtained from <u>desorption</u> experiments were calculated in a slightly different way. By observing diffusion at short times, the D's could be calculated by comparing the experimentally observed rise in pressure with a corresponding <u>numerical</u> solution for diffusion out of a cube (see Figure 14). Run 47 will be used as an illustration. First, one calculates the parameter, ffu., which for <u>desorption</u> is defined as:

$$\text{ffu.} = 1 - \frac{\text{total amount of gas in polymer at equilibrium}}{\text{total amount of gas in polymer initially}}$$

$$= 1 - \frac{(1-f)P_i - \Delta P}{(1-f)P_i} = 1 - \frac{434.6}{472.8} \cong 0.08$$

..... (34)

Since the curves shown in Figure 14 are essentially linear at low values of M_t/M_∞, interpolation for values of ffu. not given is quite accurate, if the lower section of the curves is enlarged.

Thus at ffu. = 0.08 and $M_t/M_\infty = 0.3$,

$$\left(\frac{Dt}{\ell^2}\right)^{1/2} = 0.0914$$

$$\therefore \text{(Slope)}_N = \frac{(M_t/M_\infty)}{(Dt/\ell^2)^{1/2}} \qquad \text{(B-1)}$$

$$= \frac{0.3}{0.0914} = 3.28$$

where (Slope)_N = the slope taken from the numerical solution.

Rearranging, $$\frac{M_t/M_\infty}{t^{1/2}} = \frac{(3.28)(D)^{1/2}}{\ell} \qquad \text{(B-2)}$$

The slope from the plot of the experimental data for run 47 (see Figure 68) is

$$\text{(Slope)}_E = \frac{P_t/P_e}{t^{1/2}} \qquad \text{(B-3)}$$

$$= 0.1455\ (\text{min})^{-1/2} = 0.0188\ (\text{sec})^{-1/2}$$

Comparing equations (B-2) and (B-3),

$$\frac{(3.28)(D)^{1/2}}{\ell} = 0.0188$$

and $$D = \left[\frac{(0.0188)(\ell)}{(3.28)}\right]^2 \qquad \text{(B-4)}$$

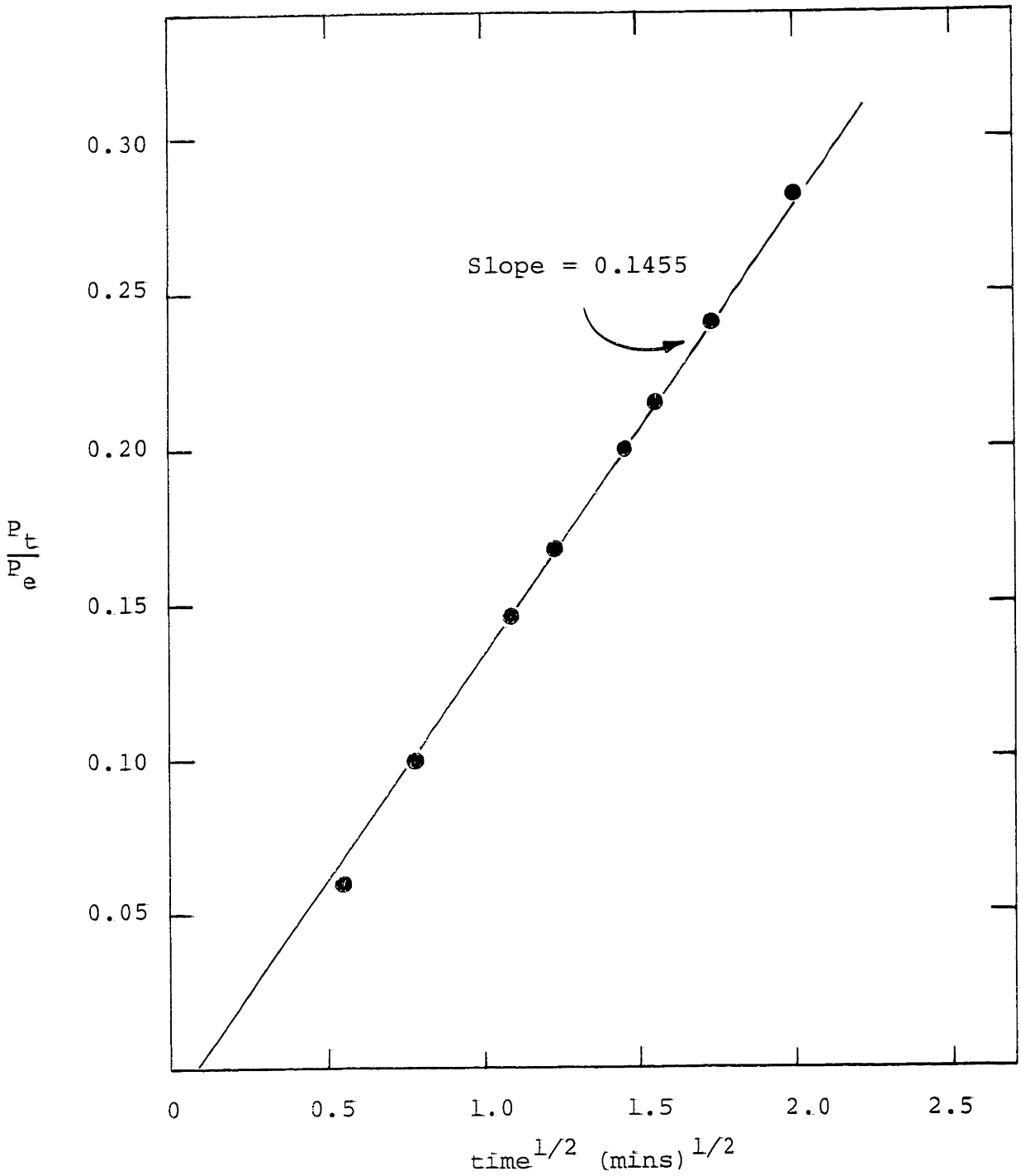

Figure 68 Desorption of Argon from Atactic Polypropylene Run 47, T = 40°C

Then with $\ell = 0.3$ cm,

$$D = \left[\frac{(0.0188)(0.3)}{(3.28)} \right]^2 = 2.95 \times 10^{-6} \ \frac{cm^2}{sec}$$

In the case of runs 41, 42, 48 and 49 the diffusion constants were calculated on the basis of equation (35) which, as already mentioned, describes radial diffusion out of a sphere into a limited volume:

$$\frac{M_t}{M_\infty} = 1 - \sum_{n=1}^{\infty} \frac{6\phi(1+\phi)}{(9 + 9\phi + \phi^2 q_n^2)} \exp - \frac{Dq_n^2 t}{\ell^2} \qquad (35)$$

At long times, this reduces to

$$\frac{M_t}{M_\infty} = 1 - \frac{6\phi(1+\phi)}{9 + 9\phi + \phi^2 q_n^2} \exp - \frac{Dq_1^2 t}{\ell^2} \qquad (36)$$

For ease of computation, equation (36) can be simplified by replacing the coefficient $[6\phi(1+\phi)/(9+9\phi+\phi^2 q_n^2)]$ by Z and denoting the time corresponding to $(1 - M_t/M_\infty) = 0.1$ by $t_{0.1}$.

Therefore,

$$D = \frac{\ell n\ (10Z)}{q_1^2} \cdot \frac{r^2}{t_{0.1}} \qquad (36a)$$

To illustrate the calculation of D, run 49 will be used.

$$\phi = \frac{V_V}{V_p} \cdot \frac{1}{k}$$

with

$$V_V = 81.5 \text{ cc}$$

$$V_p = 46.0 \text{ cc}$$

and $k = 13.64 \times 10^{-2} \ \frac{cc(STP)}{cc_p\text{-atm}}$

$$\phi = \frac{81.5}{46.0} \cdot \frac{1}{13.64 \times 10^{-2}} = 12.95$$

From Table 6-1 in Crank (29)

at $\phi = 12.95$, $q_1 = 3.16$ (by extrapolation)

$$\therefore Z = \frac{6\phi(\phi + 1)}{9 + 9\phi + q_1^2\phi^2} = \frac{(6)(12.95)(13.95)}{(9) + (9)(12.95) + (3.16)^2(12.95)^2}$$

$$= 0.602$$

From the plot of the experimental data for this run, Figure 15,

$$t_{0.1} = 92.5 \text{ mins} = 5.55 \times 10^3 \text{ sec}$$

Then with $r = 0.3$ cm

$$D = \frac{\ln(10Z)}{q_1^2} \cdot \frac{r^2}{t_{0.1}}$$

$$= \frac{\ln(6.02)}{(3.16)^2} \cdot \frac{(0.3)^2}{(5.55 \times 10^3)}$$

$$= \frac{(1.7951)}{(10)} \cdot \frac{(9)(10^{-2})}{(5.55)(10^3)} = 29.1 \times 10^{-7} \ \frac{cm^2}{sec}$$

3. High Pressure Sorption Data

In the high pressure sorption work the solubility constants were calculated as illustrated for run 16, Table XIV.

The amount of gas sorbed after each equilibration is given by equation (41)

$$C = \left(\frac{273 Z_o V_b}{V_P T}\right)\left(\frac{P_i}{Z_i} - \frac{P_f}{Z_f}\right) + \left(\frac{273 Z_o V_a}{V_P}\right)\left(\frac{P_i}{Z_{a_i} T_{a_i}} - \frac{P_f}{T_{a_f} Z_{a_f}}\right) \qquad (41)$$

the parameters for the system were:

$$V_P = 158.0 \text{ cc}$$

$$V_b = 154.5 \text{ cc}$$

$$V_a = 21.5 \text{ cc}$$

The conditions at the first equilibration were:

$$T = -20°C = 253°K$$

$$P_i = 4.36 \text{ atm}$$

$$P_f = 2.48 \text{ atm}$$

$\Big\}\ \Delta P = 1.88$ atm

$$T_{a_i} = 7°C = 280°C$$

$$T_{a_f} = 5°C = 278°K$$

For CO_2 the critical properties are:

$$T_c = 304.3°K$$

$$P_c = 73.0 \text{ atm}$$

then the reduced properties are:

$$P_{o_R} = \frac{1.0}{73.0} = 0.0137$$

$$T_{o_R} = \frac{273}{304.3} = 0.898$$

$$\therefore \quad Z_o = 0.992$$

$$P_{i_R} = \frac{4.36}{73.0} = 0.060$$

$$T_R = \frac{253}{304.2} = 0.833$$

$$\therefore \quad Z_i = 0.959$$

$$P_{f_R} = \frac{2.48}{73.0} = 0.034$$

$$T_R = \frac{253}{304.3} = .833$$

$$\therefore \quad Z_f = 0.977$$

$$P_{i_R} = 0.060$$

$$T_{a_{i_R}} = \frac{280}{304.3} = 0.922$$

$$\therefore \quad Z_{a_i} = 0.971$$

$$P_{f_R} = 0.034$$

$$T_{a_{f_R}} = \frac{278}{304.3} = 0.915$$

$$\therefore \quad Z_{a_f} = 0.983$$

The compressibilities were obtained from the generalized compressibility chart in Reid and Sherwood (93). Substituting these values in equation (41)

$$C_1 = \frac{(273)(0.992)(154.5)}{(158)(253)}\left(\frac{4.36}{0.959} - \frac{2.48}{0.977}\right) +$$

$$+ \frac{(273)(0.992)(21.5)}{(158)}\left[\frac{(4.36)}{(0.971)(280)} - \frac{(2.48)}{(278)(0.983)}\right]$$

$$= 2.38 \frac{cc(STP)}{cc_p}$$

Thus after the first equilibration the pressure was 2.48 atmospheres and the gas concentration in the polymer 2.38 $cc(STP)/cc_p$. The concentration after the second pressurization and equilibration is

$$C_T = C_1 + C_2$$

The values of C_T are then plotted against their respective equilibration pressures. This results in a linear relationship whose slope is equal to the solubility constant, k, (see Figure 31).

4. Calculation of Micro-void Size, U_{oo} and ΔH_{ads}

a. Size of Voids

Assuming the voids are spherical and all of the same size, then

$$V = \frac{4}{3}\pi R^3$$

and

$$A = 4\pi R^2$$

Therefore $$\frac{V}{A} = \frac{R}{3} \text{ and } R = 3\frac{V}{A}$$

Assume that below T_g, all the WLF free volume is in the form of these spherical micro-voids.

$$\therefore \quad V = V_{WLF} = 0.025 \text{ cc/cc}_p$$

$$A = \text{total surface area of voids/cc}_p$$

However, A can be estimated from C_H', the hole saturation constant, cc(STP)/cc_p

$$\text{i.e.,} \quad A = \frac{C_H' N a}{22{,}400} \text{ cm}^2 \qquad \text{(B-5)}$$

where

N = Avogadro's number

a = area of molecule for hexagonal close packing, cm^2

Since no value of C_H' was available for poly(propylene), the size of its voids was estimated from data for poly(styrene), P_s, (112) and poly(ethylene terephthalate), PET, (114).

The calculation will be illustrated for CO_2 sorption in glassy, crystalline PET.

For PET, $C_H' = 4.2$ at $\alpha = 0.57$

$d = 3.7\text{Å}$ (molecular diameter of CO_2)

and $a = 3D^2/2\sqrt{3} = 11.86 \times 10^{-16} \text{ cm}^2$

Since the WLF free volume applies only to the amorphous fraction, $V_{WLF} = (0.57)(0.025)$

$$= 0.0142 \text{ cc/cc}_p$$

$$\therefore \quad A = \frac{(4.2)(6.023)(10^{23})(11.86)(10^{-16})}{(22{,}400)}$$

$$= 1.34 \times 10^5 \text{ cm}^2$$

$$\therefore \quad R = 3\frac{V_{WLF}}{A} = \frac{(3)\ (0.0142)}{(1.34)(10^5)} = 31.8\text{Å}$$

Therefore, the voids in crystalline PET have an average radius of 32Å.

b. Hole Affinity Constant, b.

For crystalline poly(propylene), the estimated value for R = 32Å. Then, C_H' can be calculated from

$$A = \frac{C_H' \, Na}{22,400} \qquad \text{(B-5)}$$

The calculation will be illustrated for argon sorption in film 27, Table III.

For Film 27, $\alpha = 0.58$

$$\therefore \quad V_{WLF} = (0.58)(0.025) = 0.0145 \text{ cc/cc}_p$$

From above $R = 3\frac{V}{A}$

$$(32)(10^{-8}) = \frac{(3)(0.0145)}{A}$$

$$\therefore \quad A = 1.36 \times 10^5 \text{ cm}^2/\text{cc}_p$$

For argon $d = 3.6\text{Å}$

and

$$a = \frac{3D^2}{2\sqrt{3}} = 11.22 \times 10^{-16} \text{ cm}^2$$

$$\therefore \quad C_H' = \frac{22,400A}{Na} = \frac{(22,400)(1.36)(10^{-5})}{(6.023)(10^{23})(11.22)(10^{-16})}$$

$$= 4.51 \text{ cc(STP)/cc}_p$$

From Figure 30, a plot of k versus 1/T, the following values for argon solubility at 40°C have been obtained by extrapolation.

$$k = 0.190 \frac{cc(STP)}{cc_p\text{-atm}}$$

$$k_D = 0.091 \frac{cc(STP)}{cc_p\text{-atm}}$$

where k and k_D are the solubility constants in the equation,

$$C = C_D + C_H = k_D P + \frac{C'_H bP}{1 + bP} \qquad (B\text{-}6)$$

where
- C = concentration of gas in polymer $cc(STP)/cc_p$
- C_D = ordinary dissolution
- C_H = "hole-filling" sorption
- k_D = Henry's law constant
- P = equilibrium pressure, atm.
- C'_H = hole saturation constant
- b = hole affinity constant

at low pressures, $bP \ll 1$

$$\therefore \quad C = k_D P + C'_H bP \qquad (B\text{-}7)$$

and

$$k = k_D + C'_H b \qquad (B\text{-}8)$$

Substituting in values from above

$$C'_H b = k - k_D = 0.190 - 0.091 = 0.099$$

Then knowing $C'_H = 4.51$

$$\therefore \qquad b = \frac{0.099}{4.51} = 0.022$$

c. Evaluating U_{oo}.

From Hill (43) equation (7-21)

$$x'(T) = \left(\frac{2\pi m \bar{k} T}{h^2} \right) q_z \, e^{-U_{oo}/\bar{k}T} \, e^{\mu^\circ/\bar{k}T} \qquad \text{(B-9)}$$

$$\text{But } x'(T) = \frac{(C'_H b)\ (N)}{(22{,}400)\,(A)} \qquad \text{(B-10)}$$

$$= \frac{(0.099)\,(6.023)\,(10^{23})}{(22{,}400)\,(1.36)\,(10^5)\,(1.013)\,(10^6)}$$

$$= 1.932 \times 10^{7}$$

From Hill (43) equation (5-6)

$$q_Z = \frac{e^{-\vartheta/2T}}{1 - e^{-\vartheta/T}} \qquad \text{(B-11)}$$

where $\vartheta = \frac{h\nu}{\bar{k}}$

h = Planck's constant

$\bar{k}$ = Boltzmann's constant

ν = vibrational frequency, sec^{-1}

The values of ν were esimated from data by Meares (62) and an interpolation of a plot of ν versus $\varepsilon/\bar{k}$.

Evaluating,

$$\theta = \frac{(6.625)(10^{-27})(0.7)(10^{12})}{(1.38)(10^{-16})}$$

$$= 33.6$$

<u>at T = -40°C</u>

$$q_Z = \frac{e^{-33.6/466}}{1 - e^{-33.6/233}} = 6.928$$

$$\left(\frac{2\pi m\bar{k}T}{h^2}\right) = \frac{(2)(3.14)(40)(1.38 \times 10^{-16})(233)}{(6.025)(10^{23})(6.625)^2(10^{-27})^2}$$

$$= 3.04 \times 10^{17}$$

From Hill (<u>42</u>) equation (4-26),

$$\mu^\circ(T) = -\bar{k}T\ell n\left[\left(\frac{2\pi m\bar{k}T}{h^2}\right)^{3/2}\bar{k}T\right] \qquad \text{(B-13)}$$

$$\therefore \quad e^{\frac{\mu^\circ(T)}{\bar{k}T}} = \frac{1}{\left[\left(\frac{2\pi m\bar{k}T}{h^2}\right)^{3/2}\bar{k}T\right]}$$

$$= \frac{1}{[(3.04 \times 10^{17})^{3/2}(1.38 \times 10^{-16})(233)]}$$

$$= 1.855 \times 10^{-13}$$

Then rearranging the expression for x'(T)

$$e^{-U_{oo}/\bar{k}T} = \frac{x'(T)}{\left(\frac{2\pi m\bar{k}T}{h^2}\right) q_Z e^{\mu^\circ/\bar{k}T}} \qquad \text{(B-9a)}$$

$$= \frac{(1.918)\ (10^7)}{(3.04)\,(10^{17})\,(6.928)\,(1.855)\,(10^{-13})}$$

$$= 49.09$$

$$\therefore \quad U_{oo} = -(\ell n 49.09)\bar{k}T \text{ ergs/molecule}$$

$$= -(3.894)\,(1.38)\,(10^{-16})\,(233)\,(6.023)\,(10^{23})\cdot \cdot(2.389)\,(10^{-8})$$

$$= -1801 \text{ cals/gmole of argon}$$

d. Heat of Adsorption, ΔH_{ads}.

$$\Delta H_{ads} = U_{oo} + \frac{h\nu_Z}{2} + \frac{3}{2}\bar{k}T \qquad \text{(B-14)}$$

For argon at 25°C

$$\frac{h\nu_Z}{2} = \frac{(6.625)\,(10^{-27})\,(0.7)\,(10^{12})}{2} = 2.32 \times 10^{-15} \text{ ergs}$$

$$\frac{3}{2}\bar{k}T = \left(\frac{3}{2}\right)(1.38 \times 10^{-16})\,(298) = 61.7 \times 10^{-15} \text{ ergs}$$

$$\Delta H_{ads} = -1801 + (6.023)(10^{23})(2.389)(10^{-8}) \cdot [2.32 \times 10^{-15} + 61.7 \times 10^{-15}]$$

$$= -1801 + 921 \cong -880 \text{ cals/gmole}$$

5. Entropies of Activation for Diffusion

The calculations of λ, ΔS^*_G, ΔS^*_p, ΔS^*_o will be illustrated for film 14.

From run 94, Table XII

$$D = 2.58 \times 10^{-7} \text{ cm}^2/\text{sec}$$

$$T = 313°K$$

and $E_D = 11.4$ Kcals/gmole (Table V)

∴ From equation (12)

$$D_o = D\, e^{E_D/RT} \qquad (12a)$$

$$D_o = (2.58)(10^{-7})e^{11400/(2)(313)}$$

$$= 21.08 \text{ cm}^2/\text{sec}$$

If one assumes that the activation energy is all expended in the formation of a cavity for the diffusing molecule to slide through, then the length of the diffusion jump, λ, is equal to the length of the cavity with cross-section $\frac{1}{4}\pi d^2$.

$$\therefore E_D = (\text{C.E.D.})(\tfrac{1}{4})(\pi)(d^2)(N)(\lambda) \qquad (66)$$

where C.E.D. = the cohesive energy density, cals/cc

d = $3.6\mathring{A}$

N = Avogadro's number = 6.023×10^{23}

λ = diffusion jump length, $\mathring{A}$

For crystalline poly(propylene), $\delta = 8.1\ (cal/cc)^{1/2}$

$$\therefore \text{ C.E.D.} = \delta^2 = (8.1)^2 = 65.6 \text{ cal/cc}$$

$$\text{Then } 11400 = \frac{(65.6)}{(10^{24})} \left(\frac{1}{4}\right)(3.14)(3.6)^2(6.023)(10^{23})\lambda$$

$$\therefore \lambda = 28.4\mathring{A}$$

Then applying Eyring's transition state theory (42) to diffusion,

$$D_o = \frac{e\lambda^2 \bar{k} T}{h} \exp \frac{\Delta S_o^*}{R} \qquad (65)$$

where: $\bar{k}$ = Boltzmann's Constant = 1.38×10^{-16} erg/°K

h = Planck's Constant = 6.625×10^{-27} erg-sec

T = 40°C = 313°K

$$\therefore \Delta S_o^* = R\ell n \frac{(D_o)\ (h)}{(e\lambda^2 \bar{k} T)}$$

$$= 2\ell n \frac{(21.08)(10^{16})(6.625)(10^{-27})}{(2.303)(28.5)^2(1.38)(10^{-16})(313)}$$

$$\Delta S_o^* = 5.70 \text{ cals/gmole-°K}$$

ΔS_o^* contains contributions from the diffusing gas molecule, ΔS_G^*, and from the medium, ΔS_D^*.

Meares (64) defines

$$\Delta S_G^* = S_{trans} - S_{vib} \qquad (69)$$

where:

$$S_{trans} = R\ell n\left[\frac{(2\pi m\bar{k}t)^{1/2}\lambda}{h}\right] + \frac{1}{2}R \qquad (67)$$

and

$$m = \text{molecular mass} = \frac{\text{mol. wt.}}{N} = \frac{40}{(6.023 \times 10^{23})}$$

$$S_{trans} = 2\ell n\left\{\left[\frac{(2)(3.14)(40)(1.38)(10^{-16})(313)}{(6.023)(10^{23})}\right]^{1/2} \cdot \frac{(28.5)(10^{-8})}{(6.625)(10^{-27})}\right\} + 1$$

$$= 11.40 \text{ cals/gmole-°K}$$

$$S_{vib} = 3\left[\frac{Nh\nu}{T(e^{h\nu/\bar{k}T} - 1)} - R\ell n(1 - e^{-h\nu/\bar{k}T})\right] \qquad \ldots\ldots (68)$$

$$\text{if } e^{h\nu/\bar{k}T} = e^{\frac{[(6.625)(10^{-27})(0.70)(10^{12})]}{[(1.38)(10^{-16})(313)]}} = 1.113$$

$$\therefore S_{vib} = 3\left[\frac{(6.023)(10^{23})(6.625)(10^{-27})(2.39)(10^{-8})(0.7)(10^{12})}{(313)(1.113 - 1)} - 2\ell n(1 - 0.898)\right]$$

$$= 19.35 \text{ cals/gmole-°K}$$

Then $\Delta S_G^* = 11.40 - 19.35 = -7.95$ cals/gmole-°K

Then knowing ΔS^* overall and ΔS^*_G, one obtains ΔS^*_p by difference, i.e.,

$$\Delta S^*_p = \Delta S^*_o - \Delta S^*_G \qquad (70)$$

$$= 5.70 - (-7.95)$$

$$= 13.65 \text{ cals/gmole-°K}$$

6. Isosteric Heats and Entropies of Solution

The calculations will be illustrated for the case of CF_4 sorption in atactic poly(propylene).

The isosteric heat, q_s, was calculated from the expression

$$q_s = -R\left(\frac{d\ell nP}{d\frac{1}{T}}\right)_C \qquad (63)$$

From Table XIII, for run 51, T = 25°C, $k = 7.0 \times 10^{-2}$ $\frac{cc(STP)}{cc_p\text{-atm}}$

and for run 57, T = 70°C, $k = 8.6 \times 10^{-2}$ $\frac{cc(STP)}{cc_p\text{-atm}}$

Constructing a linear plot of C versus P from these values of k, and interpolating for values of P at the random value of $C = 6.0 \times 10^{-2}$ $cc(STP)/cc_p$, one obtains the values of $P_1 = 6.51$ mm Hg at T = 25°C and $P_2 = 530$ mm Hg at T = 70°C. Then integrating equation (63) and substituting

$$q_s = -R \frac{(\ell nP_1 - \ell nP_2)}{(\frac{1}{T_1} - \frac{1}{T_2})} \quad \text{at } C = 6 \times 10^{-2}$$

$$= -2 \frac{(\ell n \frac{651}{760} - \ell n \frac{530}{760})}{(\frac{1}{298} - \frac{1}{343})}$$

$$= -0.932 \quad \text{Kcals/gmole}$$

Now, the entropy of solution can be calculated from the relationship

$$(\bar{S}_2 - S_2^g) = R\ell nx - \frac{q_s}{T} \qquad (62)$$

where

$(\bar{S}_2 - S_2^g) \equiv$ the entropy change in going from the gas phase at one atmosphere into solution at the equilibrium concentration x_2.

Substituting the values from above in equation (62), one obtains

$$(\bar{S}_2 - S_2^g) = 2 \left(\frac{\frac{6 \times 10^{-2}}{22,400}}{\frac{6 \times 10^{-2}}{22,400} + \frac{0.858}{16,000}} \right) + \frac{932}{298}$$

$$= -2.96 \text{ cals/gmole-°K}$$

Appendix C

Error Analysis

I. Estimated Precision of Experimental Methods

The expected error in the determination of $\bar{P}$, D and k by the various experimental methods was estimated using statistical methods. A detailed error analysis was performed for a representative run of each method. The formulae and nomenclature of Volk (115) were generally followed.

A. Time-Lag

As in Appendix B, the data for film 14 and run number 94, Table XII, were considered to be representative of the time-lag results. The pressure-time data for this run are shown in Figure 8.

1. Diffusion Constant

The equation used was

$$D = \frac{\ell^2}{360\theta} \qquad (23)$$

From Figure 8, θ = 14.9 min. and the estimated standard deviation, $\sigma(\theta) = \pm 0.1$ min. The thickness of film 14 was ℓ = .0372 cm with $\sigma(\ell) = \pm 0.0009$, on the basis of fifteen separate measurements.

Therefore, D = 2.58 x 10^{-7} cm^2/sec and from elementary statistics

$$\sigma^2(D) = D^2 \left[\frac{4\sigma^2(\ell)}{\ell^2} + \frac{\sigma^2(\theta)}{\theta^2} \right] \qquad \text{(C-1)}$$

$$= (2.58 \times 10^{-7})^2 \left[\frac{324 \times 10^{-8}}{13.8 \times 10^{-4}} + \frac{10^{-2}}{222} \right]$$

$$= 6.66 \times 10^{-14} [23.5 \times 10^{-4} + 4.50 \times 10^{-5}]$$

$$= 1.60 \times 10^{-16}$$

$$\therefore \quad \sigma(D) = 1.26 \times 10^{-8}$$

For a normal distribution the 95% confidence limits are given by:

$$D \pm 1.96\ \sigma(D) = (2.58 \pm 0.247) \times 10^{-7}\ \text{cm}^2/\text{sec}$$

This corresponds to a $\pm 9.6\%$ estimated precision on the measurement of D.

2. Permeability Constant

The equation used to evaluate $\bar{P}$ was

$$\bar{P} = \frac{(dP/dt \times 10^{-3})(\ell)(V_s)(273)}{(A)(P_1)(60)(T_a + 273)} \qquad (24)$$

The relevant data for determining the precision of $\bar{P}$ are summarized below:

$\bar{P}$	$= 14.1 \times 10^{-9}$		
dP/dt	$= 3.49$ u/min	$\sigma(dP/dt)$	$= 0.02$
ℓ	$= .0372$ cm	$\sigma(\ell)$	$= 0.0009$
V_s	$= 107.5$ cc	$\sigma(V_s)$	$= 1.0$
A	$= 32.2\ \text{cm}^2$	$\sigma(A)$	$= 0.15$
P_1	$= 468$ mm Hg	$\sigma(P)$	$= 0.5$
T_a	$= 25.8°C$	$\sigma(T_a)$	$= 0.1$

The standard deviation of the volume, V_s, and the area, A, are based on several duplicate measurements. The variation in T_a represents the range of T experimentally observed.

The estimated precision is then given by:

$$\sigma^2(\bar{P}) = \bar{P}^2 \left[\frac{\sigma^2(dP/dt \times 10^{-3})}{(dP/dt \times 10^{-3})^2} + \frac{\sigma^2(\ell)}{\ell^2} + \frac{\sigma^2(V_s)}{V_s^2} + \frac{\sigma^2(A)}{A^2} + \right.$$

$$\left. + \frac{\sigma^2(P_1)}{P_1^2} + \frac{\sigma^2(T_a)}{(T_a + 273)^2} \right] \qquad \text{(C-2)}$$

$$= (14.1 \times 10^{-9})^2 \left[\frac{4 \times 10^{-10}}{12.2 \times 10^{-6}} + \frac{81 \times 10^{-8}}{13.8 \times 10^{-4}} + \right.$$

$$\left. + \frac{1.0}{1.15 \times 10^{4}} + \frac{2.25 \times 10^{-2}}{10.37 \times 10^{2}} + \frac{0.25}{21.9 \times 10^{4}} \quad \frac{10^{-2}}{8.9 \times 10^{4}} \right]$$

$$= 198.8 \times 10^{-18} [32.8 \times 10^{-6} + 5.87 \times 10^{-4} +$$

$$+ 0.87 \times 10^{-4} + 2.17 \times 10^{-5} + 1.14 \times 10^{-6} + 1.12 \times 10^{-7}]$$

$$= 198.8 \times 10^{-18} [7.30 \times 10^{-4}]$$

$$= 1451 \times 10^{-22} = 14.51 \times 10^{-20}$$

$$\sigma(\bar{P}) = 3.81 \times 10^{-10}$$

Therefore, the 95% confidence limits are

$$\bar{P} \pm 1.96\sigma(\bar{P}) = (14.1 \pm 0.747) \times 10^{-9}$$

The estimated precision is, then, $\pm 5.2\%$.

3. Solubility Constant

The solubility is determined from the ratio of the permeability to the diffusivity,

$$k = \frac{\bar{P}}{D} \qquad (25)$$

Using the results from the above two sections and the experimental solubility for run 94, i.e., $k = 5.50 \times 10^{-2}$ cc(STP)/cc-atm.

$$\sigma^2(k) = k^2\left[\frac{\sigma^2(\bar{P})}{\bar{P}^2} + \frac{\sigma^2(D)}{D^2}\right] \qquad (C\text{-}3)$$

$$= (5.50 \times 10^{-2})^2\left[\frac{14.51 \times 10^{-20}}{198.8 \times 10^{-18}} + \frac{1.60 \times 10^{-16}}{6.66 \times 10^{-14}}\right]$$

$$= 30.3 \times 10^{-4}[7.30 \times 10^{-4} + 2.40 \times 10^{-3}]$$

$$= 9.48 \times 10^{-6}$$

$$\sigma(k) = 3.08 \times 10^{-3}$$

The 95% confidence limits are

$$k \pm 1.96\sigma(k) = (5.50 \pm .603) \times 10^{-2}$$

This corresponds to an estimated precision of ±11.0%

B. Low Pressure Sorption

1. Solubility Constant

The precision of the low pressure sorption method will be estimated by considering run number 42, Table XIII.

$$k = \frac{V_V}{V_P} \cdot \frac{273}{T} \cdot \frac{P_e}{[(1 - f)P_i - P_e]} \quad (27)$$

The equilibrium values and the estimated deviations for the parameters in equation (27) are:

$$k = 13.62 \times 10^{-2} \ \frac{cc(STP)}{cc\text{-}atm}$$

V_V	= 81.5 cc	$\sigma(V_V)$	= 0.02
V_P	= 46.0 cc	$\sigma(V_P)$	= 0.002
T	= 26°C = 299°K	$\sigma(T)$	= 0.02
P_e	= 34.4 mm Hg	$\sigma(P_e)$	= 0.001
P_i	= 437 mm Hg	$\sigma(P_i)$	= 0.5

Since (1 - f) is a derived quantity, its standard deviation will be calculated first. (1 - f) was determined from equation (32), namely

$$(1 - f) = [1 - 2(\frac{Dt}{\pi \ell^2})^{1/2}]^3 \quad (32)$$

where (1 - f) = 0.955 and f = 0.045

D	= 11.0×10^{-7} cm^2/sec	$\sigma(D)$	= 1.26×10^{-8}
t	= 15 sec	$\sigma(t)$	= 1.0
ℓ	= 0.3 cm	$\sigma(\ell)$	= 0.01

Then

$$\sigma^2(f) = (f)^2(\frac{9}{4})[\frac{\sigma^2(D)}{D} + \frac{\sigma^2(t)}{t^2} + \frac{4\sigma^2(\ell)}{\ell^2}] \quad (C\text{-}4)$$

$$= (20.2 \times 10^{-4})(2.25)[\frac{1.59 \times 10^{-16}}{121 \times 10^{-14}} + \frac{1}{225} + \frac{4 \times 10^{-4}}{9 \times 10^{-2}}]$$

$$= (20.2 \times 10^{-4})(2.25)(1.31 \times 10^{-4} + 4.44 \times 10^{-3} + 4.44 \times 10^{-3})$$

$$= 41.0 \times 10^{-6}$$

and $\sigma(f) = 0.006 = (1 - f)$

Both V_P and V_V are derived quantities and consequently their deviations have been calculated from the appropriate relationships.

$$V_P = \frac{w}{\rho} \quad \text{where:} \quad \begin{matrix} w = 39.45 \text{ gms}, \sigma(w) = .001 \\ \rho = 0.858 \text{ g/cc}, \sigma(\rho) = .001 \end{matrix}$$

$$V_V = V_T - V_P$$

$$\text{where} \quad V_T = V_1 \frac{(P_1 - P_2)}{P_2} \qquad (26)$$

and

V_T	= 127.5 cc	$\sigma(V_T)$	= 0.05
V_1	= 60.9 cc	$\sigma(V_1)$	= 0.01
P_1	= 27.474 mm Hg	$\sigma(P_1)$	= .001
P_2	= 8.882 mm Hg	$\sigma(P_2)$	= .001

From the above data the values of $\sigma(V_P)$ and $\sigma(V_V)$ were readily calculated.

Thus having established values for all the parameters in equation (27), it becomes possible to evaluate the standard deviation of k

$$\sigma^2(k) = k^2\{ \frac{\sigma^2(V_V)}{V_V^2} + \frac{\sigma^2(V_P)}{V_P^2} + \frac{\sigma^2(T)}{T^2} + \frac{\sigma^2(P_e)}{P_e^2} + \frac{\sigma^2[(1-f)P_i - P_e]}{[(1-f)P_i - P_e]^2} \} \qquad \text{(C-5)}$$

$$= k^2\{ \frac{\sigma^2(V_V)}{V_V^2} + \frac{\sigma^2(V_P)}{V_P^2} + \frac{\sigma^2(T)}{T^2} + \frac{\sigma^2(P_e)}{P_2^2} + \frac{[(1-f)P_i]^2[\frac{\sigma^2(1-f)}{(1-f)^2} + \frac{\sigma^2(P_i)}{P_i^2}] + \sigma^2(P_e)\}}{[(1-f)P_i - P_e]^2}$$

Therefore,

$$\sigma^2(k) = (13.62 \times 10^{-2})^2 \{\frac{4 \times 10^{-4}}{6.64 \times 10^3} + \frac{4 \times 10^{-6}}{2.12 \times 10^3} + \frac{4 \times 10^{-4}}{8.94 \times 10^4} + \frac{1 \times 10^{-6}}{11.8 \times 10^2} + \frac{[417]^2[\frac{36 \times 10^{-6}}{.912} + \frac{.25}{19.1 \times 10^4}] + 1 \times 10^{-6}}{[417 - 34.4]^2}\}$$

$$= (1.855 \times 10^{-2}) \{6.02 \times 10^{-8} + 1.9 \times 10^{-9} + 4.47 \times 10^{-9} + 8.48 \times 10^{-10} + \frac{(1.74 \times 10^5)(39.5 \times 10^{-6} + 1.31 \times 10^{-6}) + 1 \times 10^{-6}}{(14.6 \times 10^4)}\}$$

$$= (1.855 \times 10^{-2}) \{6.74 \times 10^{-8} + \frac{7.10 + 1 \times 10^{-6}}{14.6 \times 10^4}\}$$

$$= (1.855 \times 10^{-2})(6.76 \times 10^{-8} + 4.86 \times 10^{-5})$$

$$= (1.855 \times 10^{-2})(48.67 \times 10^{-6})$$

$$= 90.3 \times 10^{-8}$$

or,

$$\sigma(k) = 9.5 \times 10^{-4}$$

Then, at the 95% confidence level the precision limits for this method are

$$k \pm 1.96\sigma(k) = .1362 \pm .002$$

or

$$\pm 1.5\%$$

2. Diffusion Constant

a. For part of the low pressure sorption data the diffusion constants were calculated on the basis of equation (30)

$$\frac{M_t}{M_\infty} = 2 \left(\frac{Dt}{\ell^2 \pi} \right)^{1/2} \qquad (30)$$

where

$$\frac{M_t}{M_\infty} = \frac{P_t}{P_e}$$

On rearranging $(P_t/P_e)/t^{1/2} = 2(D/\pi\ell^2)^{1/2}$ (30a)

where $(P/P_e)/t^{1/2}$ is the slope of the plot P_t/P_e vs $t^{1/2}$ (see Figure 13).

Therefore, $$D = \frac{(\text{slope})^2 (\pi) (\ell^2)}{(4)} \qquad (30b)$$

Again, using run 24 (see Appendix B) as an "average" run for all values of D determined in this way, the precision of this method will be estimated.

The parameters and the estimates of their standard deviations are:

$D = 2.91 \times 10^{-7}$ cm^2/sec

$\ell = 0.0449$ cm $\qquad \sigma(\ell) = .0009$

slope $= 1.355 \times 10^{-2}$ (sec)$^{-1/2}$ $\qquad \sigma$(slope) $= 1.02 \times 10^{-4}$

Since the "slope" is a derived quantity, its standard deviation must be calculated separately.

$$\text{Slope} = \frac{P_t/P_e}{t^{1/2}} = \frac{P_t}{P_e t^{1/2}} \qquad \text{(B-3)}$$

where:

slope $= 1.355 \times 10^{-2}$ (sec)$^{-1/2}$

$P_t = 203$ mm Hg $\qquad \sigma(P_t) = 0.5$

$P_e = 204$ mm Hg $\qquad \sigma(P_e) = 0.5$

$t = 375$ sec $\qquad \sigma(t) = 5$

$$\sigma^2(\text{slope}) = (\text{slope})^2\left[\frac{\sigma^2(P_t)}{P_t^2} + \frac{\sigma^2(P_e)}{P_e^2} + \frac{\sigma^2(t)}{4t^2}\right]$$

$$= (1.355 \times 10^{-2})^2\left[\frac{25 \times 10^{-2}}{4.12 \times 10^4} + \frac{25 \times 10^{-2}}{4.16 \times 10^4} + \frac{25}{5.63 \times 10^5}\right]$$

$$= (1.84 \times 10^{-4})[6.07 \times 10^{-6} + 6.01 \times 10^{-6} + 4.44 \times 10^{-5}]$$

$$= (1.84 \times 10^{-4})(56.48 \times 10^{-6})$$

$$= 103.9 \times 10^{-10}$$

$$\sigma(\text{slope}) = 1.02 \times 10^{-4}$$

$$\text{Then,}\quad \sigma^2(D) = D^2\left[\frac{4\sigma^2(\text{slope})}{(\text{slope})^2} + \frac{4\sigma^2(\ell)}{\ell^2}\right] \qquad \text{(C-7)}$$

$$= (2.91 \times 10^{-7})^2\left[\frac{416 \times 10^{-10}}{1.84 \times 10^{-4}} + \frac{324 \times 10^{-8}}{20.2 \times 10^{-4}}\right]$$

$$= (8.47)(10^{-14})[2.26 \times 10^{-4} + 16.04 \times 10^{-4}]$$

$$= (8.47)(10^{-14})(18.30)(10^{-4})$$

$$= 1.55 \times 10^{-16}$$

$$\sigma(D) = 1.25 \times 10^{-8}$$

The precision limits, at the 95% confidence limit, are

$$D \pm 1.96\sigma(D) = (2.91 \pm 0.245) \times 10^{-7} \ \text{cm}^2/\text{sec}$$

or

$\pm$ 8.4% of the diffusion constant.

b. In the case of the atactic samples, the diffusion constants were calculated from a numerical solution for diffusion out of a cube. The precision of this method was estimated on the basis of run 47 (see Appendix B). First, the σ(ffu.) was estimated from the relationship

$$\text{ffu.} = 1 - \frac{(1 - f)P_i - \Delta P}{(1 - f)P_i} \qquad (34)$$

where

ffu.	= 0.081		
$(1 - f)$	= 0.927	$\sigma(1 - f)$	= .006
P_i	= 510 mm Hg	$\sigma(P_i)$	= 0.5
ΔP	= 38.25 mm Hg	$\sigma(\Delta P)$	= 0.001

Simplifying (34) $\quad ffu. = \dfrac{\Delta P}{(1 - f)P_i}$

Therefore,

$$\sigma^2(ffu.) = (ffu.)^2\left[\frac{\sigma^2\Delta P}{\Delta P^2} + \frac{\sigma^2(1 - f)}{(1 - f)^2} + \frac{\sigma^2(P_i)}{P_i^2}\right] \qquad (C\text{-}8)$$

$$= (0.081)^2\left[\frac{1 \times 10^{-6}}{(38.25)^2} + \frac{36 \times 10^{-6}}{(0.927)^2} + \frac{25 \times 10^{-2}}{(510)^2}\right]$$

$$= (65.5 \times 10^{-4})[6.84 \times 10^{-10} + 41.9 \times 10^{-6} + + 9.62 \times 10^{-7}]$$

$$= 28.10 \times 10^{-8}$$

$$\therefore \qquad \sigma(ffu.) = 5.3 \times 10^{-4}$$

Then at the 95% confidence limit, the precision limits are $\pm 1.96\sigma(ffu.) = \pm 10.4 \times 10^{-4}$ or $\pm 1.3\%$.

From an enlarged plot of M_t/M_∞ versus $(Dt/\ell^2)^{1/2}$, of the numerical solution, it was estimated that a standard deviation of $\pm 1.3\%$ in the value of (ffu.) would result in a standard deviation of $\pm 1.6\%$ in $(slope)_N$, the slope from the numerical solution. Thus from (B-1), $(slope)_N = 3.28$ with $\sigma(slope)_N = 0.0525$.

The standard deviation of $(slope)_E$, the slope from the plot of the experimental data, was estimated from the relationship

$$(Slope)_E = \frac{M_t/M_\infty}{t^{1/2}} = \frac{P_t/P_e}{P_e t^{1/2}} \qquad (B\text{-}3)$$

where: $(\text{Slope})_E = 0.0188\ (\text{sec})^{1/2}$

$P_t = 502$ mm Hg $\qquad \sigma(P_t) = 0.5$

$P_e = 434$ mm Hg $\qquad \sigma(P_e) = 0.5$

$t = 126$ sec $\qquad \sigma(t) = 5$

The calculation is identical to that in the previous section and yields $\sigma(\text{slope})_E = 3.74 \times 10^{-4}$.

Then from equation (B-3) the standard deviation for D can be calculated.

$$D = \left[\frac{(\text{Slope})_E (\ell)}{(\text{Slope})_N}\right]^2 \qquad \text{(C-9)}$$

where:

$D = 2.95 \times 10^{-6}\ \text{cm}^2/\text{sec}$

$(\text{Slope})_E = 0.0188\ (\text{sec})^{-1/2} \qquad \sigma(\text{Slope})_E = 3.74 \times 10^{-4}$

$(\text{Slope})_N = 3.28 \qquad \sigma(\text{Slope})_N = .0525$

$\ell = 0.3$ cm $\qquad \sigma(\ell) = .01$

$$\sigma^2(D) = D^2\left[\frac{\sigma^2(\text{Slope})_E}{(\text{Slope})_E^2} + \frac{\sigma^2(\ell)}{\ell^2} + \frac{\sigma^2(\text{Slope})_N}{(\text{Slope})_N^2}\right] \qquad \text{(C-10)}$$

$$= (2.95 \times 10^{-6})^2\left[\frac{(3.74 \times 10^{-4})^2}{(0.0188)^2} + \frac{(.01)^2}{(0.3)^2} + \frac{(.0525)^2}{(3.28)^2}\right]$$

$$= (8.7 \times 10^{-12})[3.96 \times 10^{-4} + 1.11 \times 10^{-3} + 2.57 \times 10^{-4}]$$

$$= (8.7 \times 10^{-12})(17.63 \times 10^{-4})$$

$$= 1.53 \times 10^{-14}$$

$$\sigma(D) = 1.24 \times 10^{-7}$$

Thus the precision limits at the 95% confidence are
$D \pm 1.96\sigma(D) = (2.95 \pm .242) \times 10^{-6}$ cm^2/sec or $D \pm 8.2\%$.

c. In the case of runs 41, 42, 48 and 49 (see Table XIII) the D was calculated from desorption data by equation (36a) in conjunction with a plot such as Figure 15.

$$D = \frac{\ell n(10Z)}{q_1^2} \cdot \frac{r^2}{t_{0.1}} \qquad (36a)$$

Run 49 was considered a run representative of this method. The parameters in equation (36a) and the estimated standard deviations are then

$$D = 2.91 \times 10^{-6} \quad \frac{cm^2}{sec}$$

q_1	= 3.16	$\sigma(q_1)$	= 0.002
r	= 0.3 cm	$\sigma(r)$	= 0.01
$t_{0.1}$	= 5.55×10^3 sec	$\sigma(t_{0.1})$	= 150
Z	= 0.602	$\sigma(Z)$	= 0.005

Therefore,

$$\sigma^2(D) = D^2\left[\frac{\sigma^2(Z)}{Z} \quad \frac{4\sigma^2(r)}{r^2} \quad \frac{4\sigma^2(q_1)}{(q_1)^2} \quad \frac{\sigma^2(t_{0.1})}{(t_{0.1})^2}\right] \qquad (C\text{-}11)$$

$$= (2.91 \times 10^{-6})^2\left[\frac{(0.005)^2}{0.602} + \frac{4(0.01)^2}{(0.3)^2} + \frac{4(0.002)^2}{(3.16)^2} + \right.$$

$$\left. + \frac{(150)^2}{(5.55 \times 10^3)^2}\right]$$

$$= (8.47 \times 10^{-12})(5.21 \times 10^{-3})$$

$$= 4.41 \times 10^{-14}$$

$$\therefore \quad \sigma(D) = 2.10 \times 10^{-7}$$

The precision limits are $\pm 1.96\ (D) = \pm 4.12 \times 10^{-7}$ and $D = (2.91 \pm 0.41) \times 10^{-6}$ cm^2/sec or $D \pm 14.1\%$ with ~85% of this error arising from the variations in the particle size.

C. High Pressure Sorption

The precision of the solubilities determined from the high pressure sorption work was estimated on the basis of run 16, Table XIV.

Firstly, the variance of the amount sorbed will be estimated.

$$C = \left(\frac{273 Z_o V_b}{V_p T}\right)\left(\frac{P_i}{Z_i} - \frac{P_f}{Z_f}\right) + \left(\frac{273 Z_o V_a}{V_p}\right)\left(\frac{P_i}{Z_{a_i} T_{a_i}} - \frac{P_f}{T_{a_f} Z_{a_f}}\right) \quad (41)$$

or

$$C = \frac{273 Z_o V_b P_i}{V_p T Z_i} - \frac{273 Z_o V_b P_f}{V_p T Z_f} + \frac{273 Z_o V_a P_i}{V_p Z_{a_i} T_{a_i}} - \frac{273 Z_o V_a P_f}{V_p T_{a_f} Z_{a_f}} \quad (41a)$$

Table XVIII

Parameters for Determining $\sigma^2(c)$

Variable	Mean Value	Standard Deviation
C	2.38 cc(STP)/cc$_p$	
V_p	158.0 cc	$\pm$ 0.02
V_b	154.5 cc	$\pm$ 1.0
V_a	21.5 cc	$\pm$ 1.0
T	253°K	$\pm$ 0.1

Variable	Mean Value	Standard Deviation
P_i	4.36 atm.	$\pm$ 0.08
P_f	2.48 atm.	$\pm$ 0.1
T_{a_i}	280°K	$\pm$ .1
T_{a_f}	278°K	$\pm$ .1
Z_o	0.992	$\pm$ .001
Z_i	0.959	$\pm$ .001
Z_f	0.977	$\pm$ .001
Z_{a_i}	0.971	$\pm$ .001
Z_{a_f}	0.983	$\pm$ .001

The compressibility factors are derived values and their standard deviations were estimated by evaluating $\sigma(Z_i)$.

$$(P_i)_R = \frac{P_i}{P_c} \quad \text{where:} \quad (P_i)_R = 0.060$$

$$P_i = 4.36 \text{ atm}, \ \sigma(P_i) = 0.08$$

$$P_c = 73.0 \text{ atm}, \ \sigma(P_c) = 0.1$$

$$T_R = \frac{T}{T_c} \quad \text{where:} \quad T_R = 0.833$$

$$T = 253°K, \quad \sigma(T) = 0.1$$

$$T_c = 304.3°K, \ \sigma(T_c) = 0.1$$

$$\therefore \sigma^2(Z_i) = \sigma^2(P_i)_R + \sigma^2(T_R)$$

$$= (1.22 \times 10^{-6}) + (0.19 \times 10^{-6})$$

$$= 1.41 \times 10^{-6}$$

$$\text{and } \sigma(Z_i) = 1.19 \times 10^{-3} \cong 1.2 \times 10^{-3}$$

Now, taking each term in equation (41a) individually and summing the variances for the various terms, $\sigma(c)$ can be evaluated.

$$\text{Let } M = \frac{273 Z_o V_b P_i}{V_P T Z_i}$$

Then

$$\sigma^2(M) = M^2 \left[\frac{\sigma^2(Z_o)}{(Z_o)^2} + \frac{\sigma^2(V_b)}{(V_b)^2} + \frac{\sigma^2(P_i)}{(P_i)^2} + \frac{\sigma^2(V_P)}{(V_P)^2} + \right.$$

$$\left. + \frac{\sigma^2(T)}{T^2} + \frac{\sigma^2(Z_i)}{(Z_i)^2}\right] \qquad \text{(C-12)}$$

$$\sigma^2(M) = \left[\frac{(273)(0.992)(154.5)(4.36)}{(158.0)(253)(0.959)}\right]^2 \left[\frac{(.001)^2}{(0.992)^2} + \frac{1}{(154.5)^2} + \right.$$

$$\left. + \frac{(0.08)^2}{(4.36)^2} \quad \frac{(0.02)^2}{(158)^2} \quad \frac{(0.1)^2}{(253)^2} \quad \frac{(.001)^2}{(0.959)^2}\right]$$

$$= (22.65)(3.81 \times 10^{-4})$$

$$= 86.3 \times 10^{-4}$$

$$\text{Let } N = \frac{273 Z_o V_b P_f}{V_P T Z_f}$$

$$\sigma^2(N) = N^2 \left[\frac{\sigma^2(Z_o)}{(Z_o)^2} + \frac{\sigma^2(V_b)}{(V_b)^2} + \frac{\sigma^2(P_f)}{(P_f)^2} + \frac{\sigma^2(V_P)}{(V_P)^2} + \frac{\sigma^2(T)}{T^2} + \frac{\sigma^2(Z_f)}{(Z_f)^2}\right]$$

... (C-13)

$$= \left[\frac{(273)(0.992)(154.5)(2.48)}{(158)(253)(0.977)}\right]^2 \left[\frac{(0.001)^2}{(0.992)^2} + \frac{1}{(154.5)^2} + \right.$$

$$\left. + \frac{(0.1)^2}{(2.48)^2} + \frac{(0.02)^2}{(158)^2} + \frac{(0.1)^2}{(253)^2} + \frac{(.001)^2}{(0.977)^2}\right]$$

$$= (7.06)(1.67 \times 10^{-3}) = 11.79 \times 10^{-3}$$

Let $P = \dfrac{273 Z_o V_a P_i}{V_P Z_{a_i} T_{a_i}}$

$$\sigma^2(P) = P^2\left[\frac{\sigma^2(Z_o)}{(Z_o)^2} + \frac{\sigma^2(V_a)}{(V_a)^2} + \frac{\sigma^2(P_i)}{(P_i)^2} + \frac{\sigma^2(V_p)}{(V_p)^2} + \frac{\sigma^2(Z_{a_i})}{(Z_{a_i})^2} + \frac{\sigma^2(T_{a_i})}{(T_{a_i})^2}\right]$$

$$= \left[\frac{(273)(0.992)(21.5)(4.36)}{(158)(0.971)(280)}\right]^2 \left[\frac{(.001)^2}{(.992)^2} + \frac{1}{(21.5)^2} + \frac{(.08)^2}{(4.36)^2} + \right.$$

$$\left. + \frac{(.02)^2}{(158)^2} + \frac{(.001)^2}{(0.971)^2} + \frac{(.001)^2}{(280)^2}\right]$$

$$= (0.349)(2.50 \times 10^{-3})$$

$$= 8.73 \times 10^{-4}$$

Let $Q = \dfrac{273 Z_o V_a P_f}{V_P T_{a_f} Z_{a_f}}$

$$\sigma^2 Q = Q^2\left[\frac{\sigma^2(Z_o)}{(Z_o)^2} + \frac{\sigma^2(V_a)}{(V_a)^2} + \frac{\sigma^2(P_f)}{(P_f)^2} + \frac{\sigma^2(V_p)}{(V_p)^2} + \frac{\sigma^2(T_{a_f})}{(T_{a_f})^2} + \frac{\sigma^2(Z_{a_f})}{(Z_{a_f})^2}\right]$$

..... (C-15)

$$= \left[\frac{(273)(0.992)(21.5)(2.48)}{(158)(278)(0.983)}\right]^2 \left[\frac{(.001)^2}{(.992)^2} + \frac{1}{(21.5)^2} + \right.$$

$$\left. + \frac{(0.1)^2}{(2.48)^2} + \frac{(.02)^2}{(158)^2} + \frac{(.1)^2}{(278)^2} + \frac{(.001)^2}{(.983)^2}\right]$$

$$= (0.112)(3.79 \times 10^{-3}) = 4.24 \times 10^{-4}$$

Then

$$\sigma^2(c) = \sigma^2(M) + \sigma^2(N) + \sigma^2(P) + \sigma^2(Q) \qquad \text{(C-16)}$$

$$= (86.3 + 117.9 + 8.73 + 4.24) \times 10^{-4}$$

$$= 2.17 \times 10^{-2}$$

$$\therefore \quad \sigma(c) = 0.147$$

Then, assuming the variance for each pressure increment is equal to this average variance, the variance of the solubility constant can be estimated.

$$k = \frac{C_2 - C_1}{P_2 - P_1} \qquad \text{(C-17)}$$

From Figure 31,

$C_1 = 4.0$ cc/cc$_p$ $\qquad \sigma(c) = 0.147$

$C_2 = 10.0$ cc/cc$_p$ $\qquad \sigma(c) = 0.147$

$P_1 = 4.4$ atm. $\qquad \sigma(P_1) = 0.08$

$P_2 = 11.0$ atm. $\qquad \sigma(P_2) = 0.13$

$$\therefore \quad \sigma^2(k) = k^2\left[\frac{\sigma^2(C_2 - C_1)}{(C_2 - C_1)^2} + \frac{\sigma^2(P_2 - P_1)}{(P_2 - P_1)^2}\right] \qquad \text{(C-18)}$$

$$= k^2\left[\frac{2\sigma^2(C)}{(C_2 - C_1)^2} + \frac{\sigma^2(P_2) + \sigma^2(P_1)}{(P_2 - P_1)^2}\right]$$

$$= (0.910)^2\left[\frac{2(0.147)^2}{(10 - 4)^2} + \frac{(.13)^2 + (.08)^2}{(11.0 - 4.4)^2}\right]$$

$$= (0.828)(1.2 \times 10^{-3} + 0.535 \times 10^{-3})$$

$$= (0.828)(1.735 \times 10^{-3})$$

$$= 14.37 \times 10^{-4}$$

Therefore, $\sigma(k) = 0.0379$ and the precision at the 95% confidence level is $k \pm 1.96\sigma(k) = 0.910 \pm .0743$ or $\pm$ 8.2%.

II. Measured Precision

To check on the estimated precision, as presented in the previous sections, the standard deviation of several repeat runs was estimated.

Mickley, Sherwood and Reed (72) outline a method for assigning confidence limits to the mean of a small number of measurements. Their formulae and nomenclature are used throughout this section.

1. Time-Lag

Runs 96 through 99, Table XII, were all performed at 60°C with argon.

Run	$\bar{P} \times 10^9$	$(x - \bar{x})$	$(x - \bar{x})^2$
96	43.1	.2	.04
97	43.0	.1	.01
98	43.6	.7	.49
99	41.9	1.0	1.00

Sample mean = $\bar{x} = 42.9 \times 10^{-9}$. The variance of the population of means equals

$$S_m^2 = \frac{\sum^n (x - \bar{x})^2}{n(n - 1)} \qquad \text{(C-19)}$$

where x is the value of an individual measurement and n is the total number of measurements.

$$\therefore \quad S_m^2 = \frac{\sum^n (x - \bar{x})^2}{n(n - 1)} \qquad \text{(C-20)}$$

$$= \frac{1.54}{4 \times 3} = 0.128$$

Then, the best estimate of the standard deviation of the population of means is

$$S_m = \sqrt{0.128} = 0.358$$

Now referring to the "t table", the standard deviation at the 95% confidence limits, for three degrees of freedom, is

$$\bar{P} \pm (S_m)(t) = \bar{P} \pm (0.358)(3.18)$$

$$= (4.29 \pm 1.1) \times 10^{-9} \quad \frac{cc(STP)}{cc\text{-}sec\text{-}atm}$$

Thus the precision in the measurement of $\bar{P}$ is $\pm$ 2.7% and considerably better than predicted.

Similarly for D

Run	$D \times 10^7$	$(x - \bar{x})$	$(x - \bar{x})^2$
96	7.72	0.13	0.0169
97	7.90	0.05	0.0025
08	7.86	0.01	0.0001
99	7.90	0.05	0.0025
			0.0220

$$\bar{x} = 7.85 \times 10^{-7}$$

$$S_m^2 = \frac{\sum_n (x - \bar{x})^2}{n(n-1)} = \frac{0.0220}{4 \times 3} = .00183$$

$$S_m = 0.0428$$

$$D \pm (S_m)(t) = D \pm (0.0428)(3.18)$$

$$= (7.85 \pm .136) \times 10^{-7} \quad \frac{cm^2}{sec}$$

or at the 95% confidence level D's determined by the time-lag method are precise to ±1.7%. Again, the actually observed precision is considerably greater than predicted.

2. Low Pressure Sorption Method

Runs 43 through 48, Table XIII represent repeat determinations of D and k for argon using the low pressure sorption method.

Run	$D \times 10^7$	$(x - \bar{x})$	$(x - \bar{x})^2$
43	29.5	.3	.09
44	29.9	.7	.49
45	29.5	.3	.09
46	29.5	.3	.09
47	29.5	.3	.09
48	27.3	1.9	3.61
49	29.1	.1	.01
			4.47

$$\bar{x} = 29.2 \times 10^{-7}$$

$$S_m^2 = \frac{4.47}{7 \times 6} = 0.106$$

$$S_m = 0.326$$

$$D \pm (S_m)(t) = D \pm (0.326)(2.45)$$

$$= (29.2 \pm 0.80) \times 10^{-7} \ \frac{cm^2}{sec}$$

At the 95% confidence level the estimated precision is ±2.7%. The observed precision is, again, considerably better than estimated.

Similarily for values of k

Run	$k \times 10^{-2}$	$(x - \bar{x})$	$(x - \bar{x})^2$
43	13.60	.14	.0196
44	12.45	1.01	1.0200
45	14.00	.54	.2916
46	13.50	.04	.0016
47	13.58	.12	.0144
48	-	-	-
49	13.64	.18	.0324
			1.3796

$$\bar{x} = 13.46 \times 10^{-2}$$

$$S_m^2 = \frac{1.38}{6 \times 5} = 0.046$$

$$S_m = 0.046 = 0.214$$

$$\therefore \quad k \pm (S_m)(t) = k \pm (0.214)(2.57)$$

$$= (13.46 \pm 0.551) \times 10^{-2} \quad \frac{cc(STP)}{cc_p\text{-atm}}$$

Thus at the 95% confidence level the measured precision of k is $\pm 4.1\%$. Thus, in this case, the observed precision is lower than that predicted.

3. High Pressure Sorption

The measured precision of k's from high pressure sorption experiments is estimated from runs 14 and 15, Table XIV. Both runs measured CO_2 solubility within a range of 0.5°C.

Run	k	$(x - \bar{x})$	$(x - \bar{x})^2$
14	0.942	0.024	5.76×10^{-4}
15	0.990	0.024	5.76×10^{-4}
			11.52×10^{-4}

$$\bar{x} = 0.966$$

$$S_m^2 = \frac{11.52 \times 10^{-4}}{2} = 5.76 \times 10^{-2}$$

$$Sm = 0.024$$

$$\therefore \quad k \pm (S_m)(t) = k \pm (0.024)(12.7)$$

$$= 0.966 \pm .305$$

or the precision at the 95% confidence level is ±32%. The low level of precision is simply the result of estimating the precision from only two measurements rather than the result of poor reproducibility in the experimental method.

Appendix D

Calculations for Low Pressure Sorption System

1. Calibration of the Sample Volume, V_T

Before the polymer was introduced into the system the volume of the sample bulb and its associated connecting tubing was determined by the following, simple experiment.

With stopcocks S_3 and S_5 (Figure 16) closed, 20 to 30 mm Hg of gas (i.e., not more than the pressure transducer was designed for) were fed to the system comprising the manometer, the sample volume, and the calibration bulb. Next, stopcock S_1 was closed, stopcocks S_3 and S_5 opened and the system thoroughly evacuated. Then the pressure, P_1, in the sample side of the system was recorded. Now stopcock S_9 was closed, S_1 was opened and that part of the system evacuated. Finally S_1 was closed and S_9 opened, allowing the gas previously isolated in the calibration bulb to expand into the sample volume. The volume of the calibration bulb had been determined before the apparatus was built by weighing the amount of water it held.

The sample volume, V_T, was then readily calculated from a simple mass balance.

$$P_1V_c = P_2V_c + P_2V_T \qquad \text{(D-1)}$$

$$V_c(P_1 - P_2) = P_2V_T$$

$$\therefore \quad V_T = \frac{(P_1 - P_2)}{P_2} \cdot V_c$$

where V_c is the volume of the calibration bulb up to stopcock S_9, and, V_T is the volume of the sample bulb (empty) plus the tubing to the right of stopcock S_1 but excluding V_c.

2. Derivation of Equation (27)

By a mass balance on the sample bulb and its associated tubing:

$$\frac{P_i V_V}{RT} = \frac{P_e V_V}{RT} + \frac{P_e V_P k}{22,400} \qquad \text{(D-2)}$$

Then

$$\frac{(P_i - P_e)}{RT} V_V = \frac{P_e V_P k}{22,400} \qquad \text{(D-3)}$$

and

$$k = \frac{V_V}{V_P} \cdot \frac{(P_i - P_e)}{P_e} \cdot \frac{22,400}{RT}$$

or

$$k = \frac{V_V}{V_P} \cdot \frac{273}{T} \cdot \frac{(P_i - P_e)}{P_e} \quad \frac{cc(STP)}{cc_p\text{-atm}} \qquad (27)$$

where V_V = void volume in cc

V_P = volume of the polymer in cc

V_T = $V_V + V_P$ = sample volume in cc

P_i = pressure at time zero in mm Hg

P_e = pressure at equilibrium in mm Hg

T = temperature of system in °K

3. Derivation of Equation (28)

Again from a mass balance on the sample side of the system,

$$\frac{(1 - f)P_i V_P k}{22,400} = \frac{P_e V_P k}{22,400} + \frac{P_e V_V}{RT} \qquad (D\text{-}4)$$

$$\frac{V_P k}{22,400}\,[(1 - f)P_i - P_e] = P_e \frac{V_V}{RT} \qquad (D\text{-}5)$$

$$\therefore \quad k = \frac{V_V}{V_P} \cdot \frac{22,400}{RT} \cdot \frac{P_e}{[(1 - f)P_i - P_e]}$$

$$k = \frac{V_V}{V_P} \cdot \frac{273}{T} \cdot \frac{P_e}{[(1 - f)P_i - P_e]} \quad \frac{cc(STP)}{cc_p\text{-atm}} \qquad (28)$$

where: V_V = void volume in cc

V_P = polymer volume in cc

T = temperature of system in °K

P_i = initial equilibration pressure in mm Hg

P_e = final equilibration pressure in mm Hg

$(1 - f)$ = fraction of gas lost from polymer during pump-down

$(1 - f)$ is estimated from equation (30), namely

$$(1 - f) = \left[1 - 2\left(\frac{Dt}{\pi \ell^2}\right)^{1/2}\right]^3 \qquad (30)$$

and $P_e = P'_e - P'$

where: P'_e = observed final equilibration pressure

P' = residual pressure after pump-down.

4. Adiabatic Compression Effect Observed in Sorption Experiments

Sorption experiments include a sudden pressurization step of the sample volume and its contents, which results in a marked temperature rise and destroys the usefulness of sorption experiments for diffusivity measurements. Although the compression is not completely adiabatic, one can estimate the magnitude of the effect by assuming the sample volume and contents have negligible heat capacity and are perfect insulators.

In a typical experimental run, gas at 500 mm Hg expands from a volume A of 1000 cc into the sample volume B of 50 cc. Temperatures are initially the same and the gas is argon.

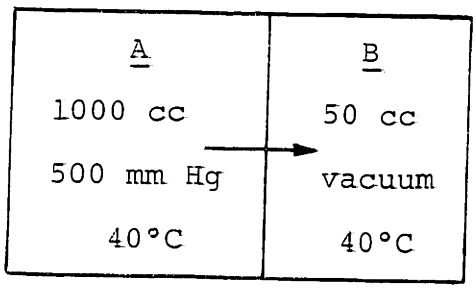

(a) First, taking contents of compartment A as an open system,

$$d(m_s e_s) = -h_o dm_o = m_s de_s + e_s dm_s$$

Since $dm_s = -dm_o$

$$mde + edm = h_o dm = (e + pv)dm$$

$$mde = pvdm$$

$$\frac{de}{pv} = \frac{dm}{m} = \frac{c_v dT}{RT}$$

$$\therefore \quad \ln \frac{m_{A_2}}{m_{A_1}} = \frac{c_v}{R} \ln \frac{T_{A_2}}{T_{A_1}}$$

or

$$\frac{m_{A_2}}{m_{A_1}} = \left(\frac{T_{A_2}}{T_{A_1}} \right)^{\frac{c_v}{R}} \qquad \text{(i)}$$

where m_{A_1} = moles of gas originally in compartment A
m_{A_2} = moles of gas finally in compartment A
T_{A_1} = temperature originally in compartment A
T_{A_2} = temperature finally in compartment A

(b) Now taking contents of both compartments as a closed system.

$$Q - w = \Delta u = 0$$

$$\therefore \quad \Delta e_A = \Delta e_B$$

$$m_{A_1}(c_v T_{A_1} + b) - m_{A_2}(c_v T_{A_2} + b) = (m_{A_1} - m_{A_2})(c_v T_{B_2} + b)$$

$$m_{A_1} T_{A_1} = m_{A_2} T_{A_2} + (m_{A_1} - m_{A_2}) T_{B_2} \qquad \text{(ii)}$$

after pressure equilization

$$(PV)_{A_2} = 20\ (PV)_{B_2}$$

and

$$m_{A_2} RT_{A_2} = 20(m_{A_1} - m_{A_2}) RT_{B_2}$$

$$m_{A_2} T_{A_2} = 20(m_{A_1} - m_{A_2}) T_{B_2} \qquad \text{(iii)}$$

substituting in (ii)

$$m_{A_1} T_{A_1} = m_{A_2} T_{A_2} + \frac{1}{20} m_{A_2} T_{A_2}$$

$$m_{A_1} T_{A_1} = \frac{21}{20} m_{A_2} T_{A_2}$$

$$\therefore \quad \frac{m_{A_2}}{m_{A_1}} = \frac{20}{21} \frac{T_{A_1}}{T_{A_2}} = \left(\frac{T_{A_2}}{T_{A_1}} \right)^{c_v/R} \qquad \text{(iv)}$$

for argon, a monatomic gas $c_v = 3$, $c_p = 5$

$$\therefore \quad \frac{c_v}{R} = \frac{3}{2} = 1.5$$

$$\therefore \quad \frac{20}{21} \left(\frac{T_{A_1}}{T_{A_2}} \right) = \left(\frac{T_{A_2}}{T_{A_1}} \right)^{1.5}$$

$$\frac{20}{21} (T_{A_1})^{2.5} = (T_{A_2})^{2.5}$$

$$T_{A_2} = \left(\frac{20}{21} \right)^{1/2.5} T_{A_1} = 0.9809 \ (313)$$

$$= 307°K = 34°C$$

(c) Then evaluating the mass in volume A before and after the expansion.

$$m_{A_1} = \frac{P_{A_1} V}{R T_{A_1}} = \frac{(500)(1)}{(62.3)(313)} = 0.0257 \text{ gmoles}$$

Then from (iv)

$$m_{A_2} = m_{A_1} \left(\frac{T_{A_2}}{T_{A_1}} \right)^{1.5}$$

$$\therefore \quad m_{A_2} = (0.0257)\left(\frac{307}{313}\right)^{1.5} = 0.0250 \text{ gmoles}$$

The gram moles ending up in volume B are

$$m_{B_2} = (m_{A_1} - m_{A_2}) = 0.0007$$

Then from equation (iii)

$$T_{B_2} = \frac{m_{A_2} T_{A_2}}{20(m_{A_1} - m_{A_2})}$$

$$= \frac{(0.0250)(307)}{(20)(0.0007)} = 548°K$$

$$= 275°C$$

This represents a temperature rise of 235°C for the volume <u>into</u> which the gas is expanded. In practice, the compression is not completely adiabatic because of the finite heat capacity of the glass tubing and the polymer. Nevertheless, the effect is considerable and responsible for the anomalous diffusion behavior observed for sorption experiments.

Appendix E

The Unit Cell of Poly(propylene) Crystals

(a) Monoclinic Crystals

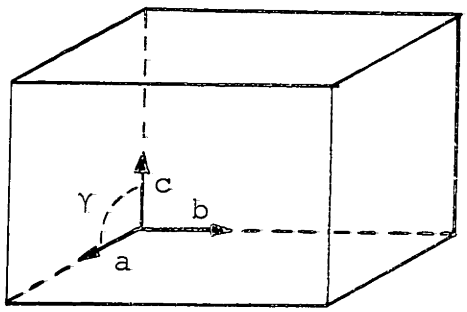

The monoclinic crystal form is defined by Bunn (21) as: a and $c \perp b$, 3 axes unequal in length, a and c are inclined to each other at an obtuse angle γ.

The unit cell constants for annealed poly(propylene) are:

$a = 6.65$ Å

$b = 20.96$ Å

$c = 6.50$ Å

$\gamma = 99°20'$

and the helical chains are parallel to the c-axis of the cell.

(b) Hexagonal

The quenched crystal habit of poly(propylene) is believed to be hexagonal.

Bunn (21) defines the unit cell of hexagonal crystals as having:

> a hexagonal base, a and b edges at 120° to each other and equal in length; $c \perp$ to a and b and different in length.

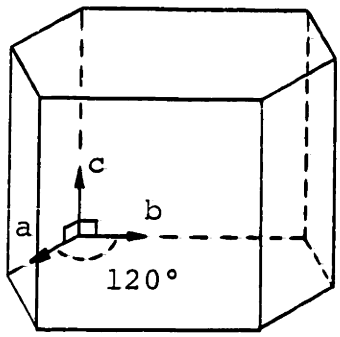

the hexagonal unit cell

Appendix F

Analysis of the Crystal Lattice

The following analysis was made (1) to determine if the smallest gas molecule, helium, could possibly pass unhindered through the lattice of a perfect crystal of poly(propylene), and (2) to estimate the size of the largest, continuous cavity left when a chain is removed from the crystal lattice.

A section of poly(propylene) chain, in its helical conformation, was constructed from Stuart models and approximate chain dimensions measured on it. It was found that the helix had a triangular cross-section when viewed end on. The dimensions of the equilateral triangle are: height = 6.6 Å, side = 7.36 Å.

In Figure 1 is shown a projection of the monoclinic unit cell of crystalline poly(propylene). If equilateral triangles with a height of 6.6 Å are superimposed upon the outlines of each chain, it is found that the largest molecule that could possibly slip unhindered through the crystal lattice is 1.5 Å (see sketch below). Since helium, the smallest molecule considered in this study, is 2.2 Å in diameter, it is fairly safe to assume that gas will not dissolve or diffuse through the perfect, crystal lattice.

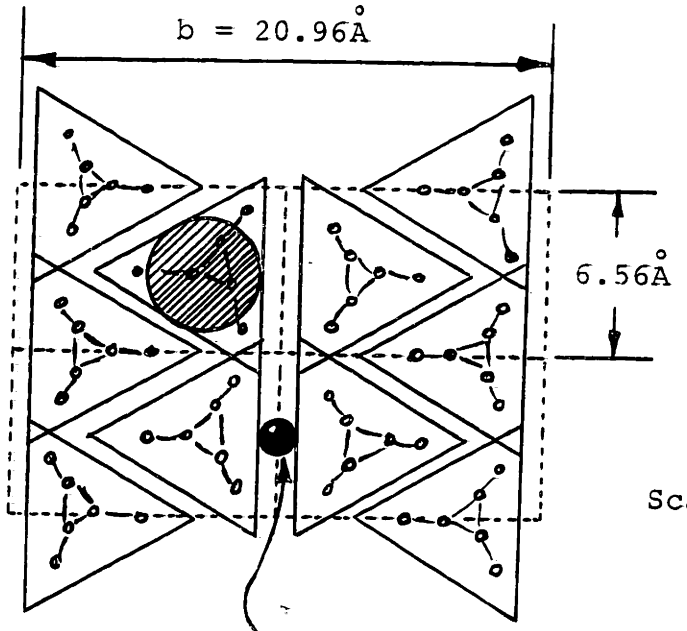

In the sketch above is also shown a cricle inscribed in one of the equilateral triangles. The diameter of this circle is ~4.5 Å. Since the chains in the lattice are helices, the largest uniform cavity left by the removal of <u>one</u> chain would be a "straight-through" cylinder (perpendicular to the paper) with a diameter of 4.5 Å.

Appendix G

1. Row Vacancy Defect Formation

The formation of row vacancies can be qualitatively evaluated by an analysis of the lamellar thickening process on annealing.

Hoffman and coworkers (45) visualize the thickening process of lamellae as a two-stage process in which the second step involves a high rate of row vacancy defect formation. They propose the following relationship for the second stage of the thickening process:

$$\ell = \ell^*_g + B_2 \log \left[\left(\frac{t - t_o}{t_o} \right) \right] \qquad (3)$$

where ℓ = the average thickness of the crystal at any time, cm

ℓ^*_g = the initial thickness of the crystal, cm

t = annealing time, min

t_o = time when crystal first appears, min

$$B_2 = \frac{2.303\ \bar{k}T}{\left(2g\ \frac{\sigma^2}{\sigma_e} + \frac{E}{\ell_o}\right)}$$

$\bar{k}$ = Boltzmann constant

T = annealing temperature, °K

σ = surface free energy, erg/cm^2

σ_e = surface free energy of edge, erg/cm^2

ℓ_o = 1.27×10^{-8} cm

E = the energy required to form a row vacancy per-C-unit, erg

Rearranging equation (3)

$$(\ell - \ell_g^*) = \frac{2.303\ \bar{k}T}{(2g\frac{\sigma^2}{\sigma_e} + \frac{E}{\ell_o})} \log\left(\frac{t - t_o}{t_o}\right) \qquad (3a)$$

$$= a_1 T \log\left(\frac{t - t_o}{t_o}\right)$$

where $(\ell - \ell_g^*)$ is the average increase in lamellar thickness and a_1 is a constant.

Since all samples were annealed for exactly 60 minutes, the age of the crystal $(t - t_o)$ is the same for every case and $\log\left(\frac{t - t_o}{t_o}\right)$ can be included in the constant.

$$\therefore \quad (\ell - \ell_g^*) = a_2 T$$

But Defect Formation $= f(\ell - \ell_g^*)$

$$\therefore \text{ Defect Formation } = a_3 T$$

or the rate of defect formation is directly proportional to the annealing temperature.

2. Estimating the Fraction of Sample That is Defects

a. Comparing Knudsen and activated diffusion.

Consider the case of helium diffusing in a pore 4.5Å in diameter,

$$D_K = 9700\ r_e\ (T/M)^{1/2}$$

$$= (9700)\ \frac{(4.5)}{2}\ (10^{-8})\left(\frac{313}{4}\right)^{1/2}$$

$$\cong 2 \times 10^{-3} \text{ cm}^2/\text{sec}$$

The average activated diffusivity for helium is on the order of 1×10^{-5} cm^2/sec. Therefore, Knudsen diffusion in a pore only 4.5Å in diameter is ~200 times greater than activated diffusion in the polymer.

b. Volume fraction of defects.

For a molecule to be never more than 30Å, i.e., <u>one</u> diffusional jump length, from a defect when it reaches a crystal it would require the following volume fraction of defects.

(i) Based on crystalline content

$$= \frac{2\pi(r_e)^2}{60 \times 60}$$

$$= \frac{(2)(3.14)(\frac{4.5}{2})^2}{(60)(60)}$$

$$= .0088$$

$$= .009 \text{ or } .9\%$$

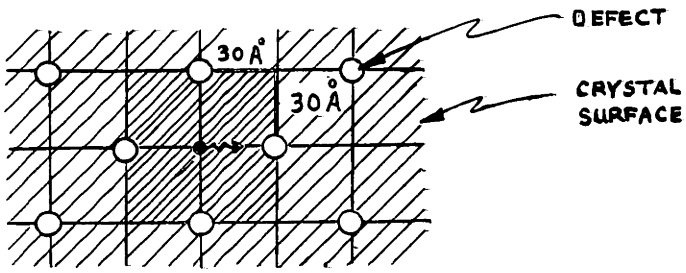

(ii) Based on crystalline plus amorphous, at $\alpha = 0.30$

$$\varepsilon = (.0088) \times \frac{70}{100}$$

$$= 0.006$$

Appendix H

Size Distribution of Accessible Defects

On the basis of the diffusional enhancement for the three gases at the 30% amorphous content, it becomes possible to calculate a size distribution for the defects. The basic assumption is that the mode of transport in the defects is non-activated and that the diffusional resistance of the defects is thus negligible compared to the resistance in the amorphous regions.

From Figures 55, 56 and 57 the average diffusional enhancements at $\alpha = 0.30$ are 97%, 66% and 44% for helium, argon and CF_4, respectively. If one assumes that the defects offer no resistance to diffusion, one can calculate a decrease in the sinuosity of the diffusion path, τ_{eff}/τ, from the different diffusional enhancements. If one only considers the accessible defects, i.e., the fraction of defects larger than the minimum size required for passage of the smallest molecule, helium, then it becomes possible to estimate a size distribution for the accessible defects.

The minimum size of the defects accessible to He, A and CF_4, respectively, was estimated from a comparison of d and σ values, where d is the molecular diameter and σ is the distance of closest approach of two non-polar molecules in the Lennard-Jones potential energy function. It was concluded that for the free passage of a gas molecule the smallest diameter of any

defect must be at least d plus 0.4 Å (i.e., a minimum separation of 0.2 Å between defect wall and gas molecule), otherwise repulsive forces due to polymer-gas interactions may come into play.

The calculations for estimating the size distribution of the accessible defects are summarized in Table H-1.

Table H-1

Gas	d(Å)	Diameter of Smallest Accessible Defect (A)	Diffusional Enhancement, (%)	$\frac{\tau_{eff}}{\tau}$	Fraction of Defects Accessible to Gas
He	2.2	2.6	97	0.51	1.00
A	3.6	4.0	66	0.60	0.82
AF_4	4.6	5.0	44	0.69	0.63

To illustrate the calculations:

(1) for helium, using the data in Figure 55 at $\alpha = 30\%$,

$$\frac{\tau_{eff}}{\tau} = \frac{D_1(\text{without defects})}{D_2(\text{with defects})} = \frac{0.74 \times 10^{-5}}{1.45 \times 10^{-5}} = 0.51$$

where τ_{eff} is the sinuosity of the diffusion path in the presence of row vacancy defects, and τ is the tortuosity at the same crystalline content but without defects.

(2) for argon, using the data in Figure 56 at $\alpha = 30\%$.

$$\frac{\tau_{eff}}{\tau} = \frac{1.60 \times 10^{-7}}{2.67 \times 10^{-7}} = 0.60$$

(3) If, by definition, fraction of defects accessible to helium = 1.0 then, fraction of defects accessible to argon =

$$= \frac{1 - \text{reduction in sinuosity for argon}}{1 - \text{reduction in sinuosity for helium}}$$

$$= \frac{1 - (\tau_{eff}/\tau)_A}{1 - (\tau_{eff}/\tau)_{H_e}} = \frac{1 - 0.60}{1 - 0.51} = 0.82$$

Now plotting these values (last column, Table H-1) against the corresponding "diameter of smallest accessible defect", one obtains the cumulative defect curve shown in Figure 59.

From this plot, in turn, one constructs graphically Figure 60, showing the size distribution of the accessible defects.

Appendix I

Location of Original Data

The original data and notebooks are located in the files of:

Professor W. R. Vieth
Room 12 - 146
Department of Chemical Engineering
Massachusetts Institute of Technology
Cambridge, Massachusetts 02139

Appendix J

List of Symbols

a	area of molecule for hexagonal close packing, $\mathring{A}^2$
A	area of film exposed to gas in diffusion cell, cm^2
b	hole affinity constant, atm^{-1}
B_1	quantity defined by equation (2)
B_2	quantity defined by equation (3)
C	concentration, cc(STP)/cc
C'_H	hole saturation constant, cc(STP)/cc
C_D	concentration due to dissolution, cc(STP)/cc
C_H	concentration due to micro-void filling, cc(STP)/cc
C_v	heat capacity at constant volume, cal/gmole-°C
C_p	heat capacity at constant pressure, cal/gmole-°C
d	diameter of diffusing gas molecule, $\mathring{A}$ or cm^2
D	diffusion constant, cm^2/sec
D^*	diffusion constant in completely amorphous poly(propylene), cm^2/sec
D_o	constant defined by equation (12)
E	energy required to form a row vacancy
E_D	energy of activation for diffusion, Kcals/gmole
$E_{\bar{P}}$	energy of activation for permeation, Kcals/gmole
f	fraction of gas lost from polymer during pump-down in static sorption studies
ffu.	final fractional uptake, defined by equation (34)
ΔF_c	free energy of condensation, Kcals/gmole
$\Delta \bar{F}_m$	partial molar free energy of mixing, Kcals/gmole
h	Planck's constant, erg-sec

h_o	enthalpy of mass leaving system, cals/gmole
ΔH_c	heat of condensation, Kcals/gmole
$\Delta \bar{H}_m$	partial molar heat of mixing, Kcals/gmole
ΔH_s	enthalpy of sorption, Kcals/gmole
ΔH_{ads}	enthalpy of adsorption, Kcals/gmole
ΔH_v	heat of vaporization, Kcals/gmole
J	permeation rate per unit area, cc(STP)/cm^2-sec
k	solubility constant, cc(STP)/cc-atm
k^*	solubility constant in completely amorphous poly(propylene), cc(STP)/cc-atm
k_o	constant defined by equation (13)
$\bar{k}$	Boltzmann's constant, erg/degree
ℓ	thickness, cm
ℓ_o	length along carbon backbone
ℓ^*	initial thickness, cm
m	steady-state pressure increase in time-lag experiments, μ/min
m_L	leak rate in time-lag experiment, μ/min
m_s	mass of system, gmole
m_o	mass leaving system, gmole
M	molecular weight, g/gmole
M_t	amount of gas sorbed or desorbed in time t, cc(STP)
M_∞	amount of gas sorbed or desorbed at equilibrium, cc(STP)
p	pressure, mm Hg or atm
p_1	upstream pressure in time-lag experiments, mm Hg or atm
p_i	initial pressure, mm Hg
p_f	final pressure, mm Hg

P_e	actual equilibrium pressure, mm Hg
P'_e	observed equilibrium pressure, mm Hg
P'	pressure at end of pump-down, mm Hg
$\bar{P}$	permeability constant, cc(STP)/cm-sec-atm
$\bar{P}_o$	constant defined by equation (11)
dP/dt	steady-state pressure rise in time-lag experiments, μ/min
q_n	positive, non-zero roots of equation (39)
q_s	isosteric heat of sorption, cals/gmole
Q	amount of gas permeated through film up to time t, cc(STP)
r	radius, cm, or distance between two approaching molecules, A
R	universal gas constant, 1.987 cal/gmole-°K or 82.057 cm^3-atm/gmole-°K
S_1	stopcock designation on schematic diagrams of apparatus
ΔS^*_o	overall entropy of activation for diffusion, cals/gmole-°K
ΔS^*_P	entropy of activation for diffusion for polymer, cals/gmole-°K
ΔS^*_G	entropy of activation for diffusion for gas, cals/gmole-°K
ΔS_c	entropy change of condensation, Kcals/gmole-°K
S_{vib}	vibrational entropy of gas molecule, cals/gmole-°K
S_{trans}	translational entropy of gas molecule, cals/gmole-°K
$\bar{S}_2$	partial molar entropy of solution, cals/gmole-°K
S^g_2	entropy of molecule in gas phase at one atmosphere, cals/gmole-°K
t	time, sec
T	temperature, °C or °K

T_a	ambient temperature, °C
T_{a_i}	initial ambient temperature, °K
T_{a_f}	final ambient temperature, °K
T_B	normal boiling point, °K
T_c	critical temperature, °K
U_{oo}	potential energy at closest approach of an adsorbed molecule, Kcals/gmole
ΔU	change in internal energy, cals/gmole
V	volume, cc
V_a	volume of tubing in high pressure sorption system, cc
V_b	void volume of bomb, cc
V_c	volume of calibration bulb, cc
V_o	potential energy barrier to movement of an adsorbed molecule along the surface
V_P	polymer volume, cc
V_s	downstream collecting volume of time-lag apparatus, cc
V_v	void volume in low pressure sorption system, cc
V_T	$(V_v + V_p)$ = collecting volume or sample side volume, cc
$\bar{V}$	partial molar volume of gas, cc/gmole
x_2	molefraction of gas in solution
x	distance, cm
Z_i	compressibility factor at T and P_i
Z_f	compressibility factor at T and P_f
Z_{a_i}	compressibility factor at T_{a_i} and P_i
Z_{a_f}	compressibility factor at T_{a_f} and P_f
Z_o	compressibility factor at 273°K and 1 atmosphere

α	volume fraction or percent amorphous volume
β	chain immobilization factor
$\varepsilon/\bar{k}$	force constant in Lennard-Jones (6, 12) potential
θ	time-lag, min
λ	length of diffusion jump, $\mathring{A}$
μ	micron, 10^{-3} mm Hg, or Flory-Huggins parameter related to heat of mixing
ρ	density of sample, gm/cc
ρ_a	density of completely amorphous polymer, gm/cc
ρ_c	density of crystalline polyer, gm/cc
σ	surface free energy, dynes/cm, or standard deviation
σ_e	surface free energy of edges, dynes/cm
τ	geometric impedance factor
ϕ	partition parameter defined by equation (38)
Φ	potential energy, ergs or Kcals

Appendix K

Literature Citations

1. Alcalay, H. H., "Fluid Transport in Structurally Modified Poly(propylene) Membranes", Sc.D. thesis, M.I.T., Cambridge, Massachusetts (1966).

2. van Amerongen, G. J., J. Polymer Sci., 5, 307 (1950).

3. Anderson, F. R., J. Appl. Phys., 35, 65 (1964).

4. Ashby, G. E. and D. F. Hoeg, J. Polymer Sci., 39, 535 (1959).

5. Barrer, R. M. and G. Skirrow, J. Polymer Sci., 3, 549 (1948).

6. Barrer, R. M., J. Phys. Chem., 61, 178 (1951).

7. Barrer, R. M., Trans. Faraday Soc., 39, 237 (1943).

8. Barrer, R. M., Barrie, J. A. and J. Slater, J. Polymer Sci., 27, 315 (1958).

9. Barrer, R. M., Trans. Faraday Soc., 35, 628 (1939).

10. Beck, D. L., A. A. Hiltz, and J. R. Knox, SPE Trans., 3-4, 279 (1963).

11. Billmeyer, F. W., Jr., "Textbook of Polymer Science", 1st ed., Interscience, New York (1962).

12. Ibid, p. 141.

13. Ibid, p. 372.

14. Binning, R. C., R. J. Lee, J. F. Jennings, and E. C. Martin, Ind. Eng. Chem., 53, 45 (1961).

15. Bixler, H. J., "Solution and Flow of Gases in Poly(ethylene)", Sc.D. thesis, M.I.T., Cambridge, Massachusetts (1959).

16. Brandt, W. W., J. Phys. Chem., 63, 1080 (1959).

17. Brandt, W. W., J. Polymer Sci., 41, 403 (1959).

18. Bunn, C. W., and T. C. Alcock, Trans. Faraday Soc., 41, 317 (1945).

19. Bunn, C. W., and E. V. Garner, Proc. Roy. Soc. (London), A189, 39 (1947).

20. Bunn, C. W., A. J. Cobbold, and R. P. Palmer, J. Polymer Sci., 28, 365 (1958).

21. Bunn, C. W., "Chemical Crystallography", 2nd ed., Clarendon Press, Oxford (1961).

22. Campbell, G., Plastics, 29, 59 (July, 1964).

23. Conner, W. P. and G. L. Schertz, SPE Trans., 3, 186 (1963).

24. Ibid., p. 190.

25. Crank, J., "The Mathematics of Diffusion", 1st ed., p. 48, Oxford University Press (London), (1956).

26. Ibid., p. 45, equation (4.20).

27. Ibid., p. 87, equation (6.22).

28. Ibid., p. 88.

29. Ibid, p. 330, Table 6.1.

30. Dainton, F. S., Evans, D. M., Hoare, F. E. and T. P. Melia, Polymer 3, 3, 286 (1962).

31. Draisbach, H. C., D. Jeschke, and H. A. Stuart, Z. Naturforsch., 17a, 447 (1962).

32. Evans, L. B. and Y. H. Ma, paper entitled "Transient Diffusion from a Well-Stirred Reservoir to a Body of Arbitrary Shape", Department of Chemical Engineering, Massachusetts Institute of Technology (1967).

33. Fein, H. L., "Diffusion of Gases in Poly(ethylene)", Sc.D. thesis, M.I.T., Cambridge, Massachusetts (1963).

34. Fisher, E. W., Ann. N. Y. Acad. Sci., 89, 620 (1960).

35. Fisher, E. W., Z. Naturforsch., 12a, 753 (1957).

36. Gailey, J. A. and R. H. Ralston, SPE Trans., 4, 29 (1964).

37. Gee, G., Quart. Revs., 1, 265 (1947).

38. Geil, P. H., J. Polymer Sci., 47, 65 (1960).

39. Geil, P. H., J. Appl. Phys., 33, 642 (1961).

40. Geil, P. H., C & EN, 16, 79 (1965).

41. Geil, P. H., "Polymer Single Crystals", pp. 211-220, 270, 1st. ed., Interscience, New York (1963).

42. Glasstone, S., Laidler, K. J. and H. Eyring, "The Theory of Rate Processes", 1st ed., p. 524, McGraw-Hill, New York (1941).

43. Hill, T. L., "An Introduction to Statistical Thermodynamics", 1st. ed., Addison-Wesley, Reading, Mass. (1960).

44. Hoffman, J. D., and J. J. Weeks, J. Res. Nat'l, Bur. Std, 66A, 13 (1962).

45. Hoffman, J. D., G. Williams and E. Passaglia, J. Polymer Sci., C14, 180 (1966).

46. Ibid., pp. 173-235.

47. Hoffman, J. D., SPE Trans., 4, 315 (1964).

48. Hoffman, J. D., and J. J. Weeks, J. Chem. Phys., 42, 4301 (1965).

49. Hosemann, R., Acta Crysta., 4, 520 (1951).

50. Jack, J., British Plastics, 34, 312 (1961).

51. Jeschke, D. and H. A. Stuart, Z. Naturforsch., 16a, 37 (1961).

52. Jolley, J. E., and J. H. Hildebrand, J. Am. Chem. Soc., 80, 1050 (1958).

53. Keith, H. D., F. J. Padden, Jr., N. M. Walter and H. W. Wyckoff, J. Appl. Phys., 30, 1485 (1959).

54. Keller, A., Phil. Mag., 2, 1171 (1957).

55. Khoury, F., J. Res. Nat'l. Bur. Std., 70A, 29 (1966).

56. Klug, H. P. and L. E. Alexander, "X-Ray Diffraction Procedures for Polycrystalline and Amorphous Materials", Wiley, New York (1954).

57. Klute, C. H. and P. J. Franklin, J. Polymer Sci., 32, 161 (1958).

58. Lasoski, S. W., Jr., and W. H. Cobbs, J. Polymer Sci., 36, 21 (1959).

59. Luongo, J. P., J. Appl. Pol. Sci., 3, 302 (1960).

60. Magill, J. H. and P. H. Harris, Polymer, 3, 252 (1962).

61. Matulevicius, E. S., Personal Communication, M.I.T., Cambridge, Massachusetts (September 1965).

62. Meares, P., Trans. Faraday Soc., 53, 101 (1957).

63. Meares, P., J. Am. Chem. Soc., 76, 3415-3422 (1954).

64. Ibid., p. 3421.

65. Meares, P., Trans. Faraday Soc., 54, 40 (1958).

66. Mencik, Z., Chem. Prumysl., 10, 377 (1960).

67. Michaels, A. S., H. J. Bixler and H. L. Fein, J. Appl. Phys., 35, 3165 (1964).

68. Michaels, A. S., and R. B. Parker, Jr., J. Polymer Sci., 41, 53 (1959).

69. Michaels, A. S., W. R. Vieth, and J. A. Barrie, paper presented at the Annual Meeting of the American Physical Society, Division of High Polymer Physics, Baltimore, Maryland, March 27-30, 1962.

70. Michaels, A. S., and H. J. Bixler, J. Polymer Sci., 50, 413 (1961).

71. Ibid., p. 393.

72. Mickley, H. S., T. K. Sherwood and C. E. Reed, "Applied Mathematics in Chemical Engineering", 2nd ed., McGraw-Hill New York (1957).

73. Miller, R. L., Polymer J., 1, 135 (1960).

74. Miller, R. L., and L. E. Nielson, J. Polymer Sci., 55, 643 (1961).

75. Mock, W. L., and H. H. Zabusky, "Permeability of Poly-(propylene) Films", S.B. thesis, M.I.T., Cambridge, Massachusetts (1959).

76. Moore, E. P., Jr., Personal Communication, Hercules Inc., Wilmington, Delaware (August 26, 1965).

77. Morrow, D. R., J. A. Sauer and A. E. Woodward, "Morphology of Solution-Crystallized Poly(propylene)", article in preparation (1967).

78. Muus, L. T., N. G. McGrum, and F. C. McGrew, SPE J., 15, 368 (1959).

79. Myers, A. W., V. Stannett, and M. Szwarc, J. Polymer Sci., 35, 285 (1959).

80. Myers, A. W., C. E. Rogers, V. Stannett and M. Szwarc, Modern Plastics, 34, 157 (1957).

81. Natta, G., Die Makromolekulare Chemie, 34-35, 94 (1960).

82. Natta, G., M. Peraldo, and P. Corradini, Atti. accad. nazl. Lincei., Rend., 26, 14 (1959).

83. Natta, G., J. Polymer Sci., 16, 143 (1955).

84. Natta, G., Chimica e Industria (Milan), 41, 647 (1959).

85. Padden, F. J., Jr., and H. D. Keith, J. Appl. Phys., 37, 4013 (1966).

86. Pae, K. D., D. R. Morrow and J. A. Sauer, "The Interior Morphology of Bulk Poly(propylene)", paper in preparation Rutgers University, New Brunswick, New Jersey (1967).

87. Palmer, R. P. and J. A. Cobbold, Die Makromolekulare Chemie, 74, 174 (1964).

88. Parker, R. B., Jr., "Sorption and Flow Behavior of Gases in Poly(ethylene)", Sc.D. thesis, M.I.T., Cambridge, Massachusetts (1958).

89. Pinsky, J., and H. A. Bent, W. A. D. C. Report, Vol. II, 53 (1955).

90. Prausnitz, J. M., A.I.Ch.E. Journal, 4, 269 (1958).

91. Quynn, R. G., J. L. Riley, D. A. Young, and H. D. Noether, J. Appl. Pol. Sci., 2, 166 (1959).

92. Ralston, R. H., Personal Communication, Hercules Inc., Wilmington, Delaware (August 26, 1965).

93. Reid, R. C. and T. K. Sherwood, "The Properties of Gases and Liquids", 1st ed., p. 43, McGraw-Hill, New York (1958).

94. Ruland, W., Acta. Cryst., 14, 1130 (1961).

95. Samuels, R. J., J. Polymer Sci., A3, 1741 (1965).

96. Satterfield, C. N., and T. K. Sherwood, "The Role of Diffusion in Catalysis", Addison-Wesley, Reading, Mass. (1963).

97. Sauer, J. A., D. R. Morrow, and G. C. Richardson, J. Appl. Phys., 36, 3017 (1965).

98. Sobue, H., and Y. Tabata, J. Appl. Pol. Sci., 4, 66 (1959).

99. Stannett, V., and I. L. Williams, paper presented at the Detroit Meeting of the American Chemical Society, Division of Organic Coatings and Plastic Chemistry, April 1965.

100. Stannet, V., M. Szwarc, R. L. Bhargava, J. A. Meyer, A. W. Meyer, and E. E. Rogers, "Permeability of Plastic Films and Coated Paper to Gases and Vapors", TAPPI (1962).

101. Stein, R. S., lecture at M.I.T., October (1966).

102. Symons, N. K., J. Polymer Sci., A1, 2843 (1963).

103. Tam, P. M., "High Pressure Sorption in Glassy Polymer", S.M. Thesis, M.I.T., Cambridge, Massachusetts (1965).

104. Till, P. H., J. Polymer Sci., 24, 301 (1957).

105. Treybal, R. E., "Mass Transfer Operations", 1st ed., p. 66, McGraw-Hill, New York (1955).

106. Turley, S. G., and H. Keskkula, J. Appl. Pol. Sci., 9, 2693 (1965).

107. Turley, S. G., Personal communication, Dow Chemical Co., Midland, Michigan (June 23, 1966).

108. Wilbourne, A. H., Trans. Faraday Soc., 54, 717 (1958)

109. Wilkinson, R. W., and M. Dole, J. Polymer Sci., 58, 1089 (1962).

110. Wyckoff, H. W., J. Polymer Sci., 62, 83 (1962).

111. Vieth, W. R., "A Study of Poly(ethylene terephthalate) by Gas Permeation", Sc.D. thesis, M.I.T., Cambridge, Massachusetts (1961).

112. Vieth, W. R., P. M. Tam, and A. S. Michaels, "Dual-Sorption Mechanism in Glassy Poly(styrene)", Department of Chemical Engineering, M.I.T., Cambridge, Massachusetts (1965).

113. Vieth, W. R., E. S. Matuleviscius, and S. R. Mitchell, "Detection of Stress-Induced Morphological Alteration of Poly(ethylene terephthalate) by Gas Permeation", Kolloid Zeitschrift und Zeitschrift für Polymere (November 1967).

114. Vieth, W. R., H. H. Alcalay, and A. J. Frabetti, J. Appl. Pol. Sci., 8, 2125 (1964).

115. Volk, W., "Applied Statistics for Engineers", 1st ed., Chapter 7, McGraw-Hill, New York (1958).

BIOGRAPHICAL NOTE

Walter Fritz Theodor Wuerth was born on February 27, 1939, in Salzwedel, Germany. He grew up in Bavaria, emigrated to the United States in 1952 and nine months later moved to Toronto, Canada. There the author completed highschool and attended the University of Toronto where he studied chemical engineering.

In 1962, Mr. Wuerth entered M.I.T. and was awarded a Master's degree in Chemical Engineering in February 1964. For the 1964-65 school year he served as Assistant Director of the Chemical Engineering Practice School stationed at the Humble Oil Refinery at Bayway. On his return to the Institute, the author continued his doctoral program.

In May 1967, Mr. Wuerth married the former Sandra Najat of Toronto.

Upon graduation the author will join the Esso Research and Engineering Company in Florham Park, New Jersey.

Mr. Wuerth is a member of Phi Lambda Upsilon, Sigma Xi, and the Association of Professional Engineers of Ontario.


ted
ILM
or
he
IND